Measurement techniques for the analysis of surface layers on grain oriented electrical steel.

Poultney, Darren

EPSRC

Engineering & Physical Sciences Research Council

corus

Measurement Techniques for the Analysis of Surface Layers on Grain Oriented Electrical Steel

Darren Poultney

A thesis submitted to the University of Wales, Swansea in candidature for the degree of Engineering Doctorate

University of Wales

cogent

Academic Supervisor

Prof. V. Randle
University of Wales, Swansea

Industrial Supervisor

Dr. D. Snell
Cogent Power Ltd.

Declaration

This work has not previously been accepted in substance for any degree and is not being concurrently submitted in candidature for any degree.

Signed ..... (candidate)

Date 26th October 2007.

Statement 1

This thesis is the result of my own investigations, except where otherwise stated. Other sources are acknowledged by footnotes giving explicit references. A bibliography is appended.

Signed .... (candidate)

Date 26th October 2007.

Statement 2

I hereby give consent for my thesis, if accepted, to be available for photocopying and for inter-library loan, and for the title and summary to be made available to outside organisations.

Signed ... (candidate)

Date 26th October 2007

Summary

Fully processed, grain oriented electrical steel possesses a forsterite glass film and a phosphate-based insulation coating on both of its surfaces. The composition, quality and thickness of these layers, in addition to a preceding decarburisation oxide layer, are known to have a significant effect on the properties of the material on which the final product is assessed. This includes physical properties, such as appearance, as well as the magnetic properties upon which the electrical steel is routinely graded.

Due to their importance, methods of rapidly and accurately assessing these surface layers would provide great benefits as the characteristics could be monitored to ensure the optimum processing conditions are achieved. Unfortunately, it has previously been found that the complexity of the layers has made their analysis problematical, particularly in terms of accuracy and the time required for testing.

A number of experimental techniques have been investigated to establish their potential for the analysis of the aforementioned surface layers, including Fourier Transform Infrared (FTIR), Electrochemical Potential (ECP), X-ray Photoelectron Spectroscopy (XPS) and Sputtered Neutral Mass Spectrometry (SNMS). Further methods were also used to determine characteristics of the coated material such as magnetostriction and magnetic loss, which provided an insight into the stressing capability of the material. As a result of these investigations:

- Combining a number of techniques resulted in a correlation between ECP profiles and the composition and / or morphology of the decarburisation oxide layer.
- A link has been established between the transmittance levels of the FTIR spectra and the thickness of the forsterite glass film layer.
- FTIR absorption bands have been linked to the constituents of the insulation coating.

Further to the study into the feasibility of these methods, a number of the techniques were used to analyse material during the development of an alternative, chrome-free insulation coating, which has subsequently been adopted as the standard production coating for the grain oriented electrical steel produced at Orb Works.

Acknowledgements

I would like to show my appreciation and gratitude for Dr. D. Snell of the Development and Market Research department at Orb Works for his continued assistance and encouragement throughout the duration of this course.

I would like to thank my academic supervisor, Professor V. Randle, for the guidance she has given me, and also Mr. Bryan Jones and Mr. Byron Tucker (Corus) for their generous support.

I would also like to show my appreciation to many members of both the Technical and DMR (Development and Market Research) departments at Orb Works, employees of ECM^2 and Swinden Technology Centre, and also the staff and students with which I have been involved at University of Wales, Swansea.
Particular thanks must go to Ms. P. Cummings, Mr. A. Green, Ms. D. Hammond, Mr. R. Ireson, Mr. K. Jenkins, Mr. J. McGettrick, Mr. A. Nolan, Mr. G. Thomas and Mr. K. Tinkham.

The author would like to thank the sponsoring company, Cogent Power Ltd., for the excellent facilities afforded to me.
Acknowledgements also go to Corus and the Engineering and Physical Sciences Research Council (EPSRC) who provide the funding for the Engineering Doctorate course.

Table of Contents

Chapter 4 Fourier Transform Infrared (FTIR) Analysis of the Decarburisation Oxide Layer

Chapter 5 Electrochemical Potential (ECP) Analysis of the Decarburisation Oxide Layer

Chapter 7 Evaluation of Forsterite Glass Film Using FTIR

Chapter 8 Evaluation of Final Insulation Coating Using FTIR

Chapter 9 Development of a New Chrome-Free Coating

Chapter 10 In-Depth Analysis of Two Alternative Chrome-Free Coatings

Chapter 11 Conclusions and Future Work

Chapter One

Review of Electrical Steels

1.1 Introduction

Electrical steels can be described as a highly specialised, magnetically soft material i.e. they can be magnetised easily but lose this magnetism as soon as the magnetising force is removed and they are subjected to any small demagnetising influence (coercive force). Laminations of electrical steel are punched from the strip and used in the construction of motors, generators and transformers.

The structure of electrical steel at room temperature is body centred cubic (unit cell with atoms at each corner and one in the centre of the cube). Regions of crystal lattice extend to form grains that vary in size, but can extend up to the order of a few of centimetres. The grains are sub-divided into domains based on their electron spins, as this acts to minimise the external field, thus minimising the stored energy in the steel. This causes a high degree of magnetisation within each domain, but no net magnetisation overall.

When the steel is exposed to an applied external field, as in its final application, the domains containing the spins that are aligned in the same direction as the field will preferentially increase in size due to movement of the domain wall. This will cause the magnetism to increase. At very small fields, this occurs reversibly, where the domain walls will move back to their original position when the field is removed. However, as the applied field is increased further, it will cause the domain walls to move away from the sites at which they were pinned. Eventually, a condition of

magnetic saturation will be reached, where all of the possible domain wall movement has occurred, and the field has rotated any grains that were not mutually aligned when they were in their initial state.

Electrical steels require domains that can move unhindered when they are magnetised. Therefore every effort is made to minimise the number of unwanted inclusions present in the steel by improving the purity of the steel, reducing the levels of carbon, nitrogen, sulphur and titanium in particular.

Grain boundaries also hinder the domain movement, meaning that larger grains are generally better for electrical steels. However, an optimal size exists where further grain growth is detrimental to the magnetic properties of the steel. This is due to the wider domain spacing that occurs in large grains. In their final application, the domain walls will be required to move a greater distance, and therefore at a higher velocity, as this domain wall spacing increases and this results in higher magnetic losses.

The main difference between electrical steel and conventional carbon steel is the addition of silicon. The discovery that silicon improved the magnetic performance of electrical steel was in the 1900's by Barrett, Brown and Hadfield [1, 2]. This improvement occurs due to the silicon causing the resistivity of the steel to increase. The variation of resistivity within Fe-Si alloys has previously been studied, and can be seen in Figure 1.1 [3]. The increased resistivity decreases the eddy currents that can flow in the core, which in turn decreases the overall losses. However, there is a limit to the amount of silicon that may be used (commercially ~ 3.4%) as it also decreases

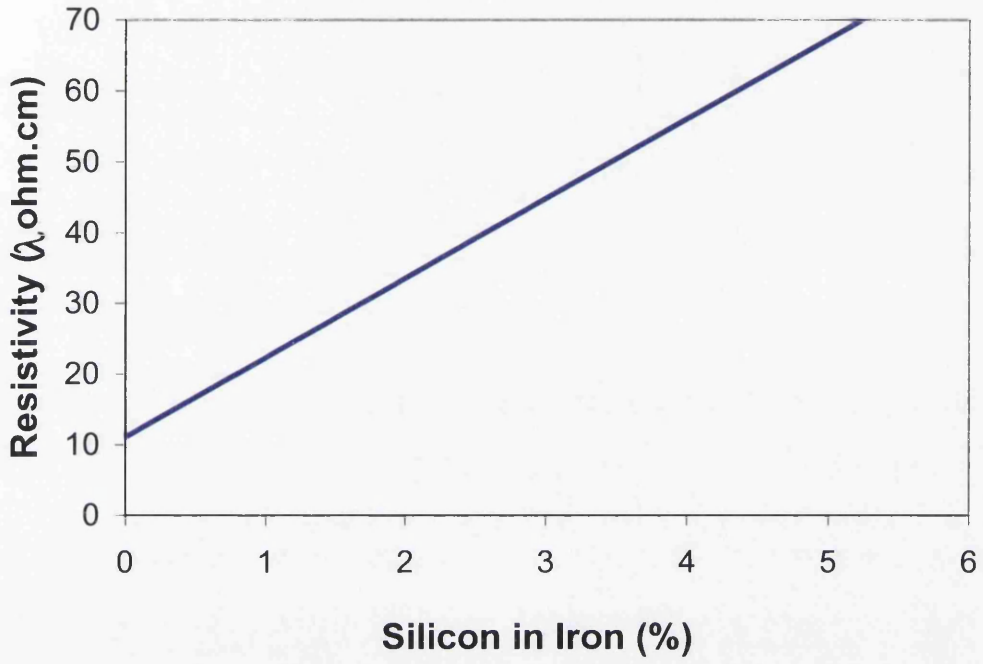

Figure 1.1: Diagram showing the effect that silicon content has on the resistivity of iron [3]

the saturation magnetisation and permeability of the material, as well as making it more brittle and difficult to roll.

The steel is used in the form of punched or cut laminations, which are assembled to form the cores that carry the magnetic flux in electrical machines. The use of the steel in lamination form acts to further reduce the flow of eddy currents within the core, which again reduces the power losses of the core. Electrical steel can be found in almost every form of machinery from large power transformers to small components in an electric shaver.

The material processed at Orb Works site of Cogent Power Ltd., where the work described in this thesis took place, can be classified as being either grain oriented material or non-oriented material. These are described in greater detail below.

1.1.1 Non-Oriented Electrical Steel.

Non-oriented electrical steel contains a lower percentage of silicon than is found in grain-oriented steel. It has grains that are in a random arrangement and hence the strip can be magnetised easily in all directions (magnetically isotropic). This material is generally used for applications where low cost takes priority over efficiency. This category can be split further into (a) fully finished and (b) semi-finished material.

(a) Non-Oriented, Fully Finished Electrical Steel.

This is used for small generators and medium sized electric motors. As the name suggests, the strip is sold in a fully processed condition. The motor manufacturers themselves, or the intermediate 'stampers', punch the material into the laminations required, and the appropriate

magnetic properties are achieved without further annealing of the sheets.

(b) Non-Oriented, Semi-Finished Electrical Steel.

This material is used in the construction of small and fractional horsepower motors. Unlike the fully-finished material, described above, it does not receive a final anneal before being dispatched. This anneal is instead carried out by the motor manufacturers or stampers themselves. This is vital to achieve the desired magnetic properties.

1.1.2 Grain Oriented Electrical Steel

The work associated with this thesis has been focussed exclusively on grain oriented material.

This product is used in the construction of power generators and distribution transformers used by the national grid. The material used for these applications must be of a very high grade as it is necessary for these machines to be very efficient and long lasting due to their cost [4].

Large grains are formed in this material due to the way in which it is processed. These grains are oriented to provide preferential magnetic properties along the rolling direction of the strip i.e. the material is magnetically anisotropic.

The idea of grain-oriented steel arose due to the discovery that certain chemistries and processing conditions could be used to produce material with highly directional properties. This discovery was patented in 1934 by Dr. Norman P Goss [5] who gives his name to the "Goss" [001](110) orientation, also known as the cube on edge (COE) texture. It denotes a texture with a [001] orientation close to the rolling direction and

(110) planes close to the sheet plane, shown in Figure 1.2. This is the arrangement of the crystalline structure of the iron that is highly desirable in electrical steels.

The orientation of the grains causes the material to show magnetic anisotropy due to the fact that there is an easy direction of magnetization along the edges of the cubes belonging to the iron crystals. This arrangement causes the material to be easily magnetised in the rolling direction, but magnetisation in any other directions proves very difficult. For this reason it is useful for applications that require a preferential magnetizing direction, for example a transformer core as shown in Figure 1.3.

Grain-oriented electrical steels can be split further into two separate categories. These are conventional grain oriented (CGO) material and high permeability (Hi-B) material. The Hi-B material was developed by Nippon Steel in 1966 and has a higher degree of orientation and a larger grain size [6] than CGO material. There are variations in the ways in which the two types of grain oriented steel are processed (discussed in Section 1.2), resulting in Hi-B having a superior grain orientation. The consequence of this is that Hi-B material exhibits lower hysteresis losses (see Section 1.5) than CGO material.

1.2 Process Route

The various steps involved in the manufacture of the two types of grain-oriented steels [7] are shown in Figure 1.4.

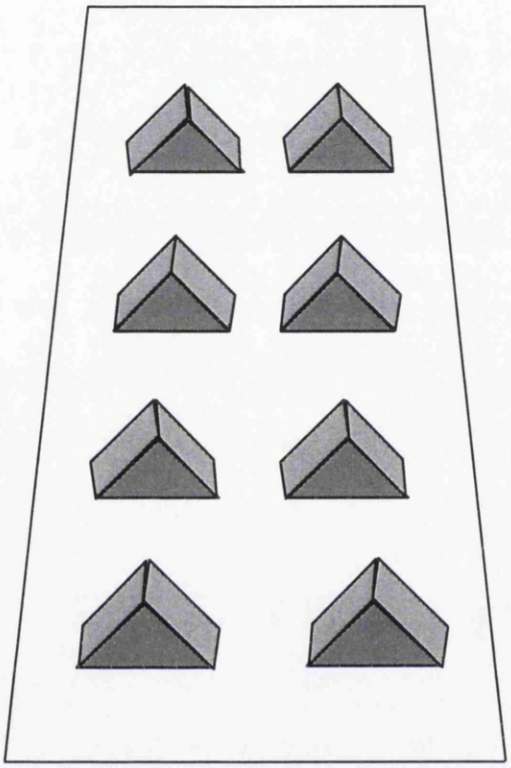

Figure 1.2: Diagram showing the Goss orientation of grains in grain oriented steel.

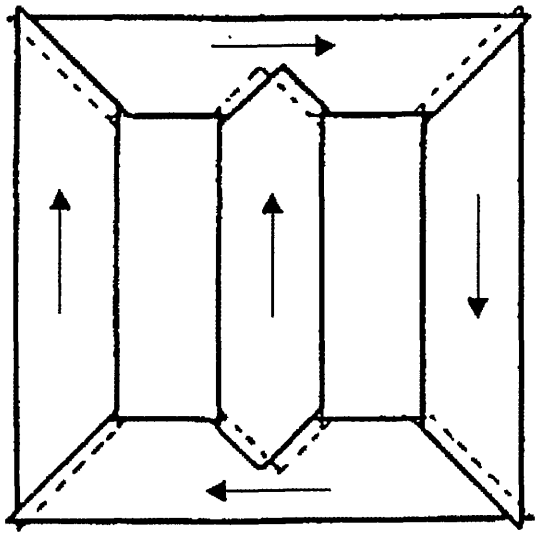

Figure 1.3: A transformer core showing the rolling direction of the laminations.

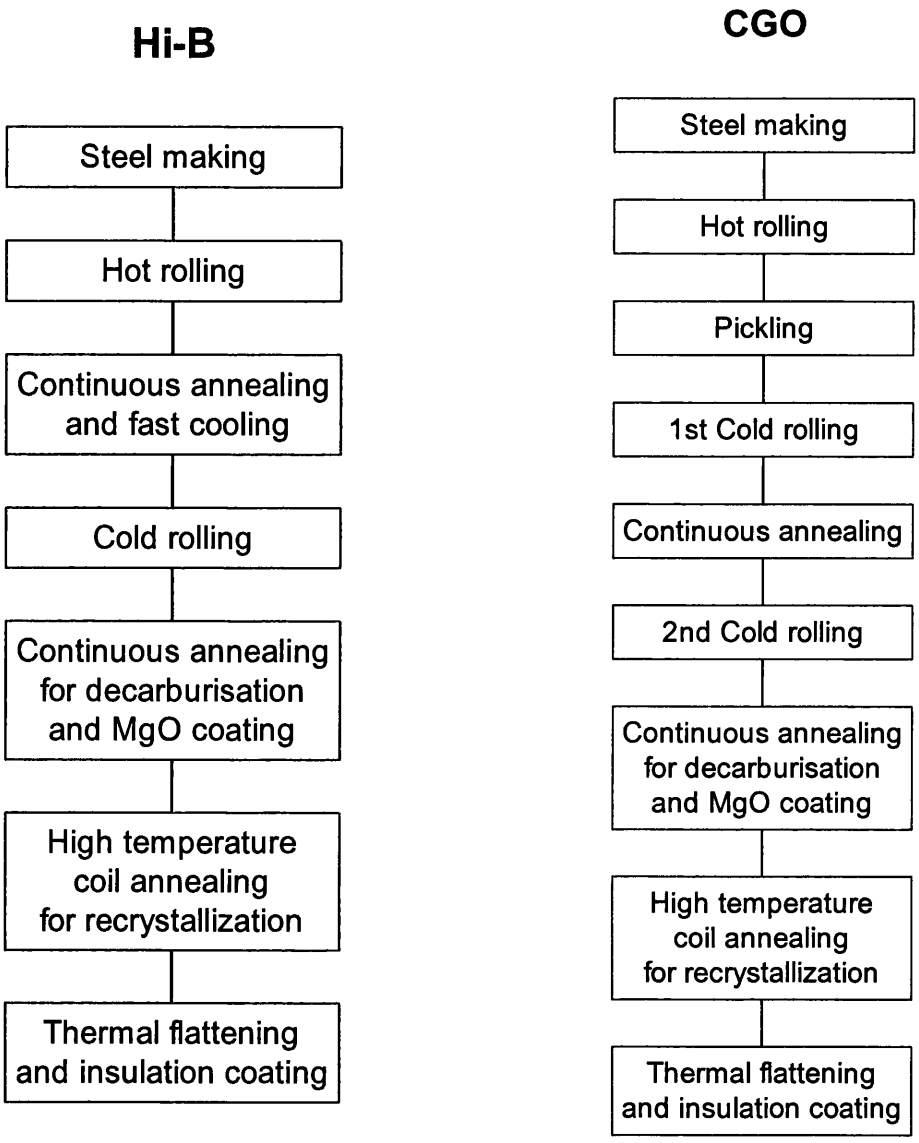

Figure 1.4: Diagram showing the process routes involved in CGO and Hi-B production.

It can be seen that the processes are very similar. The main differences are that the CGO does not undergo the continuous annealing and fast cooling stage prior to cold rolling, and that the CGO route involves a two stage cold rolling process, either side of a continuous anneal.

Aluminium nitride (AlN) is also introduced into the Hi-B material at the steel making stage to act as a grain growth inhibitor. The restriction in the grain growth caused by the AlN addition increases the amount of stored energy. This energy is then released when the inhibitor is removed during the high temperature annealing stage, resulting in the growth of larger grains (i.e. it is beneficial to minimise the grain size in every stage up to the high temperature annealing stage).

1.2.1 Feedstock

The processes up to and including hot rolling are carried out on the site of the steel making itself. All of the remaining steps are carried out at electrical steel plants, such as Orb Works.

When the steel feedstock arrives at Orb Works, it is in the form of coils of approximately 20 tonnes in weight, and with a strip width of ~ 1050mm. At this stage, the thickness of the steel is ~2.1mm and the orientation within the material is generally random. It contains approximately 3.15% silicon, as well as impurities such as carbon, oxygen, nitrogen, manganese and sulphur.

An in depth look at each of the stages of the production process is given in the following sections.

1.2.2 Anneal and Pickle Line

This process is carried out to remove the scale from the hot band and generate a surface at a standard that will facilitate cold rolling. The annealing also has the following effects on the material:

- To obtain a fine dispersion of the grain growth inhibitor (AlN).
- To obtain the correct amount of AlN precipitation.
- To cause the martensite and / or bainite phases to be precipitated.
- To develop equiaxed crystals at the surface layer
- To secure carbon and nitrogen in solution

The material first passes through a furnace that has a carefully controlled atmosphere. The gas used in the furnace is 3HN gas (3% hydrogen in nitrogen) as this prevents oxidisation. The furnace is heated to a temperature of ~1000-1100°C, using four gas-fired zones and six electrically heated zones. Upon leaving the annealing furnace, the strip must be cooled to a temperature of less than 100°C for a subsequent shot-blasting section. However, the strip should not be allowed to cool too much as this will result in it becoming too brittle, which could result in a snap. The required cooling is achieved using a number of water sprays and cooling fans.

It should be noted that CGO material very rarely undergoes this annealing treatment (unless it is of a very high grade), as the benefits that can be gained do not justify the cost of this operation.

Prior to pickling, the strip passes through the wheelabrator section where blasting it with steel shot breaks down the surface scale. The purpose of this is to assist in the pickling process, in which it passes through two pickling tanks where the strip is sprayed with hydrochloric acid. Further cleaning of the strip using water and rotating

brushes follows the pickling, and ensures that all the acid has been removed. Before the strip is recoiled, oil is applied to the surface. This acts to prevent rusting of the strip prior to rolling and provides the required standard of surface quality for rolling.

1.2.3 Cold Reduction

The mills sited at Orb Works are four high cold reduction reversing mills.

This process is used to reduce the thickness of the strip to a precise, specified gauge. The range of material produced at Orb usually has a final gauge of 0.23, 0.27, 0.30 or 0.35 millimetres.

Other advantages of cold rolling are that it increases the stored energy of the material, creating a homogeneous structure, and forms nuclei of secondary recrystallization with improved orientation of the crystals.

1.2.4 Decarburising Anneal (and MgO Coating)

This is a continuous process that is carried out in a furnace of approximately 140 metres in length. At Orb, a combination of gas and electrical heaters are used to maintain the furnace at the correct temperature. Before the strip passes into the furnace, it passes through a natural gas fired burn-off section (~6m) to remove any milling oil and other dirt and debris from the surface. The main furnace section is maintained at a temperature of ~850°C, and the atmosphere is carefully controlled to be 75% hydrogen / 25% nitrogen. The gas is passed through a saturator before passing into the furnace with the aim of controlling the dew-point of the atmosphere. This is the temperature to which a gas must be cooled so that it will be saturated with respect to water vapour. Any cooling below this temperature will result in the formation of water vapour on the cooled surface.

The strip speed on the decarburisation line is ~50-55 m/min, meaning that this process causes the strip to be at elevated temperatures in the furnace for approximately 150 seconds (including the time in the burn-off oven).

A diagram of this line can be seen in Figure 1.5 [8].

This process serves the following three purposes:

- Reduces the level of carbon in the steel from approximately 0.05% to below ~ 0.0025%. This figure depends slightly on the material being processed.
- Promotes primary recrystallization, in which old grains disappear and new grains grow.
- Causes the formation of a surface oxide layer. This layer is very important in the context of this project, as it is directly related to the formation of a forsterite glass film at a later stage of processing.

Coating of the strip with a magnesium oxide (MgO) slurry [9] occurs at the end of the decarburising line, prior to the strip being coiled. This coating is required to prevent adjacent laps of the coil from sticking together in the High Temperature Coil Anneal (HTCA) furnace, which would cause defects along the strip.

Coating the steel with MgO also enables the amount of nitrogen absorbed in the steel during the high temperature anneal stage to be controlled, and also reduces the sulphur content.

The presence of the MgO powder is also influential in secondary recrystallization.

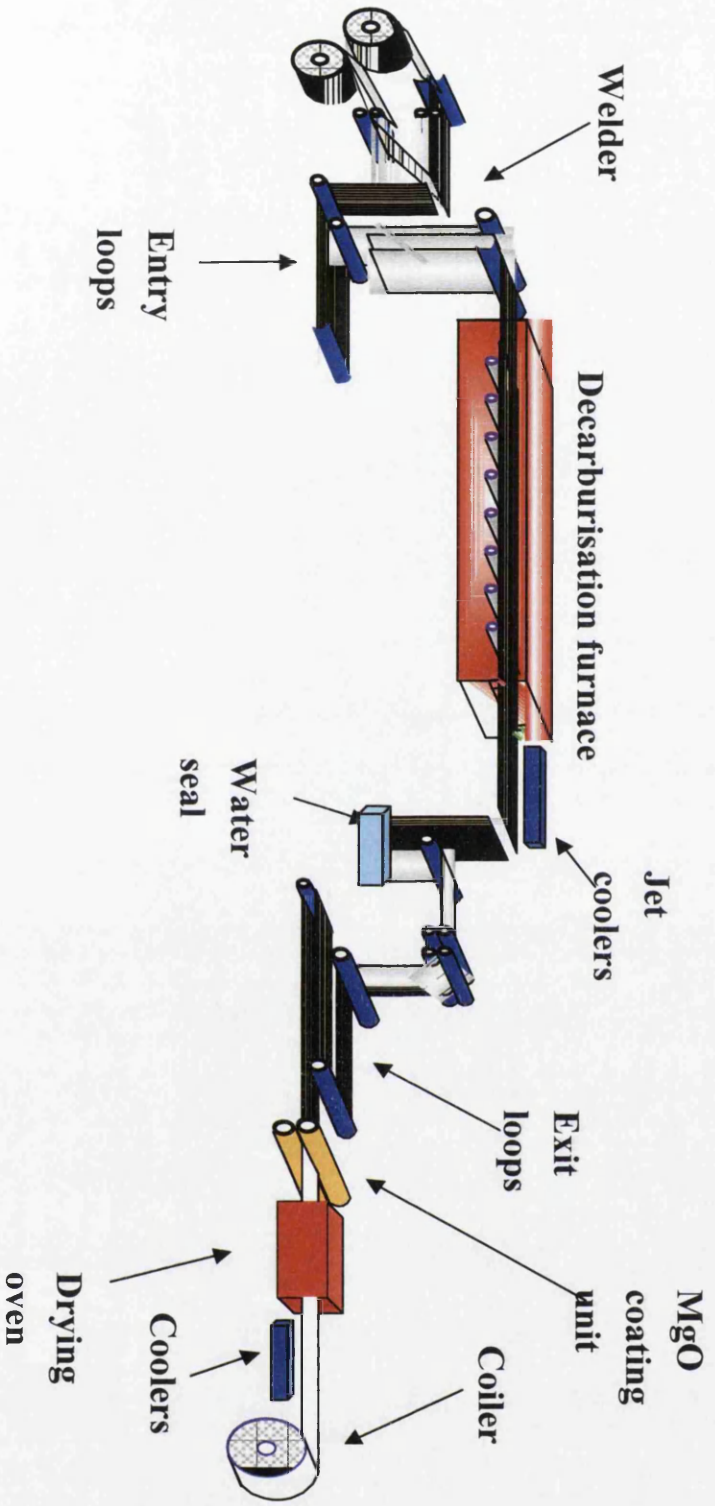

Figure 1.5: Schematic diagram of a decarburisation line [8].

The MgO is applied to the strip in the form of a slurry. This is formed by mixing a magnesia powder with water, and should contain ~13% MgO in suspension. Grooved rubber rolls are used on both the top and bottom surfaces to impart a coating weight of ~4.5gm^{-2} onto either side of the strip. Once coated, the strip passes through a furnace which is heated to approximately 650°C, which increases the temperature of the steel to ~140°C. This removes any excess water, leaving a white powder coating adhered to the surface.

As time passes within the mixing chamber, magnesium hydroxide will slowly be formed as the magnesium oxide powder hydrates. This magnesium hydroxide is useful as it stabilises the aqueous slurry of MgO and also promotes the covering activity. It is possible to use magnesium hydroxide alone, although it may decompose to produce a large amount of water. This would subsequently result in a reduction of the magnetic quality of the coated steel, as the water carried in the form of the hydrate will remain in this coating even after the drying process that occurs after coating.

The amount of hydration achieved is one of the variables that can affect the quality of the glass film that is formed at a later stage [10], as the forsterite grains are affected by the amount of water carried into the coil in the form of the hydrate. The amount of water carried into the coil in this way is determined by:

- Type of magnesia used
- Temperature of the slurry
- Time the MgO is held as a slurry
- The amount of magnesia applied
- The drying process
- Particle size distribution

Two or more different sources of magnesia are often mixed together to obtain the optimum properties.

It is undesirable that the magnesia should hydrate above approximately 3%. However, the amount of magnesium hydroxide should always exceed 1% by weight as it creates an electric repulsive force. This acts to repel the suspended MgO particles from each other.

To ensure that the correct amount of hydration is achieved, it is necessary to maintain the slurry at a temperature of between 10 and 20°C.

Magnesia powder is always provided with a statement of the range in particle sizes that is present in the batch. It is believed that the particle size distribution, and the shape of these particles, may also have an effect on the glass film that is formed. At present, current working practices state that 70% weight or more of the particles should be of a size of 0.5 microns or less.

It is desirable that there are no impurities in the MgO (for example chlorine and sulphur). However, the magnesia is often doped with various other elements to affect its properties. These doping elements, and their effects are listed below [11].

- Aluminium compounds (preferably 0.1-1%) may be used to provide a similar electric repulsive effect to that of the magnesium hydroxide. This is added in the form of aluminium hydroxide or aluminium nitride. However, the strip sometimes absorbs some of the nitrogen from the AlN compound, which obstructs secondary recrystallization. This results in fine grains, which results in poor magnetic quality of the final product.
- Magnesium nitrate may be used to stabilize the magnesia slurry. However, it is a necessity that the separator does not contain magnesium in any other

forms such as magnesium chloride or magnesium sulphate as they will have a detrimental effect if they are absorbed into the steel.

- Boron, in quantities of less than 2.5%, is another element that helps to stabilize the solution. It also enhances the coating property and improves the magnetic properties of the strip. Another advantage of adding boron is that it can hinder the absorption of nitrogen into the strip.
- Sodium (in the form of a sulphide, hydroxide or thiosulphate) may be used in amounts between 0.005-0.2%. This decreases the core loss of the strip by greatly increasing the tension characteristics of the final coating on the strip. This effect occurs due to the sodium causing the particles of MgO to combine with each other. However, the amount of sodium added must be limited to 0.2%. If the sodium exceeds this amount it will result in a reduction of the melting point of the 'glass' material formed in the HTCA. This will prevent the material from forming a forsterite glass film on the surface of the strip.
- The presence of ~5% TiO_2 will stabilize the solution and enhance the magnetic properties of the strip.
- Lithium (0.02-0.7%) will enhance the magnetic flux density of the material.

In addition to these elements, the way in which the slurry is prepared may also affect the coating properties. For example, when preparing the aqueous slurry, a stirring impellor (rotating shaft and blades) is used. Past experience has shown that the quality of the coating varies according to the stirring speed.

1.2.5 High Temperature Coil Anneal (HTCA)

During this process, the coils of MgO coated steel are placed in a furnace with their bore vertical and heated in a hydrogen atmosphere (Figure 1.6 [8]).

The HTCA furnace has a base made from refractory brick. This is surrounded by sand, which acts to provide a gas seal between the base and the inner cover that is placed over the coils. Each of these inner covers contains two coils, with the upper coil supported by a stalk and a stainless steel 'mushroom'. Four of these covers are contained within the shell of one heating furnace, as shown in Figure 1.7.

Heating elements are located both within this shell and also within the base. Both water and sand seals are used to prevent gas or heat escaping from this furnace.

Current practice states that all parts of the coil should reach a temperature of 1180-1200°C, and soak at this temperature for at least four hours. However, due to the size of the coils, the outer laps attain this temperature much more quickly than the inner windings. It may take up to 30 hours for the whole coil to attain the correct temperature, and a further 24 hours for it to cool.

Under the correct conditions, selective secondary recrystallization will occur. The MnS in the steel acts as a grain growth inhibitor, which causes the grains with the desired Goss orientation to grow preferentially over others. Once this has occurred, the MgO acts to remove the remaining sulphur in the steel, ensuring that any sulphide inclusions do not remain, as these could inhibit movement of the domain walls.

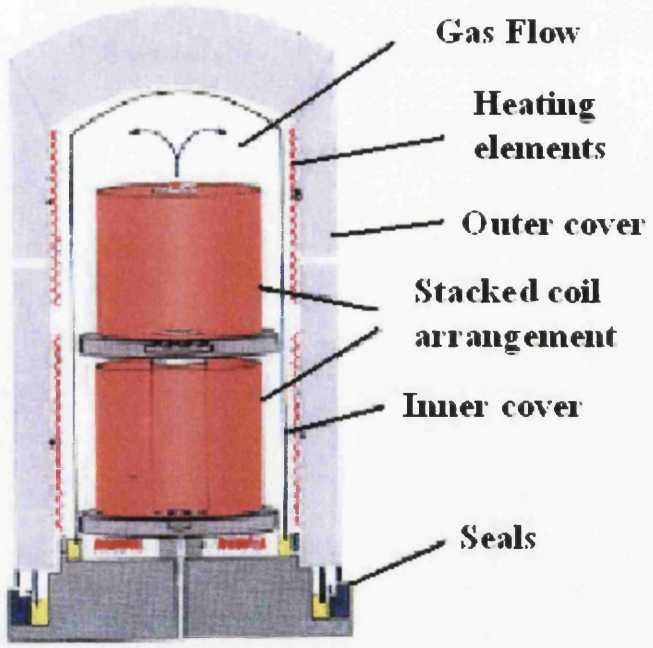

Figure 1.6: Schematic diagram of H.T.C.A furnace [8].

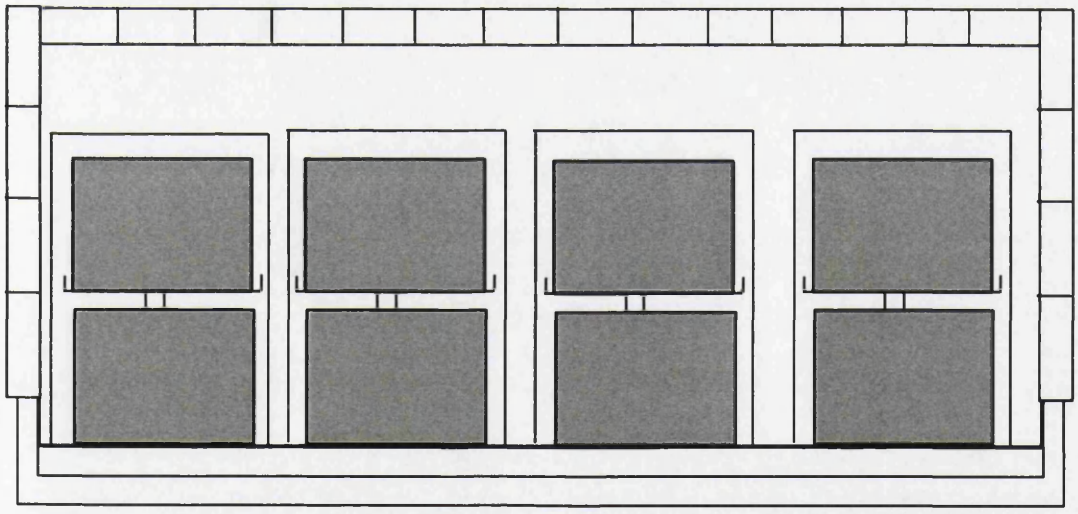

Figure 1.7: Coils stacked in High Temperature Coil Anneal (HTCA) furnace.

It is also the stage at which the forsterite "glass" film is formed [12, 13]. For forsterite to be formed successfully, the temperature must exceed 1003 to 1017°C, depending on the magnesia that is used [14].

1.2.6 Thermal Flattening and Final Coating

This is a continuous process, at the end of which the material will be at a stage where it is suitable for customer use (following the necessary slitting / punching processes). A schematic diagram of this processing line is shown in Figure 1.8 [8].

Before being coated, the strip passes through a cleaning section to remove any excess magnesia that remains from the high temperature annealing process and to prepare the surface. The strip is firstly brushed and washed with water, before passing into a pickling bath containing a dilute sulphuric acid (H_2SO_4). As well as removing any remaining magnesia, this acid provides a light etch of the forsterite glass film, which helps the final coating to key into it. The strip is then rewashed to remove any trace of pickling acid, firstly with cold water and then in a hot water (90-95°C) rinse tank. It is then dried with hot air blowers, leaving it ready for the coating process. It is important to ensure that the strip is dried thoroughly after this process to prevent any rust developing on the surface during the time it is held within the storage loops. Water on the strip may also have an effect on the tracking of the strip if it is transferred onto the rolls contained within the loop storage section.

The coating (covered in more detail in Section 1.3.3.) primarily contains a phosphate solution, colloidal silica and water. These constituents are mixed on the site of the coating line.

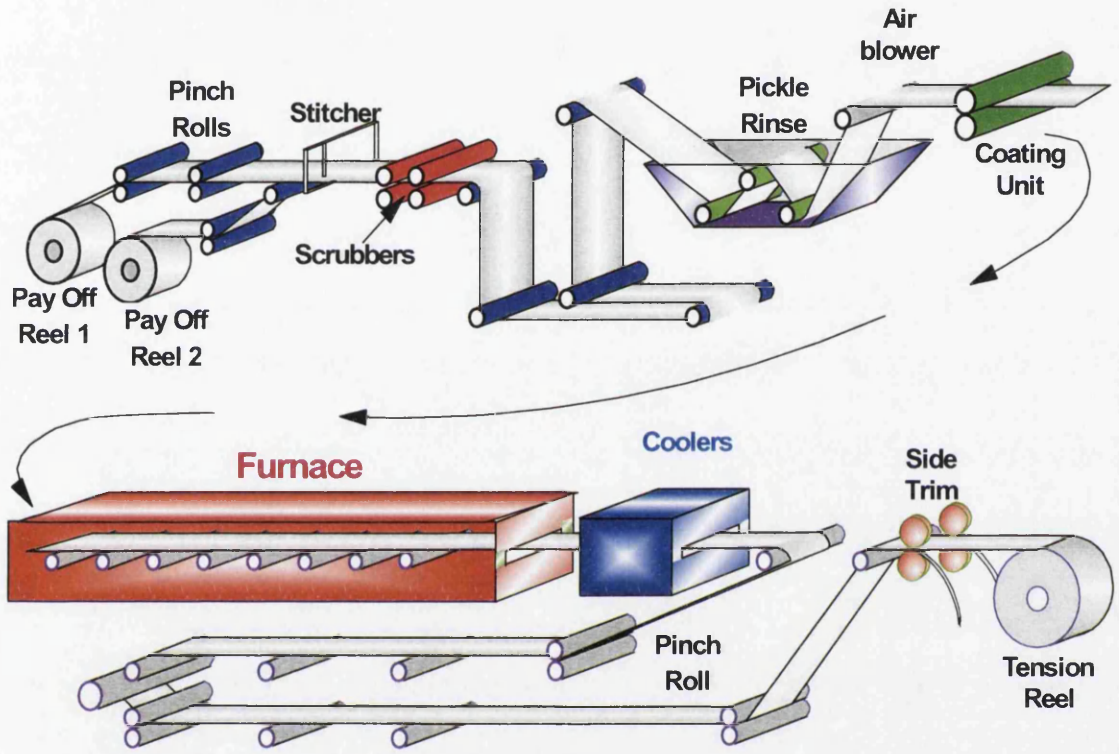

Figure 1.8: Schematic diagram of the thermal flattening and final coating line [8].

Following the application of the insulation coating the strip passes through a pre-heat furnace to ensure that it is fully cured before the first roll of the main furnace is reached. This is ensured by heating the strip in a furnace with a temperature of ~650°C.

The main thermal flattening furnace has an atmosphere of ~3% hydrogen in nitrogen and raises the temperature of the strip to approximately 850°C for a duration of 25-30 seconds. The atmosphere is purely to ensure that a clean processing environment is maintained and helps to ensure a good final appearance of the steel. The strip passes through a series of flattening rolls that penetrate the natural pass line of the strip. It is then cooled slowly to temperature of ~675°C, before undergoing a period of faster cooling. All that then remains is for the strip to pass through a section where its appearance is inspected before being re-coiled, ready for slitting and packing procedures.

1.3 Surface Layers

1.3.1 Decarburisation Oxide Layer

As described in Section 1.2.4, the strip passes through a furnace with an atmosphere of 75%H / 25%N and at a temperature of 850°C. These conditions promote the formation of an oxide layer on the surface of the steel.

A layer of amorphous silica will form adjacent to the surface of the steel. After a certain length of time in the decarburisation furnace, a layer of fayalite will be formed on top of this silica. This will occur to a greater extent if the dew point is raised to above its optimal level. Therefore the oxide layer will be more silicon-rich if the dew

point of the furnace is lowered. The graph shown in Figure 1.9 [14] shows the effect that the dew-point (and also temperature) has on the oxide layer that is formed.

There is also a subscale presence of crystalline silica due to diffusive effects, which penetrates into the steel strip itself. Figure 1.10 shows a schematic diagram of the layers that are present in the oxide scale formed on the material produced at Orb Works.

A presence of iron oxides may also be found in this oxide layer. It is believed that optimum conditions should be those at which silica alone is formed because any fayalite formed will decompose into metallic iron and silica at later stages of processing. This conductive metallic iron will then reduce the insulation, as it will become embedded in the glass film.

As well as the dew point, the quality of this layer can also be affected by other factors, such as the atmosphere of the furnace and by the speed at which the strip passes along the line.

The oxide layer formed during decarburisation is the first of the three layers of interest for this thesis, as its composition has a direct effect on the formation of the insulating glass film layer.

1.3.2 Forsterite Glass Film

The 'glass' film is the first of the insulating layers to appear on the steel substrate. The name given to this layer is misleading, as it is not actually a glass at all; it is in fact of a crystalline nature and does not contain any glassy phases. It consists of a

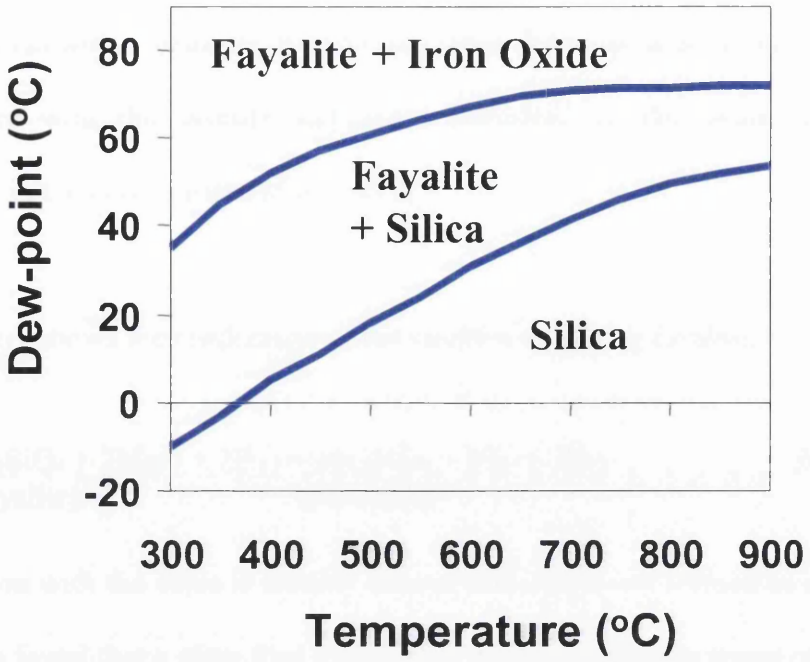

Figure 1.9: Effect of dew-point and temperature on the formation of the oxide layer [14].

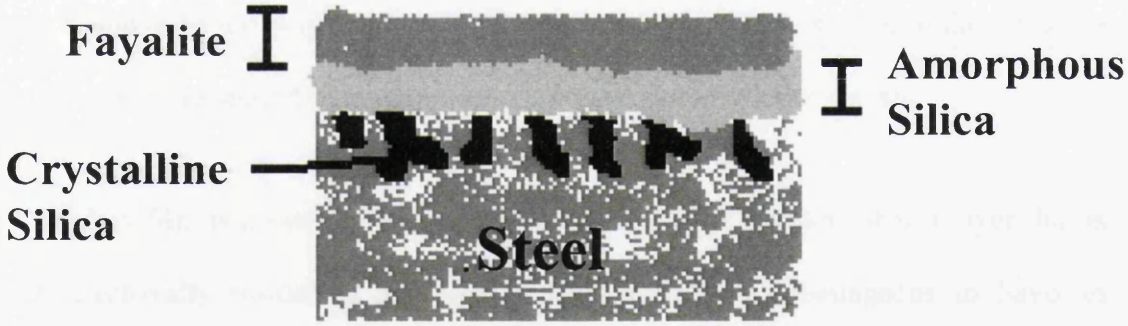

Figure 1.10: The structure of the oxide layer formed during decarburisation

compound known as forsterite. It is formed when the magnesium oxide reacts at high temperature with the fayalite and silica contained in the oxide layer, formed previously in the decarburisation furnace.

Equation 1.1 shows the mechanism of the reaction involving fayalite.

$$\underset{\text{(fayalite)}}{Fe_2SiO_4} + 2MgO + 2H_2 \rightarrow \underset{\text{(forsterite)}}{Mg_2SiO_4} + 2Fe + 2H_2O \qquad \textbf{Equation 1.1}$$

The reaction with the silica is similar, except that iron is not formed as a by-product. It has been found that a glass film will exhibit good properties in terms of appearance, bending adhesion, uniformity and insulation if the grains of forsterite are smaller than 0.7 microns [15]. The size of the forsterite grains is proportional to the amount of water carried into the coil. This is affected by the amount of H_2O and / or CaO present in the magnesia coating. The additives may cause the effect on their own, but the effect is greater if they are both present. To ensure the forsterite grains are of the required size, the amount of water should be less than 1.2 g/m^2 (both sides). CaO has been found to be the only addition to the magnesia that affects the size of the forsterite grains, and there should be no more than 0.08g/m^2 present (both sides).

The glass film is a very important element of the final product. It is a layer that is both electrically insulating and stress inducing. It is advantageous to have an electrically insulating layer on the surface of the steel as it prevents the flow of eddy currents between adjacent laminations in the final application. The coefficient of thermal expansion of the glass film is different to that of the steel itself. Therefore as they cool, the layer becomes stress inducing due the tensile stress in the steel, coupled with the compressive stress in the forsterite. This reduces the amount of

magnetostriction that occurs, which is the main source of transformer noise. It is caused by the expansion and contraction of the steel during the magnetisation process. This magnetostriction causes energy to be lost from the system, and therefore the stress induced by the forsterite results in a reduction in the final power loss data of the material. It also acts to modify the crystal orientation so that is in greater alignment with the desired Goss texture [14].

As well as these properties, a good glass film should have other desirable characteristics [16]. It is required to be heat resistant and non-oxidising in reducing or inert gases at 1000°C and above. It should obviously not modify the orientation of the grains to the detriment of the steel.

Although the glass film provides many benefits it is important that the forsterite does not become too thick, as this would cause the stacking factor of the core it is used in to decrease, as a smaller percentage of the core would be steel. This would have an unfavourable effect and decrease the efficiency of the core.

Despite the importance of the glass film, the quality of this layer is not routinely monitored. It is only examined to discover the cause of defects that arise in the film. When the glass film is of good quality, it is a dull mid-grey in appearance and is uniform across the width of the strip. It is also found to have good adherence to the strip. However, defects in this surface layer may sometimes occur, affecting the appearance and / or the performance of the steel [17].

1.3.3 Final Insulation Coating

A further coating is applied to the strip on the final coating and thermal flattening line. It is coated directly on top of the layer of forsterite that has previously been formed in the H.T.C.A.

At present, the coating comprises mainly of colloidal silica, phosphate and water. The composition of the mix has recently been modified to remove all trace of chrome, which was used in the formulation at the time when this project commenced.

Once mixed, the coating passes onto the top surface of the strip and a weir spreader is used prior to the coating roll to ensure that the coating is distributed uniformly across the strip width. The excess coating is collected in a bottom coating tray beneath the strip, where it is applied to the underside of the steel after being picked up by a bottom coating roll. It is the pressure between the strip and these two grooved, rubber coating rolls that is used to carefully control the thickness of the coating, as well as the groove specification (grooves per inch and groove depth).

Previous research, illustrated in Figure 1.11 [18], has shown that the ratio between silica and phosphate in the coating mix considerably affects core loss values associated with the material. Therefore, a mix that does not contain the optimum ratio will result in material being produced that does not reach its full potential in terms of magnetic loss data.

The coating acts to improve the magnetic properties of the steel in two ways.

Firstly, the coating provides an insulating layer between laminations when they are assembled for their final application. This reduces the eddy currents that can flow within the core.

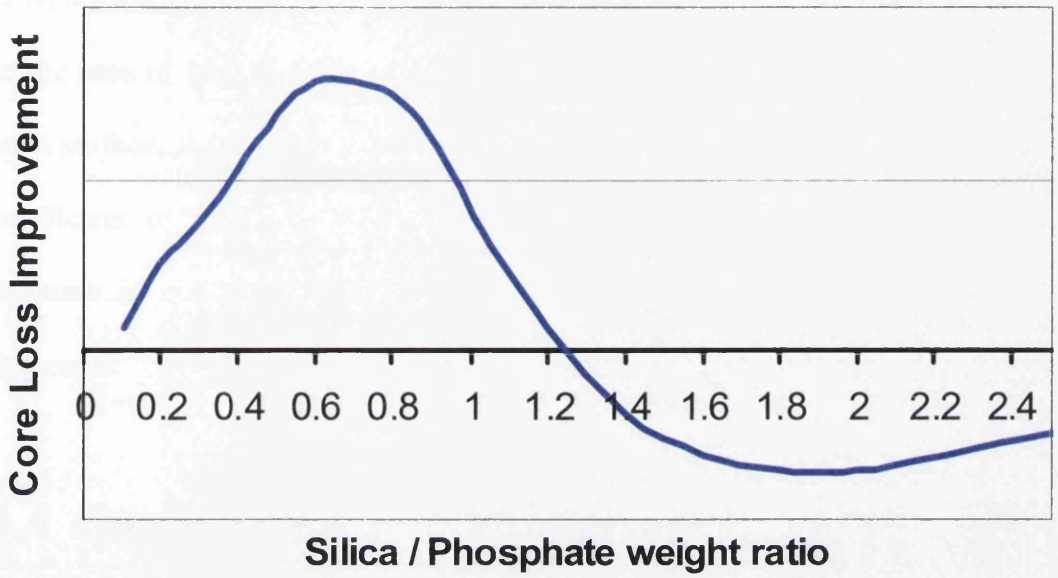

Figure 1.11: Variation in core loss improvement as the silica / phosphate ratio is varied [18].

Secondly, the coating acts to apply a tension to the surface of the steel that reduces the magnetostriction losses that occur during magnetisation. These losses occur due to the rotation of the magnetic domain walls, and are the greatest cause of transformer noise. When the transformer is assembled, compressive stresses are applied to the steel sheets that cause the magnetostriction effects to increase. However, a tension coating, such as those applied to the steel at Orb, minimises this effect, therefore reducing the losses.

In the case of this coating, and the forsterite that has previously been formed on the steel surface, the tension is applied upon cooling. Each of these layers has a lower coefficient of thermal expansion that the steel itself, ensuring that the steel will decrease in size far more that the surface layers as the temperature of the strip decreases.

1.4 Coating Defects

Some of the defects that can occasionally arise in the forsterite glass film are given below:

- Bright spot defects – These vary in size from just visible to having a diameter of up to a few millimetres. They can be seen as an almost circular area of bright, metallic material. They occur on both the top and bottom surfaces, and are more commonly found around the centre of the strip. They sometimes occur in rows in the rolling direction. These bright spots are an undesirable feature as they have the effect of causing the steel to exhibit poor resistivity. It has been found that this type of defect is caused by local oxidation as a result of processing conditions favouring over-oxidation,

- Dark spot defects – These defects appear as almost round dark spots with a diameter of up to approximately 5 millimetres. It has been found that the coating is more readily removed (i.e. it is flakier) away from the defect. This defect is similar to the bright spot defect in that it is also caused by local oxidation.
- Bare edges – As the name suggests, these defects occur at the edges of the steel strip. They are seen as a combination of bright and dark bands / lines. The quality of the coating within these bands varies greatly in terms of coating thickness and adhesion to the strip. The bare edge defects occur on the part of the coil that was hottest in the high temperature anneal phase. This is due to the atmosphere being too wet when the glass film is formed.
- Bright specks / Accretions – These defects can appear randomly across the steel. At first, they appear to be a smaller version of the bright spot defect, but are found to be raised, metallic regions. They occur due to "pick-up" being transferred to the strip during processing on the decarburisation line.
- Powder grit – These small (few mm), raised white spots are found across the width of the strip. However, they usually occur on just one surface. When scraped with a scalpel, they form a powder, which has been analysed to be MgO. Powder grit is caused by the settling of over hydrated MgO accumulating in the coating tray, prior to being transferred to the strip.
- Thin glass – When this defect occurs, the underling grains of the steel can be seen. This defect causes a flaky coating, due to poor adherence, and causes the steel to exhibit poor resistivity. It occurs when the processing conditions of the decarburising line favour under-oxidisation. Upon analysis with a Transmission Electron Microscope (TEM), the grain size of the forsterite was

found to be much larger than is optimal (a few microns compared to the favoured size of ~0.7 microns).

Bare patches and thin film occur mainly on the looser outer laps. This is because the steel is more exposed to the annealing atmosphere and the water vapour concentration is at a minimum. Therefore, to prevent this there must be an adequate amount of water vapour in the annealing atmosphere adjacent to the steel surface. It is only necessary for this water vapour to be present whilst the temperature is below that at which the silica and the MgO react to form forsterite glass film. Once this temperature has been reached, the presence of water vapour will have no effect.

The amount of water in the furnace atmosphere is given by the dew point. This is the temperature at which dew will form on a chilled mirror [19]. A high dew point temperature indicates a high concentration of water vapour in the atmosphere.

Raising the dew point of the annealing atmosphere can be done by:

- Increasing the water vapour concentration in the hydrogen atmosphere
- Allowing magnesia to hydrate further
- Coating the material with a suitable mix of magnesia and magnesium hydroxide

The last two methods are preferable as they affect the area adjacent to the strip.

As well as the water vapour concentration, the temperature of the annealing furnace will also have an effect on the thickness of the glass film that is formed. It is found that once the temperature at which forsterite is formed has been reached, a further increase in temperature will result in a thicker glass film [14].

1.5 Energy Losses

Once the material has been processed, it is tested and subsequently graded. The material is sold against stringent guarantees of its magnetic performance, in terms of both power loss and permeability. Data relating to a whole range of peak induction and frequencies is available for all material produced, although the results at induction levels of Bpk = 1.5 or 1.7 T, 50 or 60 Hz are considered most important.

These loss characteristics are determined by a combination of the glass film layer, a final insulation coating and the magnetic properties of the steel. Power loss is defined as the amount of power that is dissipated during magnetisation. Permeability is related to the size of magnetic field that is required to produce a specified induced magnetisation.

The main forms of power loss in electrical steel are hysteresis loss, eddy current loss and anomalous loss [8]. It can be seen in Figure 1.12 [8] that eddy-current losses and anomalous losses vary with frequency, whereas hysteresis losses are independent of the frequency.

Hysteresis loss is due to the structures within the material, and occurs when energy is dissipated due to the rapid motion of a domain wall. It is essentially the amount of energy required to change the magnetic state of the core to be in phase with the alternating magnetic flux. This may be explained more clearly by using the example of an a.c. transformer.

A flux density (B) is induced in a core when a current is passed through copper wire that is wound around that core. This is due to the magnetic field (H) that is created. Equation 1.2 gives the relationship between the magnetic field and the flux density.

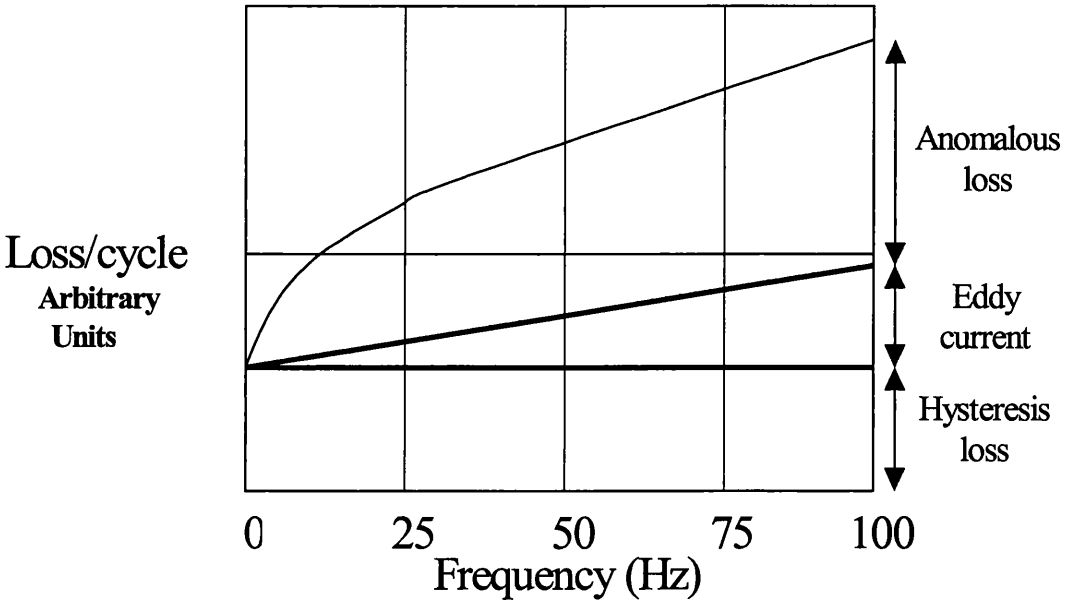

Figure 1.12: Diagram showing the losses that occur in electrical Steels [8].

$$B = \mu_0 (H + M)$$ **Equation 1.2**

Where: B = flux density (T)

μ_0 = permeability of the core (H/m)

H = magnetic field strength (A/m)

M = magnetization (A/m)

If an alternating current is passed through the windings of a transformer core, the magnetic field and flux density vary during one cycle as shown in Figure 1.13. This is known as a B-H or hysteresis loop and the difference between grain oriented and non-oriented material is shown.

The area contained by the loop is proportional to the power loss i.e. it is a measure of the energy lost during one cycle.

Eddy current losses are due to heat energy being dissipated due to the eddy currents that are induced within the core. There is a discrepancy between the magnetic losses that are calculated and those that are measured. This is attributed to anomalous loss and is due to the complex behaviour of the domains during magnetisation.
The energy lost due to eddy currents can be calculated using Equation 1.3, [20].

$$P_E = \eta (p\mathrm{dBf})^2 / 6\rho \quad W/m^3$$ **Equation 1.3**

Where: P_E = eddy current loss

η = loss anomaly factor (due to additional eddy-current losses)

d = sheet thickness

B = peak flux density

F = frequency

ρ = resistivity

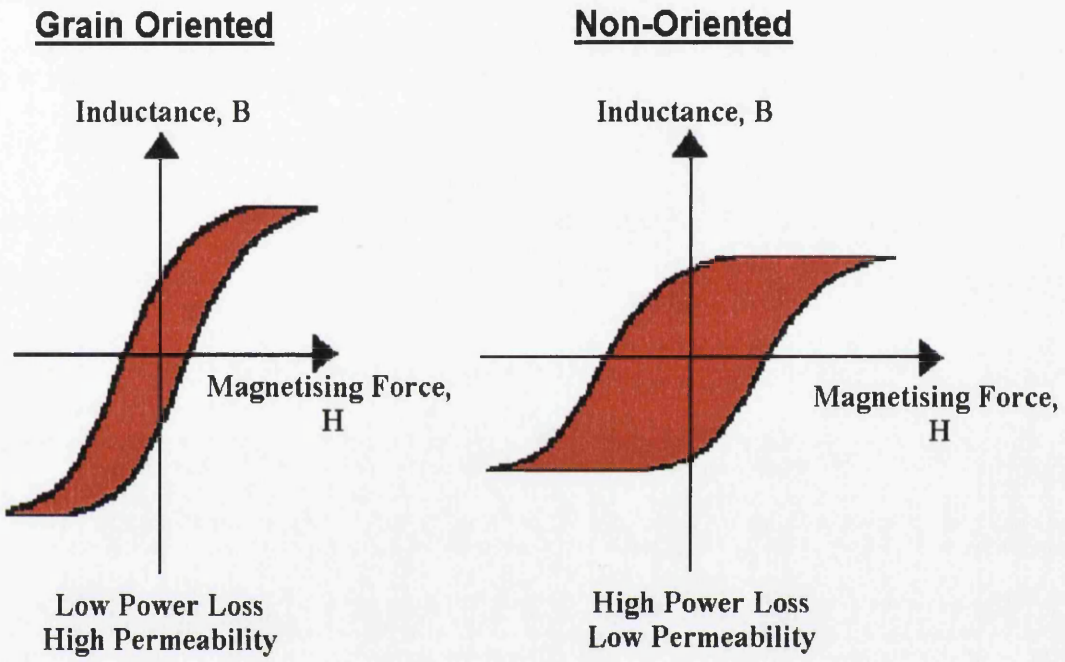

Figure 1.13: Hysteresis (B - H) loops for grain oriented and non-oriented material.

As well as increasing the losses of the material, eddy current losses also create their own field that opposes the field that was originally applied and causes the flux density to decrease progressively towards the centre of the material.

Restricting their flow throughout the core can reduce the eddy current losses. This is the reason that cores are assembled from laminations instead of using solid cores. The effect of assembling n laminations to form a core reduces the eddy current loss by a factor of $1/n^2$ when compared to a solid core [21].

It is also the reason for applying an insulating coating to the surface of the steel.

Chapter Two

Review of Measurement Techniques

2.1 Overview of Current Techniques

There are a number of techniques currently used for the analysis of the surface layers that are present throughout the production process of electrical steels. These are briefly reviewed in the following sections.

2.1.1 Decarburisation Oxide Layer

- **Optical Microscopy**

The oxide layer formed during the decarburisation process is most commonly analysed using an optical microscope. This can provide images such as that shown in Figure 2.1 [22]. It can be seen that the image does not contain a great amount of detail.

Although useful in terms of determining thickness and any unexpected inclusions, this method is time-consuming and does not provide accurate information on the components of the layer.

- **Oxygen / Nitrogen Analyser**

The oxygen content of the decarburisation oxide layer is monitored on a routine basis. Discs of approximately 100mm diameter are punched from the end of each coil and subsequently analysed using the Leco apparatus located on-site within the Chemistry Laboratory. A number of smaller discs of 6mm diameter are then taken from the larger sample, weighed and placed into a carbon crucible. The sample is then heated,

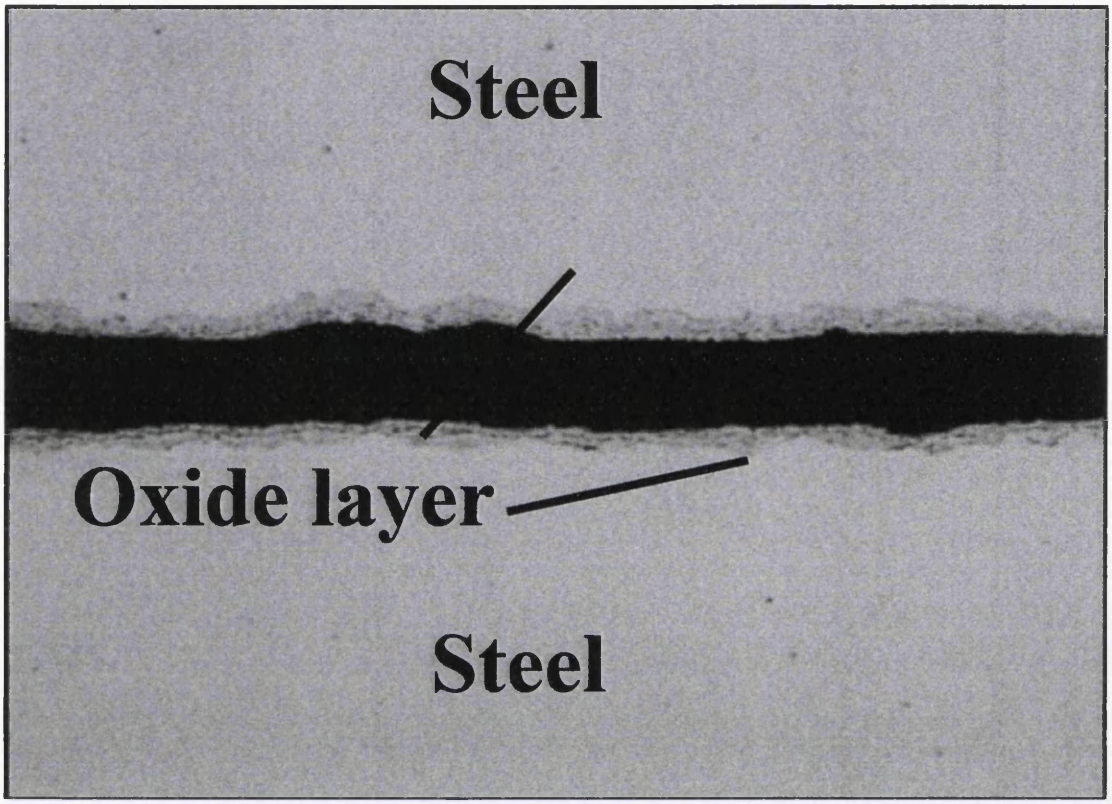

Figure 2.1: An image of the decarburisation oxide layer obtained using an optical microscope (x1000) [22].

under a helium carrier gas, which causes the oxygen within the sample to form carbon dioxide by reacting with the carbon of the crucible. This amount of CO_2 is then analysed by the machine (using infra-red technology) and compared against calibration standards to establish the oxygen content of the sample. Standard operating procedures suggest that the level of Oxygen should remain between approximately 500 and 590 p.p.m. for a sample of 0.30mm gauge, depending on the type of material being analysed. This oxygen level is believed to provide an oxide layer of a thickness that has the potential to produce a good quality forsterite glass film.

This method provides elemental results, and cannot therefore be used to determine the amount of fayalite or silica present. This is due to the presence of silicon and oxygen in both compounds making it impossible to attribute the presence of each element to a specific compound.

- **Iodine / Methanol test**

This technique is used to separate the oxide layer from the steel matrix using an iodine in methanol solution. Once the layer has been removed, the remaining oxides are fused with other compounds to make a glass. This glass is then dissolved in hydrochloric acid to form a solution that can be analysed using Atomic Absorption Spectrophotometry, which is an elemental analysis technique that utilises light absorption to provide details of the composition of a sample. The major disadvantage of this technique is that it is very time consuming.

2.1.2 Forsterite Glass Film

A continuous on-line inspection process is undertaken on the final coating and annealing line. It is a visual inspection by the operators as the defects previously mentioned in Section 1.4 can be easily seen on the strip surface when their extent becomes problematic. A line operator prior to the sample being coiled carries out the inspection, and both surfaces of the strip are observed.

The forsterite glass film is also analysed using an optical microscope. However, this is carried out only when samples have been found to contain defects or when material does not reach the magnetic standards expected. It is not carried out on a routine basis.

2.1.3 Final Insulation Coating

A sample of the final insulation coating solution is taken approximately once per week. This sample is taken directly from the mixing tank, and is therefore in liquid form. It is analysed using Atomic Absorption Spectrophotometry, which analyses the composition in terms of the elements present. The levels of phosphorous and silicon are monitored to ensure that the coating formulations are mixed to the correct specifications.

The cured coating does not undergo any routine analysis, other than coating thickness using a Fischer Permascope.

2.2 Techniques Used During This Investigation

2.2.1 Fourier Transform Infrared (FTIR)

The Fourier Transform Infrared (FTIR) instrument can be used to analyse materials and provide information about the compounds that make up that material. Compounds can be recognized due to their characteristic interaction with infrared radiation; each compound will absorb the radiation at a certain frequency.

This method is most widely used in the identification of organic materials but can also be applied to other materials.

Infrared is the term used to describe a region in the spectrum, which exists between the visible and microwave sections [23]. It is normally expressed in the units of wavelength or frequency, with units of microns and wavenumber respectively. The wavenumber is the number of waves per centimetre (cm^{-1}). The complete infrared region spans from 6 to 13300 cm^{-1}, although the section most commonly used for FTIR applications is between 400 and 4000 cm^{-1}. This is known as the 'fundamental' region and does not include near infrared or far infrared.

All molecules are made up of a number of atoms that are held together by chemical bonds. Within a molecule, the atoms will vibrate and rotate with respect to one another. The chemical bonds bind the atoms together elastically and can be thought of as acting like springs between the oscillating atoms. The frequency at which this occurs depends on a number of factors including the masses and structures of the atoms and the strength of the bonds between them. Due to these variables, each molecule will have a characteristic frequency associated with it, and it is these frequencies that correspond to the same frequencies as the waves belonging to the infrared region of the spectrum.

If infrared radiation is incident upon a molecule that has the same frequency, then the atoms are excited to a higher energy level as it affects the vibrations and other interatomic vibrations. Visible or ultraviolet light will cause electrons to be promoted to a higher orbital and microwaves affect the rotation. This occurs as a result of energy from the wave being transferred to the atoms. This is infrared absorption, which provides the basis for the Fourier Transform Infrared (FTIR) apparatus. The grazing angle technique allows the spectrum of infrared radiation to be detected after it is incident upon the specimen. By analysing the spectrum of the radiation that is detected, it is possible to determine the molecules present in the sample specimen, as the spectrum will show the frequencies of the electromagnetic waves that have been absorbed.

The difference between an FTIR instrument and a dispersive instrument is that it measures in the time domain, whereas a dispersive instrument measures in the frequency domain.

An FTIR spectrometer uses a Michelson interferometer, shown in Figure 2.2.

This produces an output signal that contains the same information as the original infrared signal, but of a much lower frequency. This output signal is known as an interferogram.

The radiation travels from the source to the beam splitter, where approximately 50% of the beam is reflected onto the stationary mirror and back to the splitter. The rest of the beam passes through the beam splitter and travels to the movable mirror, before also returning to the splitter. The beam that is reflected from the stationary mirror has a fixed path length along which it travels. However, the distance travelled by the other split beam is variable. At the point at which they meet back at the beam splitter,

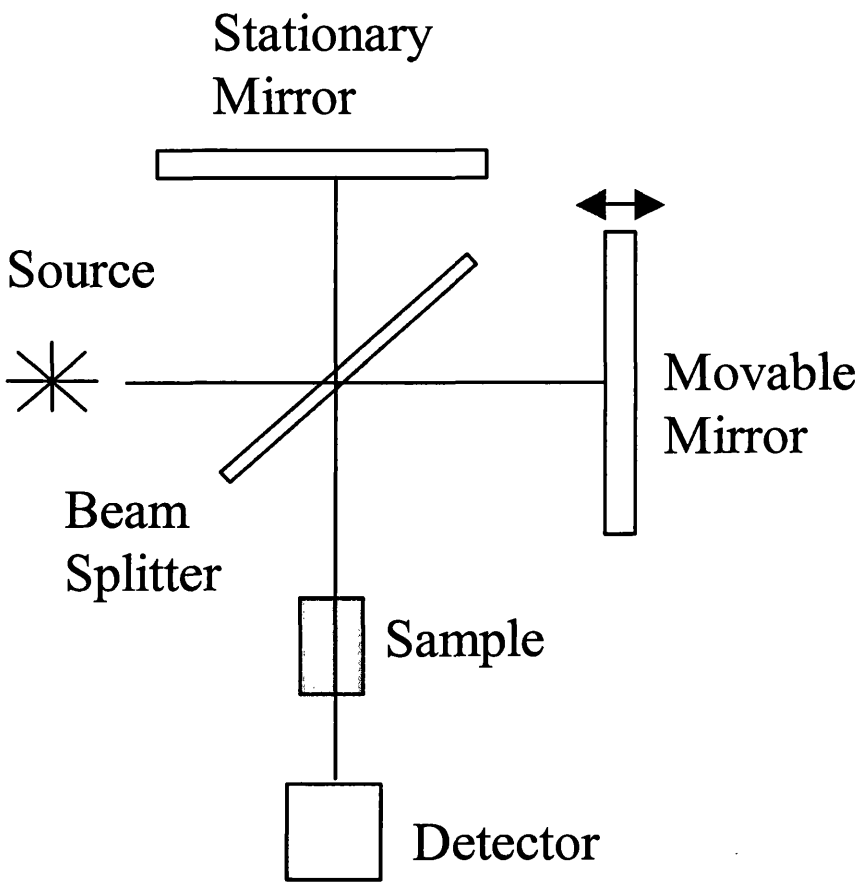

Figure 2.2: A Michelson interferometer, as used in the FTIR apparatus.

they interfere with one another and recombine. Depending on the two beams, the interference may be either constructive or destructive. If the difference between the two beams is exactly one wavelength, or a multiple of a wavelength, then the interference will be constructive. Destructive interference occurs if the two beams have a path difference of half a wavelength. Therefore, as the movable mirror moves back and forth, it will cause a sequence of maxima and minima to be detected, with each maxima indicating a mirror movement of half a wavelength (as the beam travels back and forth). Therefore, if the mirror position is altered at a constant rate, the detector will receive a signal that varies sinusoidally. However, in practice, the interferogram produced will look like that illustrated in Figure 2.3.

This is due to the resultant interferogram comprising of a combination of each of the interferograms for each separate frequency contained within the polychromatic infrared radiation source. The large maxima at the centre, known as the centreburst, is due to all interferograms being in phase when there is zero path difference (ZPD) i.e. when the path length from the beamsplitter to the fixed mirror is exactly the same as the path length between the beamsplitter and the movable mirror.

This analysis technique gets its full name from the mathematical operation that is involved in converting a time function to a frequency function. In more practical terms, this procedure converts the interferogram to the infrared absorption spectrum. The mathematical operation involved is known as a Fourier Transform.

The apparatus used for the experimentation at Orb is a Perkin Elmer BX spectrometer, shown in Figure 2.4. It is a single-beam spectrometer. This means that all the wavenumbers of the background are measured at the same time, before all of the wavenumbers for the sample spectrum are measured at once. This is different to a

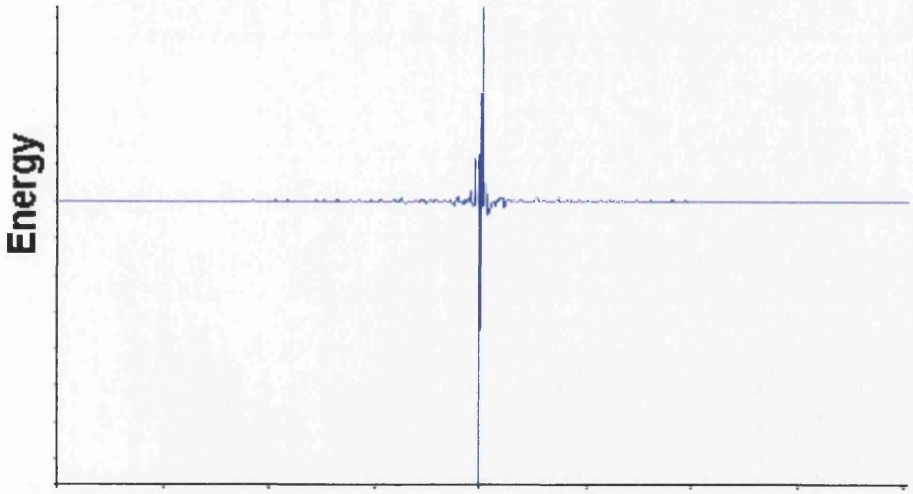

Figure 2.3: Illustration of a Typical Interferogram for a polychromatic Infrared Source.

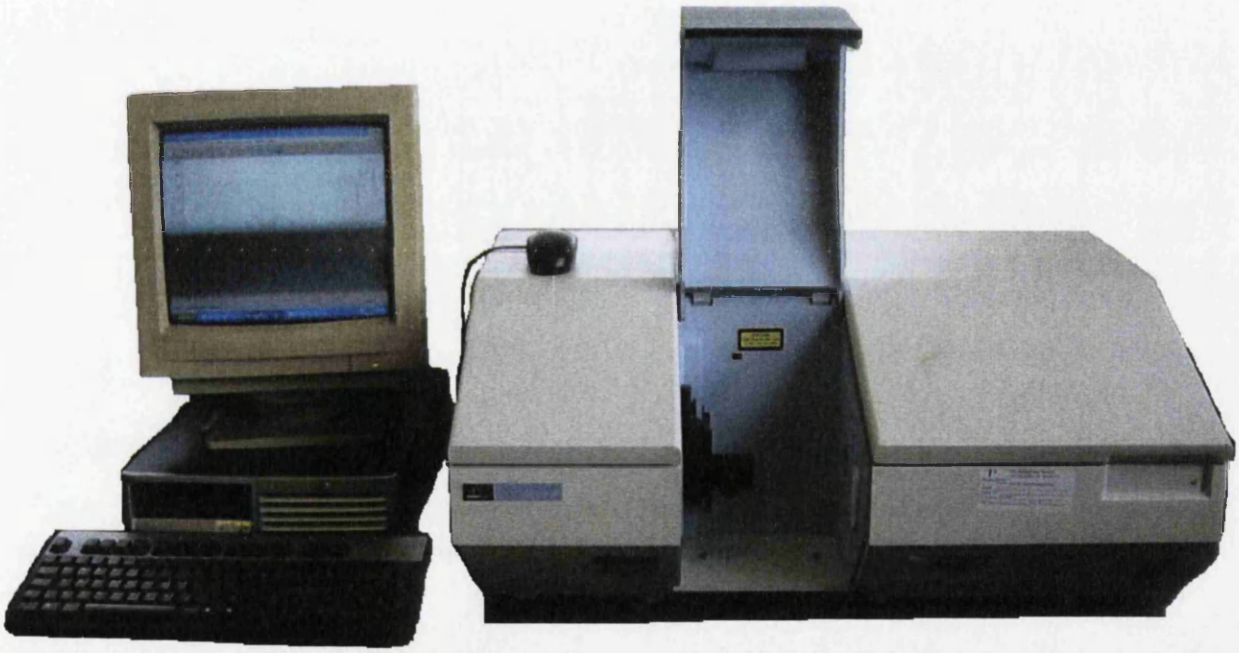

Figure 2.4: Perkin Elmer BX spectrometer, as used at Orb

double-beam dispersive instrument where the spectra for the background and the sample are taken at the same time and ratioed as the apparatus progresses through the wavenumbers. It is capable of collecting data over the range of 7800-100 cm^{-1} and has a potential optical path difference (OPD) resolution of $1cm^{-1}$.

The detector used in the instrument is a deuterated triglycine sulphate, or DTGS, detector that is optimal for frequencies in the mid-infrared region.

2.2.2 Electrochemical Potential (ECP) Analysis

A method known as the electrochemical potential (ECP) method has been developed to evaluate the surface oxide layer formed in the decarburisation furnace, and this technique has been studied in great detail at Orb Works [24, 25]. This method utilises a working electrode and a reference electrode. The process that removes the oxide layer from the surface of the steel is similar to wet corrosion. It is a REDOX reaction. This is a reaction where one species will lose electrons (i.e. it will be oxidised) and the other will gain electrons (reduced). A computerized version of the technique has been developed as part of an M.Res project [25] run by Cogent and University of Wales, Swansea. The working electrode is a sample under investigation. It has dimensions of 130mm x 50mm and is taped with acid resistant tape to ensure that only the bottom 70mm and the top 10mm of the sample is exposed. The reference electrode is a mercury / calomel electrode. Both samples are immersed in 5% sulphuric acid at 70°C for a duration of 20 minutes. This temperature is achieved by placing the beaker of acid into a water bath. To ensure the temperature of the acid remains uniform throughout, it was stirred with a mechanical glass stirrer at a speed of 266 r.p.m. The variation in the potential difference between the two electrodes is

recorded by a P.C. and can be plotted graphically. Figure 2.5 shows the set-up of apparatus used for the electrochemical potential method.

The potential difference will vary due to the dissolution of the surface oxide layer on the steel. The results will be indicative of both the thickness and composition of the layer and give a 'fingerprint' of the layer.

2.2.3 X-Ray Photoelectron Spectroscopy (XPS)

X-ray Photoelectron Spectroscopy (XPS), or Electron Spectroscopy for Chemical Analysis (ESCA) as it is also commonly known, is a non-destructive testing technique used for the compositional analysis of the surface of a sample. It is both a qualitative and quantitative technique that provides compositional data based on all elements except helium and hydrogen. It also establishes the electronic state of the surface region.

The technique was developed in mid-1960's by K. Siegbahn, who later won the Nobel Prize for Physics in 1981 for his work in this field.

The basis of this technique is provided by the photoelectric effect, first observed by Hertz in 1887 [26]. This describes the phenomenon whereby electrons are emitted by the surface of a material when light is incident upon it. Although observed many years previously, the photoelectric effect was not fully understood until 1905, when Albert Einstein postulated that light is made up of packets of energy known as photons. This theory suggested that each photon has a quantum of energy (E) calculated using Equation 2.1:

$$E = hf = hc/\lambda \qquad \textbf{Equation 2.1}$$

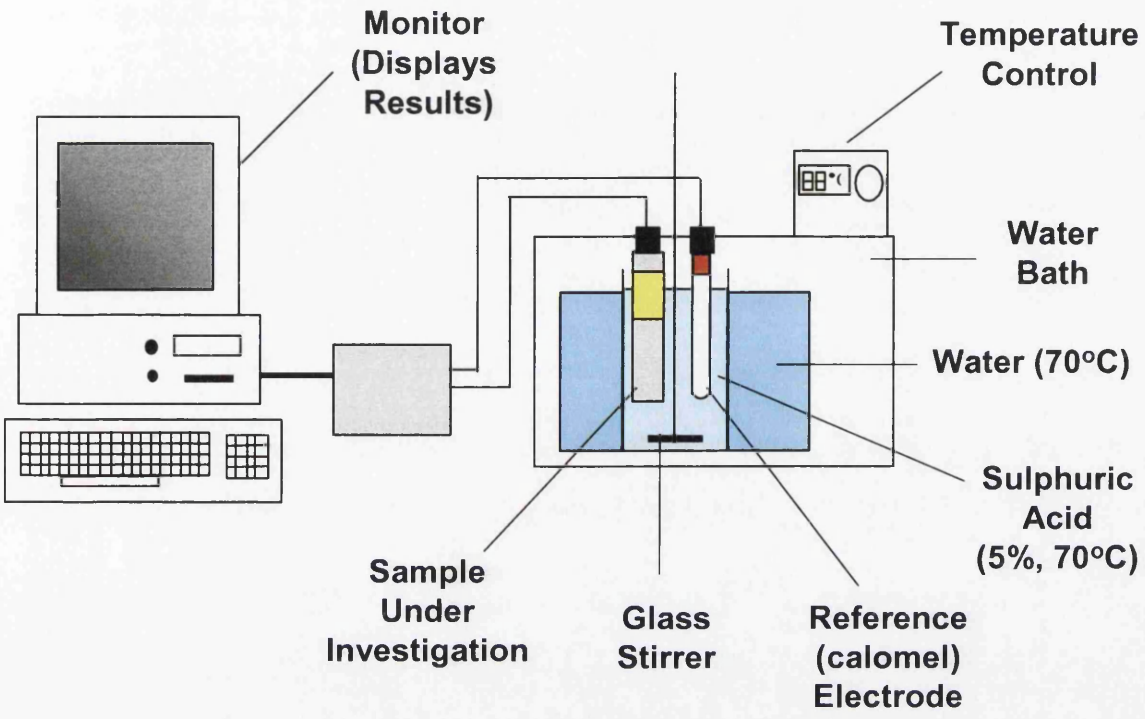

Figure 2.5: The experimental set-up for electrochemical potential investigations.

Where h is Planck's constant (6.626×10^{-34} J.s), f is the photon frequency (Hz), c is the speed of light (3×10^{8} ms^{-1}) and λ is the photon wavelength (m).

The minimum energy needed by an electron to escape the material (in the case of XPS, it is a core electron that is removed) is known as the work function, Φ. This energy acts to overcome the attractive binding energy forces holding the electrons within the material. The electron may absorb the photon when it is incident upon the surface in an 'all or nothing' event i.e. either all the energy of the photon is absorbed, or none at all. Assuming that this energy is greater than the work function of the material, the electron is liberated, with any energy greater than F converting to kinetic energy (KE). This is shown by Equation 2.2:

$$hf = F + KE_{max} \qquad \textbf{Equation 2.2}$$

This technique uses soft x-rays as the source of monochromatic (fixed-energy photons) radiation. This radiation then irradiates the surface and bombards it with photons in an ultra high vacuum (UHV) environment. This results in the removal of electrons to a depth of approximately 5 microns, which approximately relates to the top 10 atomic layers.

Upon photo-ionisation, an electron energy analyser can be used to measure the distribution in kinetic energy of the emitted electrons, leading to the display of a photoelectron spectrum.

The binding energy holding the core electrons within each atom is very characteristic of a certain element, enabling the material from which the electron is emitted to be easily identified. It is also possible to obtain information on the oxidation state and

other chemical information from small changes in the binding energy for each atomic orbital. This can be done using careful analysis of small shifts in the peaks of the spectra. Also, the intensity of the peaks is related to the concentration of a particular element within the sample, allowing the method to provide quantitative elemental analysis.

2.2.4 Sputtered Neutral Mass Spectrometry (SNMS)

Sputtered Neutral Mass Spectrometry involves the bombardment of a solid target sample by a beam of energetic ions, causing target atoms to be ejected into the gas phase. This occurs due to the exchange of momentum when the incident ions collide with the target atoms.

The neutral species emitted from the target sample when using the SNMS technique give a far more representative analysis of the sample than the ions used in other mass spectrometry techniques. They account for approximately 99% of the species emitted, but are not as readily attracted to the mass analyser as the ions due to their lack of charge. Therefore, it is necessary for these particles to pass through an ionisation region, where they undergo electron bombardment. This enables them to be analysed by a mass analyser in the normal way. Otherwise, the technique would rely on only the particles whose trajectory caused them to reach the detector.

SNMS generally has a reduced sensitivity when compared to other similar techniques, such as Secondary Ion Mass Spectrometry. For this reason, the incident beam used for SNMS is required to be of a high energy. This results in the technique eroding the surface of the sample under investigation (otherwise known as sputtering), enabling this technique to be used to produce a depth profile of the composition.

The apparatus used during this investigation (Vacuum Generators SIMSLAB, shown in Figure 2.6) is based at Swinden Technology Centre (STC), Rotherham. It utilises a 10keV argon ion beam to sputter material from the sample surface, which is generated from an argon/oxygen plasma. The beam current is maintained at 250nA, with the rate of etching controlled by the beam current density. Detection of the species is by a quadrupole mass spectrometer.

2.2.5 Magnetostriction

The term magnetostriction relates to the fractional change in dimension of a ferromagnetic material when it is magnetised. It is widely believed that this phenomenon has a considerable effect on the noise produced by a transformer core that has been assembled from electrical steel, and it is therefore highly desirable to reduce this effect.

A Magnetostriction Measurement System (Figure 2.7) has been developed as part of a PhD course in association with Cogent Power [27, 28], and is located at Orb Works. It predominantly measures the magnetostriction (from the peak fundamental to the 5^{th} harmonic) of a sample of standard Epstein size (305 x 30mm), but it has also been designed to determine the power loss, specific apparent power and permeability of the material. These measurements can be carried out at an applied compressive or tensile stress, at intervals of 1MPa over the range of -10MPa to +10MPa.

To obtain the relative data, the sample under investigation is clamped into a fixed position at one end, with the other end being attached to a low friction, non-rotating cylinder. This cylinder applies the stress uniaxally along the length and in the plane of the sample. The magnitude of the stress is controlled by the pressure of the cylinder, which is in turn regulated by electro-pneumatic valves linked to a PC

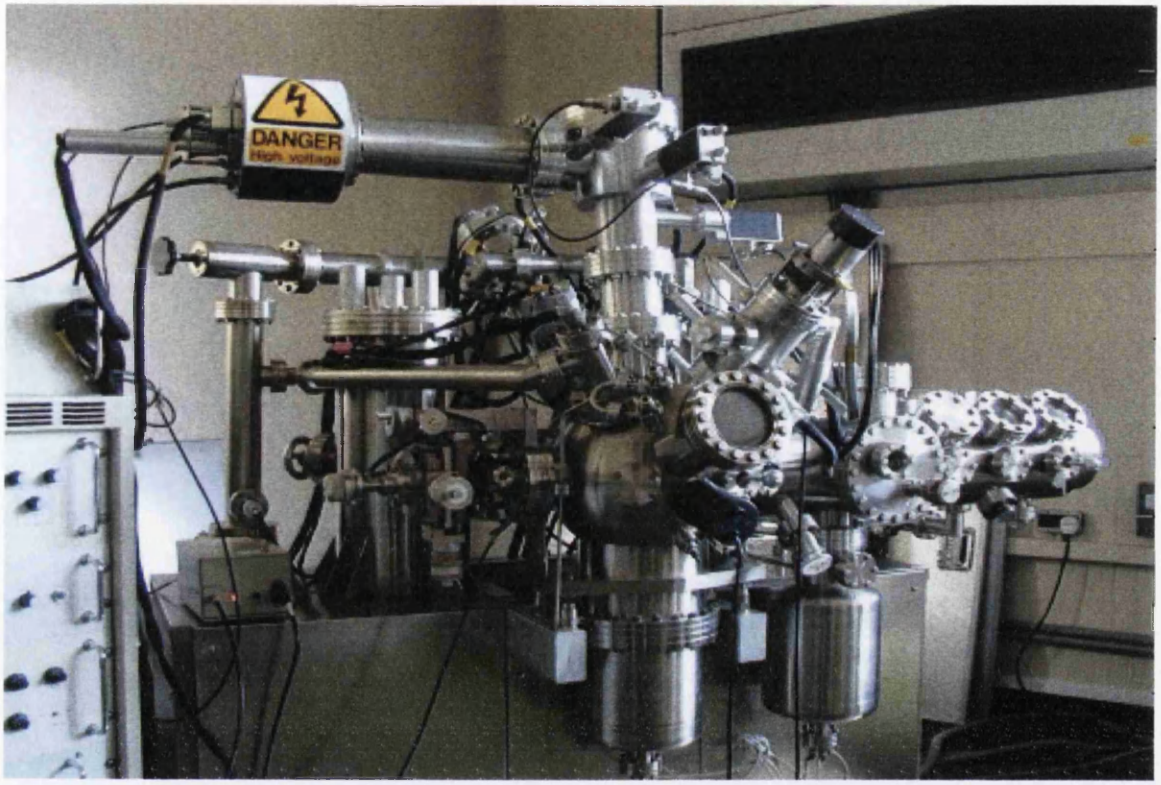

Figure 2.6: SNMS apparatus (Vacuum Generators SIMSLAB)

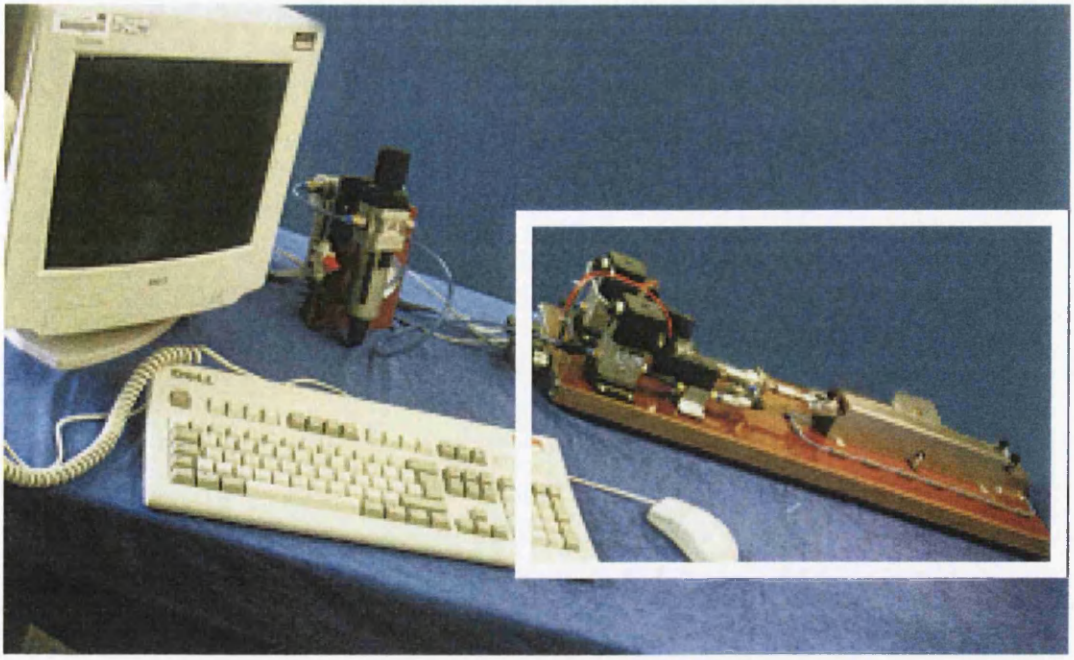

Figure 2.7 (a): Magnetostriction Measurement System.

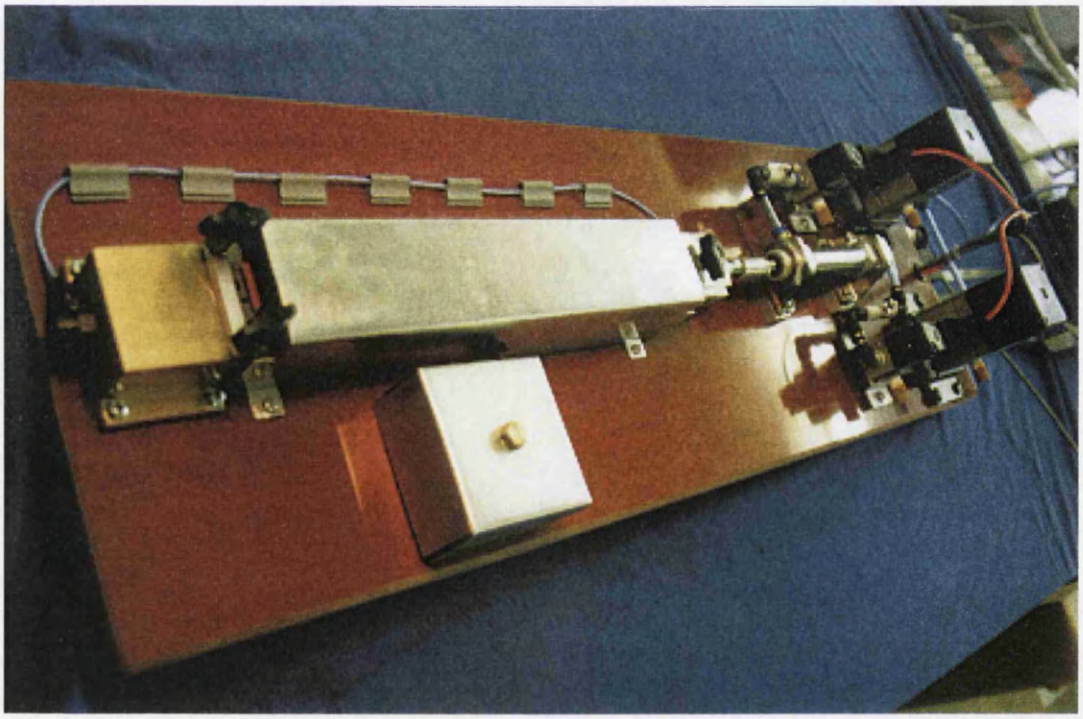

Figure 2.7 (b): Magnetostriction Measurement System. (highlighted area in 27 (a)).

containing the related software.

The magnetisation is controlled by a PMS 19000 loss tester which controls the levels of induction and also provides the measurement system for characteristics such as power loss, permeability and specific apparent power.

2.2.6 PMS 3000 Single-Strip Tester

The PMS 3000 single-strip tester (Figure 2.8(a), 2.8(b)), used to measure the magnetic properties of various samples during this investigation, was custom built at Orb Works. It is a version of the standard PMS 3000 apparatus that is used to routinely test the material from each coil produced at Orb Works in accordance with British Standards [29]. It has been modified so that it tests just a single Epstein (305mm x 30mm) sample, instead of the standard pack of 24 samples.

The sample under investigation is placed inside a solenoidal 'tunnel' containing the primary (magnetising) and secondary (sensing) windings. A flux closure yoke, manufactured using laminated electrical steel, is used to reduce the reluctance associated with the flux leaving the sample into air. The sample may then be magnetised according to the induction and frequency levels specified by the user. The associated software then produces a digital image of the B-H hysteresis loop. From this, the specific total loss, specific apparent power and permeability is automatically calculated and the results shown on screen.

2.2.7 Fischer Permascope

Coating thickness measurements at Orb, both in the laboratory and on the production lines, is manually measured using a Fischer Permascope (Figure 2.9). The magnetic

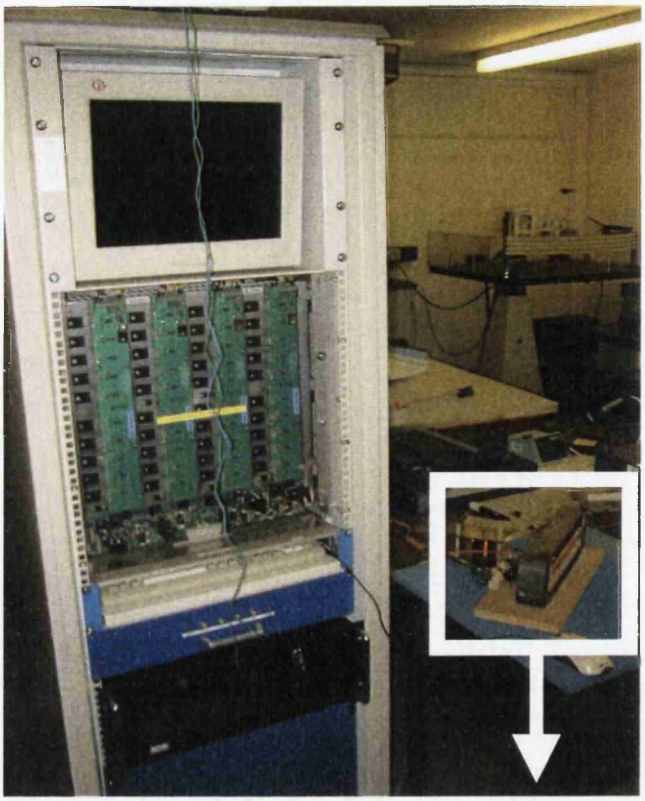

Figure 2.8 (a): PMS 3000 single-strip tester.

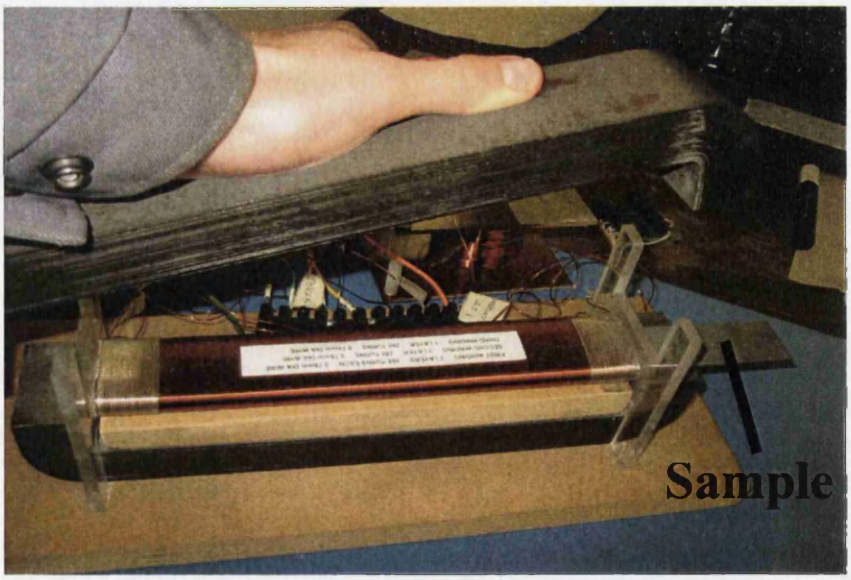

Figure 2.8 (b): PMS 3000 single-strip tester (highlighted area in 2.8(a)).

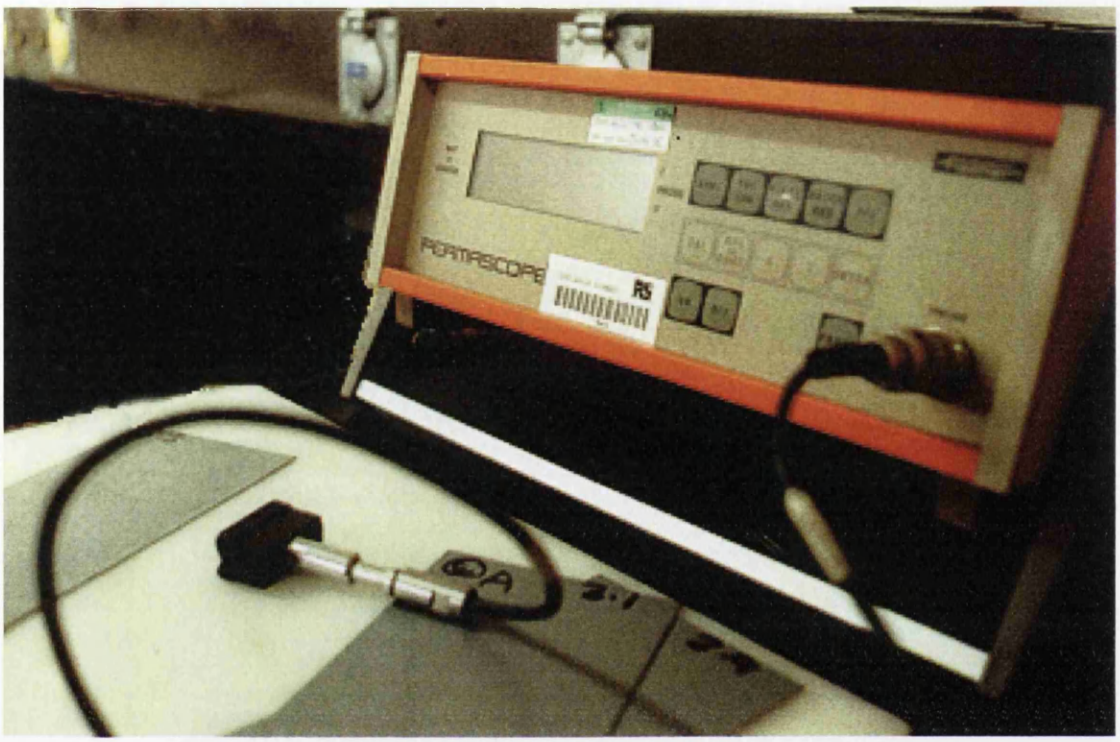

Figure 2.9: Fischer Permascope and probe.

induction method allows the non-destructive determination of coating thickness of non-magnetic coatings on a ferrous substrate, such as the forsterite glass film and final insulation layer found on electrical steels [30]. The base unit is linked to a probe, which is pushed down onto the surface of the coated sample. The probe contains a coil that generates a changing magnetic field. The magnetic flux density of this field is altered upon contact between the probe and the sample, and a secondary coil measures the change in magnetic inductance. Once the instrument has been calibrated using copper calibration foils of a known thickness, a microprocessor can convert this change into a value for coating thickness, which is shown on a digital display on the base unit.

The accuracy and reproducibility of the technique can be affected by characteristics such as surface roughness, silicon content and thickness of the steel, as well as uniformity of the coating. It is therefore necessary to ensure that the calibration is carried out on the same steel substrate that has been coated to minimise errors. Also, a minimum of 20 readings are taken from a selected area to produce an average value, and this is found to result in an accurate and reproducible coating thickness measurement.

Chapter 3

3.1 Aims of Programme

The review of literature has given an introduction into electrical steels, and in particular the surface layers that are present at various stages throughout production. It has been shown that the quality and composition of the decarburisation oxide, forsterite glass film and final insulating layers can have a great effect on the final material. This may be in terms of magnetic performance or appearance, both of which are factors that are likely to significantly influence the customers' perception of the material produced at Orb. There are also many other characteristics of the surface layers for which certain standards must be achieved if the desired quality of the final product is to be attained. Therefore, the improvement of these layers in terms of both consistency and quality will give Cogent a distinct advantage over competing manufacturers of electrical steel.

For these reasons, it would be highly beneficial for Cogent to possess analytical techniques that can be used to accurately determine the composition and quality of each of the layers. This would enable the standards to be more closely monitored, and the processing parameters to be altered, where necessary, in order to produce a more optimum product.

At present, the decarburisation oxide layer is analysed in terms of only its oxygen content, and the forsterite glass film is only analysed if problems occur i.e. there is

generally little assessment of these layers other than the crude classification of good or bad.

The final insulating layer is also only inspected visually on-line to directly assess its quality, although routine magnetic testing carried out on each processed coil might draw attention to any major deficiencies in the cured coating.

In the past, a number of analytical techniques have been evaluated in an attempt to provide a more accurate analysis of each of the layers. Unfortunately, they have been found to be extremely time consuming. In a continuous production environment such as that at Orb Works, it is necessary for analytical methods to provide a rapid assessment of the layers in order for any problems to be remedied as quickly as possible. Therefore, none of the techniques that had previously been found to be time consuming were considered to be a viable option, irrelevant of the accuracy that they could provide.

The present programme was therefore designed to evaluate a number of analysis techniques, and establish those that may be used to provide an accurate and rapid assessment of the composition and / or quality of the surface layers. Where applicable, the viable techniques can be used to determine the effect that varying certain parameters (such as final coating composition) has on the overall quality of the product.

Chapter Four

Fourier Transform Infrared (FTIR) Analysis of the Decarburisation Oxide Layer

4.1 Introduction

For a number of years, there has been a Fourier Transform Infrared (FTIR) spectrometer located within the Chemistry Department at Orb Works. Its main use at present is to provide regular analysis of oils. However, previous work has been carried out which indicates that this method may have the potential to be used to characterise the oxide layer formed on the surface of the steel during the decarburisation process [31]. This characterisation could be in terms of the thickness of the oxide layer and / or its compositional make-up.

When the oxide layer has previously been analysed with the FTIR apparatus, it has been difficult to authoritatively analyse the resultant spectrum, as the bands associated with each of the components of the oxide layer have not been seen distinctively. It has been suggested that the use of a variety of grazing angle attachments may help to solve this problem. This is a piece of apparatus that causes the radiation to be incident upon the surface at a carefully controlled angle, which in turn alters the depth to which the infrared radiation penetrates into the surface. The attachment used 'as standard' for the analysis of coated samples at Orb provided a grazing angle of 26.5°. As this attachment was found to produce inconclusive results, an attachment providing a grazing angle of 80° was acquired to carry out a further investigation into the suitability of this technique for rapidly identifying the composition of the

decarburisation oxide layer. This would allow the consistency of the material produced on the decarburisation lines at Orb Works to be quickly and easily assessed, enabling rapid detection of any variation in the oxide layer from what is expected for optimum glass film formation.

4.2 FTIR Apparatus: Effect of Scanning Parameters

4.2.1 Introduction

To ensure that any results obtained from the FTIR equipment would be valid, it was first necessary to establish the correct scanning parameters for the apparatus. Orb Works has recently taken delivery of a new FTIR spectrometer and discussions with personnel experienced in this field suggested that the default settings used on the new FTIR equipment at Orb might not be set to their optimum levels. The default settings described above are:

- Number of scans: 3
- Resolution: 4 cm^{-1}

A visit to a different Corus site allowed observation of an FTIR set-up that been operational for a number of years. Discussions with employees that are experienced in the use of FTIR indicated that a minimum of 6 scans should be carried out on each sample (in order to provide sufficient data for a single spectrum), and the necessity of this was demonstrated on the apparatus in question. Also, it was recommended that the resolution used should be either $2cm^{-1}$ or $1cm^{-1}$, although time restraints prevented any scans being carried out at the time to confirm this.

For these reasons, the effect that the variation of these parameters would have on the spectra obtained from the Orb apparatus was investigated.

4.2.2 Experimental Procedure

The FTIR spectrometer was used to obtain a spectrum from material with a variety of different coatings on the surface. This was carried out using the 'standard' 26.5° attachment, as more was known about this than the more recently acquired 80° attachment. It was found that the largest number of distinctive bands was observed on the spectrum obtained from a grain oriented sample coated with the final insulation coating. Although a requirement of the overall investigation was the analysis of a large number of decarburisation samples, it was decided that using final coated samples would provide a more accurate assessment of the required scanning parameters as the spectra relating to the oxide layer was too inconclusive at this stage. The spectra obtained from this material were not fully understood at this point in the investigation, but it was only necessary to use the bands to monitor the consistency between spectra when the scanning parameters were altered.

A single steel sample, coated with the insulation coating, was acquired from the end of the final coating line and cut to an appropriate size, ensuring that it would fit correctly in the standard reflectance attachment (26.5° grazing angle). This guaranteed that there was no bending of the sample whilst it was held in position, as this could cause minor discrepancies in the final spectra obtained. The sample remained fixed in the correct position while all scans were carried out, which ensured that the spectra obtained were representing exactly the same area of coating. This

should theoretically result in identical spectra, which will differ only due to changes in the scanning parameters.

The first setting to be varied was the number of scans. These separate scans were carried out within a short time frame and are automatically averaged by a program contained within the FTIR scanning software to produce one spectrum. It was decided to vary the number of scans at each interval between two and six. This includes both the number currently used at Orb according to the default setting (three) and the number that has been recommended (six). This was first carried out using the default resolution setting of $4cm^{-1}$, and then repeated using a resolution of $2cm^{-1}$ to determine any effects that occur due to changing this second parameter.

4.2.3 Results and Discussions

4.2.3.1 Number of Scans

Figures 4.1 and 4.2 show examples of the variation in the spectra (transmittance against wavenumber) obtained as the number of scans was altered from two through to six. Figure 4.1 shows the spectra obtained when the resolution was set to $4cm^{-1}$, and Figure 4.2 shows the spectra when a resolution of $2cm^{-1}$ was used.

It can clearly be seen on both figures that each of the spectra are very similar, irrespective of the number of scans that were carried out. It should be noted that there are five spectra on each of the figures, all of which overlap very closely. The fact that it is difficult to distinguish between each of the separate spectra emphasizes the fact that very little variation was observed.

The only area of variation that can be seen on this scale is in the wavenumber range of approximately 650 – 750 cm^{-1}. The variation appears to be slightly more prominent

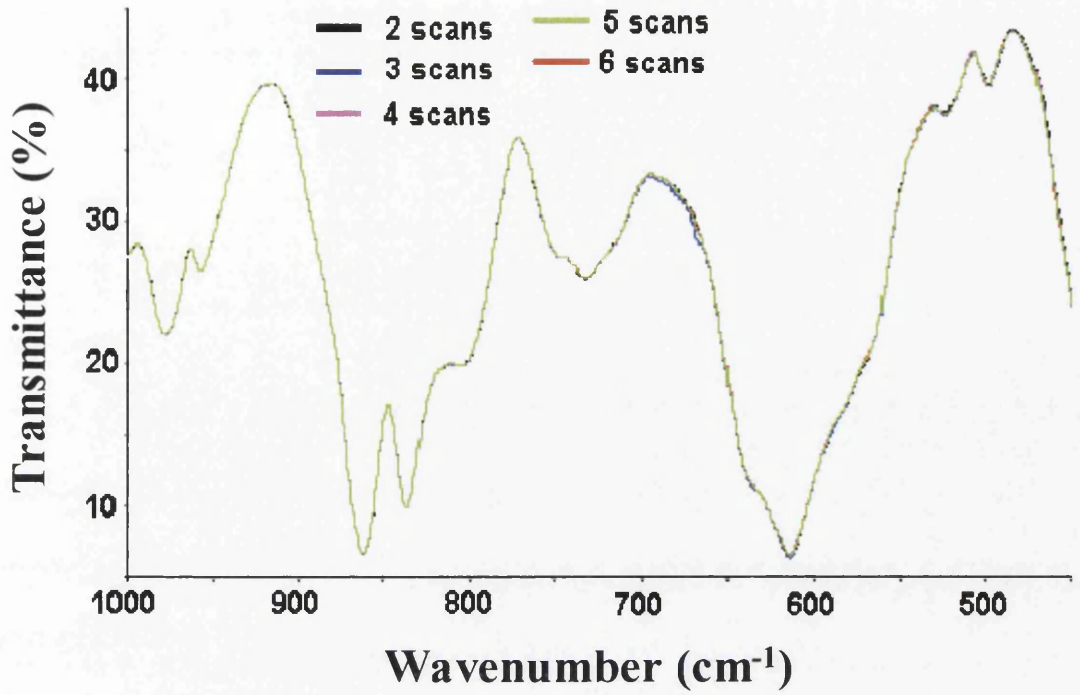

Figure 4.1: Spectra obtained when the number of scans was varied (Resolution set to 4 cm^{-1})

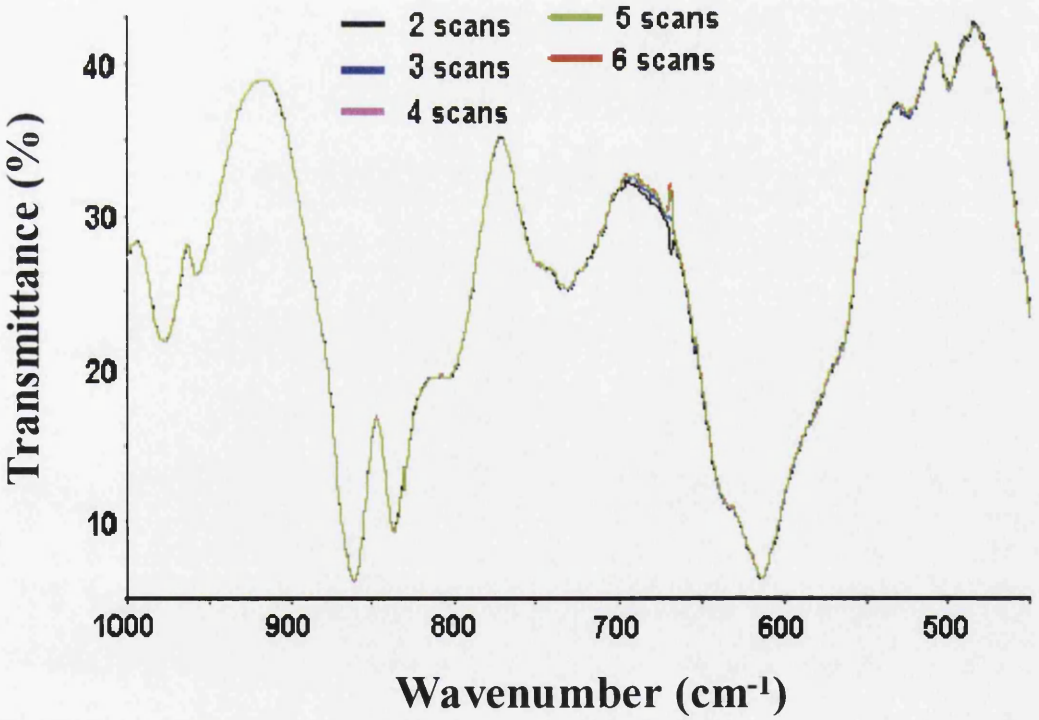

Figure 4.2: Spectra obtained when the number of scans was varied (Resolution set to 2 cm^{-1})

when a resolution of 2 cm^{-1} is used. Figure 4.3 shows a more detailed version of this region of Figure 4.2, so that it may be seen in greater detail. It can be seen that the variation is not only in the size of the band at ~670 cm^{-1}, but it actually changes from a peak to a trough in the case where two scans were carried out. The reason for this effect change has not been confirmed, but it is expected to be a result of the apparatus itself, and not the sample being analysed as there is not practical explanation as to why there should be a change between a transmittance trough and peak.

Analysing the spectra in general, it is a trough that is of most interest in the case of these transmittance spectra, because a reduction in the %T value indicates the presence of a compound that is absorbing the radiation. It is unclear how changing the number of scans carried out would influence the spectra in the way seen in this investigation, and further research may be required if this effect has an influence on the data that is taken from the spectra. However, 670cm^{-1} is not in a region that affects the maximum height of the band upon which it occurs, and therefore may not be relevant when analysing this spectrum. Also, this feature is negligible in size when compared to the size of the band on which it is found. It should be noted that a band at this wavenumber was later observed on the spectrum for plain, uncoated steel. This evidence further suggests that this band is due to an effect of the apparatus, and not of the surface being analysed.

4.2.3.2 Resolution

Figure 4.4 shows a comparison between the spectra obtained using the two resolution settings (2cm^{-1} and 4cm^{-1}). It can be seen that there is very little difference between the two sets of spectra, with only a very small offset between the two (each set contained 2 scans). This offset is negligible compared to the changes that may be

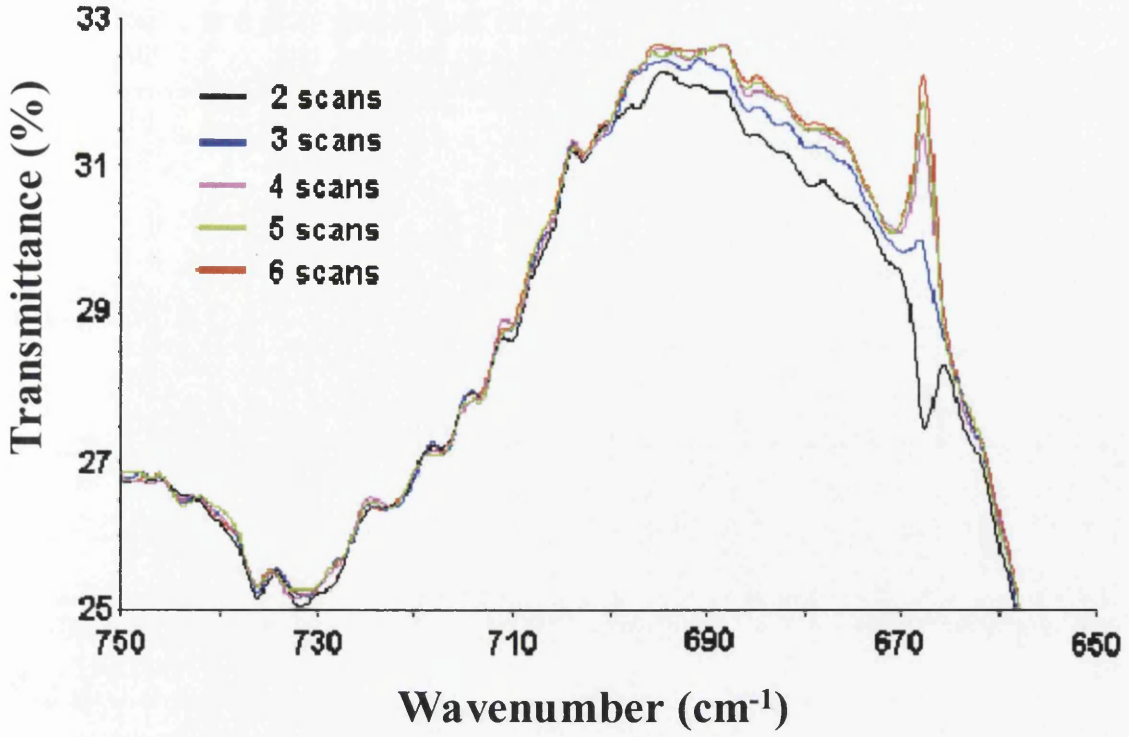

Figure 4.3: Selected region of spectra shown in Figure 4.2

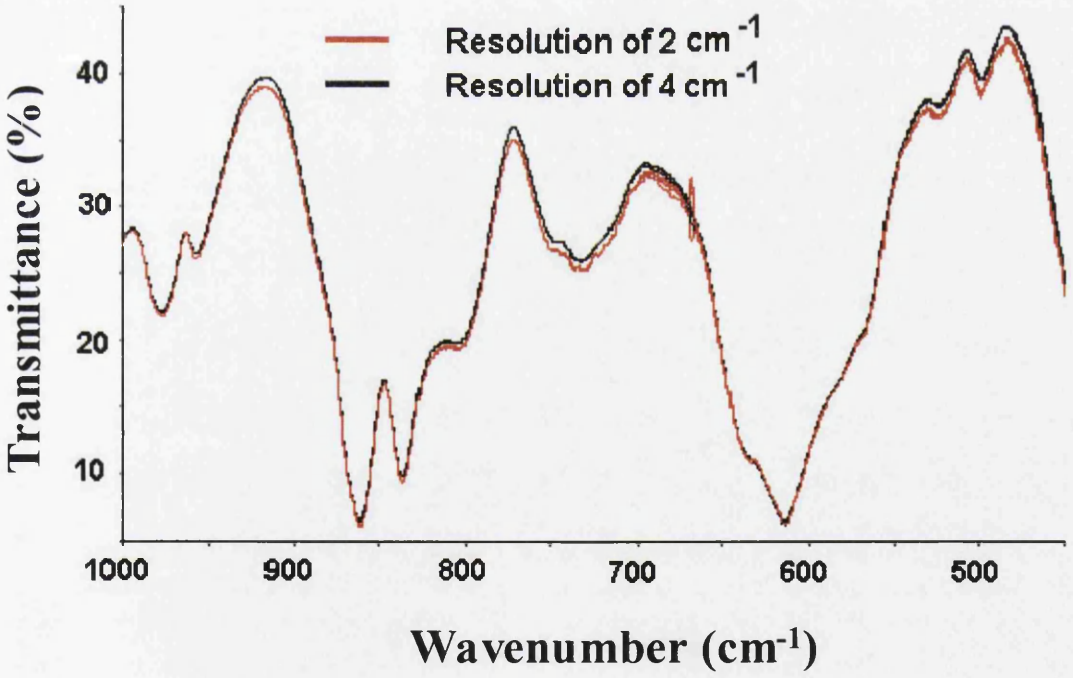

Figure 4.4: A comparison between the two sets of spectra obtained when using different resolution settings

seen along the length of a standard Epstein sample, as the effect on the areas of each of the bands, and also the maximum height of the bands, is very small.

Figure 4.5 shows a magnified region of these spectra, which displays a greater amount of detail. It shows that the spectra obtained when using a resolution of 4 cm^{-1} result in a much smoother line. This may show a small decrease in the accuracy of the apparatus, but the effect on the areas is negligible as the red spectra ($2cm^{-1}$ resolution) just appears to oscillate slightly with respect to an average which would be almost identical to that shown by the black ($4cm^{-1}$ resolution) spectra.

4.2.4 Conclusions and Recommendations of Section 4.2

4.2.4.1 Number of Scans

As the number of scans does not appear to have an effect on the spectra obtained, it is recommended that the default setting on the apparatus at Orb remains at 3 scans, as this appears to be completely adequate. Increasing the number of scans on this apparatus fails to produce a spectrum with any greater detail, and also has the disadvantage that an increased number of scans is more time consuming. This is a significant drawback, as it is envisaged that this technique could eventually be used for routine analysis on a large number of samples. Therefore, 3 scans provide the optimal compromise between the quality of a spectrum and test duration.

4.2.4.2 Resolution

The effect of improving the resolution of the equipment is more noticeable than varying the number of scans, although it is still quite slight and only observed to have a prominent effect when the selected region is magnified.

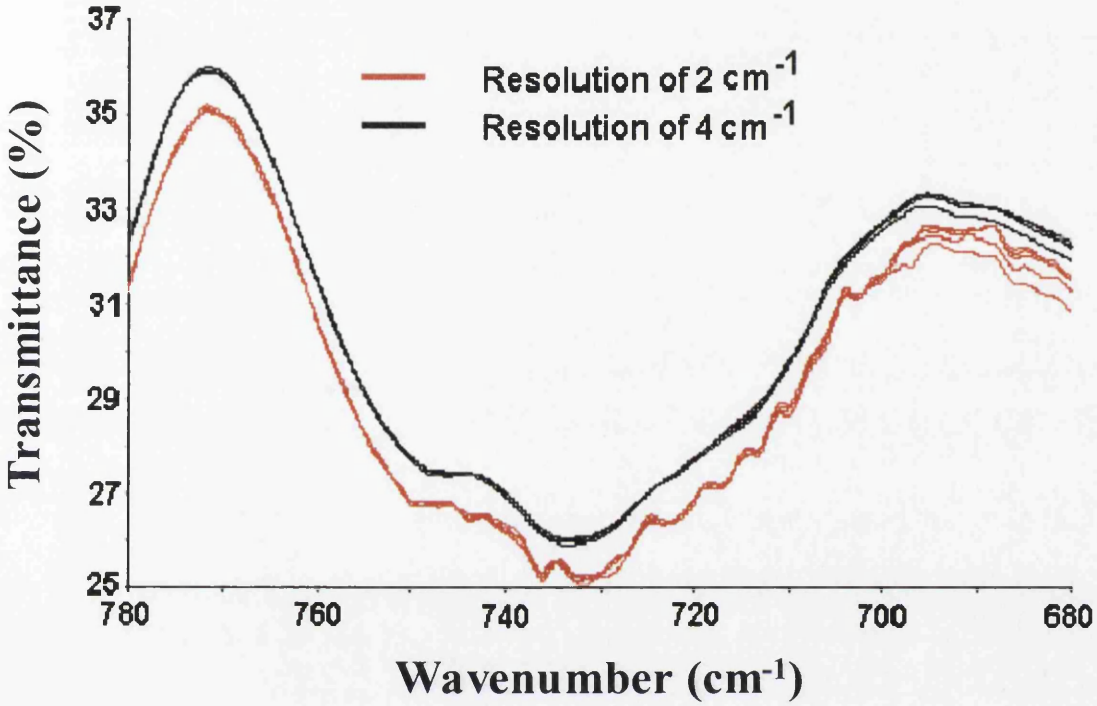

Figure 4.5: Selected region of spectra shown in Figure 4.4

Therefore it is recommended that the default setting of $4cm^{-1}$ be retained as there does not appear to be any benefits gained from changing it to 2 cm^{-1}. In fact, the reverse may be true as the oscillations may lead to further difficulties when trying to interpret the data.

The recommendations made from this investigation are only truly valid for the case being considered (i.e. phosphate-based coating analysis). This is due to the spectra having bands that are both quite large and clearly defined. As the number of coatings that are analysed using FTIR increases, it may be found that not all spectra are as clearly defined. In these cases, it is possible that there are situations where a change of resolution may be beneficial. Therefore, each case should be considered separately, although the variation caused by altering the scanning parameters in this investigation would only have a noticeable effect on very poor, undefined spectra which would probably not yield any useful results.

4.2.4.3 Comparison With Other Equipment

It was found that the initial recommendations, made by FTIR personnel based at another Corus site, did not improve upon the spectra obtained when using the initial default settings. The FTIR apparatus based at Orb Works has been recently purchased, and is therefore likely to be a more advanced version than the equipment upon which recommendations were based. It is likely that recent advances in technology have resulted in this type of apparatus being developed further in recent years, minimising the effects caused by scan number and resolution. Therefore, the spectra originally acquired when using the initial settings were already of such good quality that it was difficult to substantially improve upon them.

Although this investigation concluded that no change should be made to the default settings, it also provides a good degree of confidence in the validation and accuracy of any future spectra.

4.3 Analysis of Decarburised Sheet

4.3.1 Experimental Procedure

A total of fifteen samples were selected from the decarburisation lines at Orb Works, nine from D5 line and the remaining six from D4 line. Each sample was chosen from a different shift as this would hopefully cover a range of processing conditions and therefore lead to differences in the spectra obtained.

The samples used were selected from decarburisation discs that are routinely used by the Chemistry Laboratory for oxygen analysis, since these were readily available and the oxygen content was already known.

Following advice from Chemistry Laboratory personnel, the top side of the sample was always taken as being the side on which burrs were present from when the disc had been punched from the strip, irrespective of which side had been labelled. This would allow any difference in trends between the two surfaces to be identified. This is a possibility as there may be a difference in the processing conditions experienced by each side.

The default scan of the apparatus is from 400cm^{-1} and 4000 cm^{-1}, but all of the main bands were subsequently found to lie between 400cm^{-1} and 2000cm^{-1}. Therefore, the scans were subsequently analysed in this wavenumber range. Spectra were obtained from both the top and the bottom surfaces of each of the samples using the Orb FTIR

apparatus in conjunction with the 80° grazing angle attachment that has been specifically acquired for analysis of these types of oxide layers.

4.3.2 Results and Discussion

4.3.2.1 Identification of Bands

When the scans of all the samples had been completed, the spectra were each considered individually and then compared. Although there were many small indistinctive bands on each of the spectra, it was found that there appeared to be four main bands of interest that varied in size or shape between samples. These bands occurred at the following approximate wavenumbers:

$1050cm^{-1}$ (band 1),

$985cm^{-1}$ (band 2),

$925cm^{-1}$ (band 3),

$670cm^{-1}$ (band 4).

A typical spectrum of transmittance versus wavenumber for these samples is shown in Figure 4.6. The four main bands of interest have been labelled, each being observed as a trough as it is the reduction in transmittance that is of interest

4.3.2.2 Band Area

The area associated with each of these bands was established using the standard baseline method [32]. This utilises a baseline, which is drawn on the each spectrum between the two points where the trough of the band appears to start and finish, to define the remaining perimeter of the trough. Therefore, a specific area is outlined.

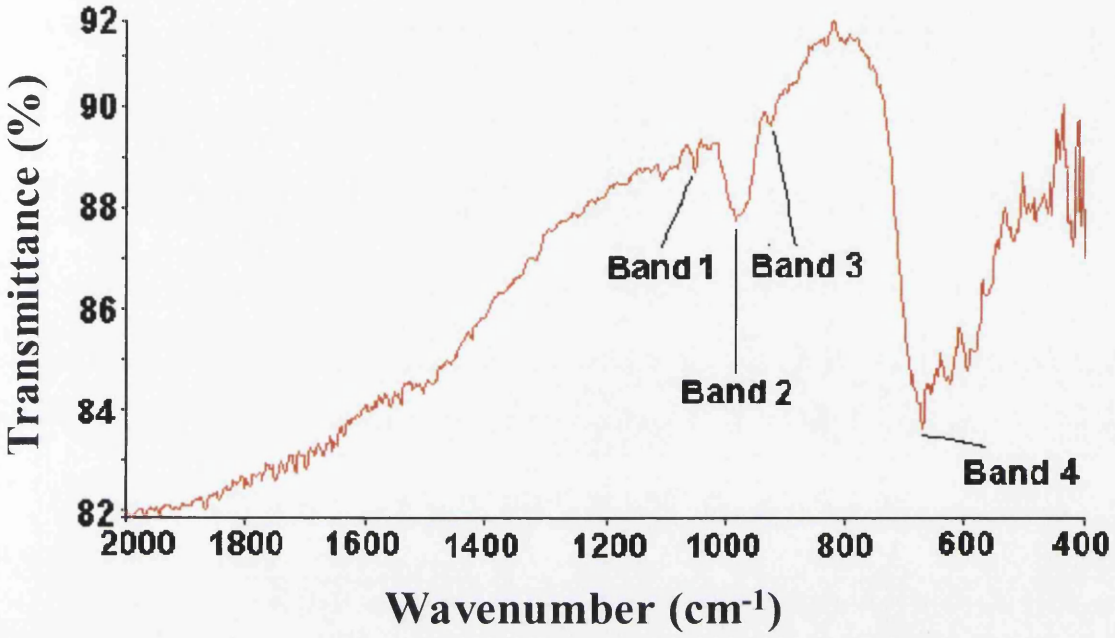

Figure 4.6: A typical example of the spectra obtained from a sample taken from the decarburisation lines

The assumption must be made that the background radiation varies linearly with wavelength.

Following further research, the various parts of the spectra were identified:

Many small bands that appear at approximately 1350 – 2000 cm^{-1} are often associated with H_2O.

Band 4 (in Figure 4.6) was found to be unrelated to the oxide layer and was in fact evidence of the presence of CO_2 [33].

However, the remaining bands were associated with compounds expected to be found in the oxide layer, namely $FeSiO_3$ (band 1) and Fe_2SiO_4 (bands 2 and 3) [31]. The compound Fe_2SiO_4 is known as fayalite, after which the entire decarburisation oxide layer is commonly (and incorrectly) named.

Graphs were plotted to establish whether or not there was a relationship between the areas of any of the bands (Figures 4.7 - 4.12), as the conclusions above suggest that bands 2 and 3 should be linked. As expected, this confirmed that these were the only two bands that showed a clear relationship. This confirms that they are both due to the same compound (fayalite).

In some cases, it was found that there was also a small component of band 2 that was due to $FeSiO_3$ as the two absorption bands overlap slightly. This is due to the resolution of the instrument being lower than desired. However, this was not a significant effect as the area of band 2 was predominantly related to fayalite.

The FTIR results were surprising due to the fact that there appeared to be no large bands corresponding to silica (SiO_2). Previous metallographic work carried out at Orb Works has proven that this compound has previously been found in the oxide

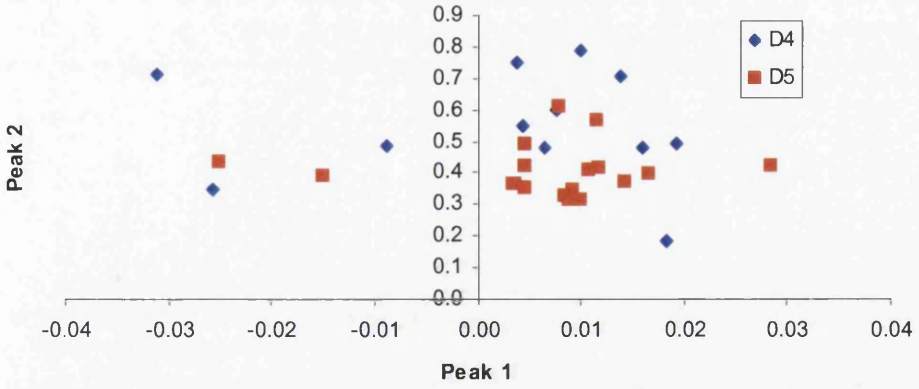

Figure 4.7 – Correlation of FTIR band area data (Band 1 vs. Band 2)

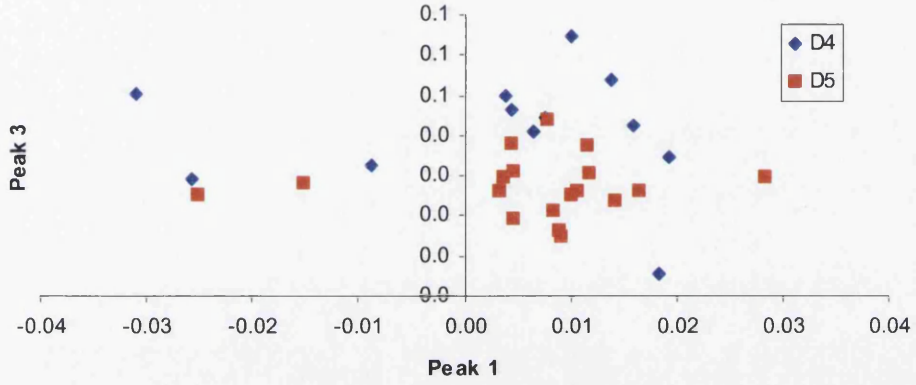

Figure 4.8 – Correlation of FTIR band area data (Band 1 vs. Band 3)

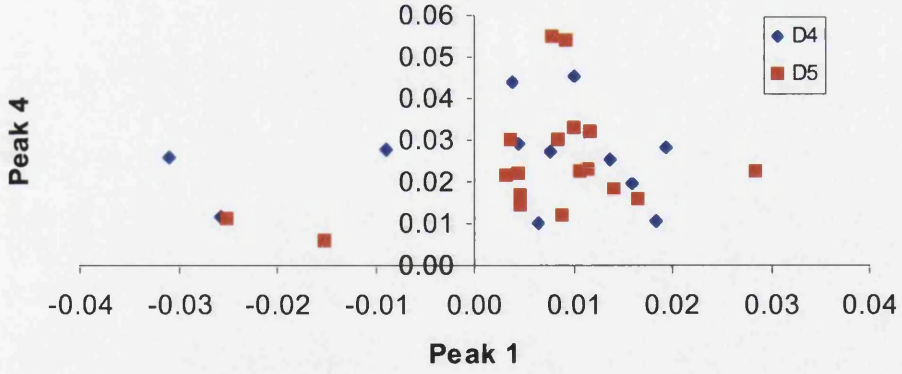

Figure 4.9 – Correlation of FTIR band area data (Band 1 vs. Band 4)

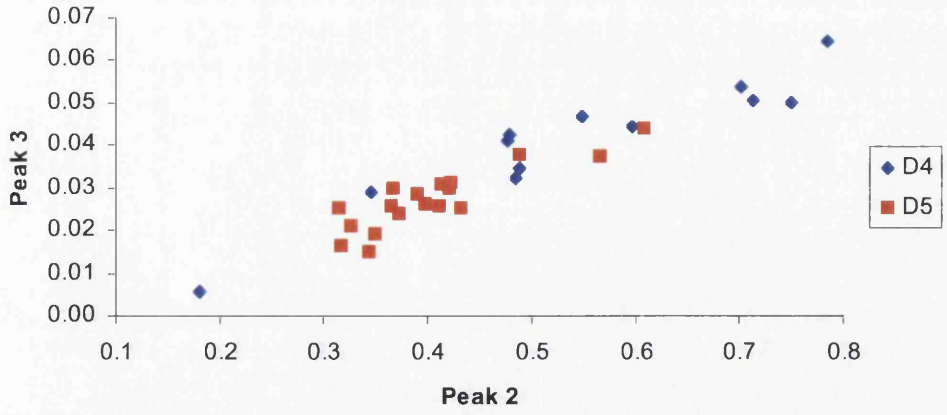

Figure 4.10 – Correlation of FTIR band area data (Band 2 vs. Band 3)

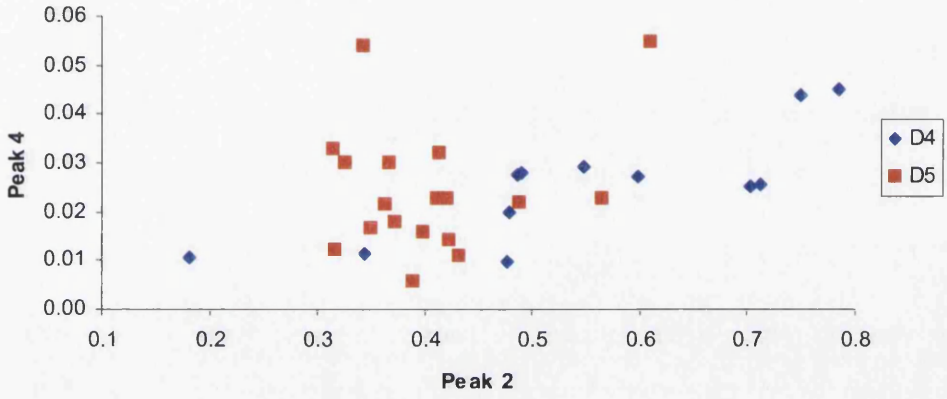

Figure 4.11 – Correlation of FTIR band area data (Band 2 vs. Band 4)

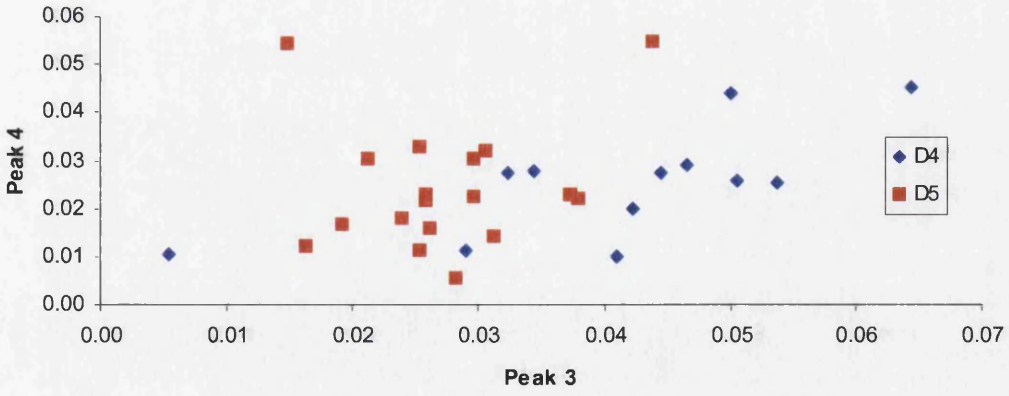

Figure 4.12 – Correlation of FTIR band area data (Band 3 vs. Band 4)

layer after the strip has undergone the standard decarburisation procedure on either one of the Works decarburisation lines. The SiO_2 in the oxide layer reacts with a magnesia (MgO) coating to form a forsterite (Mg_2SiO_4) glass film at a later stage, and so poor glass film defects would have occurred on the coils from which the samples were taken if SiO_2 had not been present. This strongly suggests that traces of SiO_2 should have been observed on these spectra. If this compound were present, the related bands would be expected between 1050 and 1250 cm^{-1}.

When a trace obtained from Orb material is compared with a trace for Japanese material (see Figure 4.6 and Figure 4.13 (also [31]) it is clear that the content of SiO_2 and fayalite is significantly different between the two specimens. It would initially appear that the Orb product is not of the optimum composition as the presence of SiO_2 is beneficial for good glass film formation. The MgO can also react with fayalite to form the forsterite glass film, but this causes conductive iron particles to become embedded in the surface layer during the glass film reaction, thus reducing the insulation properties of the final product.

4.3.3 Conclusions of Section 4.3

Significantly, this work has proven that fayalite is present in the decarburisation oxide layer, and that it can be clearly detected by using the 80° grazing angle attachment on the FTIR apparatus located at Orb. However, there appears to be no evidence of silica. From the results obtained, the most likely conclusion for this was that the FITR could only 'see' the very topmost section of the oxide layer. It seems plausible to suggest that the oxide layer is capped with a layer of fayalite that the infrared radiation is unable to penetrate with the current apparatus.

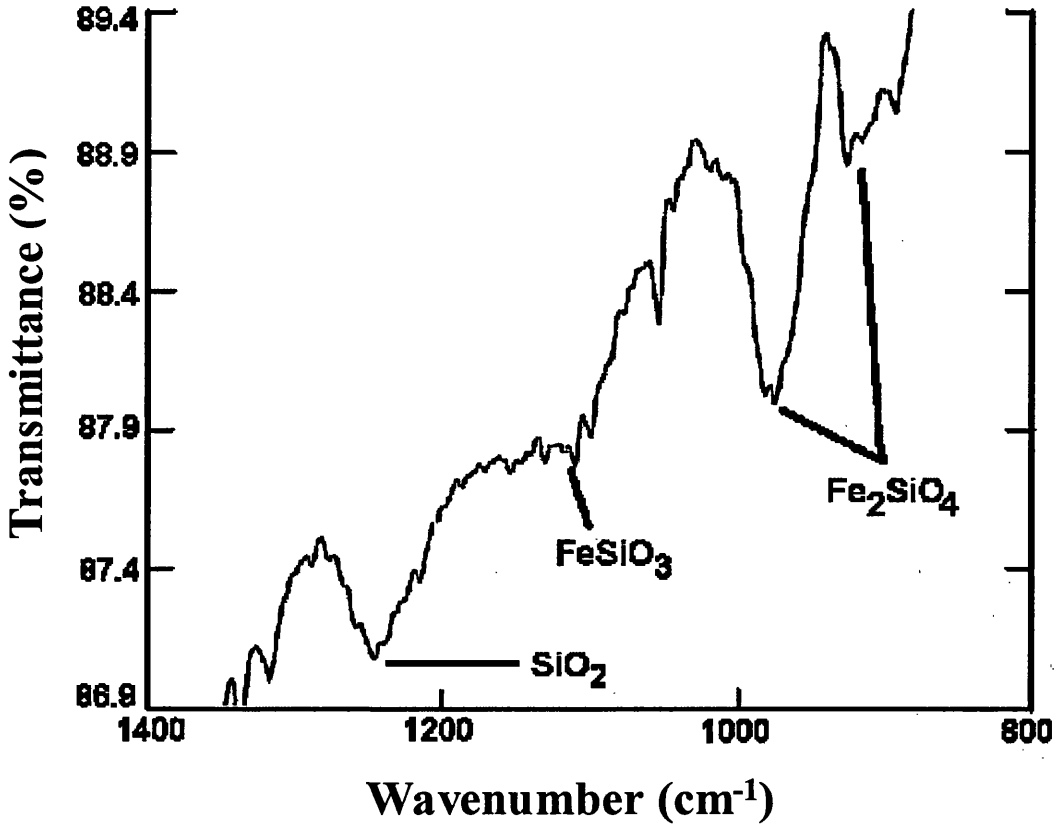

Figure 4.13: Spectrum obtained from Japanese material [31].

As mentioned previously, it is the grazing angle attachment that determines the angle at which the radiation is incident upon the surface of the sample; as the incident beam is varied towards being perpendicular to the sample, the greater the penetration depth of the radiation.

To investigate the effect of varying the angle of the incident radiation, apparatus containing a variable grazing angle attachment was utilised to further investigate the potential for FTIR analysis of the oxide layer. This piece of equipment enables the angle of incidence to be varied between over the maximum range possible (i.e. theoretically from 0^{o} to 90^{o} with respect to the sample surface). This work is covered in Section 4.4.

4.4 Analysis of the Decarburisation Oxide Layer Using a Variable Grazing Angle Attachment

4.4.1 Introduction

In this chapter, the FTIR technique has been evaluated in an attempt to establish the potential for analysis of the oxide layer formed on the surface of the strip during the decarburisation process.

The FTIR apparatus at Orb possesses two attachments for the analysis of flat steel samples. These are a standard attachment, which provides an angle of incidence of 26.5^{o}, and a separate attachment with a grazing angle of 80^{o}.

Work has shown that the standard attachment is unable to provide useful spectra as there are no clear bands observed. Use of the fixed grazing angle attachment (80^{o}) has shown that only fayalite is detected, suggesting that only the uppermost section of the oxide layer is analysed. Therefore it was necessary to utilise the FTIR apparatus

based at Swinden Technology Centre (STC), as this was complete with a variable grazing angle attachment.

The use of the variable grazing angle attachment allows the angle at which the infrared radiation is incident upon the sample surface to be varied, thereby altering the depth of penetration into the layer. It is envisaged that this would enable all the compounds contained within the oxide layer to be detected by the FTIR apparatus, with evidence of all of these compounds evident on the same spectrum. An investigation was carried out at STC to establish the effectiveness of this technique.

4.4.2 Set-up of Experimental Apparatus

The grazing angle attachment can be seen in Figure 4.14. It has the potential to theoretically vary the angle at any interval between 10^{o} and 90^{o} (with an error of $\sim 0.5^{o}$), although angles greater than $\sim 85^{o}$ prove difficult in practice. Adjusting the height of two mirrors, made possible by rotating the two 'arms', varies the angle. For the apparatus to function correctly, it is necessary that the angle to the vertical must be equal for both of the arms. An angle of 10^{o}, with the arms in an almost vertical position, gives the maximum infrared penetration depth, and a setting of 90^{o} gives the minimum penetration. The variation in angles is shown in Figure 4.15.

Figure 4.16 shows the plan view of the spectrometer set-up, indicating the path of the infrared radiation as it passes through the apparatus from source to detector.

Before any meaningful spectra could be acquired, it was necessary to calibrate the apparatus. With the aid of an in-built computer program, this was easily achieved simply by obtaining a spectrum of the background. For this investigation, the standard sample used during calibration was stainless steel. This would be sufficient

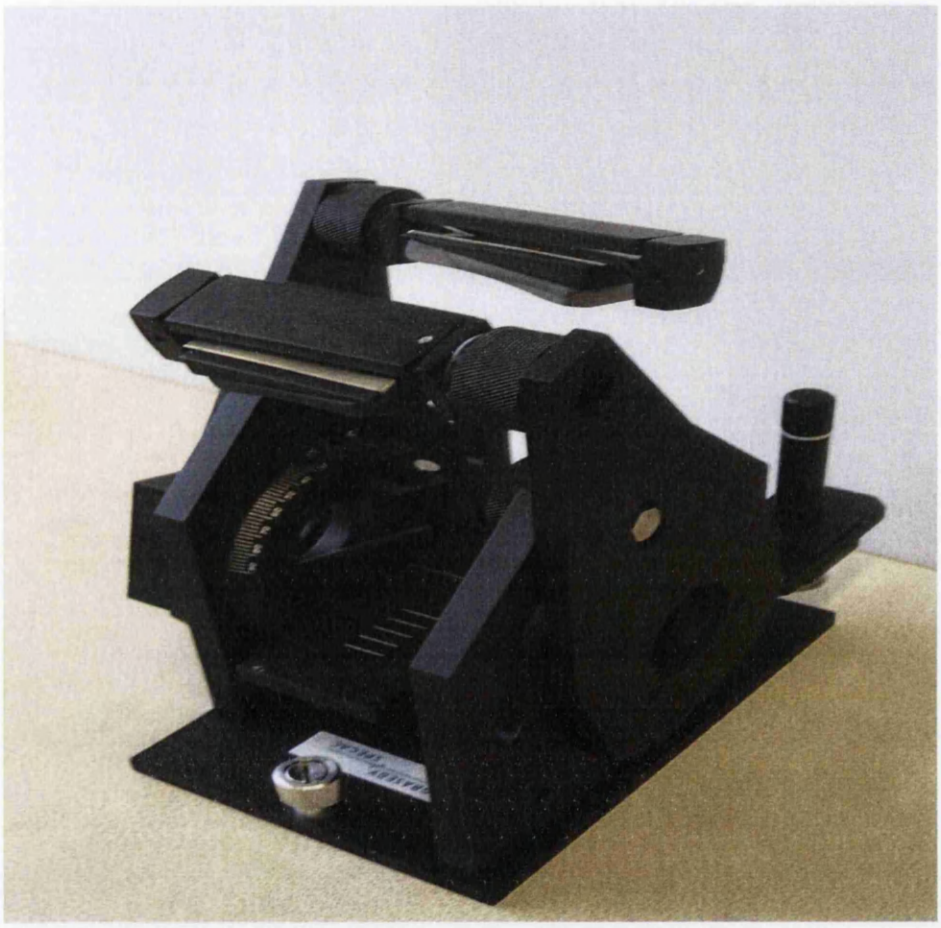

Figure 4.14: Photograph showing the grazing angle apparatus located at Swinden Technology Centre.

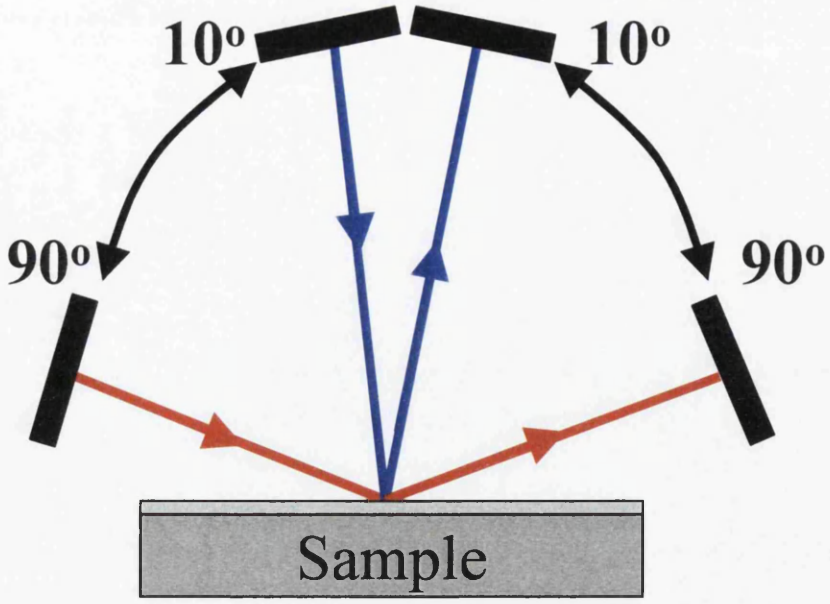

Figure 4.15: Variation of angles, enabled by moving 'arms'.

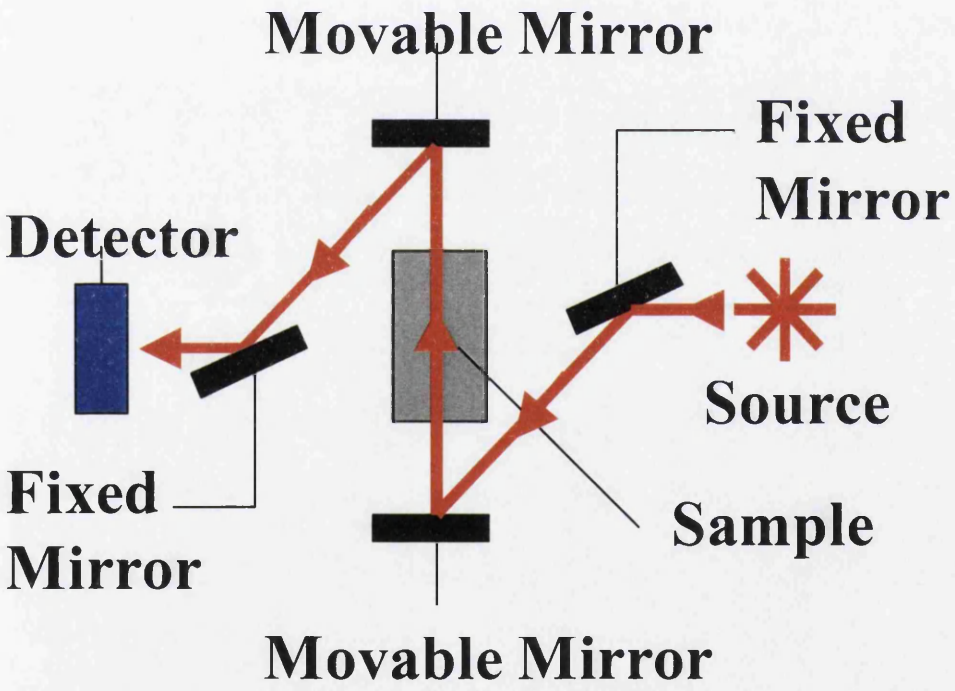

Figure 4.16: Plan view of the spectrometer set-up.

for this work, as all the spectra were to be used in comparison with one another. However, for any future quantitative work it would be beneficial to use a sample of plain (i.e. uncoated) electrical steel.

The calibration was repeated during regular intervals throughout the investigation to minimise any variation in sampling conditions.

Initially, 32 scans were performed to produce each separate spectrum. This would give a high degree of accuracy, but seemed excessive as the number of scans believed to be adequate for the Orb apparatus is 3 (see also Section 4.2.4.1). Using a setting of 32 scans was also very time consuming, considering the number of samples to be analysed. It was decided to reduce the number of scans to 16. To determine whether this would have an effect on the spectra produced, two spectra were obtained from the same area of a common sample, one with 16 scans, and one with 32. The two resultant spectra were compared, and it was found that the difference between them was negligible. These spectra can be seen in Figure 4.17, in which it is difficult to distinguish between the two spectra due to their high degree of similarity. Therefore, it was decided to proceed through the investigation with the reduced number of 16 scans, as this would allow more samples to be analysed without compromising on accuracy. It should be noted that these spectra are measured in absorbance instead of transmittance, as this was the preferred method at STC and was recommended by personnel experienced in the use of this particular piece of equipment. This scale was used for all subsequent spectra obtained from this apparatus.

In this instance, the two methods of analysis are very similar, except that it is the peaks that are of note when looking at a spectrum measured in absorbance, instead of the troughs when transmittance spectra are observed.

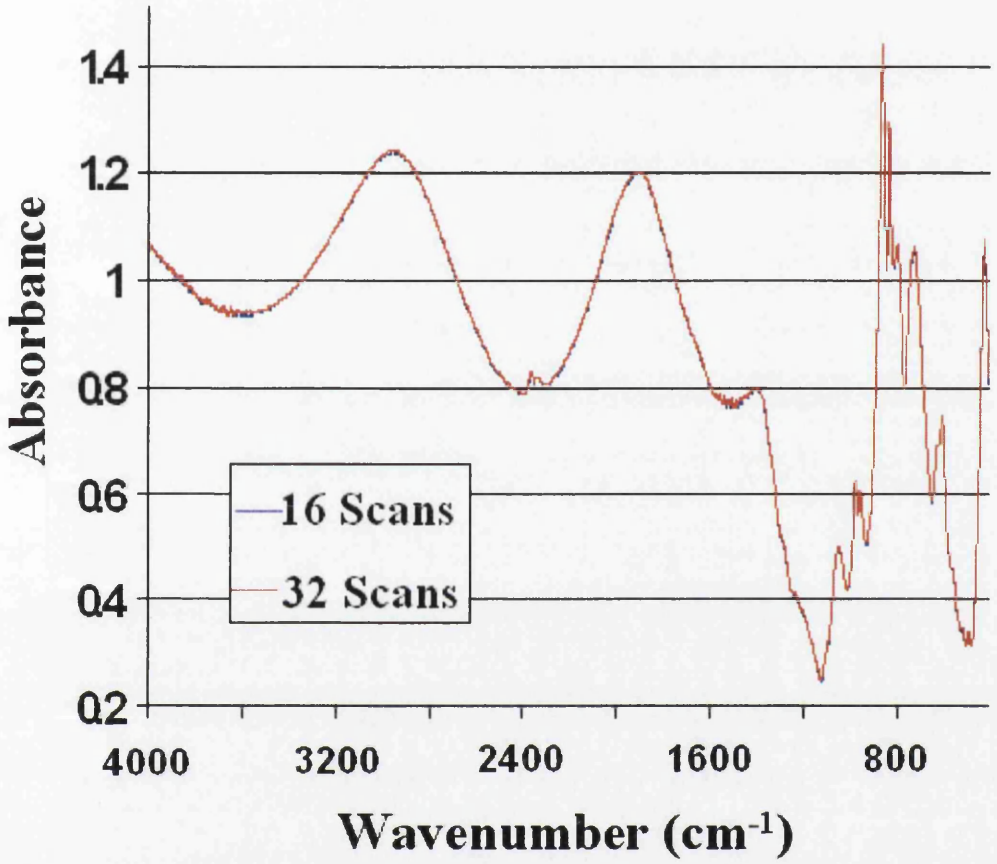

Figure 4.17: Comparison between 32 and 16 scans.

Another parameter to be considered was the strength of the signal received by the detector. As the angle was varied, the power of this signal can also vary, even if the remainder of the set-up remains unchanged. Therefore, each time the angle was varied, one of the 'fixed' mirrors was adjusted in very small increments using a sensitive screw-thread mechanism. This altered the intensity of the signal, which was depicted by a waveform on the computer display. It was therefore possible to ensure the optimal signal was used for each sample.

4.4.3 Experimental Procedure

A strip sample was obtained from the decarburisation line following a standard production run, and cut to an appropriate size for analysis. The magnesia (MgO) coating was brushed off, and the surfaces were cleaned with acetone. Once the sample was correctly positioned in the apparatus, the grazing angle was varied in 5° intervals between 85° and 10°. This should alter the depth of penetration of the radiation, which will ideally enable both the fayalite and silica layers to be detected at the same time.

Both the top and bottom surfaces of the sample were analysed to discover the levels of variation between the two surfaces.

4.4.4 Results and Discussion

The resultant spectra are displayed in Figure 4.18. Although spectra were obtained at every 5°, only spectra at intervals of every 10° are shown for clarity. It can be seen that these spectra followed a clear trend at higher angles, and the spectra at 5° intervals also agreed with this.

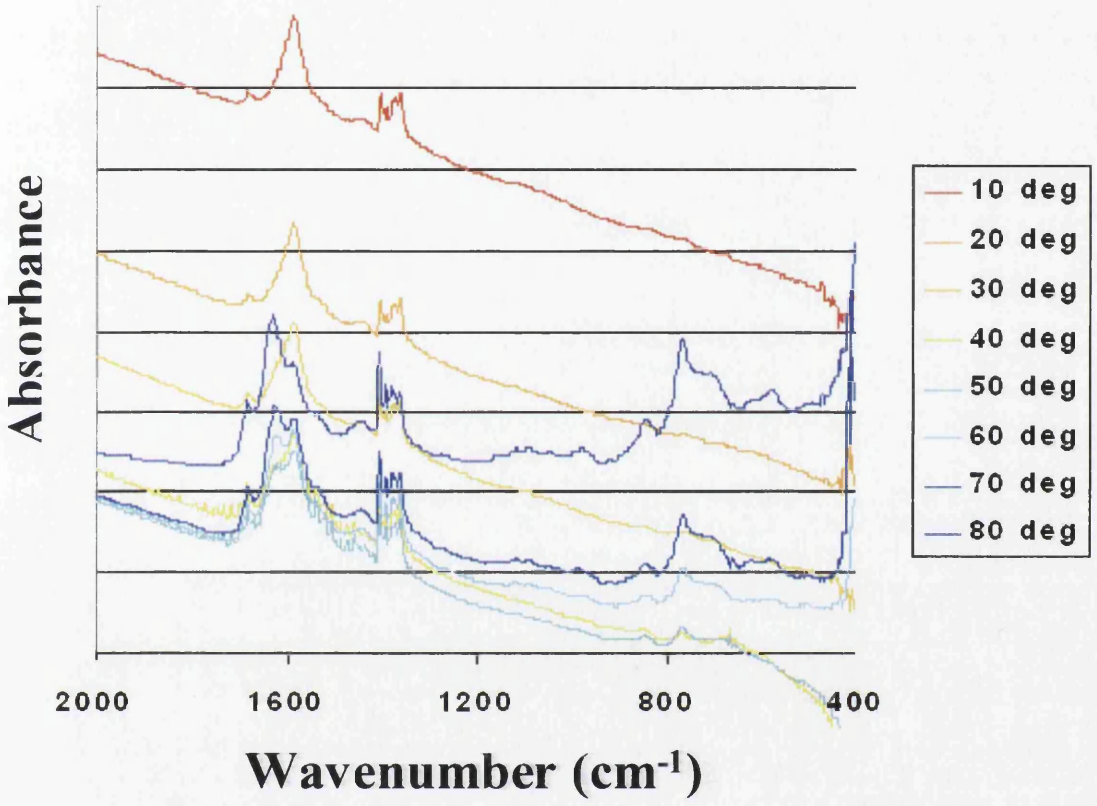

Figure 4.18: Grazing angle assessment of decarburisation oxide layer.

There are very obvious absorption bands that can be seen on each of the spectra. These correspond with the approximate wavenumber regions of 1600cm^{-1} and 1350 - 1400cm^{-1}. The reasons for the presence of these bands is unknown, as they do not relate to any of the bands expected from researched literature, and have not been evident on the spectra obtained from the FTIR apparatus at Orb Works.

Further bands began appearing in the 50° spectrum, and increased in magnitude as the angle increased. The main band was at ~750cm^{-1}, with smaller bands either side at approximately 600cm^{-1} and 850cm^{-1}. Again, these wavenumbers do not correspond with those expected.

4.4.5 Conclusions of Section 4.4

The results from these spectra appear to be incorrect, as the spectra seen do not correspond with any of the compounds expected. It was thought to be possible that the bands seen in all of the spectra could be related to the acetone that the samples were cleaned with prior to analysis. However, the sample was left to stand for a number of minutes prior to this analysis, in which time all traces of the acetone should have evaporated. Acquiring the spectrum for acetone confirmed that there was no link between this substance and the bands that were observed.

The spectrum for MgO was also obtained, as it was possible that traces of this may have remained, but none of the bands corresponded, ruling this compound out as the source of any of the bands.

It appears most likely that the unexpected results are be related to a change in the apparatus, although the position of the bands should remain constant. It was the same oxide layer being analysed, and this discrepancy could not be due to the sample under analysis. Therefore, contamination of the analysis chamber appears to be the only

plausible explanation. This hypothesis is also supported by the bands appearing to be almost identical in each of the spectra, suggesting that the contamination is at a constant level.

One interesting aspect of these results is the variation seen with the changing grazing angle. There is a clear increase in the size of band at approximately $750cm^{-1}$, suggesting that increasing the angles results in the compound responsible for this band being detected to a greater extent. However, this result also suggests that more of this compound is detected as the penetration depth decreases, suggesting that this unknown compound is found primarily on the very top surface of the oxide layer. From these results, it can be concluded that the layer responsible for this band is very thin, and requires the path of the radiation through the layer to be of a certain length before it registers on the spectrum. This path would increase in a thin top layer as the direction of the radiation got closer to the flat surface.

It is possible that this compound is a secondary oxide layer formed on the decarburisation layer in the time between taking the sample from the line and analysing it. However, it would be expected that any layer such as this would have been observed on the FTIR apparatus based at Orb Works.

The FTIR technique is most commonly used for the analysis of organic compounds, as many difficulties are experienced when looking at inorganic matter. It appears that these compounds are simply not suited to being analysed using this technique.

As these results have shown to be inconclusive, a further method was sought to establish a way of analysing a greater depth of the oxide layer to ascertain whether silica is in fact present in the decarburisation oxide layer. It appears that there is no

method of doing this in a non-destructive manner. Therefore, it was decided that a further investigation should be carried out to discover the effect of partially pickling the decarburised material to remove the uppermost part of this layer. This work is discussed in Section 4.5.

4.5 Effects of Pickling on FTIR Spectra Obtained

4.5.1 Introduction

It was found that it was not possible to analyse the full depth of the decarburisation oxide layer using FTIR, when utilizing either the standard FTIR apparatus with fixed grazing angle at Orb Works or the maximum range of the variable grazing angle attachment located at Swinden Technology Centre. This was proven by the absence of silica bands on the spectra obtained. It was therefore necessary to develop a method that would allow the infrared radiation to access the lower reaches of this layer.

As the previous investigation had exhausted the available non-destructive methods, it was necessary to devise a way of removing the very topmost surface of the oxide layer. An investigation was carried out using brief acid pickling to achieve this.

4.5.2 Experimental Procedure

Sample J20254 was acquired from the end of the decarburisation line at Orb Works and brushed free of MgO. Both sides were then analysed using the 80^{o} grazing angle attachment on the FTIR apparatus at Orb, previously found necessary to observe the bands relating to fayalite. The sample was then pickled, following the standard pickling procedure used by the Chemistry Laboratory, for 10 seconds in a mixture of

sulphuric and hydrofluoric acid, which was heated to approximately 50°C. Once removed from the acid, the sample was rinsed with water and thoroughly dried using a hot air dryer. When pickling for such a short duration, only the very top of the surface oxide layer should be etched away, leaving further parts of the layer exposed. The sample was then analysed on the same FTIR apparatus to show the effect of pickling on the spectra obtained. It was envisaged that the pickling would cause a thinning of the fayalite, possibly allowing the infrared radiation to penetrate into the region occupied by silica.

4.5.3 Results and Discussion

The spectra obtained using the FTIR apparatus both before and after the brief acid pickle are shown in Figure 4.19.

It was expected that the spectrum of the pickled sample would be similar to the spectrum obtained from the sample in its pre-pickled state, with the bands decreasing in size slightly as the amount of oxide layer was reduced. Hopefully, evidence of silica would also be present.

It was also thought that there might also be some extra bands due to traces of the pickling acid that had not been fully rinsed from the surface and/or rust that may have formed following the sample being dried.

However, the spectra generated after pickling showed no signs of the three main bands that had previously been linked to the oxide layer (Figure 4.6). There were however two very large bands at approximately 500 cm^{-1} and 1200 cm^{-1}. These bands approximately coincided with the wavenumbers at which SiO_2 was expected to be found [31]. There was also a smaller band at ~825 cm^{-1}. Spectra obtained from [32] suggest that this is related to SiO_2, although the same spectra show the main silica

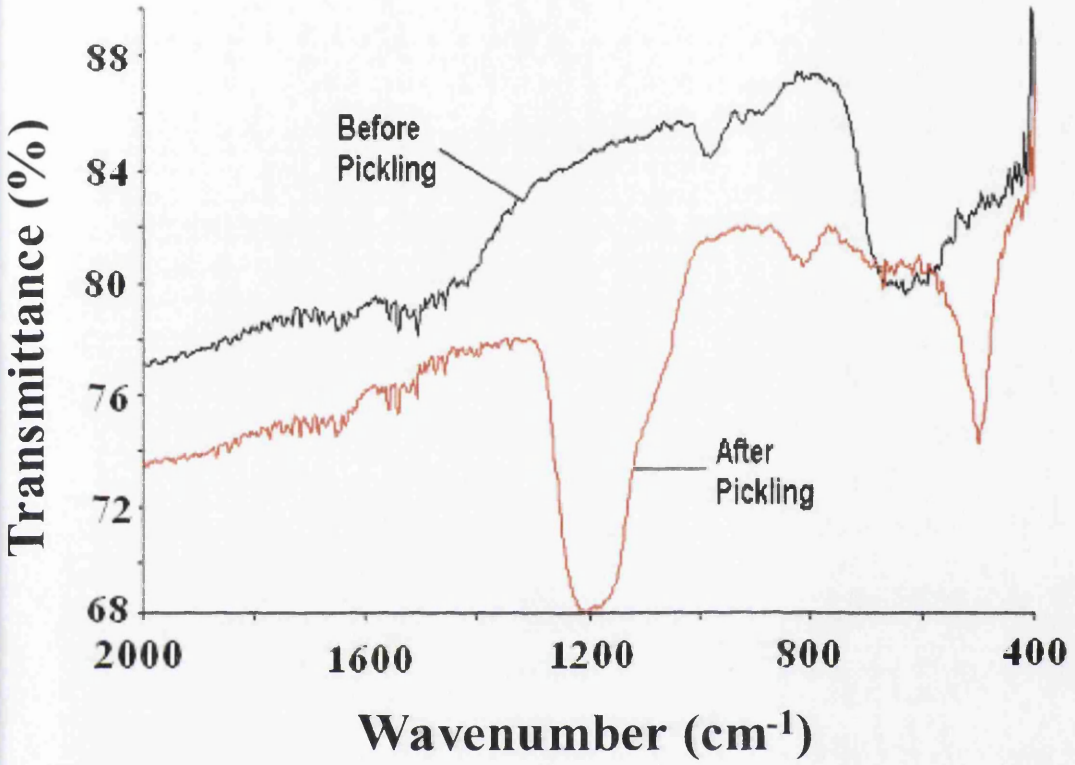

Figure 4.19 - FTIR spectra of pickled and non-pickled samples.

band at a slightly lower wavenumber than seen here (1130 cm^{-1} compared to 1200 cm^{-1}). However, from previously acquired knowledge relating to this oxide layer, it is inconceivable that the substance observed here would be anything other than silica.

4.5.4 Conclusions of Section 4.5

The infrared trace for the pickled sample, showing obvious bands relating to silica, confirms that the infrared radiation has not been able to penetrate the full depth of the oxide layer when a standard grazing angle attachment has been used. It also validates the theory that the oxide layer generally consists of a silica-rich layer directly adjacent to the steel, with a fayalite-rich layer on top. This layering effect has previously been observed under a microscope many years previously, but had not been confirmed at the exact processing conditions currently used.

Although it had been expected that the spectra obtained would be of the entire oxide layer, and that the spectra from before and after pickling would be somewhat similar, it can now be concluded that the infrared radiation is unable to penetrate the fayalite that is present on the top of the oxide layer.

Although these results have given an insight into the capabilities of the FTIR apparatus, it was considered necessary to carry out a further investigation, with spectra being obtained at smaller pickling intervals. This would enable the transition from the fayalite rich layer to the silica rich layer to be seen in more detail. It was decided that it would be best to do this by combining this investigation with another technique that is currently being developed, known as the Electrochemical Potential

(ECP) method. This method is detailed in Chapter 5, and combined with the FTIR technique in Chapter 6.

Chapter Five

Electrochemical Potential (ECP) Analysis of the Decarburisation Oxide Layer

5.1 Introduction

It is well known that the composition and thickness of the layer formed during the decarburisation process of grain oriented electrical steel has a direct influence on the glass film formed during the subsequent high temperature coil anneal. For example, the magnesia can react with both silica and fayalite contained in the oxide layer to form the forsterite glass film. However, the insulating properties of this layer will be improved if the reaction involves silica, as the reaction with fayalite will leave conductive iron as a by-product.

Due to these effects, it was considered necessary to evaluate the oxide layer of samples produced on the decarburisation lines at Orb Works to determine the consistency of the composition. It is highly desirable that the oxide layer is consistent from one coil to another, and also across the width of the strip, in terms of both thickness and composition. Unfortunately, the extent of this consistency is currently unknown. A greater understanding of the degree of variation would lead to an improved confidence in the product and is vital for good quality control.

In the future, it is likely to be considered necessary to carry out investigations into the magnesia slurry, and other parameters that may affect the quality of the resultant glass film. In order to do this, it will be necessary to ensure the starting material is the same, and has a consistent oxide layer. Otherwise, any effects seen may be attributable to unknown changes in the oxide layer.

The Electrochemical Potential (ECP) method of analysis has previously been developed to evaluate the oxide layer produced during the decarburisation process [34-39].

The cause of any variation in the oxide layer could be due to a number of factors, ranging from differences in the underlying steel throughout the length of the coil, to variable heat transfer across the strip width from the burners in the furnace. This investigation aims to examine the variation in the oxide layer both along the length and across the width of the strip. This should be seen by observation of the changes occurring in the ECP profiles relating to samples that have been selected from different areas of the strip. The potential difference between the sample and a reference electrode, measured against time for each sample, will vary due to the dissolution of the surface oxide layer on the steel surface. The resultant ECP profiles are therefore likely to be indicative of both the thickness and composition of the layer and give a 'fingerprint' of the layer.

A detailed description of the electrochemical potential technique was provided in Section 2.2.2.

5.2 Experimental Procedure

A large sheet of material measuring approximately 2.3m in length and of strip width (~950mm) was taken from the end of coil H77538 after being processed on the D4 decarburisation line at Orb Works. This was then cut into smaller samples suitable for electrochemical potential (ECP) analysis. These samples measured 130mm x 50mm.

Each sample was given an identification number so that its position from within the original sheet could be easily determined.

The following grid shows the way in which the samples were labelled on a section of the sheet.

A1	A2	A3	A4	A5	A6
B1	B2	B3	B4	B5	B6
C1	C2	C3	C4	C5	C6
D1	D2	D3	D4	D5	D6
E1	E2	E3	E4	E5	E6

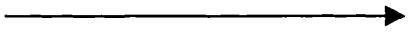

Rolling direction

Samples were selected which corresponded to both columns 2, 6,9,12 and 15, and to rows A, F, K, Q and V (i.e. A2, A6.....F2, F6 etc.). This gave a large number of samples over the whole area of the sheet, and therefore enabled trends to be identified both along the length and across the width of the sheet.

The standard ECP procedure (described in Section 2.2.2) was followed. This involved immersing both the sample and the reference calomel electrode in 5% sulphuric acid at 70°C for a duration of 20 minutes. The apparatus used can also be seen in Figure 2.5.

The desired temperature is achieved by placing the beaker of acid into a heated water bath. To ensure the temperature of the acid remains uniform throughout, it was stirred with a mechanical glass stirrer at a speed of 266 r.p.m.

The temperature of the acid was checked at regular intervals using a standard thermometer. The temperature variation during the course of a series of measurements was noted to be within ±0.5°C.

The acid was replaced after every 6 samples, as it has been shown previously that further use would lead to the possibility of incorrect results [34] due to degradation of the acid.

A precise area of the sample was covered with an acid-proof tape to ensure a consistent area of each steel sample was exposed to the acid (70mm x 50mm). The area of the sample above the tape (10mm x 50mm) was abraded to remove the oxide layer to ensure good electrical contact when it was clamped into place.

The reference electrode was a mercury / calomel electrode. This electrode was placed in the acid at least 90 minutes prior to each set of experiments to allow it to stabilise. It was suggested by Chemistry Laboratory personnel, experienced in the use of these electrodes, that this should eliminate the need for a sacrificial test sample.

5.3 Results and Discussion

5.3.1 General Shape of ECP Profiles

The ECP computer program takes a reading of the potential difference between the two electrodes every 5 seconds throughout the 20-minute duration of each test. This data can then be transferred into a Microsoft Excel file, enabling an ECP profile to be generated by plotting the potential difference against time.

The plotted profiles were found to be similar for each sample, but small features allowed them to be categorised into four groups, shown in Figures 5.1 – 5.4.

It can be seen in Figure 5.1 that the potential difference drops until it reaches what can be described as a trough (t_1, v_1). At this point it begins to increase to a peak (t_2, v_2) before falling off steadily and levelling out to a 'baseline'. This is the general trend seen in an ECP profile. The profile shown in Figure 5.1 shows what is described as a 'Type 1' curve. If the profiles in Figures 5.1 and 5.2 are compared, it can be seen that a difference is clearly evident. In Figure 5.1, the value for v_1 is at a different level to the baseline where the trace levels out, but in Figure 5.2 these points are at a similar level. This is defined as a 'Type 2' curve.

Another difference can be seen in Figures 5.3 and 5.4 where a smaller second peak can be seen between the first peak and the baseline. This feature occurs both when the trough is at a different level to the baseline, and also when these two points are at the same level. These two profiles are categorised as Types 1a and Type 2a respectively.

The reasons for this variation need to be understood further, and the effect of this variation on glass film formation, if any, clearly needs to be established. Identifying and eliminating this variation should then allow consistent, optimum surface oxide and glass film layers to be produced.

5.3.2 Consistency of Material

It was considered that due to the way that the material is processed on the line, there should be less variation in processing conditions at the centre of the strip compared to

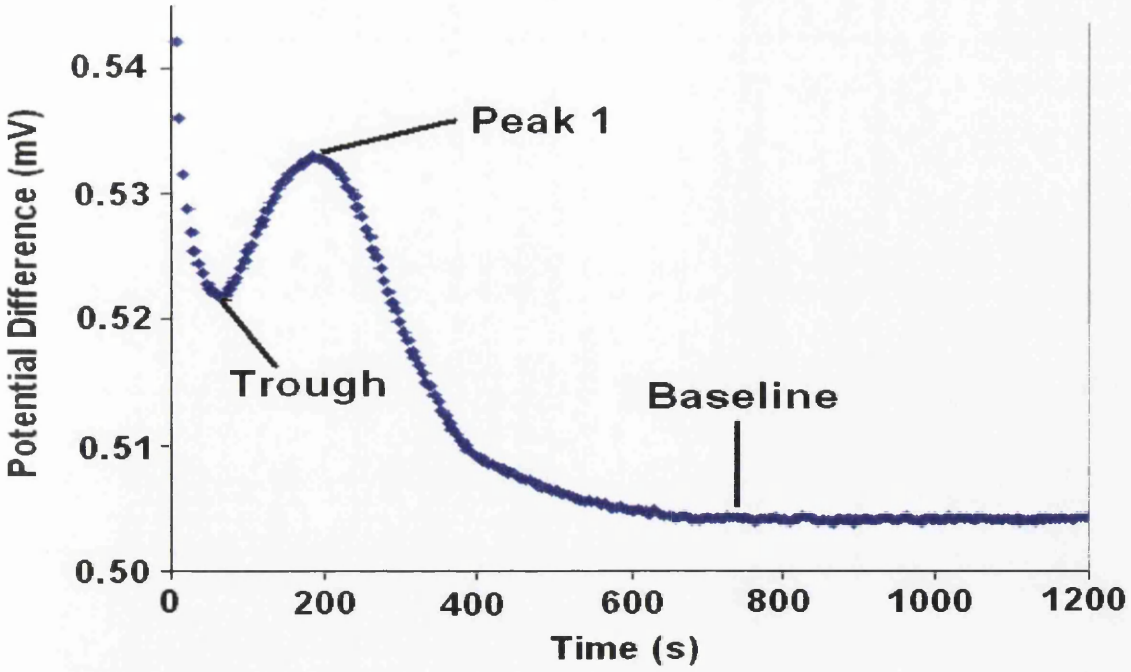

Figure 5.1: 'Type 1' ECP profile.

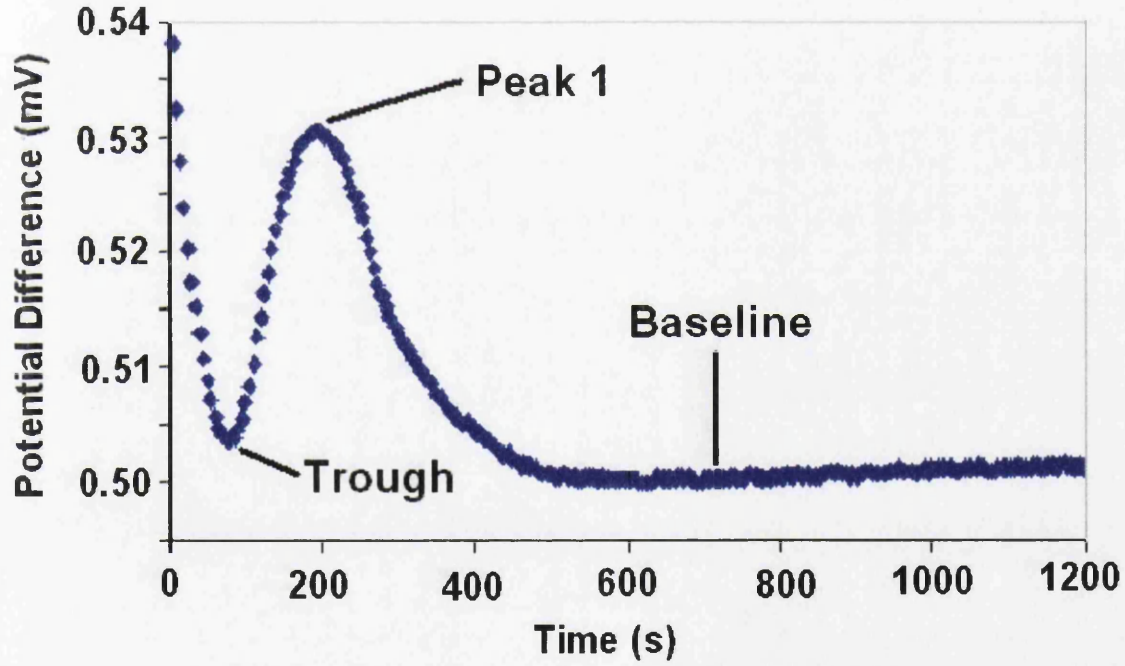

Figure 5.2: 'Type 2' ECP profile.

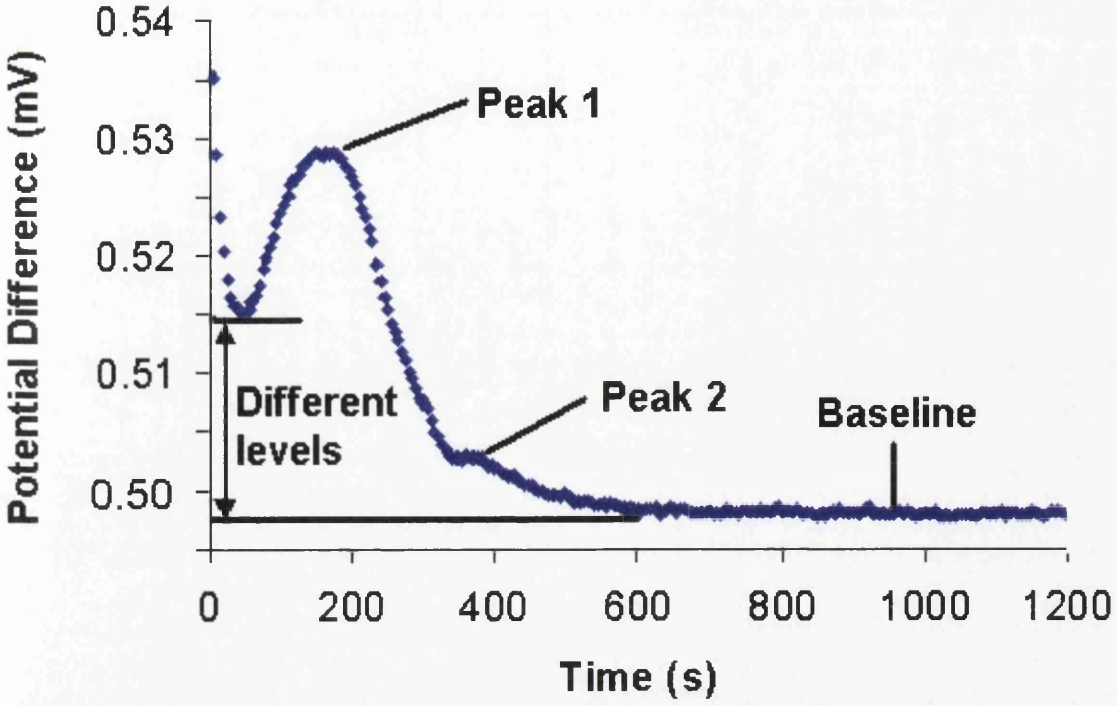

Figure 5.3: 'Type 1a' ECP profile.

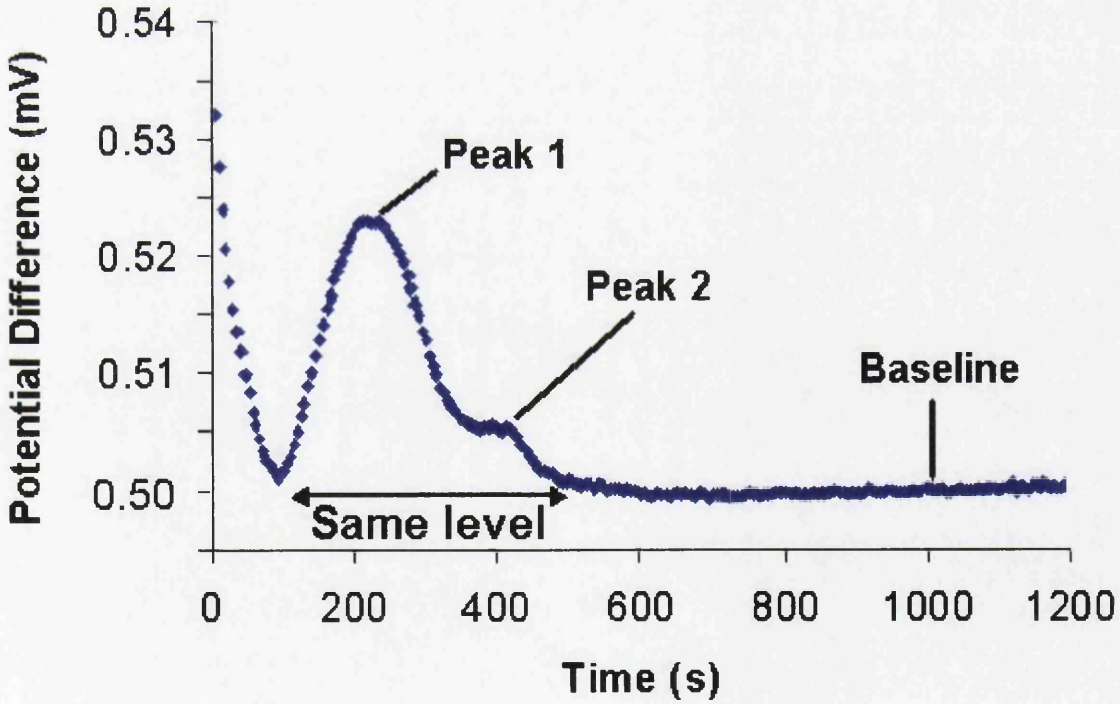

Figure 5.4: 'Type 2a' ECP profile.

the edges. For example, the edge burners utilised could have a large effect on the edge of the strip but may have little impact on the centre of the strip.

Observation of the burn-off oven indicates general turbulence in the oven and also a variation in the level of oil staining and contamination upon the strip surface. These effects could also result in a variable product, having an effect on all parts of the strip, not just at the edges.

The effect that this variability has on the oxide layer on the surface of the strip should clearly be shown by variations in the shape of the ECP profiles that are obtained.

The full set of ECP profiles obtained during this part of the investigation can be seen in Figure 5.5.

The characteristic parameters of each curve that were analysed were the time taken to reach the base of the trough (t_1) and the time taken to reach the first peak (t_2), along with the value of the potential difference at both of these points (v_1 and v_2 respectively).

The results are shown in Tables 5.1 and 5.2. The layout of these two tables shows the samples as they would have been seen on-line i.e. the columns are across the width and the rows are along the length of the strip.

The data seen in these tables is also shown graphically in Figures 5.6 – 5.13. It should be noted that the range of the y-axis (either potential difference or time, depending on the figure in question) has been kept constant for each parameter so that a direct comparison can be made. For example, it can be seen in Figures 5.6 and 5.7 that the range of both y-axes is from 45 to 85 seconds.

It can be seen that both parameters vary to a similar degree along both the length and the width of the strip. It was expected that one or both of the parameters might

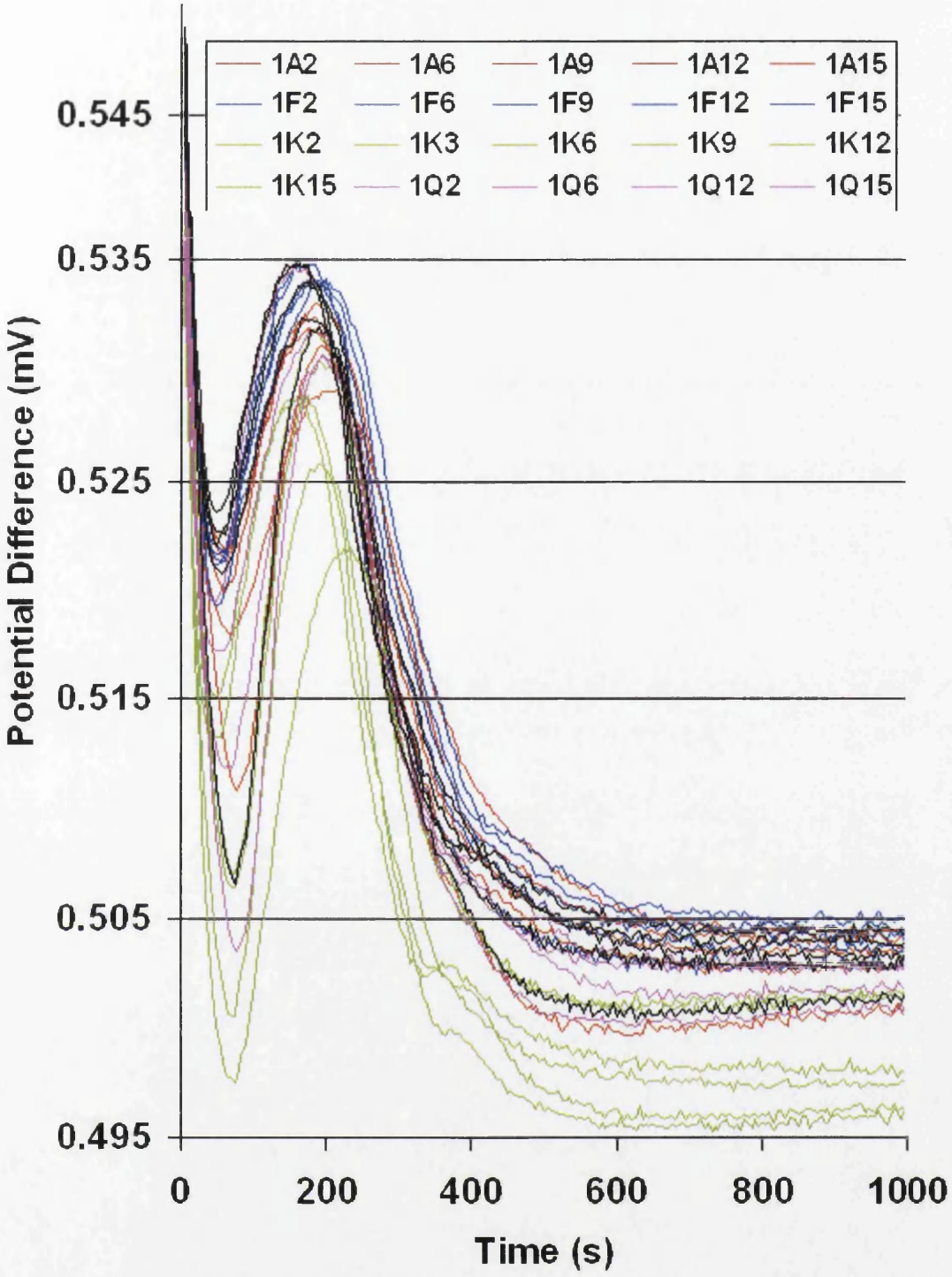

Figure 5.5: Full set of ECP profiles obtained for initial consistency assessment.

	Column 2		Column 6		Column 9		Column 12		Column 15	
	Trough	Peak	Trough	Peak	Trough	Peak	Trough	Peak	Trough	Peak
Row A	60	170	60	175	65	185	70	215	80	195
Row F	50	170	50	180	50	175	55	190	55	205
Row K	70	190	50	165	75	235	70	185	70	190
Row Q	80	195	50	155	----	----	60	195	60	180
Row V	75	190	55	180	50	160	50	160	55	175

Table 5.1: Time taken to reach trough and peak (seconds).

	Column 2		Column 6		Column 9		Column 12		Column 15	
	Trough	Peak	Trough	Peak	Trough	Peak	Trough	Peak	Trough	Peak
Row A	0.520	0.533	0.521	0.532	0.522	0.533	0.518	0.529	0.511	0.531
Row F	0.519	0.535	0.522	0.535	0.521	0.534	0.521	0.534	0.522	0.534
Row K	0.501	0.526	0.515	0.529	----	----	0.507	0.532	0.506	0.530
Row Q	0.504	0.531	0.519	0.535	0.498	0.522	511.8	0.531	0.517	0.532
Row V	0.507	0.532	0.521	0.532	0.522	0.535	0.524	0.535	0.523	0.534

Table 5.2: Potential difference at trough and peak (mV).

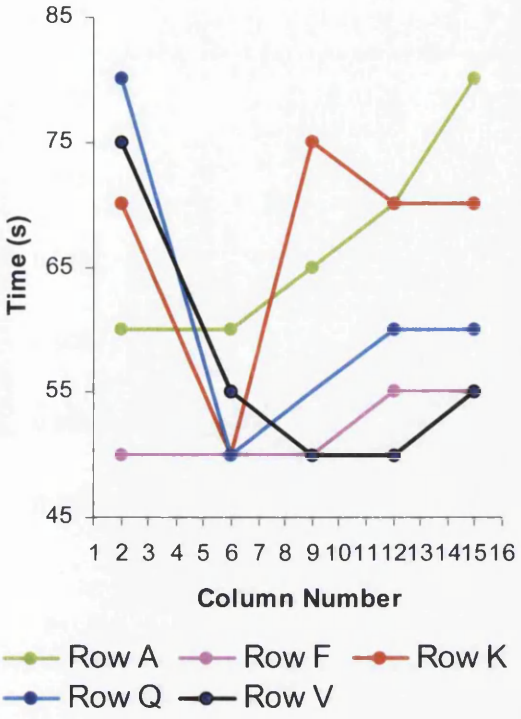

Figure 5.6: Time taken to reach the base of the trough (across the width).

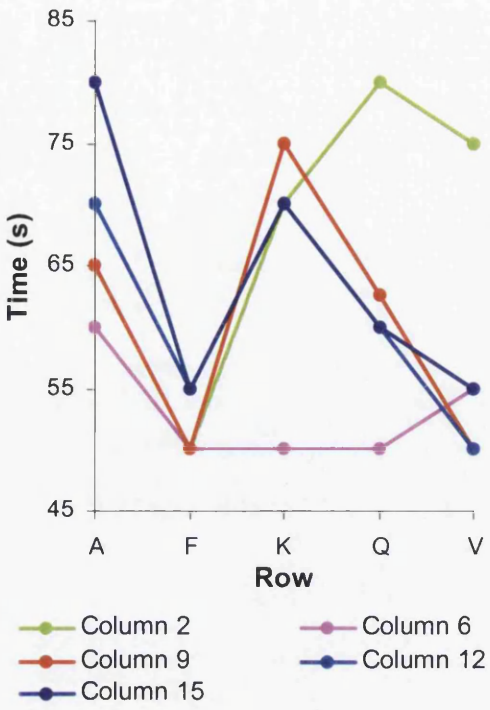

Figure 5.7: Time taken to reach the base of the trough (along the length).

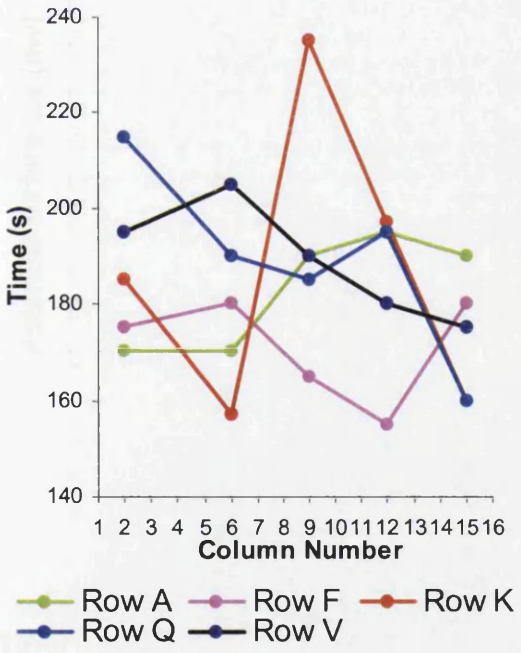

Figure 5.8: Time taken to reach the top of the peak (across the width).

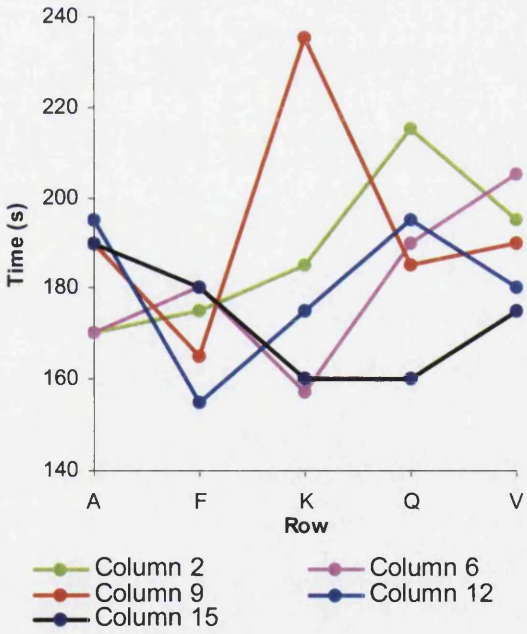

Figure 5.9: Time taken to reach the top of the peak (along the length).

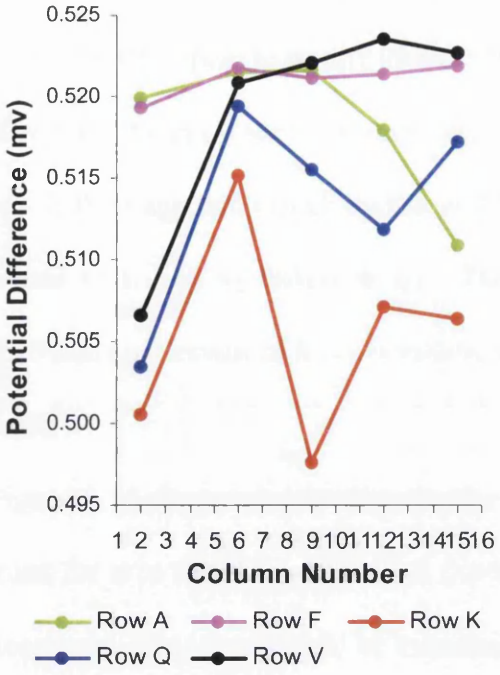

Figure 5.10: Potential difference at the base of the trough (across the width).

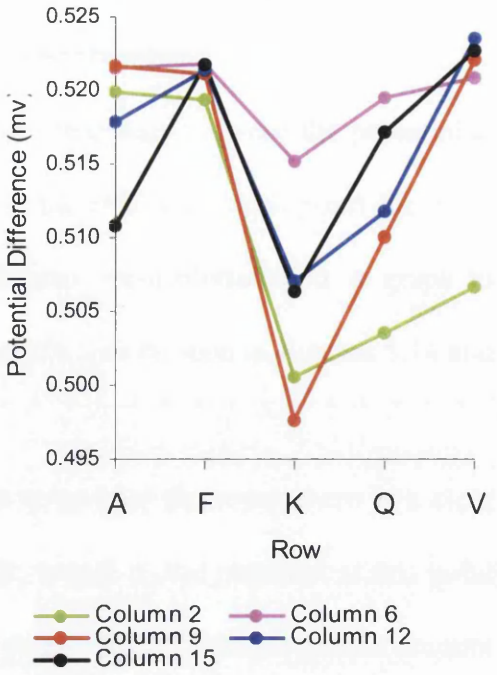

Figure 5.11: Potential difference at the base of the trough (along the length).

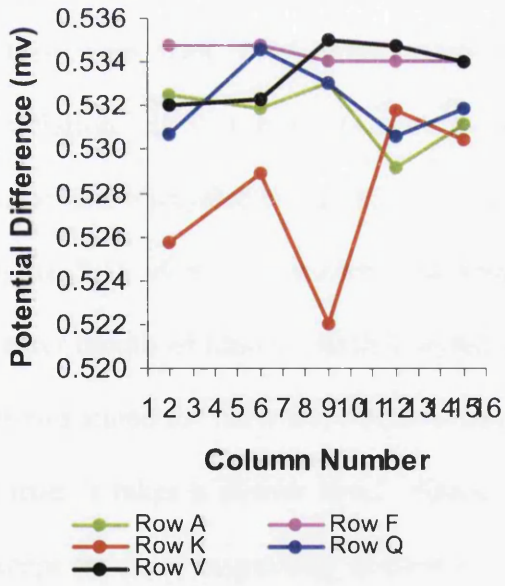

Figure 5.12: Potential difference at the top of the peak (across the width).

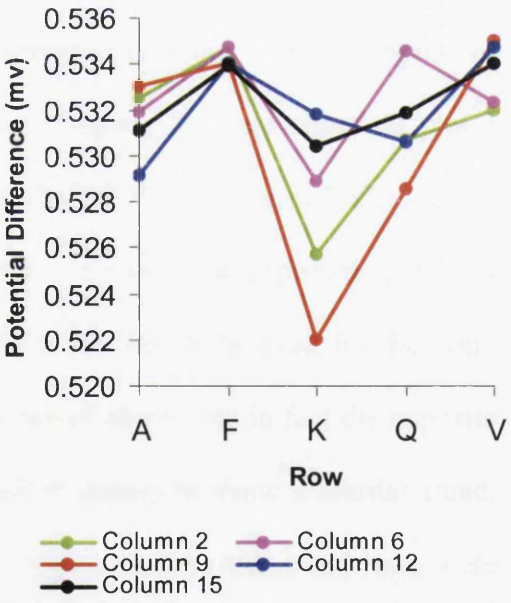

Figure 5.13: Potential difference at the top of the peak (along the length).

increase as the strip width was traversed, but this does not appear to be the case. There do not appear to be any obvious trends in either direction.

However, it can be seen that there appears to be a correlation between the potential at which the peak and trough appear and the time it takes to reach each point (i.e. v_1 is linked to t_1 and v_2 linked to t_2). These parameters were plotted onto a graph to determine the extent of this correlation and the results can be seen in Figures 5.14 and 5.15.

Figure 5.14 shows clearly that, for the samples in each of the rows, there is a clear trend for it to take longer to reach the base of the trough as the potential at this point decreases. This is as would be expected, as the potential has to drop a greater amount to get to the lower values and would therefore be expected to take longer.

The exception to this trend was the samples relating to Row F, but these points were in such close proximity to one another that a meaningful trend line could not be added. From the trend lines added to the data points for rows A, K, Q and V, the R^2 values were 0.86, 0.79, 0.90 and 0.96 respectively, showing a good degree of correlation. If all the points from each sample in Figure 5.14 are added to plot a single line, a correlation can still be seen, although the R^2 value drops to 0.62.

Figure 5.15 shows a somewhat surprising result. It would be expected to take a greater length of time to reach a higher potential at the top of the peak for the same reasons stated for the lower potential troughs discussed above, but in fact the opposite is true; it takes a shorter time. Again, all samples appear to show a similar trend, except for those originating in Row F. The R^2 values for the fitted trend lines were 0.75, 0.39, 0.58, 0.99 and 0.90 for rows A, F, K, Q and V respectively, with the R^2 dropping to 0.46 all these data points were plotted together.

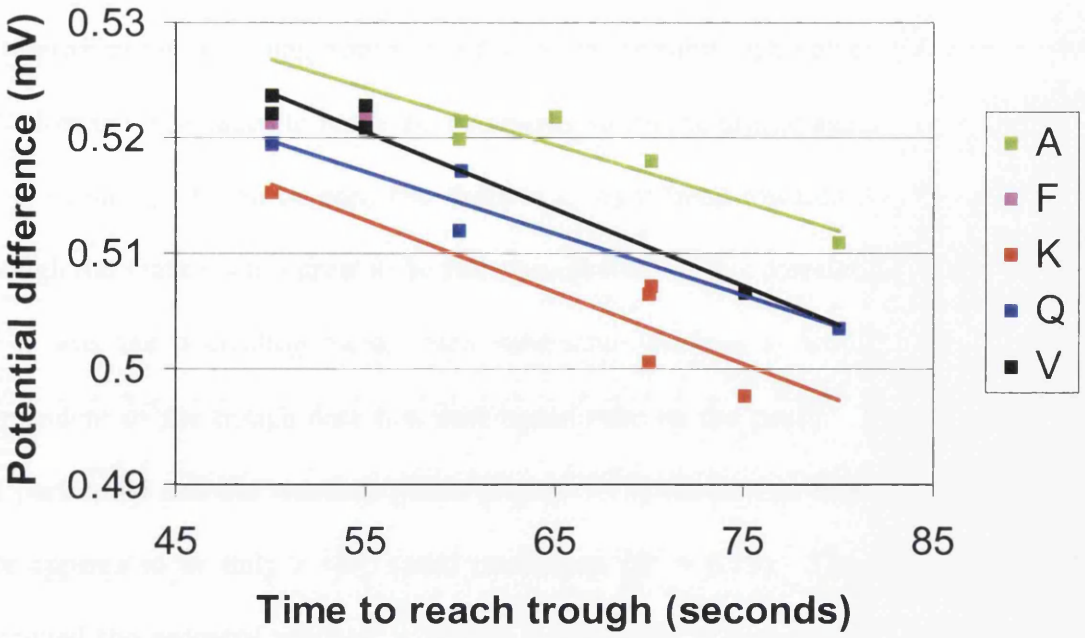

Figure 5.14: Correlation between the potential difference at the base of the trough and the time taken to reach that point.

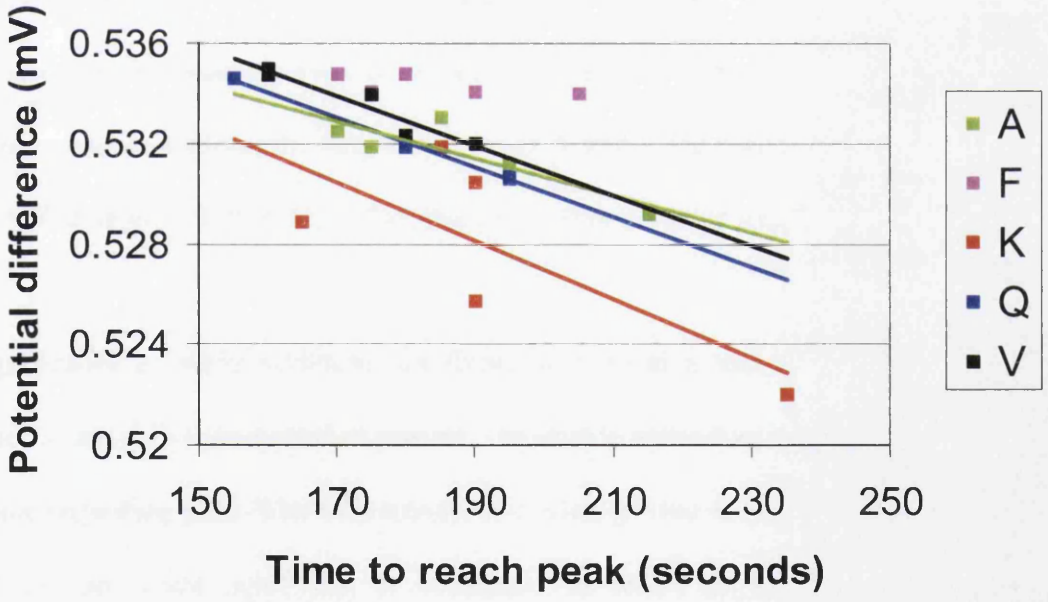

Figure 5.15: Correlation between the potential difference at the top of the peak and the time taken to reach that point.

It was considered that the value of t_1 might be an overriding factor, which would cause profiles taking a long time to reach t_1 to also exhibit high values for t_2. Figure 5.16 plots the time taken to reach the two positions on the profile against one another (i.e. t_1 versus t_2). It can be seen that there is a slight trend towards this ($R^2 = 0.46$) although the scatter is too great to be fully conclusive. If this correlation was correct, and t_1 was the overriding factor, then subtracting t_1 from t_2 would provide data independent of the trough data (i.e. data based only on the peak). This calculation was performed and the resultant graph (Figure 5.17) shows that this is incorrect, as there appears to be only a very small correlation ($R^2 = 0.19$). Therefore it can be concluded the potential reached at the top of the peak is independent of the 't_1-t_2' value.

It was observed that the 4 differently shaped curves (i.e. Types 1, 2, 1a and 2a) showed no clear pattern as to where they appeared on the strip. The position at which each type of profile was observed is shown in Table 5.3. Some rows seemed to be reasonably consistent along the length (e.g. rows A and F are predominantly Type 1, and Row K is mainly Types 2 and 2a), but there were no clear trends that were seen overall.

The significance of these variations on forsterite formation and ultimate magnetic properties in not fully understood at present. To enable authoritative investigations to take place regarding glass film technology, it is clearly vital to start with a uniform product i.e. an oxide layer that is consistent in terms of both thickness and composition. Even though the curves may not be fully understood at this stage, at least regions of uniformity may be highlighted to enable further analysis to take place.

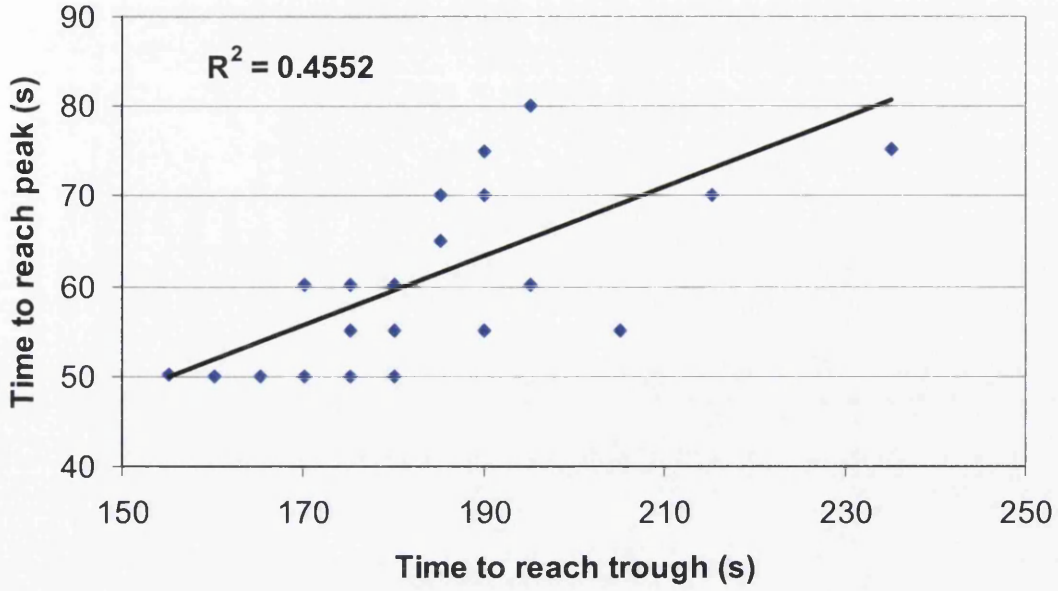

Figure 5.16: Plot of the time taken to reach the trough compared to the time taken to reach the peak.

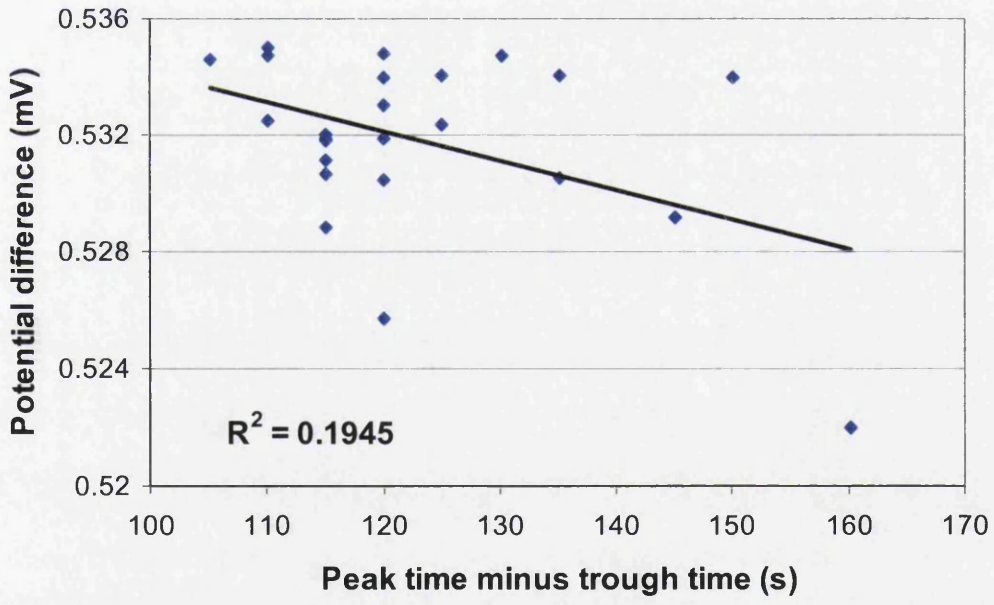

Figure 5.17: Plot of the time taken to reach the peak versus the potential at that point, independent of time taken to reach the trough.

	Column 2	Column 6	Column 9	Column 12	Column 15
Row A	**1**	**1**	**1**	**1**	**1 / 1a**
Row F	**1**	**1**	**1**	**1**	**1**
Row K	**2a**	**1a**	**2a**	**2**	**2**
Row Q	**2**	**1**	**----**	**1a/2a**	**1a**
Row V	**2**	**1a**	**1**	**1**	**1**

Table 5.3: Type of ECP profile at various positions on the strip Sample.

If it is not possible to locate regions of good uniformity, a broader than desirable band of variation may need to be tolerated until a more uniform product is produced.

5.3.3 Further Investigation Into Sample Consistency

The investigation was extended by using the ECP apparatus to analyse further samples. A majority of the remaining samples from row K and column 9 were chosen in order to gain a more detailed knowledge of the variations across the length and width of the strip.

The ECP profiles for the samples originating from Row K are shown in Figure 5.18. These are taken from along the length of the coil, in the middle section of the strip. Therefore, it expected that the profiles should show very little variance. It can be seen that the profiles vary significantly in terms of t_1, t_2, v_1 and v_2. Two of the profiles also exhibit evidence of the smaller second peak.

The variation in these profiles can also be seen in Figures 5.19 and 5.20. These show the time taken to reach the trough and the peak for each sample, and the values of potential difference at these points. It can be seen that both of these figures show what appears to be a random scatter around a mid-point, with no particular trends observed.

Similarly, Figure 5.21 shows the set of profiles obtained from the samples in column 9, and Figures 5.22 and 5.23 show the variation in the associated parameters.

It was expected that a significantly greater degree of variation would be seen across the width compared to along the length of the strip, but it can clearly be seen that there is a similar degree of variation in both directions. The data perhaps suggests

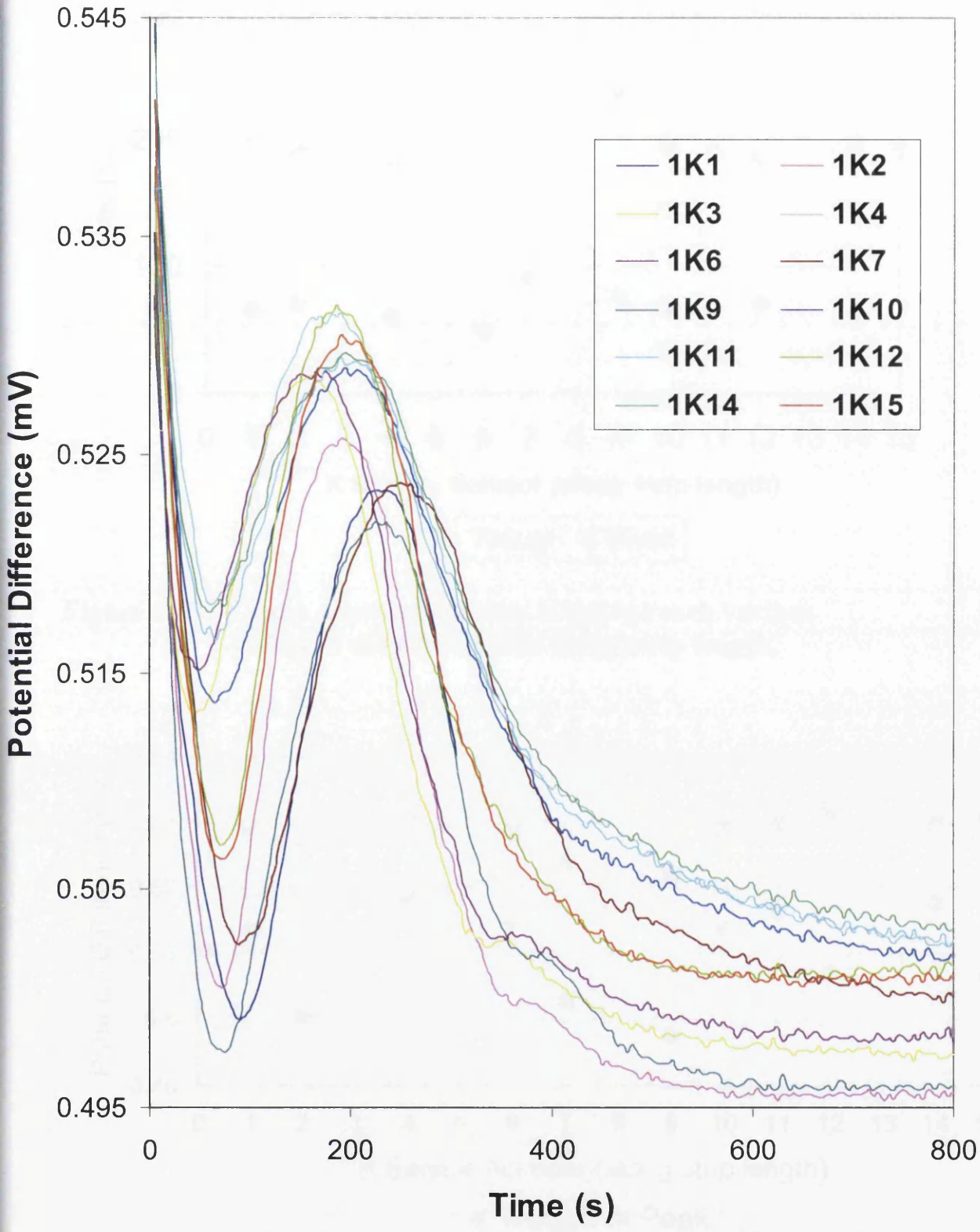

Figure 5.18: Graph showing variation in profiles along row K.

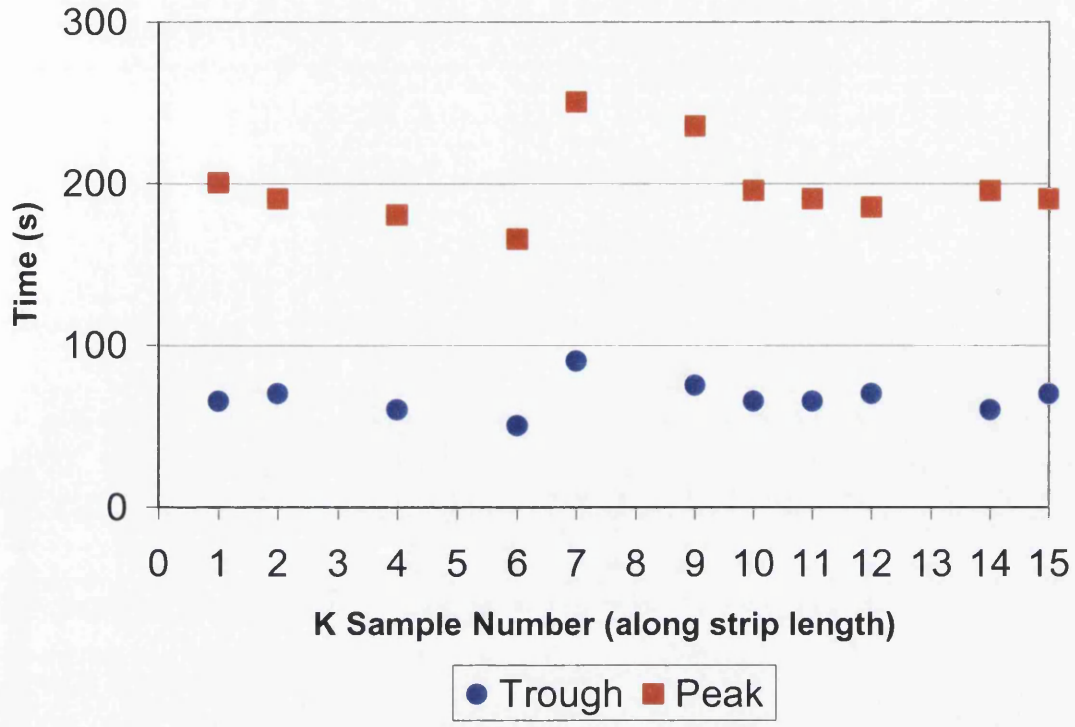

Figure 5.19: Graph showing the time taken to reach various points of the ECP profile along strip length.

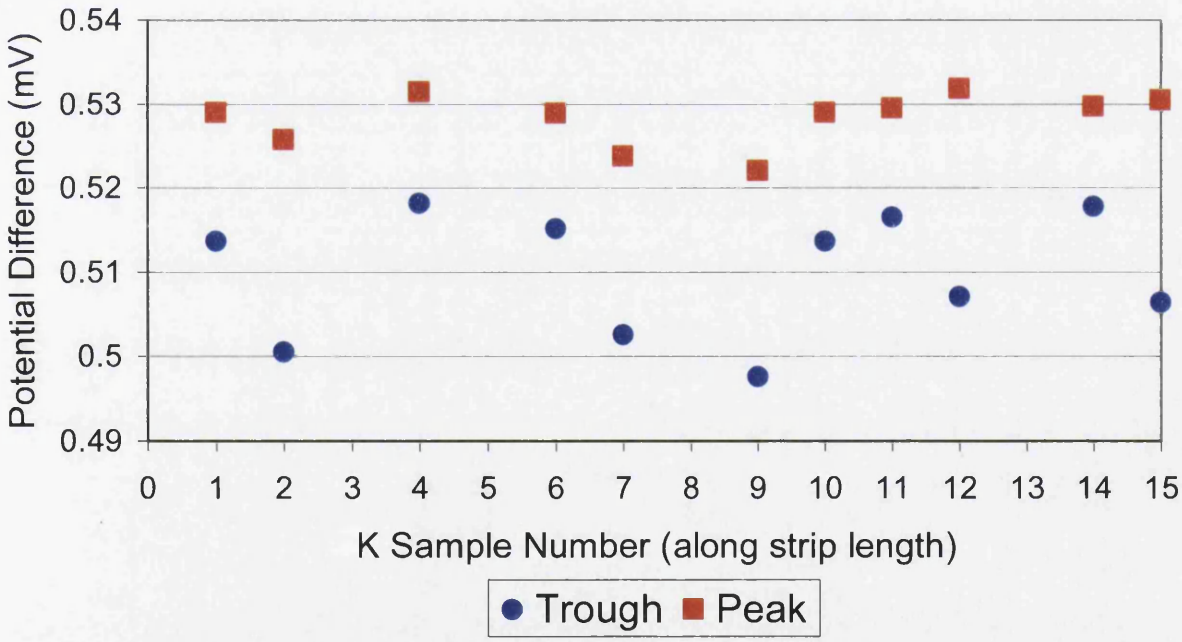

Figure 5.20: Graph showing the potential difference at various points of the ECP profile along strip length.

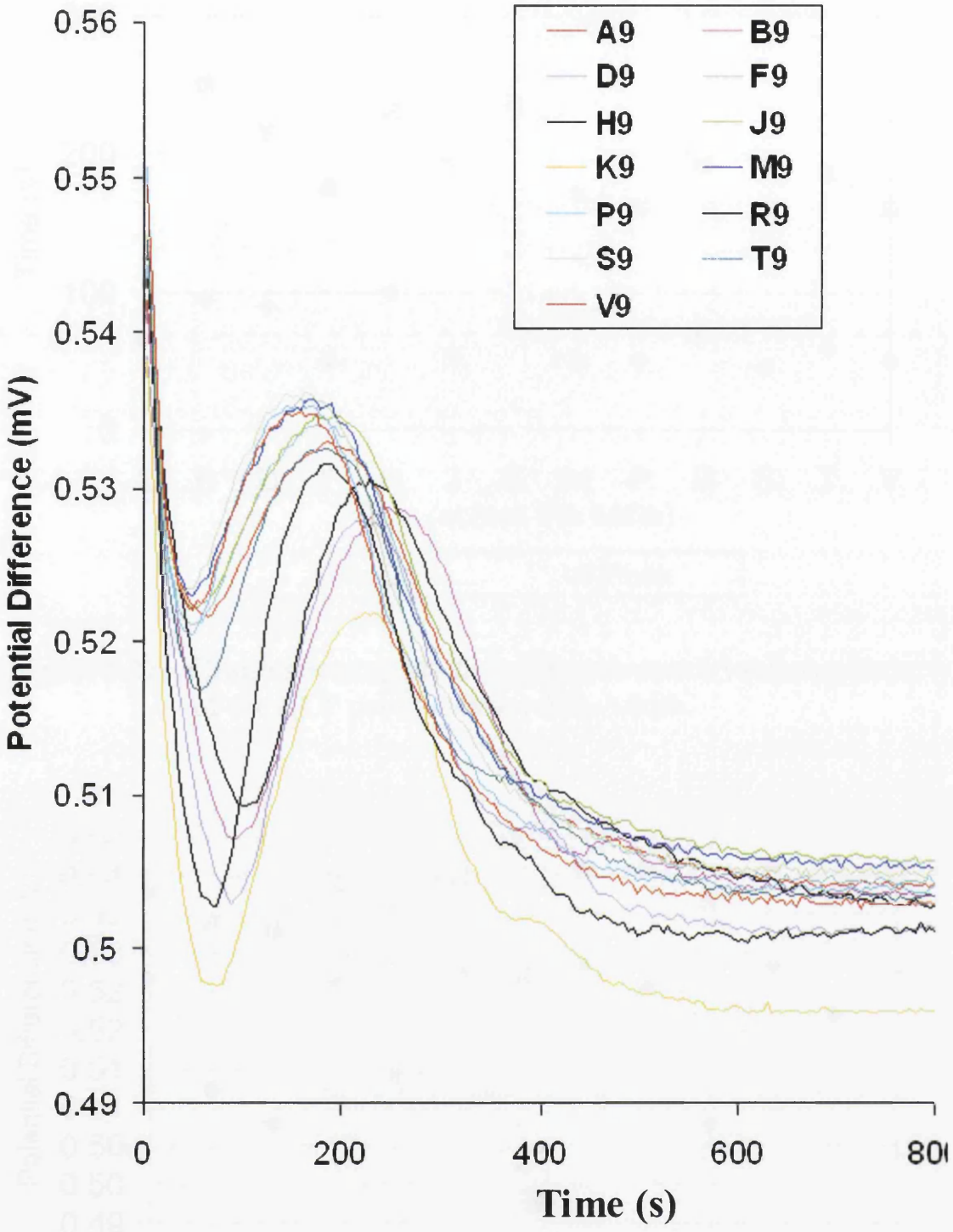

Figure 5.21: Graph showing the variation in profiles along column 9.

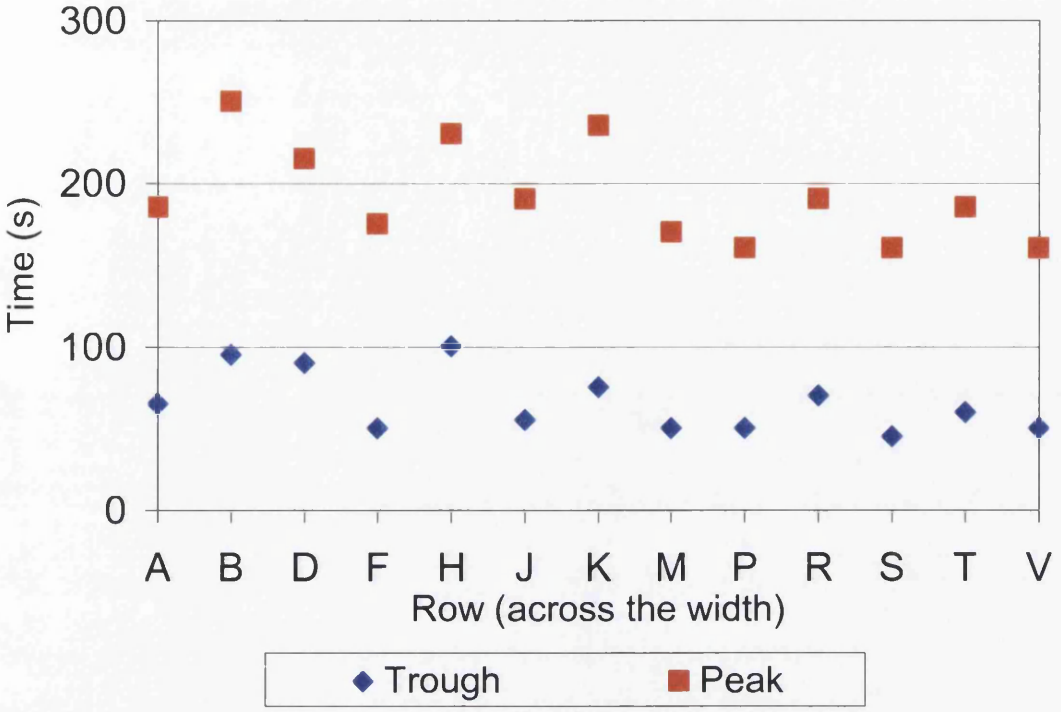

Figure 5.22: Graph showing the time taken to reach various points of the ECP profile across strip width.

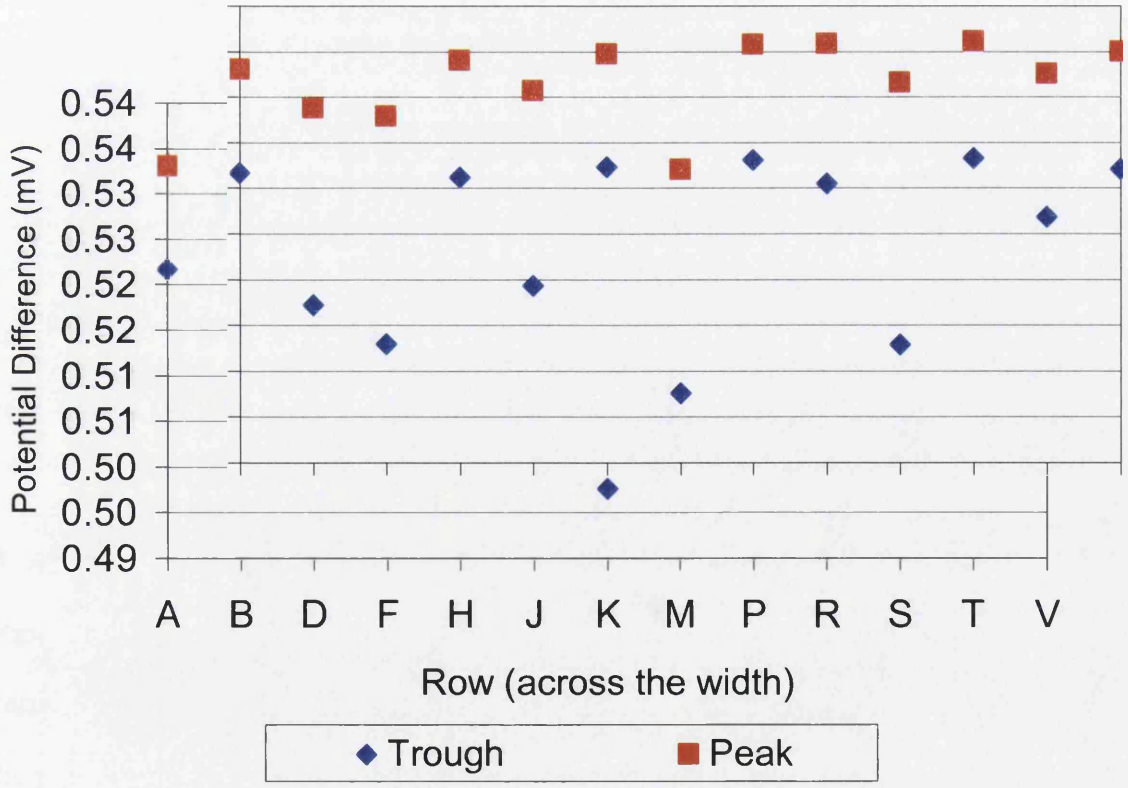

Figure 5.23: Graph showing the potential difference at various points of the ECP profile across the width.

that staining, surface roughness or other effects may be the cause of the variation, rather and temperature variation caused by the edge-burners, as these effects are more likely to be randomly scattered at various positions on the strip. In this case, it would have been expected that the temperature would result in a gradual change in profiles as the width of the strip was traversed towards the centre.

5.3.4 Effect of Sample Order

It was considered that there might be a possibility that the parameters and / or shapes of the curves could be affected by the degradation of the acid (although degradation should be negligible in a batch of only 6 tests). Figure 5.24 shows the ECP time parameters (i.e. t_1 and t_2) when the order in which the tests were carried out is taken into account. In this case, the position from which the sample was taken from the strip is not deemed to be relevant, which is a valid assumption based on the previous work. Figure 5.25 shows the corresponding values for v_1 and v_2.

A change of batch is depicted on both graphs by a change from a filled shape (square for the peak data and diamond for the trough data) to a cross. For example, the samples corresponding to the final sample in a batch (i.e. the last sample to be tested before the acid was changed) are sample numbers 4, 10, 16, 21, 27, 33 and 39.

It can be seen in Figure 5.24 that the time to reach the base of the trough is quite regularly higher for the first sample in a batch than for the rest of the samples in that particular batch. This is also shown to be a trend when looking at the time to reach the peak data.

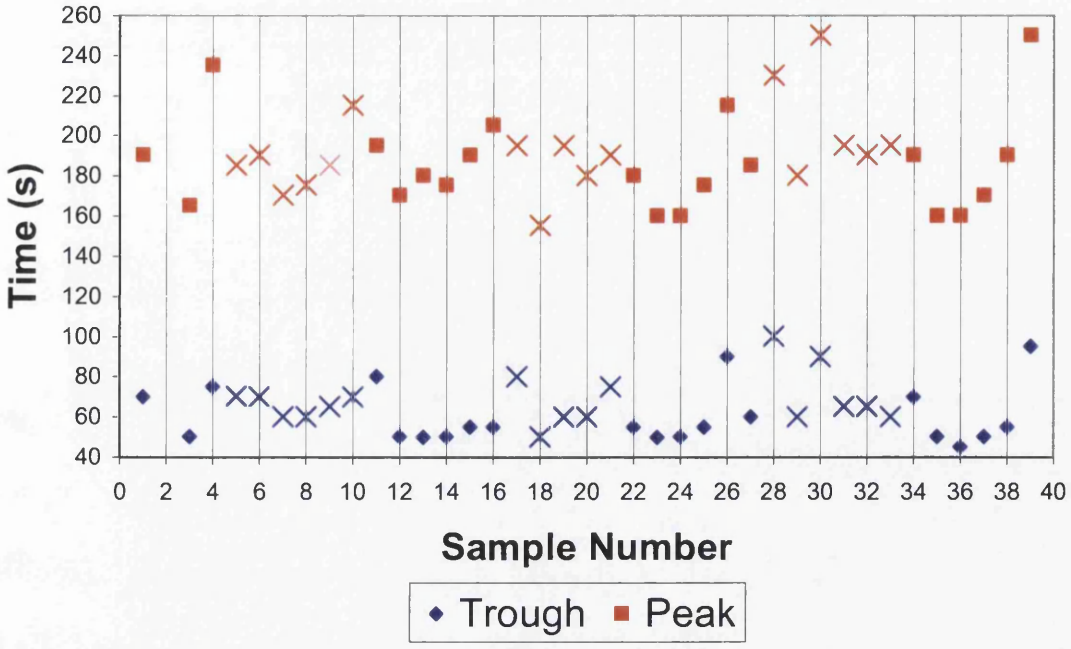

Figure 5.24: Graph showing the time taken to reach the peak and trough of an ECP profile (samples in order of testing).

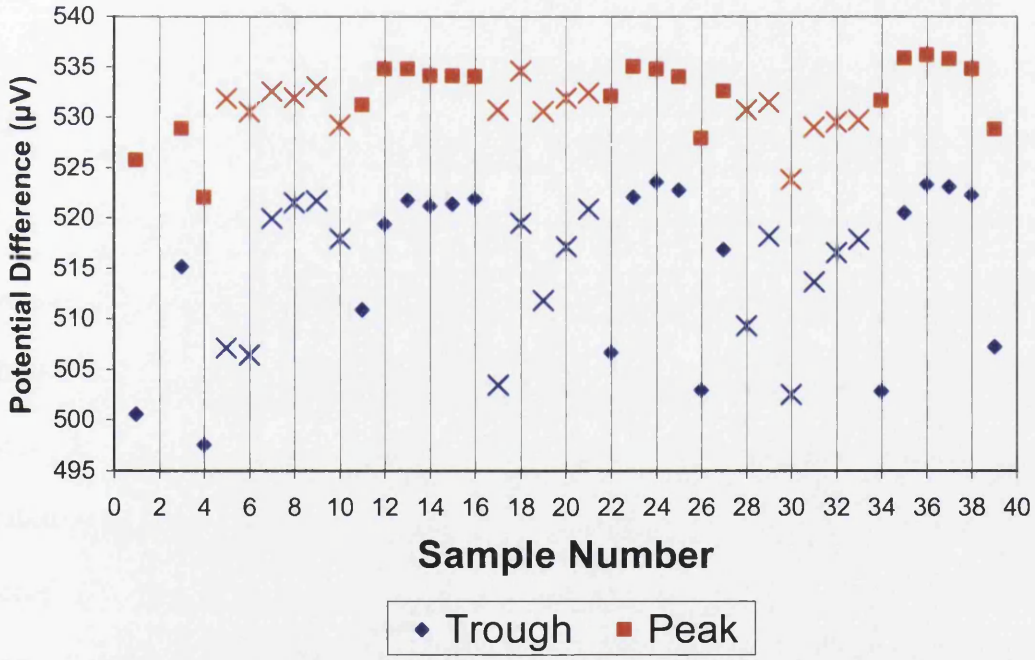

Figure 5.25: Graph showing the p.d. at which the trough and peak were reached (samples in order of testing).

In Figure 5.25, the first sample in each batch generally shows a lower potential difference. This is most obvious when looking at the potential of the trough.

Figure 5.26 shows the time difference between the base of the trough and the top of the peak (t_2-t_1). It can be seen that, in general, the time between these two points increases with the sample number in a particular batch. This suggests that the strength of the acid is decreasing as the number of samples tested increases, causing it to take longer to etch through the surface oxide layer.

A trend is also seen within each batch of samples in Figure 5.27, which shows the difference in potential between the base of the trough and the top of the peak (v_2-v_1). In this figure, the difference in potential between these two points decreases as the batch progresses. This could again suggest that the etching rate is decreasing as the batch progresses, causing the change from fayalite layer to silica layer to be less well defined.

5.4 Conclusions of Initial Trials (Sample H77538)

It was believed that the results of this investigation would show there to be a reasonable degree of consistency in ECP profiles along the length of the strip and a definite trend in the variation across the width. It was thought that this would occur due to the temperature differential across the width of the strip caused by the burners located at the sides of the furnace.

Therefore it may be concluded that the temperature differential is not as significant as previously believed. The variation was found to be far more random, with little correlation seen in either strip direction between the type of profile observed and the associated profile parameters. This suggests that the effects causing the different profiles are likely to me more localised, appearing arbitrarily at various points on the

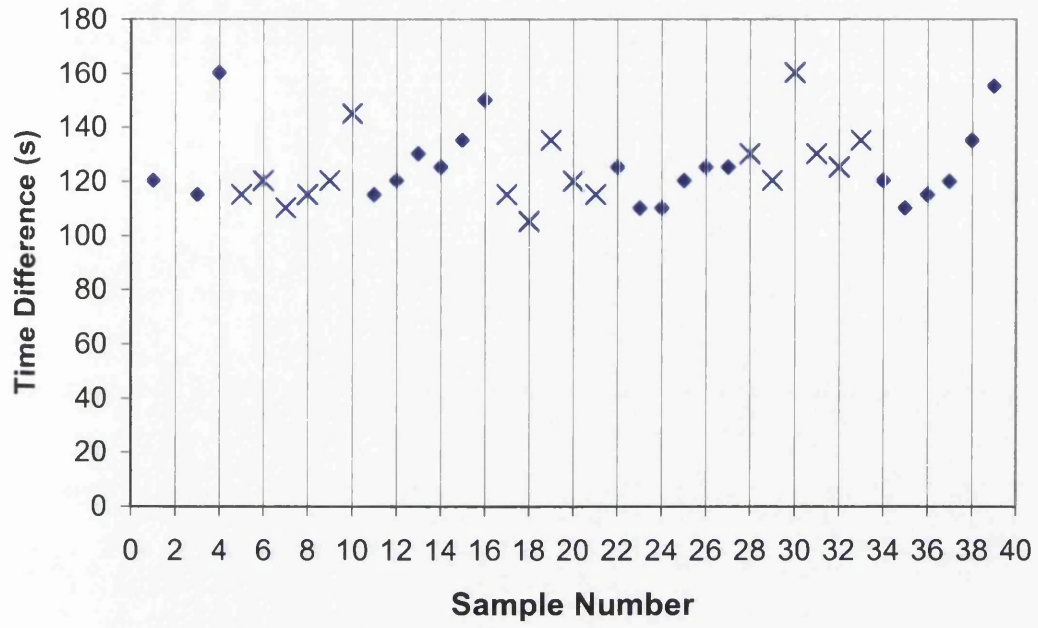

Figure 5.26: Graph showing the time difference between the base of the trough and the top of the peak.

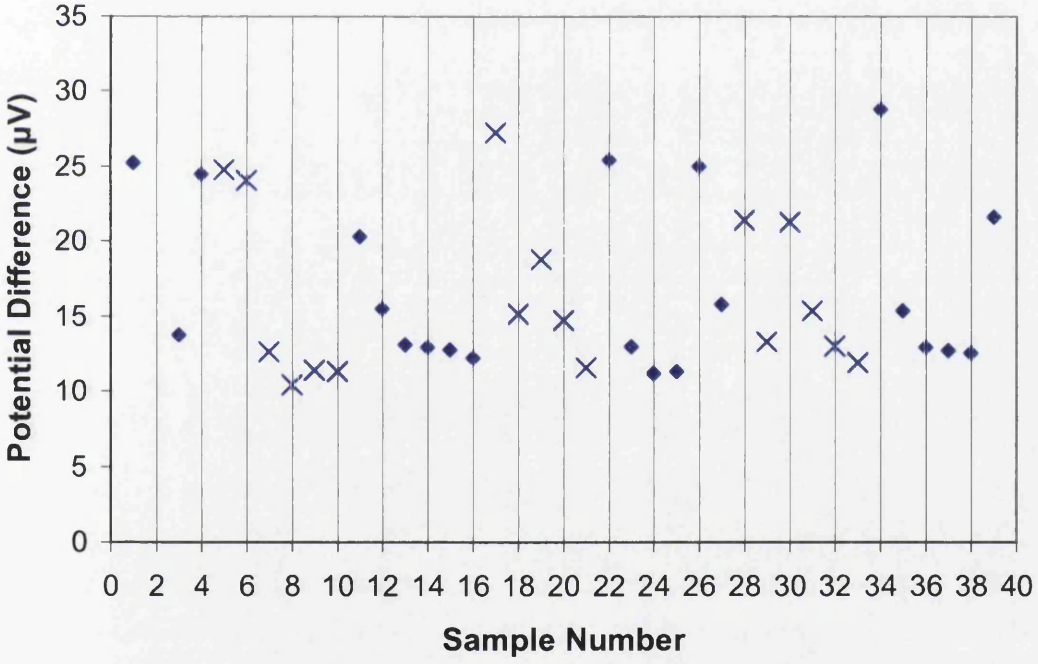

Figure 5.27: Graph showing the variation in p.d. between the base of the trough and the top of the peak.

strip surface. The most probable cause of this type of effect is likely to be strip conditions such as surface roughness or staining.

From previous work [35] and the experimentation carried out so far in this investigation, the ECP technique is considered to be quite reproducible, but effects such as staining, temperature variations and other strip conditions could cause certain areas of the strip to be variable. It would appear that sections of the strip are reasonably uniform such that they could be used as a source of material for authoritative glass film investigation. However, analysis of numerous samples would be necessary to determine the extent of the variation, and these effects would need to be taken into account until such variations are eliminated. Effort should be made to establish and rectify the causes of the variations noted.

In view of the results relating to sample order, in particular Figures 5.24 and 5.25 suggesting that the first sample may be affected differently by the acid than the remaining samples in the batch, it is suggested that a sacrificial sample is used during future experimentation. This should be carried out in the fresh acid for each new batch, prior to any samples of interest being tested. To further reduce any erroneous results caused by the effects of a new batch of acid, the reference electrode should still be left to stabilise in the acid prior to testing any further samples.

The number of samples per batch of acid should also be reconsidered for future work, to ensure that the degradation of the acid was not an overriding factor in the positioning of the parameters of the profile.

It is also possible that the profiles obtained to date during this investigation have been more similar than it first appears, and that samples from different coils may result in a much more drastic variation in profiles than has been seen in sample H77538. In order to ensure that the results from this sample were not unique, it was deemed necessary to carry out an investigation to determine the extent of ECP profile variation on a further sample. This is discussed in Section 5.5.

5.5 Further ECP Analysis - Sample H77850

5.5.1 Introduction

An investigation has previously been carried out to establish the variation in the decarburisation oxide layer, both along the length and across the width of the strip (see Sections 5.1 – 5.4). It was expected that the oxide layer would show variation across the width if temperature gradients or other position dependant variations arose during processing. In general this was not found to be the case, as variations of a similar magnitude arose both along the length of the strip as well across the width. It appeared there was no trend as to where profiles of a certain type appeared on the strip, and it is thought most likely that the variation seen is due to effects such as staining or surface roughness.

It was recommended that a further sample be obtained from one of the decarburisation lines at Orb Works and analysed in a similar way to the previous sheet (H77538), using the same electrochemical potential (ECP) apparatus. This would demonstrate whether or not the results from the previous investigation were representative of the decarburisation oxide layer and also determine the level of consistency between coils.

5.5.2 Experimental Procedure

A sheet sample was taken from coil H77850, which had recently been processed on the D5 decarburisation line at Orb Works. It measured approximately 2.2 metres in length and was of strip width (~950mm). Using a similar sized sample to that of coil H77538 would ensure that the area examined was kept constant, and the variation in profiles observed across similar distances.

The magnesia coating, with which the steel is coated on the decarburisation line prior to the coiler, was brushed off in the same manner as with the previous sample, until all visible traces had been completely removed. The removal of this magnesia should not affect the underlying oxide layer in any way.

The sheet was cut up and labelled in the same way as the previous sheet, with the rows (in the rolling direction) labelled numerically and the columns (across the strip width) labelled alphabetically.

During this investigation, the procedure was based around the standard practices described in Sections 2.2.2 and 5.2. However, the one noticeable exception to the method followed when analysing the previous sample was the use of a sacrificial sample. Following the conclusions drawn in Section 5.4, the recommendation was made that a sacrificial sample be used every time a new batch of acid was used to ensure that the acid was fully stabilised prior to any meaningful analysis was performed. This sample counted as one of the six to be used per batch of acid, thus decreasing the number of 'useful' samples that could be analysed to five per batch.

It was decided to keep the batch sizes the same based on previous recommendations from a separate investigation [35].

5.5.3 Results and Discussion

An ECP profile shows how the potential difference between an analysed specimen and a reference electrode varies as the surface oxide layer of the sample is removed by pickling in acid. The profiles obtained during this investigation, relating to the samples from sheet H77850, can be seen in Figure 5.28.

It was found that the profiles could again be split into the four categories shown in Figures 5.1-5.4, and also that there was no pattern as to where each type of profile occurred on the original sheet sample. This is demonstrated in Table 5.4 where the location of each type is shown.

As with the previous sample, the profiles were analysed in terms of the time that had elapsed before two different points were reached. These points were the base of the trough and the top of the peak, which were designated as coordinates v_1, t_1 and v_2, t_2 respectively, in relation to their values for potential difference and time.

Tables 5.5 and 5.6 show this tabulated data, which has also been plotted in Figures 5.29 - 5.36.

It was again observed that the values of t_1, t_2, v_1 and v_2 varied to a similar degree in both strip directions, confirming that the oxide layer did not vary according to any trend across the width of the strip for either of the two samples analysed.

Figures 5.37 and 5.38 show the potential difference value relating to t_1 and t_2 respectively. It can be seen in Figure 5.37 that there again appears to be a good correlation between t_1 and v_1, with R^2 values of 0.77, 0.41, 0.76, 0.78, 0.83 and 0.15 for rows F, H, K, N, Q and S, corresponding to an R^2 value of 0.67 when all plotted together.

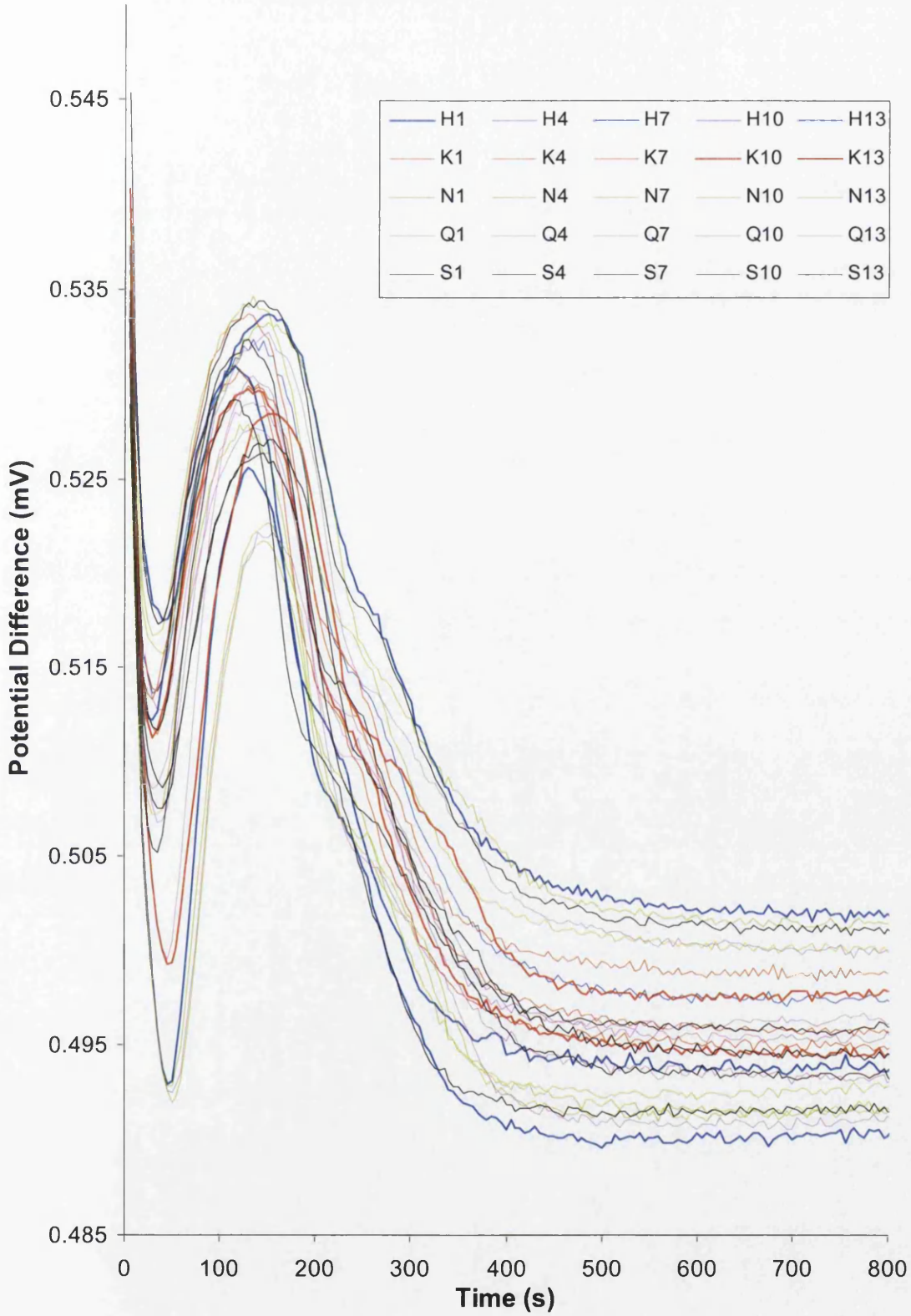

Figure 5.28: A graph showing the collection of profiles obtained from sample H77850.

	Column 1	Column 4	Column 7	Column 10	Column 13
Row F	-----	-----	1a	2 / 2a	1
Row H	1a	1 / 1a	1a	2a	1 / 1a
Row K	1a	1a	2a	1a	1a
Row N	2a	1a	1 / 1a	2a	1a
Row Q	1a	2a	1a	1a	2a
Row S	1a	1a	1a	1a / 1	1a

Table 5.4: Type of ECP profile at various positions on the H77850 strip sample.

	Column 1		Column 4		Column 7		Column 10		Column 13	
	Trough	Peak	Trough	Peak	Trough	Peak	Trough	Peak	Trough	Peak
F	---	-----	---	-----	30	125	50	150	40	155
H	30	115	40	150	30	135	45	130	35	140
K	30	120	35	130	45	150	35	135	30	130
N	50	145	30	135	40	150	50	150	35	130
Q	30	135	45	135	35	150	35	135	50	155
S	35	115	35	140	35	130	40	150	40	140

Table 5.5: Time to reach trough (t_1) and peak (t_2) (values given in seconds).

	Column 1		Column 4		Column 7		Column 10		Column 13	
	Trough	Peak	Trough	Peak	Trough	Peak	Trough	Peak	Trough	Peak
F	---	-----	---	-----	0.511	0.532	0.490	0.520	0.510	0.530
H	0.512	0.531	0.518	0.534	0.514	0.532	0.493	0.526	0.511	0.530
K	0.513	0.531	0.514	0.534	0.499	0.528	0.506	0.527	0.511	0.530
N	0.492	0.522	0.517	0.535	0.516	0.533	0.493	0.523	0.507	0.528
Q	0.509	0.528	0.500	0.531	0.513	0.533	0.507	0.529	0.492	0.522
S	0.505	0.529	0.517	0.534	0.512	0.532	0.509	0.527	0.508	0.526

Table 5.6: Potential difference at trough (v_1) and peak (v_2) (values given in mV).

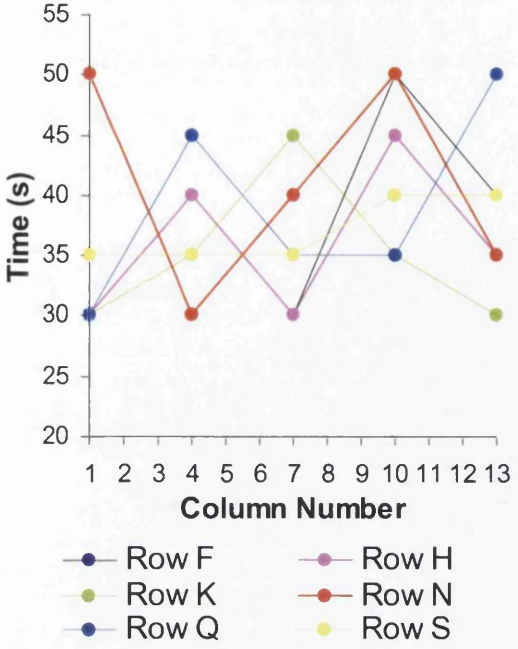

Figure 5.29: Time taken to reach the base of the trough (across the width).

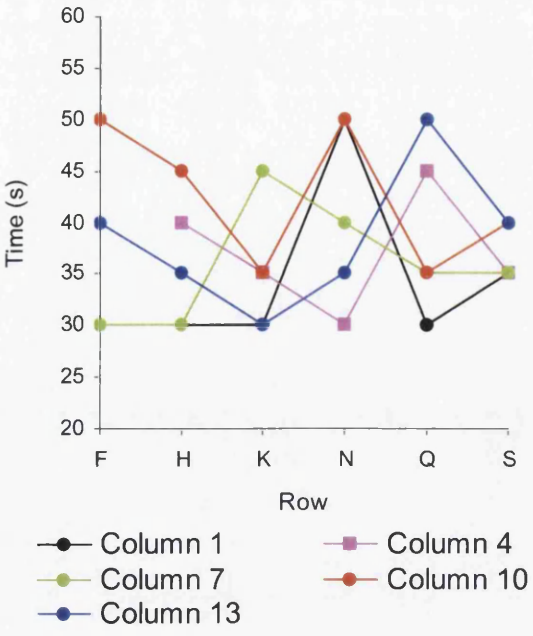

Figure 5.30: Time taken to reach the base of the trough (along the length).

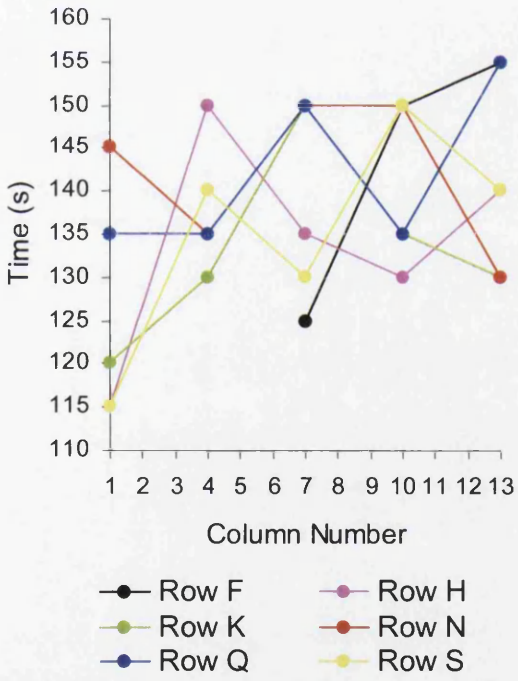

Figure 5.31: Time taken to reach the top of the peak (across the width).

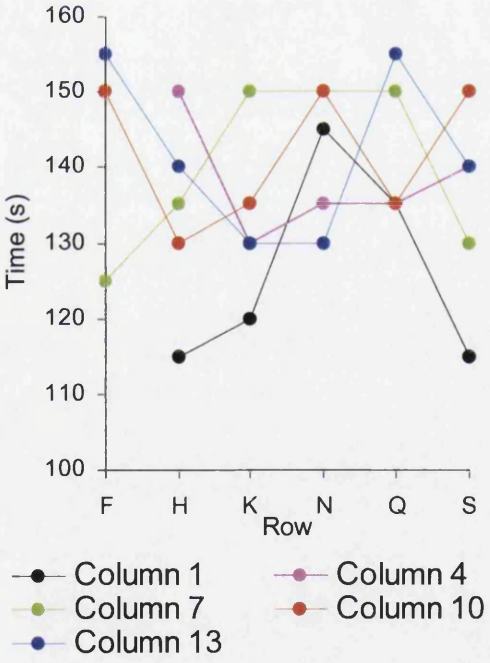

Figure 5.32: Time taken to reach the top of the peak (along the length).

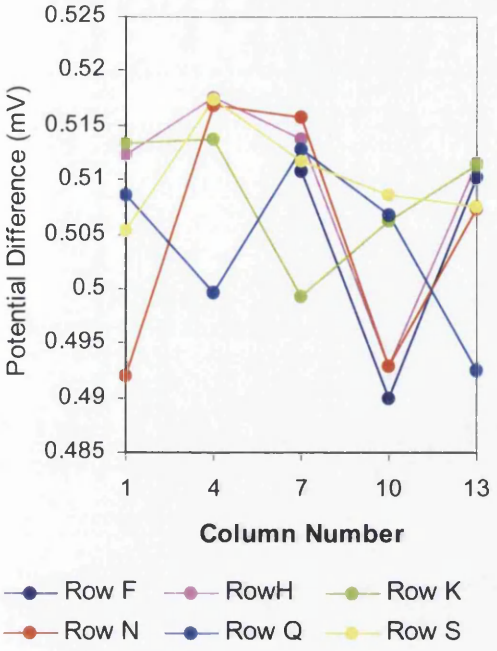

Figure 5.33: Potential difference at the base of the trough (across the width).

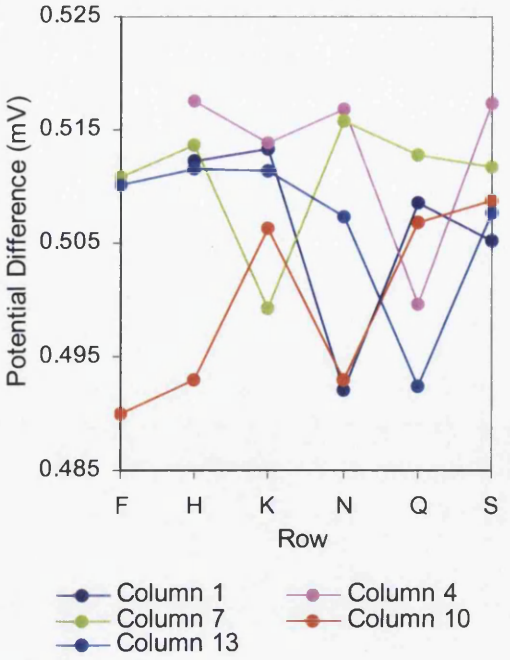

Figure 5.34: Potential difference at the base of the trough (along the length).

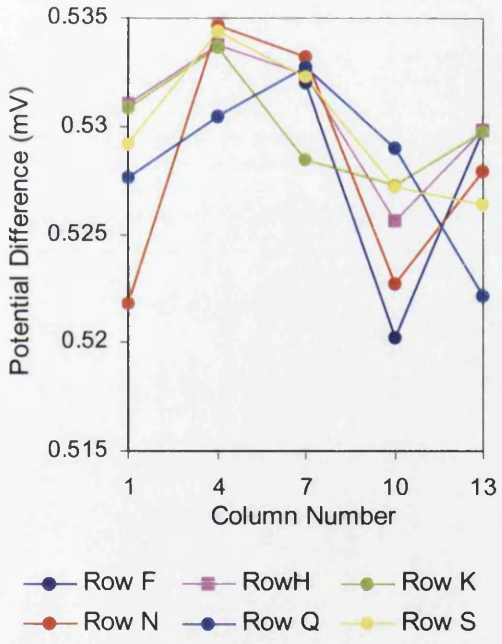

Figure 5.35: Potential difference at the top of the peak (across the width).

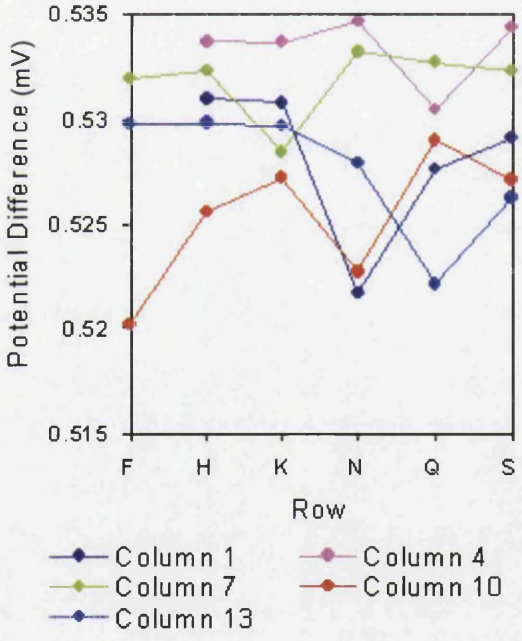

Figure 5.36: Potential difference at the top of the peak (along the length).

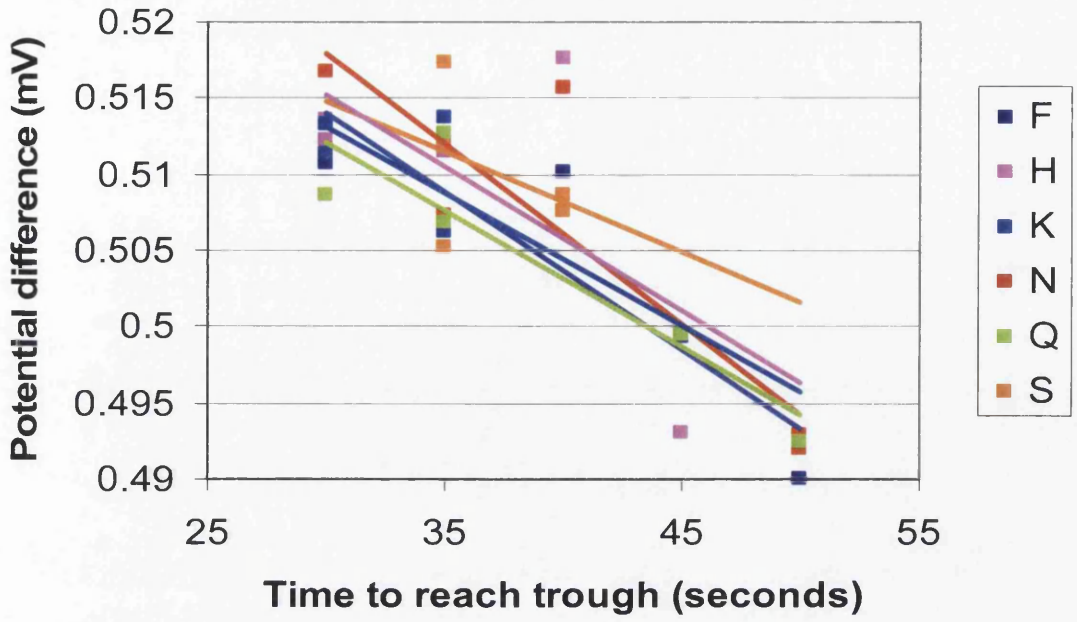

Figure 5.37: Correlation between the potential difference at the base of the trough and the time taken to reach that point.

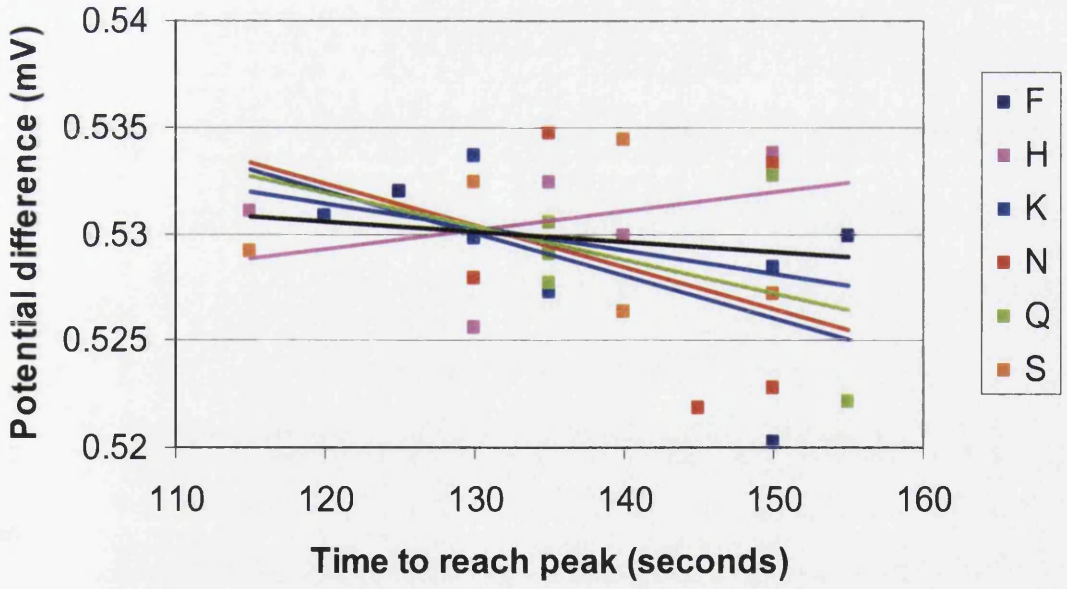

Figure 5.38: Correlation between the potential difference at the top of the peak and the time taken to reach that point.

However, Figure 5.38 shows no correlation whatsoever, suggesting that the time taken to reach the peak is independent of the potential that is reached.

When comparing Table 5.5 to the associated table for the previous sample (Table 5.1), it can immediately be seen that the time to taken to reach the points of interest was much shorter for the second sample (H77850) than it was for the first (H77538). An average was calculated for each strip sample. It was found that for sample H77538, the average values for t_1 and t_2 were 61 seconds and 184 seconds respectively. This can be compared to the values of 38 and 138 calculated for the most recent sample. This could suggest that either the oxide layer on sample H77850 is not as thick as that on the previous sample or that the acid is of a greater strength and is therefore etching the oxide layer at a greater rate. It is deemed unlikely that the acid strength could be a factor in this variation as great care was taken in mixing the correct formulation. However, the etching rate could also be affected by the surface roughness of the oxide layer, as a surface with greater roughness would leave an increased area open to acid attack. Unfortunately, surface roughness data was not obtained from these samples at the time of analysis, but should be considered in any future investigation.

Analysing the data further, it can be seen that the variation in t_1 is of a similar magnitude for both samples, with the data points spread over a range of 30s for H77538 and 20s for H77850. However, when the values for t_2 are analysed it can be seen that there is a much greater spread in values for H77538 where the range is 80s, compared to 40s for H77850. Although this may seem significant, it is likely that this is simply related to the increase in overall t_2 values for the H77538 samples, and not a

reflection of the accuracy of the technique being affected. However, it could also be linked to changes in the interface that causes this peak

When analysing the data for the values of v_1, it was observed that the values for the second sample were slightly lower than those seen previously. However, the v_2 values averaged a slightly higher level than those seen for the initial sheet sample. This resulted in the troughs seen on the profiles of the samples from the second sheet appearing to be much sharper than those for the first sheet. This could suggest that the layers of fayalite and silica are more clearly defined for the second sample.

Although it has been found that samples H77538 and H77850 display the same shaped profiles, there has been no direct comparison to discover whether they occur at the same values of potential difference. A direct comparison of the actual ECP profiles from the two strip samples can be seen in Figure 5.39.

It can be seen that the sample from each coil exhibits a similar degree of spread. However, the graph shows that the two samples have separate distinctive bands that are offset from each other. It may be that this variation in the band containing the spread is the only clear distinction between different coils.

5.6 Alterations to Decarburisation Conditions

5.6.1 Introduction

Samples from a further three coils were analysed using the ECP apparatus, although not as thoroughly as the previous two sheets. The results are not discussed in detail here, but this extension to the investigation demonstrated that the extra coils also

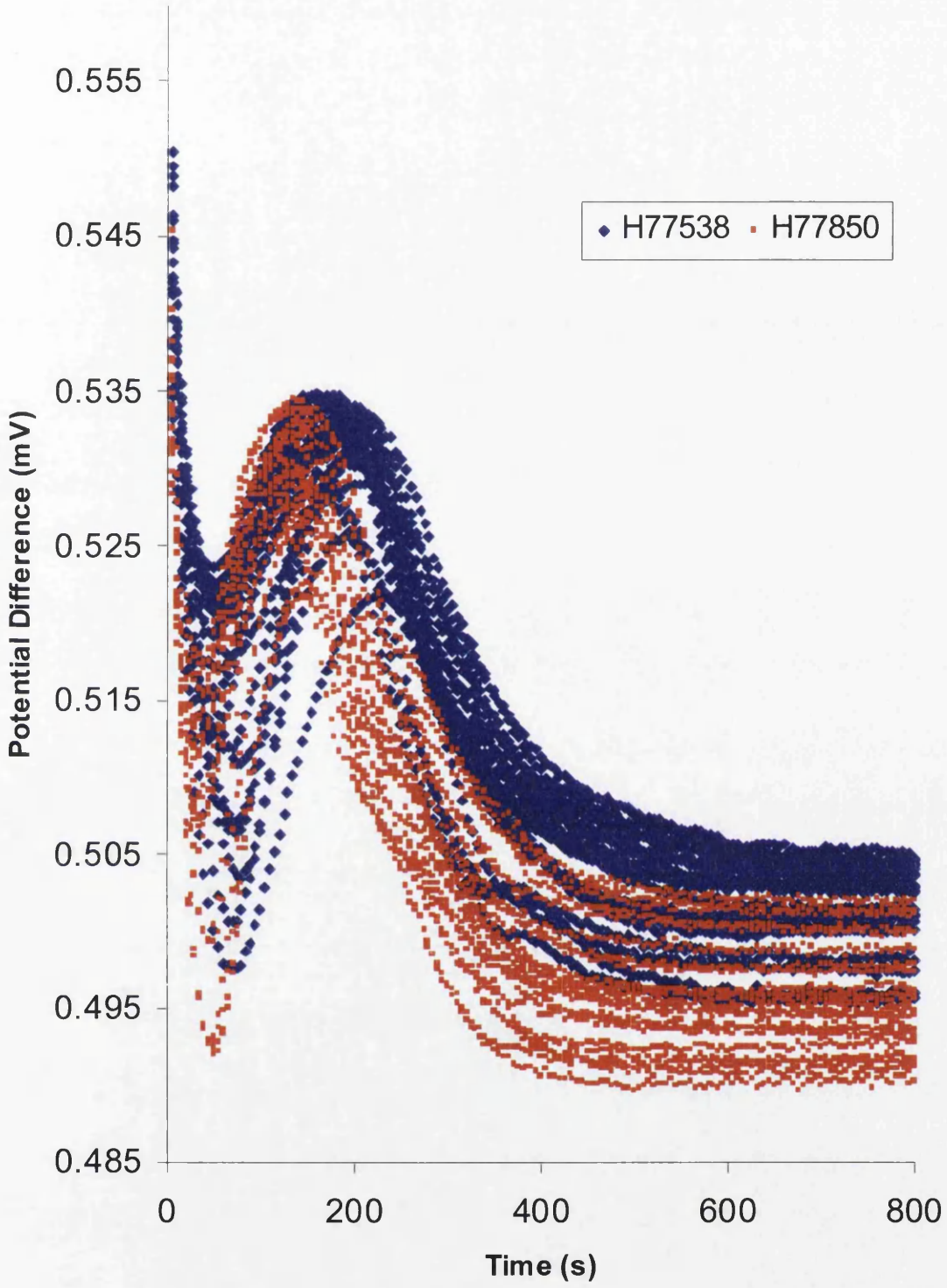

Figure 5.39: A comparison of the profiles obtained from coils H77358 and H77850.

exhibited ECP profiles of the same shapes (i.e. types 1a, 2a, 1b, and 2b). The averaged profiles for each coil are shown in Figure 5.40.

It remains unclear whether the profiles seen in this investigation show the amount of variation that is be expected to be seen between most coils, or whether the coils are coincidentally similar. It is possible that the conditions in the decarburisation furnace was stabilised over the time that the five analysed coils were processed. However, it is also possible that the ECP apparatus is not sensitive enough to detect subtle changes in the oxide layer.

As the material being produced at Orb Works was of a good, consistent quality, it was not feasible to alter the conditions of the production line in order to deliberately produce different oxide layers. It was therefore necessary to utilise a laboratory tube furnace, located at Orb, to simulate the decarburisation anneal. The aim of this work was to determine whether the ECP profiles would vary extensively if the material were decarburised under significantly different conditions.

5.6.2 Experimental Procedure

Due to operational practicalities, it was decided that the simplest way of altering the composition of the oxide layer was to vary the dew point by selectively passing the furnace gas through a saturator at different temperatures. This was done over the largest possible range in order to produce drastically different layers. The conditions chosen were:

- Dry hydrogen atmosphere (i.e. saturator bypassed),
- Hydrogen passed through a saturator at 22.5°C,
- Hydrogen passed through a saturator at 59.5 °C.

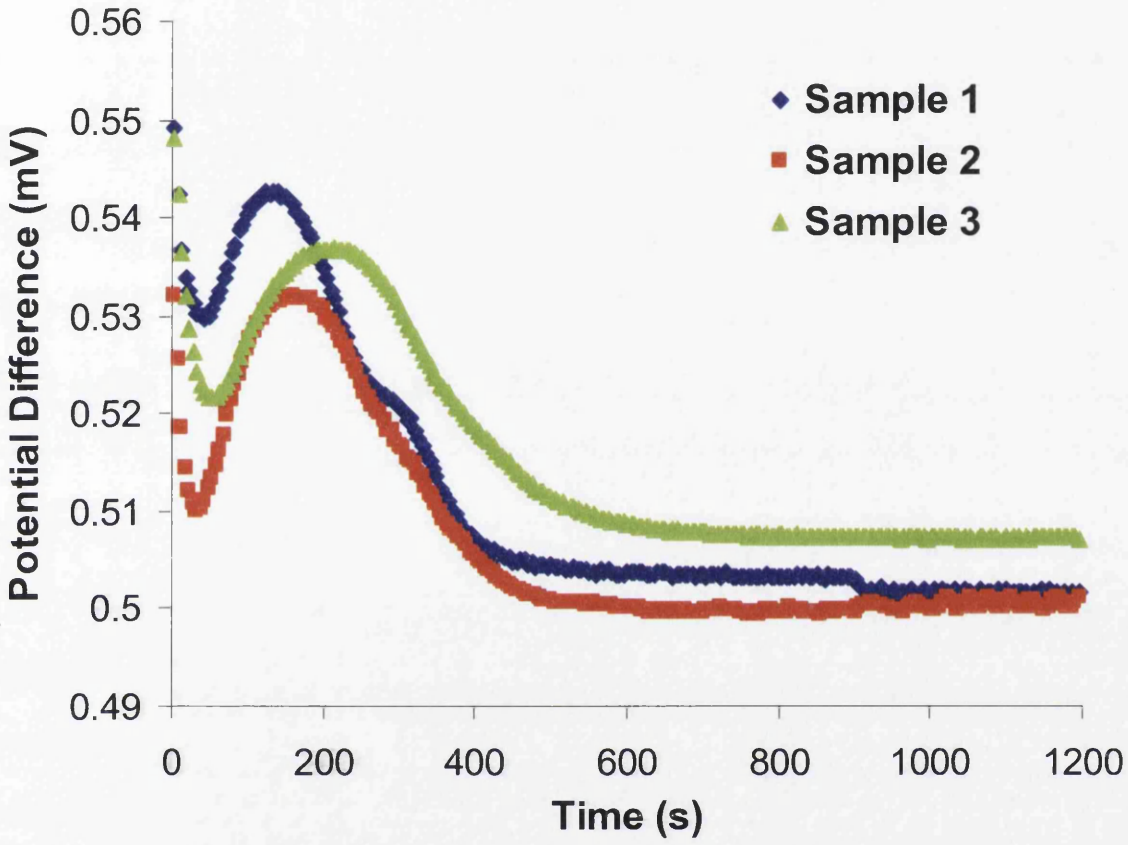

Figure 5.40: Average profiles obtained from a further three coils.

The temperature of 22.5°C was related to the room temperature at the time of the investigation, and 59.5°C was the maximum temperature that could be achieved with the saturator that was used. This compares to an average dew point temperature on the production lines of approximately 68°C.

The temperature of the furnace was kept constant at a value of ~800°C to simulate the same temperature as found on the decarburisation lines at Orb.

The samples used were taken from two coils (42539 and 42655) at the entry of the Orb decarburisation lines (i.e. prior to them passing through the decarburisation furnace). Two coils would show whether changing the material would have an effect on the resultant oxide layer.

At the stage where they were removed from the line, the samples have no oxide layers present on the surface. They were cleaned with a solvent prior to entering the tube furnace to ensure that all traces of dirt, oil etc had been removed from the surface.

To ensure efficient and accurate transportation of the samples into and out of the hot-zone (geometrical centre) of the furnace, the samples were loaded into a custom made carriage. This ensured that the samples were held at the correct temperature, but also minimised contact with the sample itself.

To replicate the conditions on the production line, the samples were rapidly manoeuvred into the hot-zone and left at temperature for 4.5 minutes. This consisted of 2.5 minutes for the sample to reach the required temperature, and 2 minutes to soak at this temperature. They were then moved to another section of the furnace to cool for a further 1.5 minutes (still in a controlled atmosphere).

Two samples from each coil were used under each different dew-point condition to determine the level of reproducibility.

Once annealed and fully cooled, the samples were analysed using the standard ECP procedure.

5.6.3 Results and Discussion

The resultant ECP profiles can be seen in Figure 5.41. A 'typical' profile from a sample obtained from the D5 decarburisation line is also included on this figure for comparison.

It can immediately be seen that differences can be seen between the profiles obtained from samples annealed under different conditions. The samples annealed under a dry atmosphere show the potential difference falling to a trough, before ascending to the baseline. The samples annealed with a furnace dew point at room temperature result in a profile that has two smaller peaks following the initial trough. However, the samples annealed with a dew point similar to that specified for the production line appeared to show a similar shaped profile to those seen previously on production material, with an initial drop in potential difference, followed by a peak and then another descent towards the baseline.

5.6.4 Conclusions

It should be noted that the differences in annealing conditions in this experiment vary by a much greater degree than would ever be seen on the production lines. However, this work does show that the ECP technique is sensitive enough to distinguish between samples annealed under different conditions, proving that the ECP profiles are affected by the changes in oxide layer composition.

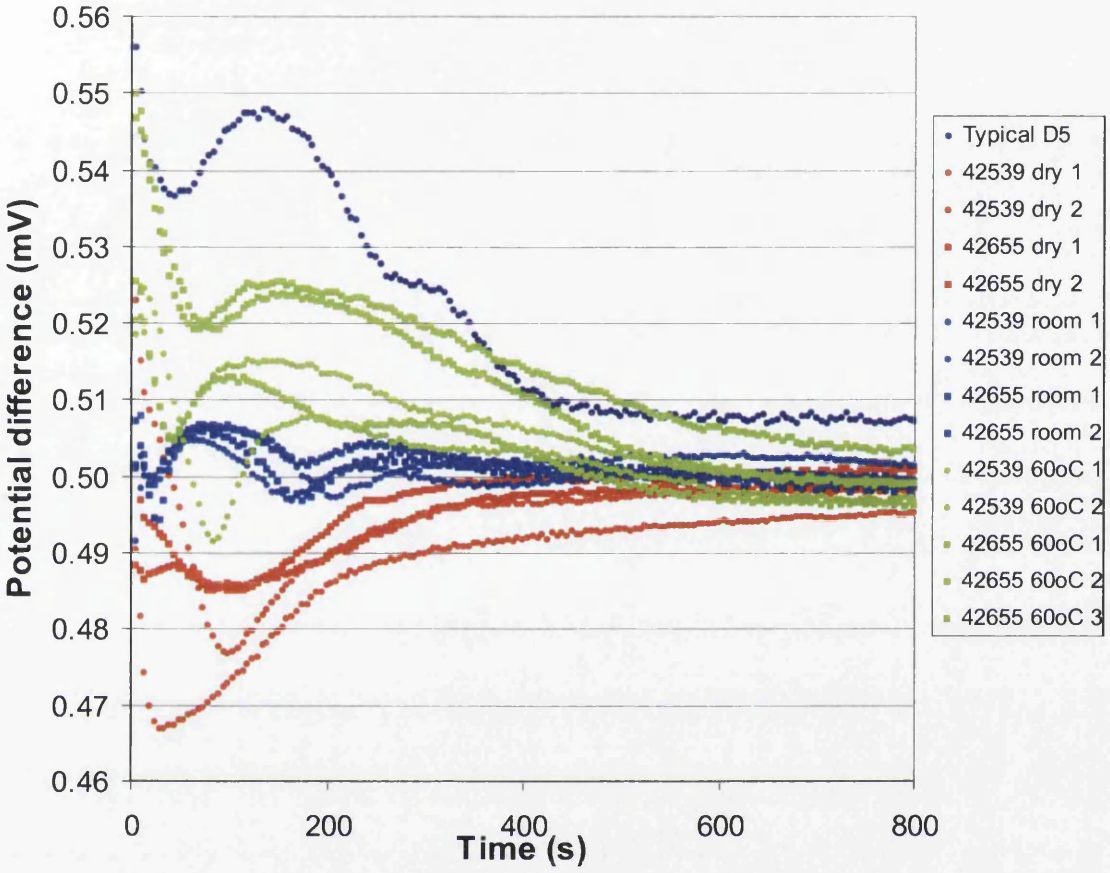

Figure 5.41: Profiles resulting from different laboratory decarburisation conditions.

5.7 Chapter Summary

It had previously been expected that the oxide layer produced during the decarburisation stage would vary to a greater extent across the width of the strip than it did along the length, if temperature gradients were prevalent. However, there were no clear trends in the variation across the width, or in variations along the length of the strip. This may indicate an effect arising from staining due to mill lubrication, or surface roughness effects. The investigations carried out on samples H77538 and sample H77850 both gave similar conclusions.

Although the profiles of production samples were found to vary in terms of the time taken to reach specified points and the potential difference at these points, they all exhibited a similar shape i.e. they all displayed a trough followed by a main peak. Internal discussions have indicated that related previous work [36-38], carried out many years prior to this study into oxide layer variation, has shown profiles that vary to a much greater extent i.e. with extra peaks and / or troughs. This may indicate that the difference between the two coils is not as great as it first appears. It is possible that the two coils have very similar oxide layers, with only a slight difference shown by the offset bands of spread seen in Figure 5.40.

Further work using the laboratory tube furnace to vary the decarburising conditions confirmed that considerably different profiles would result from samples annealed under significantly different conditions. Therefore it seems likely that the production samples analysed in this investigation actually possessed very similar decarburisation oxide layers.

The fact that the profiles are similar and no further peaks or troughs are seen for either of the two main production samples, or the three supplementary samples, suggests two possibilities. These are:

a. The processing conditions on the decarburisation lines are reasonably consistent over a number of weeks
b. The processing conditions experienced by the two coils from which the samples were taken were coincidentally similar.

To test this hypothesis, samples were occasionally taken from a number of coils over the remaining time of the Engineering Doctorate and analysed with the ECP apparatus. It was found that nearly all of the resulting profiles gave similar results to those seen previously, suggesting that the oxide layer remains consistent when the furnace conditions are unchanged. However, one production-led trial relating to the annealing conditions did take place a number of months after the initial investigations. Material was acquired from the trial coils, and resultant spectra from two of the coils that were processed under different conditions are shown in Figure 5.42. This confirms that the ECP is able to distinguish between changes in furnace conditions, not only in exaggerated laboratory trials, but also on a production basis.

It is recommended that effort should be made to determine the causes of the differences that do arise in the sheet samples when analysed using the ECP technique, and to establish how to eliminate such variations. It is likely that successfully implementing this would probably result in a more predictable glass film formation and hence less variable magnetic properties.

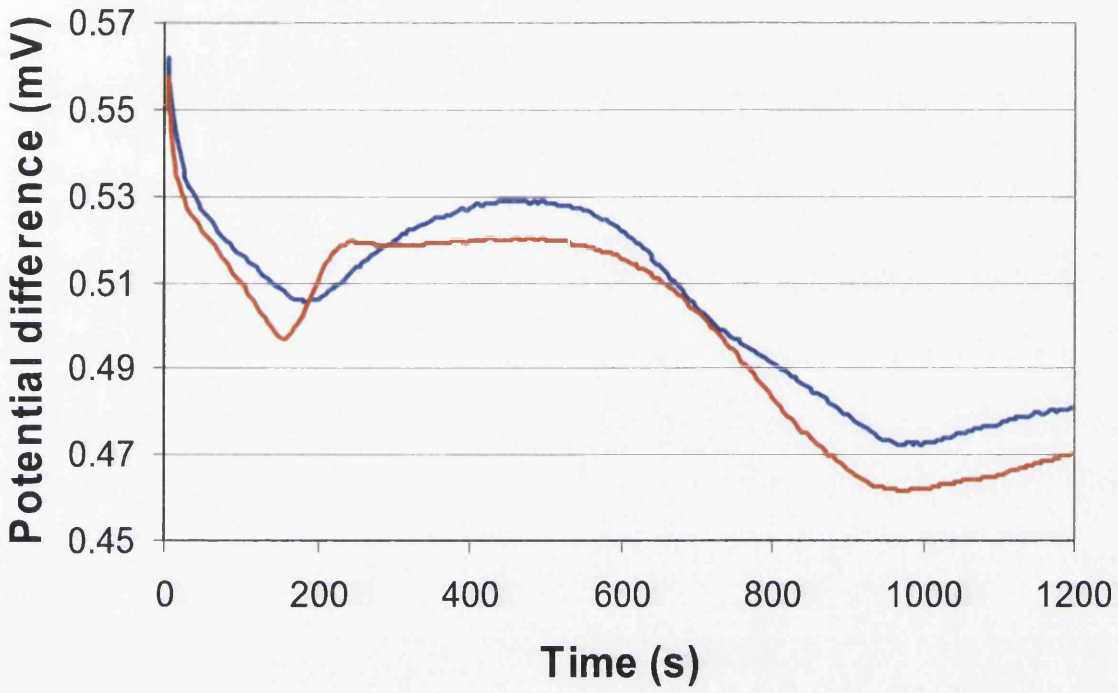

Figure 5.42: Profiles obtained from samples that underwent different Works processing conditions

Although the significance of the profiles is not currently fully understood, it has been shown that this technique is capable of distinguishing between different oxide layers. Therefore it is a useful tool for selecting samples for any investigations into the parameters that affect glass film, as it can be used to confirm whether the oxide layer on the surface is consistent on a selection of samples. This will eliminate one of the variables that could otherwise cause discrepancies.

To understand the significance of these profiles, and to determine the changes in the composition of the oxide layer that are required to cause the variation seen in this investigation, it is necessary to carry out further investigations to determine the relevance of the various characteristics of the ECP profiles. A number of analysis techniques were used to do this, and the work relating to this further investigation is described in Section 6.

Chapter Six

Interrupted Electrochemical Potential (ECP) Analysis of the Decarburisation Oxide Layer

6.1 Introduction

During the decarburisation process, an oxide layer, consisting mainly of fayalite (Fe_2SiO_4) and silica (SiO_2), is formed on the surface of the steel strip. A technique known at the electrochemical potential (ECP) method is currently being developed for the analysis of this layer (see Chapter 5). The method produces results in the form of an ECP profile. This is a plot of the change in potential difference between a reference electrode and a sample under investigation as the oxide layer is etched away. An example of these profiles is shown in Figure 6.1. It can be seen that the profiles have distinctive peaks and troughs. However, it is not known how the shape of these profiles and other characteristics (e.g. position and levels of the peak / trough, rate of change of potential difference etc.) precisely relate to the composition of the oxide layer.

Effort has previously been made to utilise the Fourier Transform Infrared (FTIR) apparatus to analyse the full depth of the oxide layer (Section 4), as this could be related to the various characteristics on the ECP profile. Unfortunately, it was found that the penetration depth of the infrared radiation was insufficient to analyse the entire layer. However, when a sample was partially pickled in acid, it was found that the FTIR spectrum of the pickled surface was significantly different to that in its un-pickled state. This suggests that the oxide layer produced on the decarburisation lines

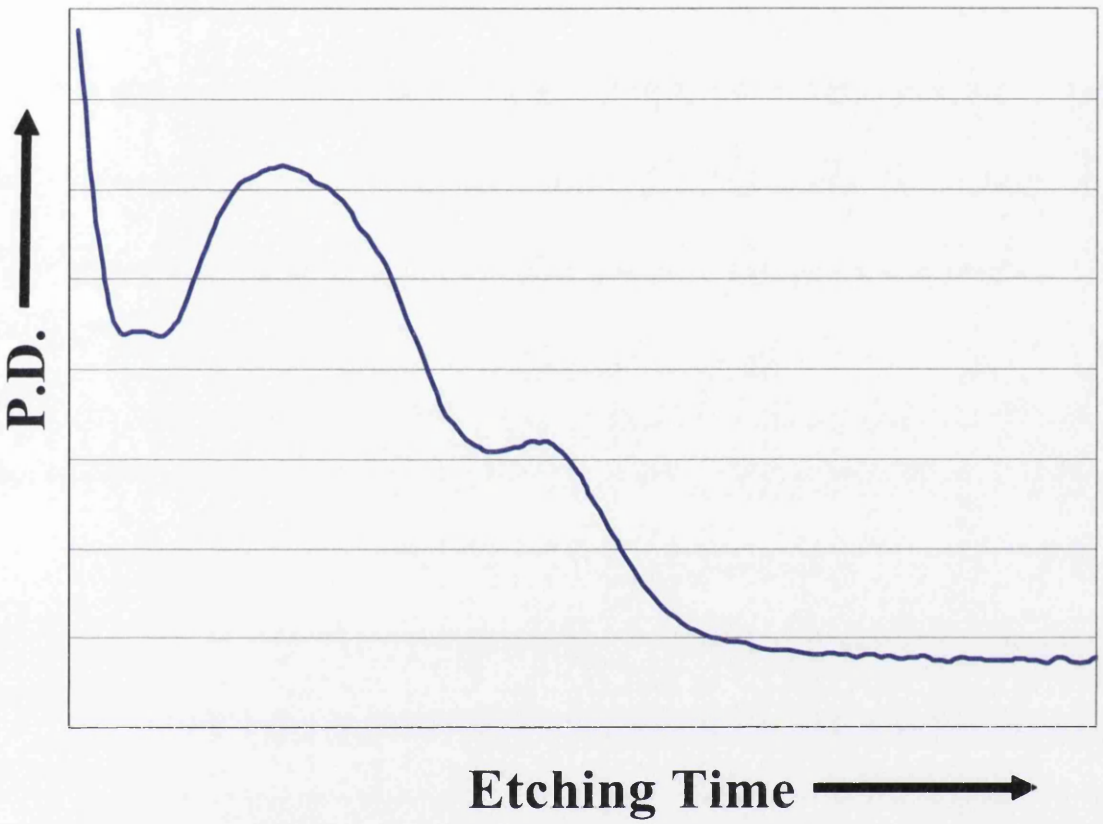

Figure 6.1: Example of an ECP profile.

at Orb Works shows a definite layering structure consisting of a layer of predominantly silica-rich material, with a thin layer of fayalite on top.

It was therefore considered necessary to carry out an investigation to determine the exact structure of the decarburisation layer that would enable the validation of the electrochemical potential (ECP) method as a technique for the analysis of decarburised material.

The pickling previously undertaken for the FTIR investigation was carried out only to discover whether any changes occurred between spectra. Therefore, the accuracy with which this was done was not deemed a priority, and accurate measurements of the many variables (pickling rate, acid strength, temperature etc.) were not considered to be of particular concern. The only desirable outcome was that the lower layers of the oxide layer were exposed, and this was successfully achieved.

To study the oxide layer in greater depth, a more accurate, and therefore less rapid, method of gradual oxide layer removal was required. Through previous experience gained from using the ECP apparatus, it was known that the 5% sulphuric acid at 70°C used for this technique caused the oxide layer to be etched away over a period of approximately fifteen minutes and would therefore be suitable. It was hoped that it would be possible to take advantage of this slow etching in order to combine the ECP method with a number of other analysis techniques in an attempt to establish the relevance of characteristics on the ECP profiles. This was achieved by carrying out 'interrupted ECP'.

Interrupted ECP is the name used to describe the manner in which ECP could be linked with other surface analysis techniques. The samples initially follow the standard ECP process under normal conditions i.e. submerged in 5% H_2SO_4 at 70°.

However, instead of completing the full 20-minute duration of the test, it was interrupted at various stages of etching and the samples were removed from the acid. The times at which the samples were removed were linked to the position that the trace had reached on the ECP profile. This was carefully monitored as the experiment progressed. Upon removal from the acid, the samples were rinsed with water and dried immediately to prevent any further acid attack on the oxide layer. This left the surface of the oxide layer in a state that directly related to a particular point of the ECP profile. This could then be analysed to establish the elements or compounds present at the surface.

A number of techniques were used to analyse the surface at various points along the ECP profile. These are discussed in the following sections.

6.2 Combination of FTIR and Interrupted ECP Techniques

As discussed in Section 6.1, previous work has suggested that the Fourier Transform Infrared (FTIR) method may be used for the analysis of the decarburisation oxide layer, but the radiation is unable to penetrate the full depth of the oxide layer. This was initially seen as a disadvantage, but now provides FTIR with the benefit of being able to be used to look more specifically at the very surface of the layer at various intervals of the etching process.

Previous experimental work (Section 4) has identified the positions of the absorption bands that are relevant. The major band associated with fayalite is expected to be

found at ~985cm^{-1}, and silica related bands are expected at approximately 1250cm^{-1}. It is also believed that the presence of any $FeSiO_3$ may result in a small band at the lower end of this range. This agrees with literature, which suggests that fayalite is found at the wavenumber specified above [31], and silica related bands are found in the approximate wavenumber range of 1050-1250cm^{-1} [31, 33, 40 and 41].

This data can be used to determine what compounds are present at the surface at various stages as the oxide layer is etched away.

6.2.1 Experimental Procedure

A sheet of strip width was taken from the end of the decarburisation line and cut into a number of smaller samples suitable for ECP analysis (dimensions of 130mm x 50mm). The samples to be analysed were taken from an area as small as possible, to minimise any variation in processing conditions that may alter the oxide layer. They were brushed free of the magnesia (MgO) powder coating, and prepared using the standard method for ECP analysis [35].

The samples were then subjected to the standard ECP conditions i.e. submerged in 5% H_2SO_4 at 70°, but removed at predetermined times relating to their position on the ECP profile.

The chosen times were

10 seconds – very brief etch in acid

20 seconds - descending the profile towards the trough

30 seconds - further along the profile, close to trough being reached

60 seconds - point at which the base of the trough is reached

85 seconds - p.d increasing after trough has been reached

95 seconds - further increase towards peak

125 seconds - point at which the top of the first (main) peak is reached

215 seconds - p.d decreasing following the peak being reached

275 seconds - profile levelling out before second peak is reached

360 seconds – descending towards baseline

One sample was also allowed to reach the baseline, as this could act as a reference sample. The p.d was allowed to stabilise to ensure that the entire oxide layer had been etched from the surface.

These positions are shown on the profile in Figure 6.2.

Upon removal from the acid, the samples were rinsed thoroughly with running water to ensure that no acid remained to further attack the surface. Once they had been dried using a hot air dryer, the samples were analysed using the FTIR apparatus at Orb Works. Since it was the oxide layer being analysed, it was necessary to employ the 80^{o} grazing angle attachment for all scans.

Each FTIR scan was performed on the etched sample as soon as was possible following the drying process. A sample was not etched until an FTIR spectrum had been obtained for the previous sample. This ensured that the time between etching and obtaining the FTIR spectrum was kept to a minimum, therefore decreasing the time in which the surface could oxidise.

A spectrum was also obtained for a sample of un-etched material so that it was known what was present on the surface following removal from the line.

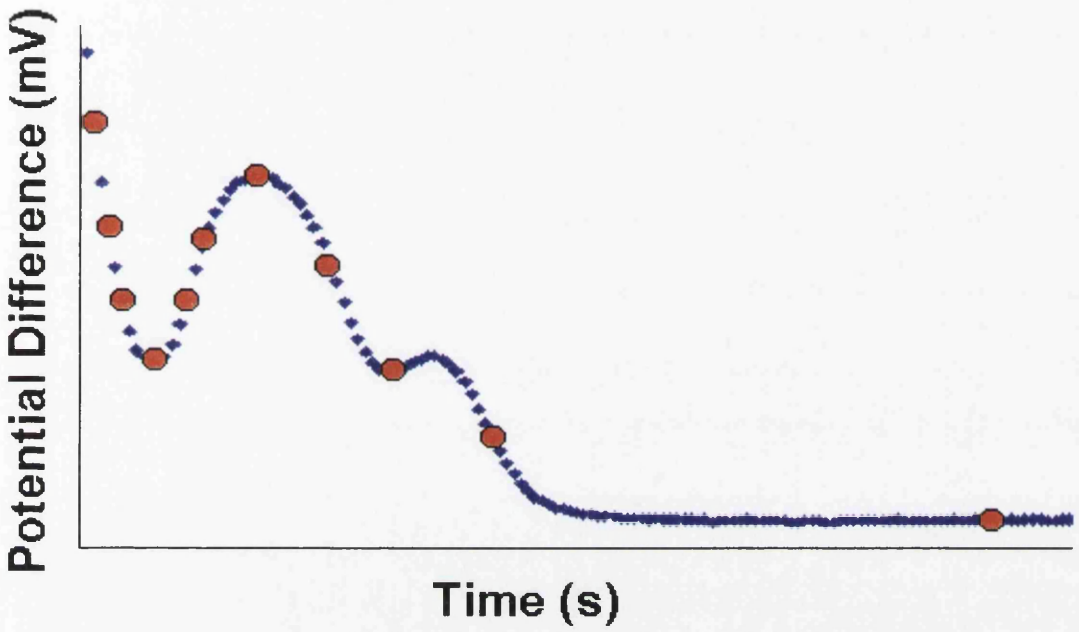

Figure 6.2: ECP profile depicting the interrupted etching intervals for the FTIR investigation.

6.2.2 Results and Discussion

The spectra obtained from each of the samples are shown in Figures 6.3 - 6.13. It should be noted that the transmittance scale is set to show the bands as large as possible so that the maximum amount of data can be extracted from each spectrum. Therefore the actual size of the bands may be different to how they appear on the following spectra.

From this data, it can be seen that at the specified points on the ECP profile:

- 0 seconds (un-etched, Figure 6.3) – There is a prominent band at ~980 cm^{-1}, which is where the band for fayalite is expected. However, there is no evidence of silica, shown by the featureless area between 1050 and 1250cm^{-1}.
- Descending to trough (Figures 6.4-6.6) – The spectrum seems to have changed drastically from that described above; the band at 980 cm^{-1} is no longer evident, but another band has appeared, centred around ~1135 cm^{-1}. This band is observed to increase in size as the etching time increases. This peak is at a lower wavenumber to that seen in Section 4, but is likely to still be silica, based on other reference spectra [33, 41]. Further evidence for this link between this absorption band and silica is given by the appearance of an additional smaller band at approximately 490cm^{-1}, as this is also related to silica [33, 41]
- At the base of the trough (Figure 6.7) – this set of spectra showed many similarities to that which preceded it. Again there was a significant band close to where it had been observed previously, but it appeared to have shifted from the original position at ~1135cm^{-1} to a wavenumber closer to 1200cm^{-1}. This is closer to the wavenumber at which silica was expected to be observed, according to [31, 40], and where it had been observed experimentally in

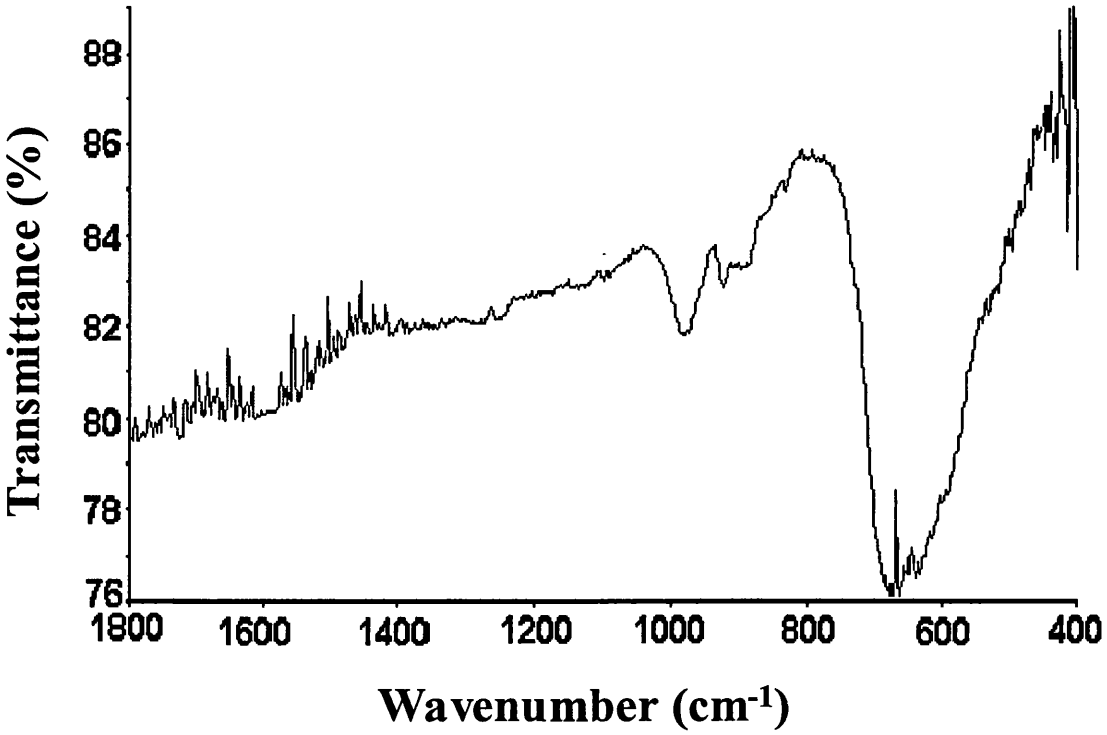

Figure 6.3: FTIR spectrum of un-etched material.

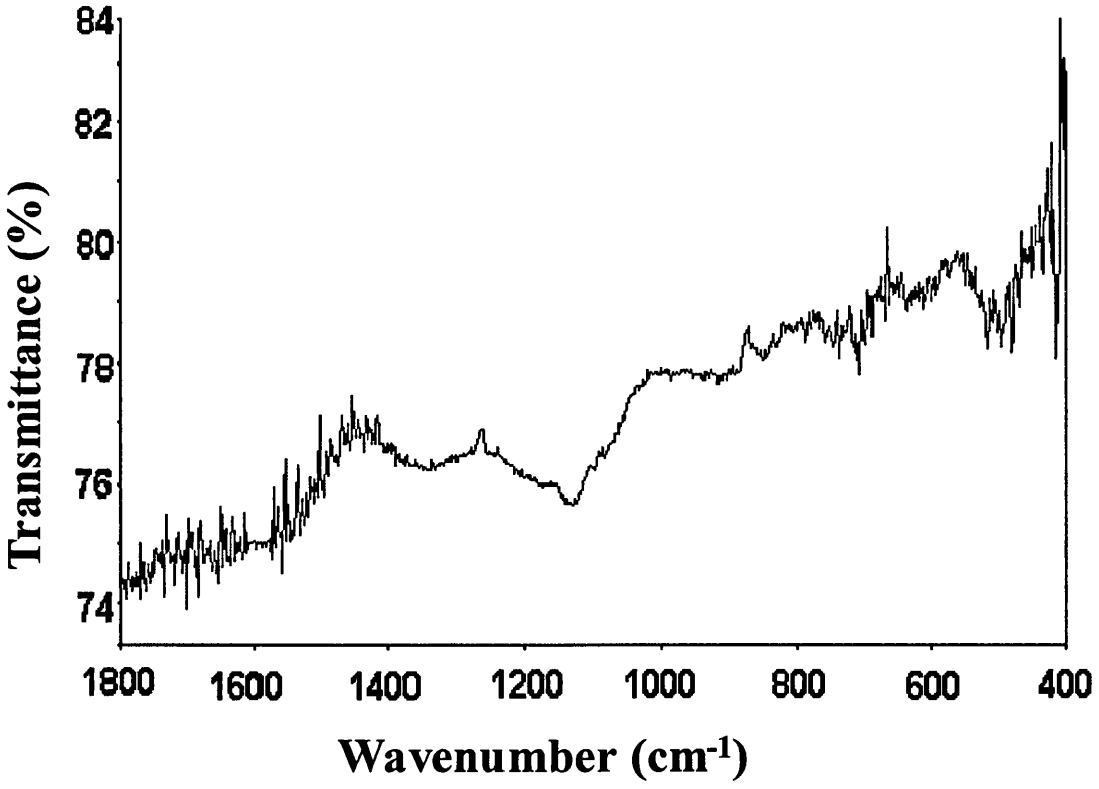

Figure 6.4: FTIR spectrum of material etched for 10 seconds.

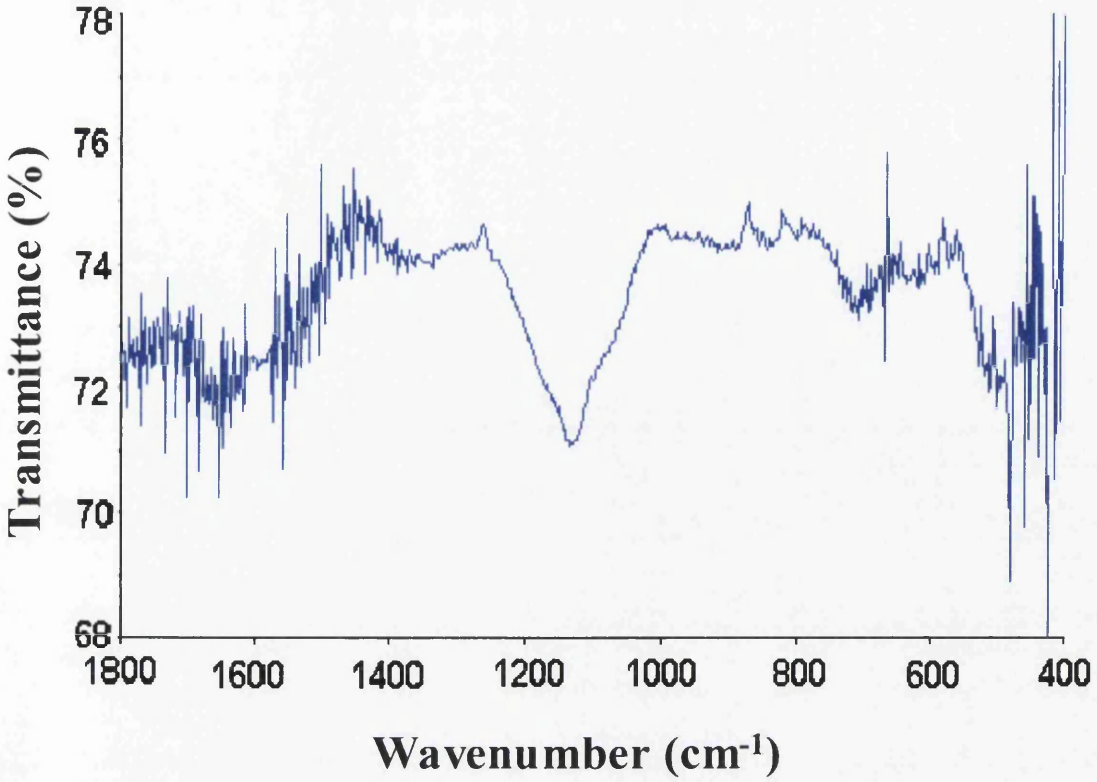

Figure 6.5: FTIR spectrum of material etched for 20 seconds.

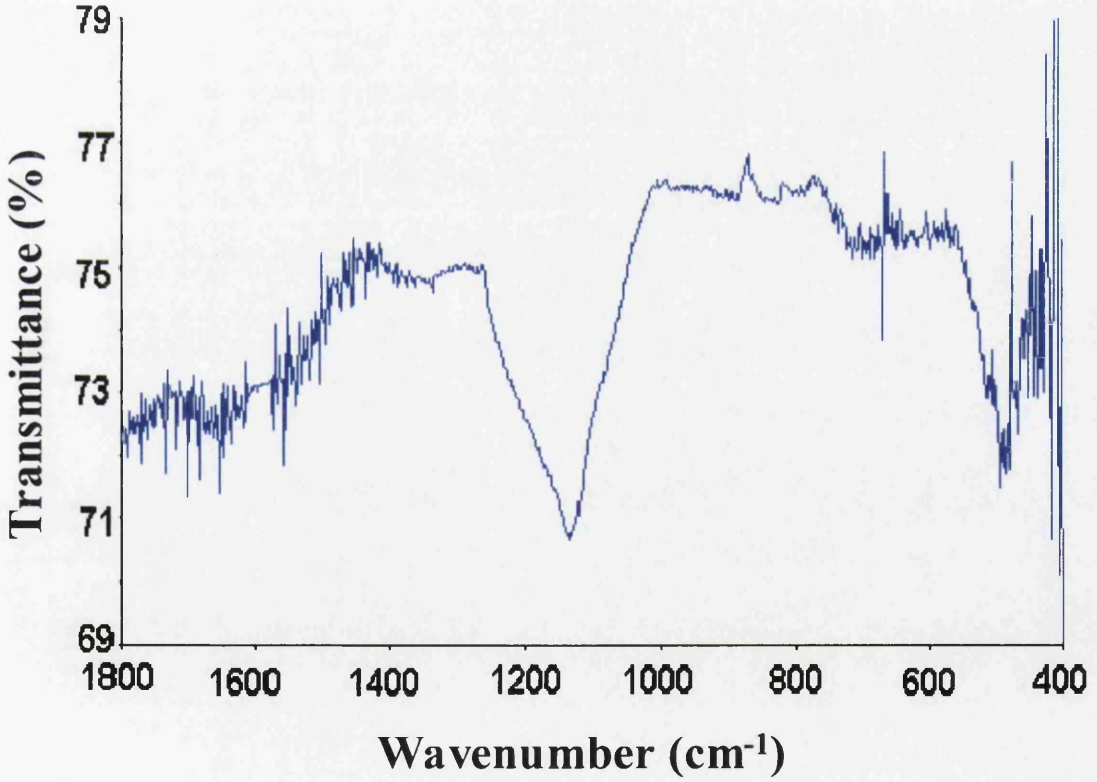

Figure 6.6: FTIR spectrum of material etched for 30 seconds.

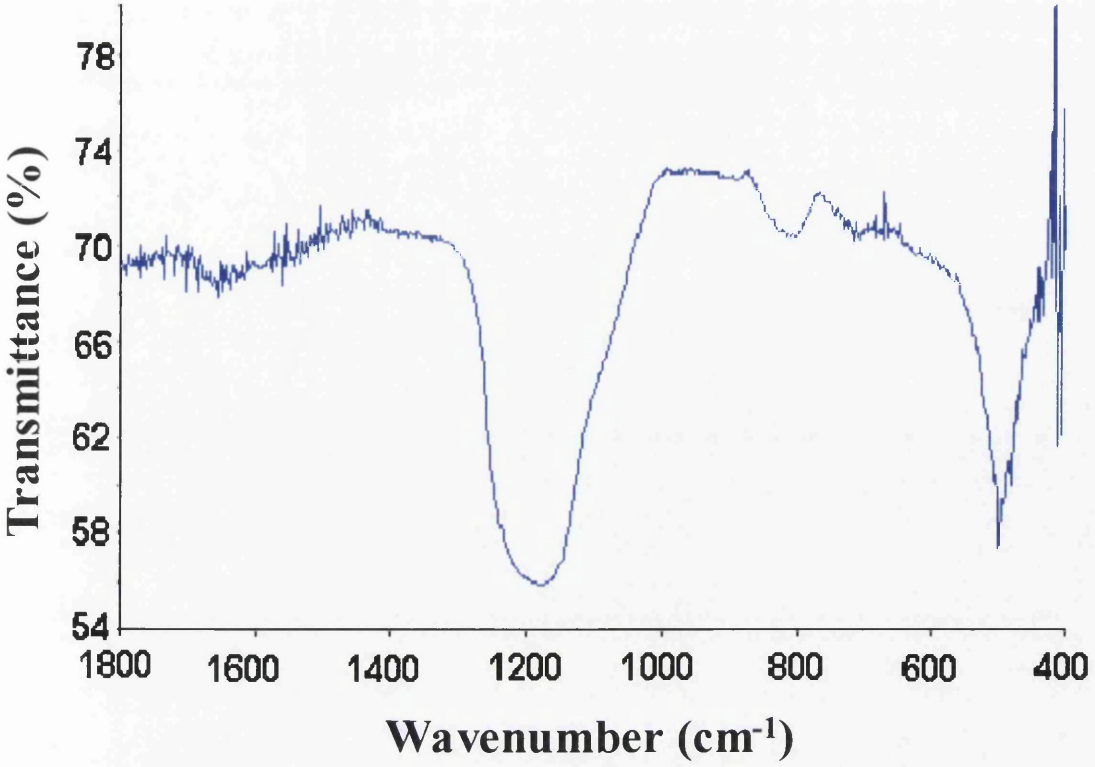

Figure 6.7: FTIR spectrum of material etched for 60 seconds.

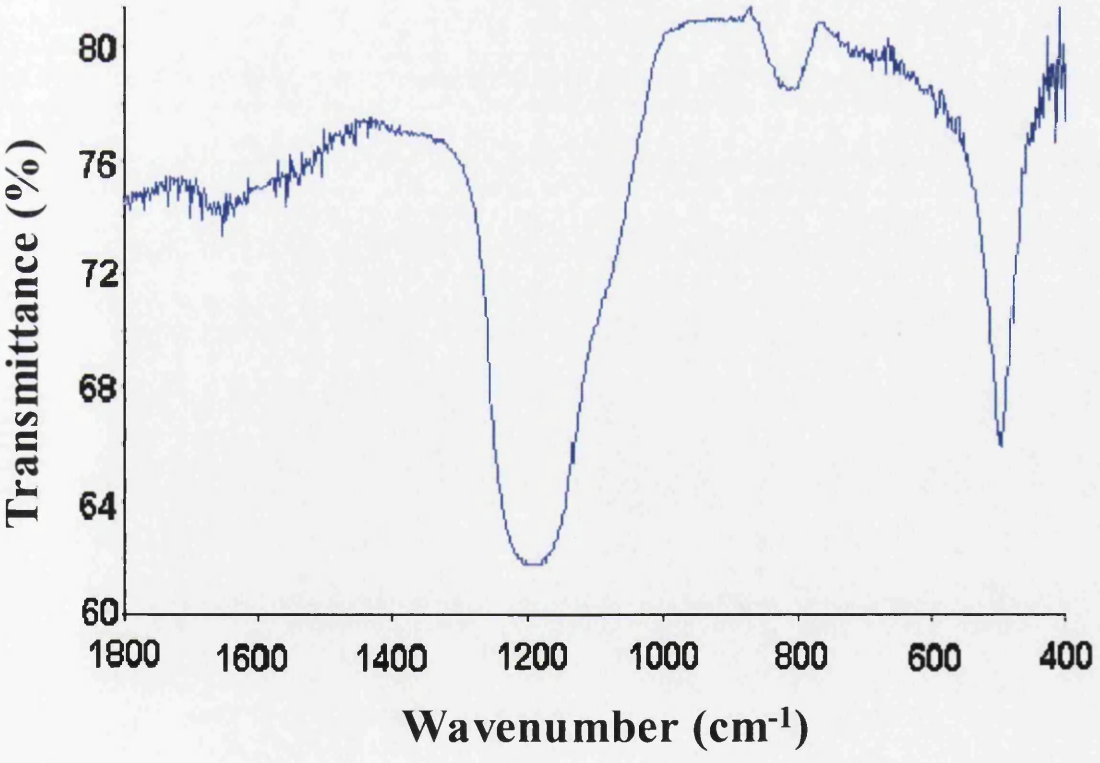

Figure 6.8: FTIR spectrum of material etched for 85 seconds.

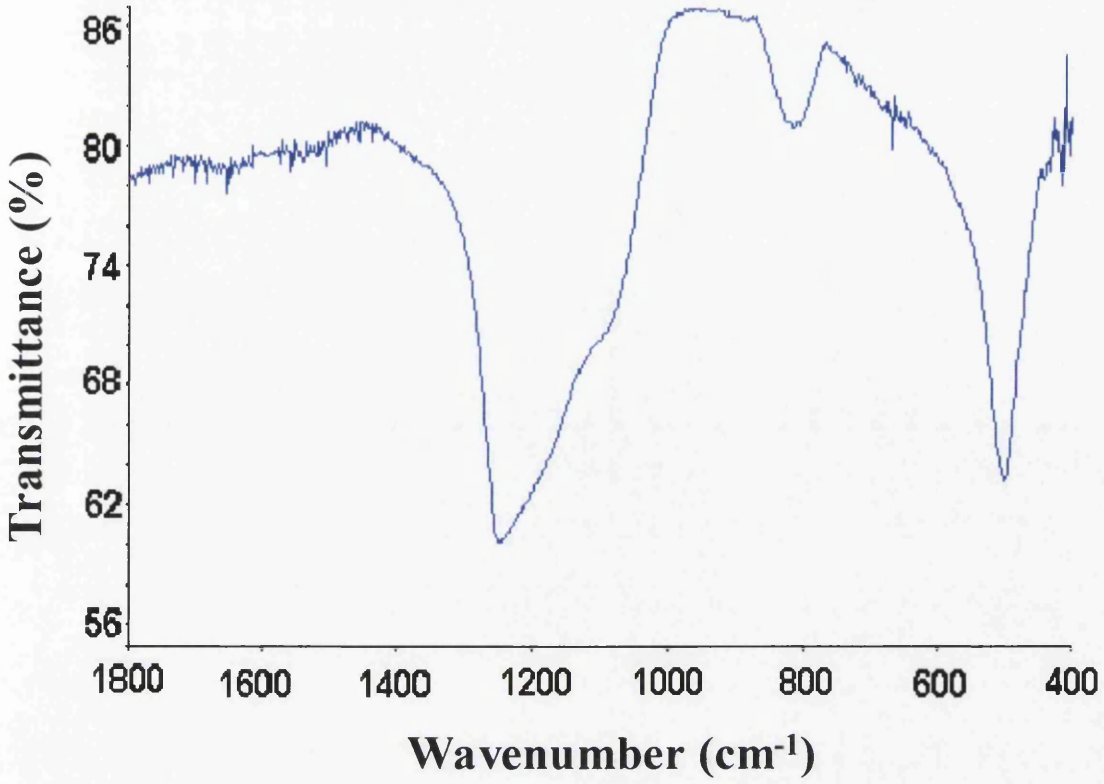

Figure 6.9: FTIR spectrum of material etched for 95 seconds.

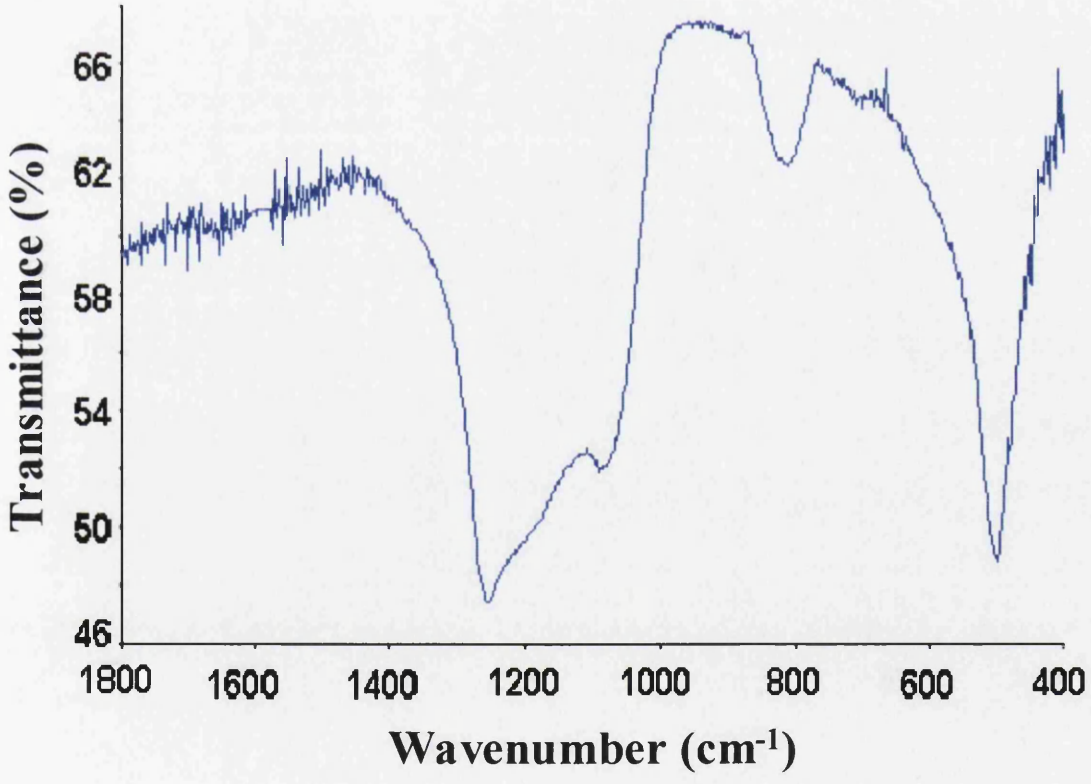

Figure 6.10: FTIR spectrum of material etched for 125 seconds.

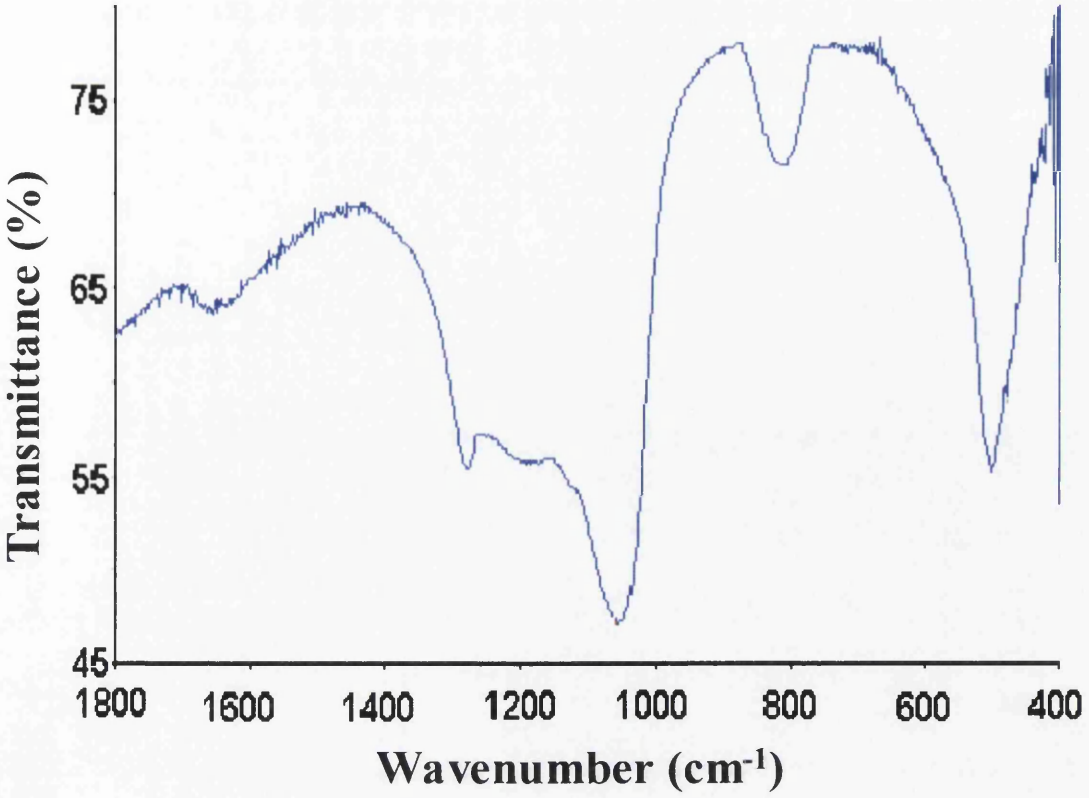

Figure 6.11: FTIR spectrum of material etched for 215 seconds.

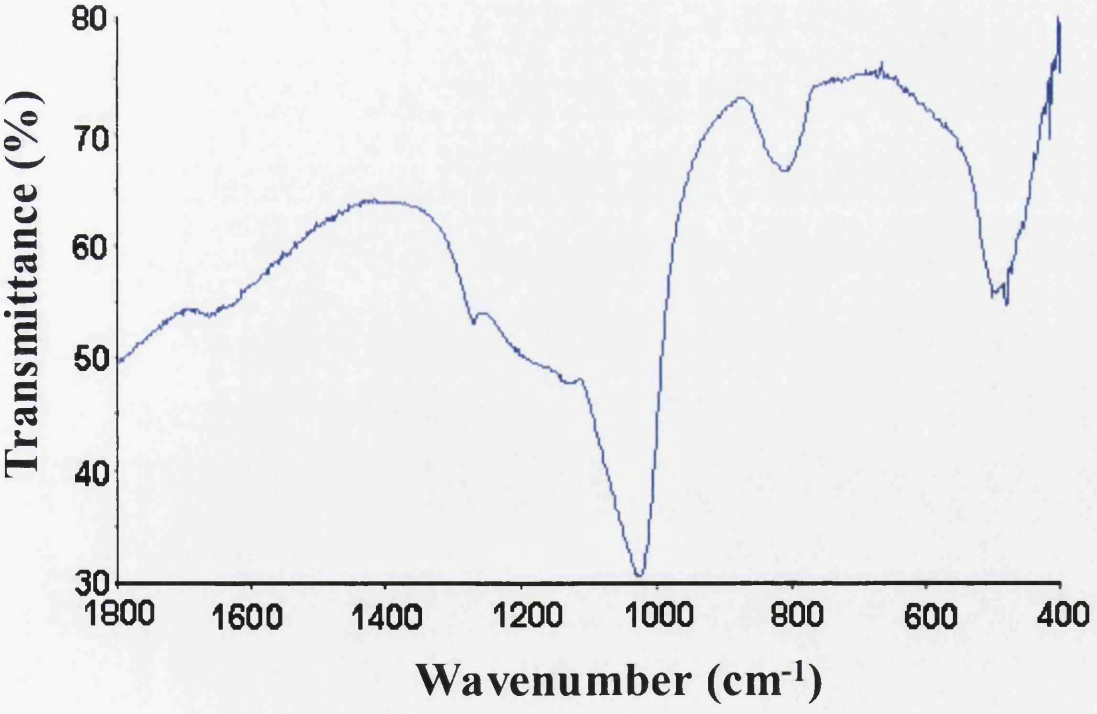

Figure 6.12: FTIR spectrum of material etched for 275 seconds.

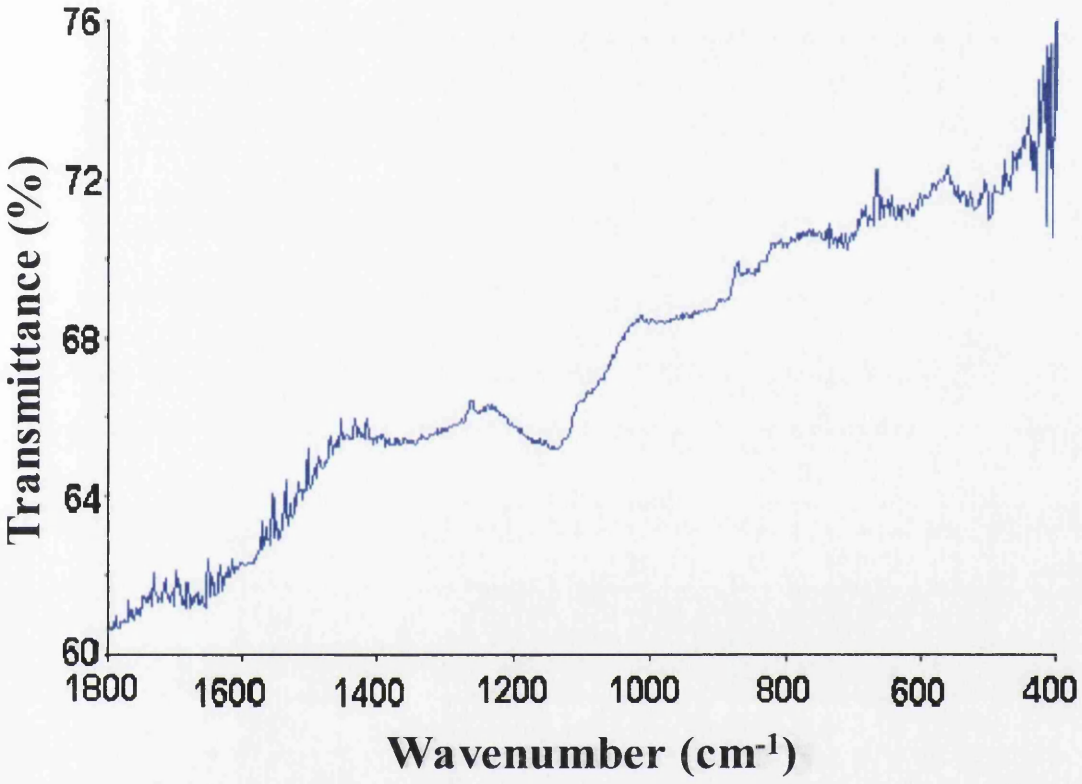

Figure 6.13: FTIR spectrum of material etched for 360 seconds.

Section 4. The trough of this band had also become more rounded than seen previously.

The band at 490cm^{-1} was again seen and was sharper than other previous spectra. It should be noted that the scale on this spectrum is significantly different to those before it, and these two bands are now far more substantial in size.

A third band also begins to appear at approximately 800cm^{-1} (Figure 6.7). Evidence links a band at this wavenumber to silica [33, 41].

- Ascending towards peak (Figures 6.8 and 6.9) – Again the three bands similar to those previously observed were present. However, the band at ~1200 cm^{-1} began rounded at the trough, but appeared to become sharper as the peak of the ECP profile was approached. The wavenumber at which this band occurred again appeared to increase, up to a maximum of ~1250cm^{-1} for the sample etched for 95 seconds (Figure 6.9). There also appeared to be a slight 'shoulder' forming at approximately 1100cm^{-1} on this band.

  The size and shape of the bands at 800 and 490cm^{-1} did not appear to alter much.

- Peak reached (Figure 6.10) – Again, this spectrum shows quite a significant change. The band that was seen with its trough at ~1200-1250 cm^{-1} has continued to widen, and has now begun to separate into separate bands, the two main ones being centralised around approximately 1250 and 1080 cm^{-1}. The evidence of any feature around 1130cm^{-1} now appears only as an almost negligible shoulder on the band at 1250cm^{-1}. It is this wavenumber (1250cm^{-1}) that silica was originally expected to be found, based on the work in Section 4. This is the most significant band in this area of the spectrum. Of

the other bands that had previously been seen, the ones at~800 and 490 cm^{-1} had now increased in size, with the latter also shifting to a slightly higher wavenumber (~500 cm^{-1}).

- Descending to baseline (Figures 6.11-6.13) – The feature between 1000-1300cm^{-1} remained resolved into two separate bands immediately after the potential of the ECP profile descended following the peak, with the base of one of the troughs at ~1080cm^{-1} and the other at ~1250cm^{-1}. However, the samples relating to points after the peak had been reached show the band at ~1080cm^{-1} becoming far more prominent, with the adjoining band (1250 cm^{-1}) becoming just a large shoulder upon it. This contrasted with the spectra related to the samples prior to the peak being reached on the ECP profile, where the band at ~1250^{-1} was far more prominent.

  The band at ~800cm^{-1} appeared to have grown further, whereas that at ~500cm^{-1} had remained almost unchanged.

  In the sample etched for 360 seconds (Figure 6.13, just before the baseline was reached) it was observed that the two main bands at 1050 and 1250cm^{-1} appeared to recombine and move to a wavenumber ~1150cm^{-1}. This spectrum only showed very slight bands at approximately 800 and 490cm^{-1}.

- Baseline reached – The spectrum for this sample showed an almost straight, featureless line. This was as expected, as this sample is at the end of a completed ECP etch, and should therefore have the entire oxide layer removed from the surface.

  The one feature present was a small band at ~670 cm^{-1}. However this band has been present on each of the spectra, suggesting that it is present at all stages of etching. This could suggest that there was slight contamination of

each of the samples, although this effect appears to be negligible due to the size of the band.

6.2.3 Conclusions of Section 6.2

The results show that following only a small amount of etching, the fayalite in the uppermost section of the decarburisation oxide layer is removed. There are no fayalite bands shown on the relevant spectrum even before the trough on the ECP profile is reached. Instead, a band is observed at ~1135cm^{-1}. Although this is at a wavenumber lower than that observed in Section 4, many reference sources suggest that this band is related to silica (SiO_2).

Once the trough has been reached on the ECP profile, this main band shifts to approximately 1250cm^{-1} where it then subsequently appears to separate due to it comprising of two separate components. This occurs on the spectrum relating to the sample that was removed when the ECP profile reached its peak. At this point, the band that previous work has suggested is linked to silica (1250cm^{-1}) was the dominant feature. However, as the potential difference decreases after the peak, the peak at ~1080cm^{-1} becomes more dominant. This is a band that, according to a number of reference sources, also relates to silica. During comparison with the spectra obtained when analysing the separate constituents of the final insulation coating, it was also noted that the pure colloidal silica also exhibited bands at approximately 1050, 800 and 500cm^{-1}.

Discussions with personnel highly skilled in the analysis of FTIR spectra suggested that it was entirely plausible that both of these bands (1080 and 1250cm^{-1}) are related to the presence of silica, but they would be of two different forms that would interact with the infrared radiation in different ways. The presence of relatively constant

bands at approximately 500 and 800cm^{-1} on the spectra containing bands at both 1080 and 1250cm^{-1} lends support to this theory.

It may be that this band is due to the change between amorphous silica that is found on the surface of the steel and the crystalline silica that protrudes into the steel substrate itself. However, this is unlikely as the spectra related to the two different forms are expected to be quite similar.

An alternative view is that the band at 1050-1100cm^{-1} is confirmed as being related to silica due to the overwhelming support of a number of articles, but the band at 1250cm^{-1} is in fact linked to a different, as yet undetermined, compound such as other silicates and / or oxides. However, this seems unlikely due to the limited number of elements that are present on such a material, and the fact that iron oxides do not appear to exhibit absorption bands on an FTIR spectrum.

An interesting feature of these results is that a link between changes in the FTIR spectra and the positions of the ECP profile can clearly be seen. The characteristic trough and peak of the ECP profile are found to coincide with the changes in the spectra where the main band of interest changes from its higher value (~1250cm^{-1}) to its lower value (~1100cm^{-1}). This suggests that the ECP technique can be used to characterise different decarburisation oxide layers.

6.3 Combination of Scanning Electron Microscopy (SEM) and Interrupted ECP Techniques

A further technique used in conjunction with the interrupted ECP method was scanning electron microscopy (SEM). This is another surface sensitive method, and is

likely to analyse only the uppermost part of the oxide layer. Therefore it would analyse only the exposed area at each etching interval, similar to the FTIR investigation described in Section 6.2. The results from the FTIR investigation led to possible conclusions as to the relevance of the different shapes and distinctive characteristics of an ECP profile. However, the conclusions that were drawn were not completely authoritative and required additional investigation in order to provide further evidence from which definitive conclusions may be drawn. Using the SEM technique enables the surface of the samples to be observed, which may be able to determine the differences between different forms of silica, and also analyses the composition of the surface layers. This compositional analysis could give the weight percentage of a number of elements, the main ones of interest in the oxide layer being oxygen, silicon and iron as these are the constituents of silica and fayalite. It is for this reason that SEM has been considered for the analysis of the decarburisation oxide layer.

6.3.1 Experimental Procedure

A length of strip was taken from a decarburisation line at Orb Works and cut into smaller samples for ECP analysis. The samples were again taken from a small area of the strip to minimise variations in the oxide layer. The experimentation was carried out using the standard ECP procedure, with the samples being removed at intervals relating to the ECP profile. These positions are shown on Figure 6.14. They corresponded to etching times of 5, 20, 40, 90, 150, 230, 300 and 1000 seconds. It can be seen that this material exhibited a smaller secondary peak, and a sample was deliberately taken at this point to determine the characteristic of the oxide layer that was causing it to be observed.

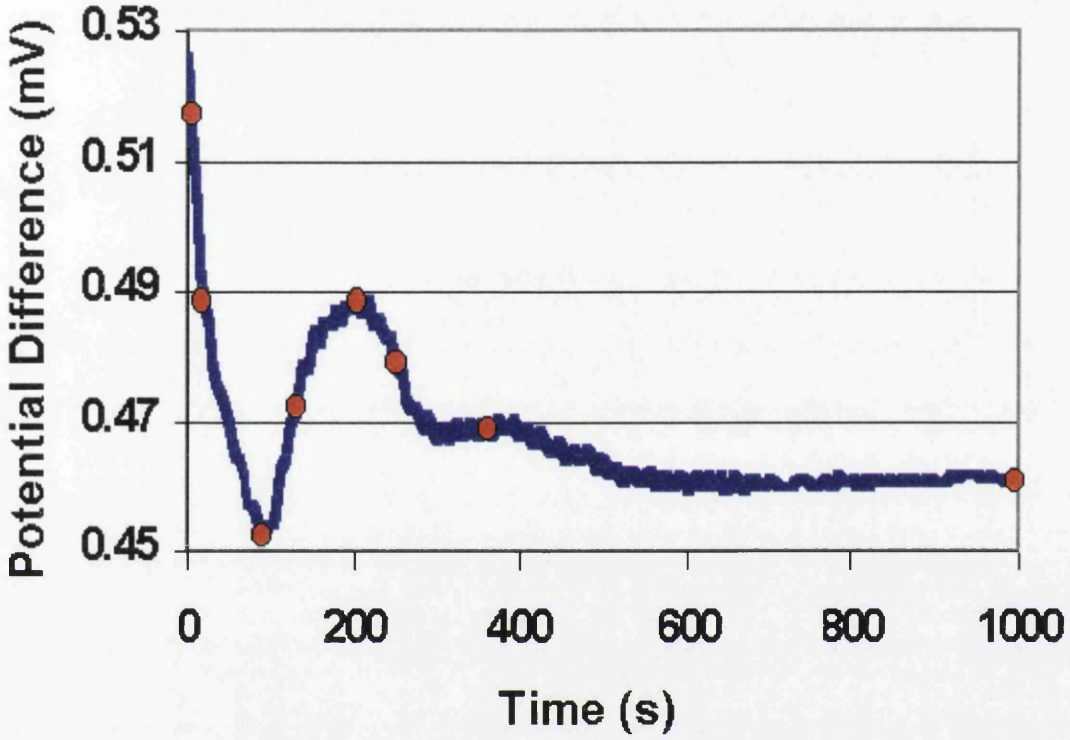

Figure 6.14: ECP profile depicting the interrupted etching intervals for the SEM investigation.

Ideally, many more samples would have been taken at other etching times, but due to time constraints in analysing the samples with the SEM apparatus, this number of samples was considered adequate. Further samples would cause an excessive amount of time to elapse between the etching process and the SEM analysis. Upon removal from the acid, it was necessary to rinse the samples with water to ensure that the acid did not continue to attack the layer, and then thoroughly dry them using a hot-air blower.

Corus personnel performed the SEM analysis of these samples using the apparatus based at ECM^2, Port Talbot.

6.3.2 Results and Discussion

The images of the oxide layer at various stages of etching (Figures 6.15 - 6.24), obtained using the SEM apparatus, proved to be inconclusive. This was due to only one area on each sample being considered for analysis (due to time constraints), and also the quality of the images themselves. However, there was still some useful information that could be extracted.

It can be seen that in Figures 6.15 - 6.18 that the lines associated with the rolling direction are clearly evident, with the rolling direction in Figure 6.17 being at 90° to that seen in the other three images. Many regions can be seen that show areas of depressions. This is similar to what is seen when using an optical microscope, and is related to the surface roughness of the material. These depressions are not merely holes through the oxide layer to the steel substrate below, but in fact also have an oxide layer formed on the surface within it. In many cases, certain parts of this oxide layer may be even thicker than on the rest of the surface due to the increased surface area of the curved depression.

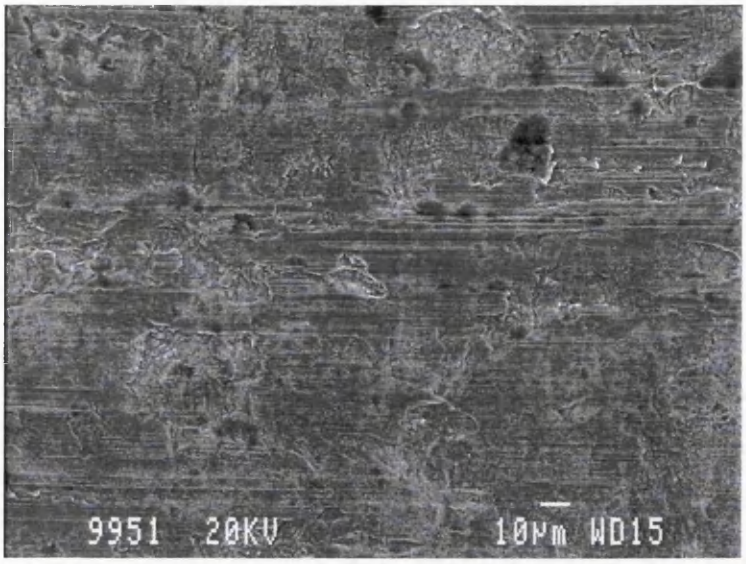

Figure 6.15: SEM Image

Etching time: 0s

(Un-etched material)

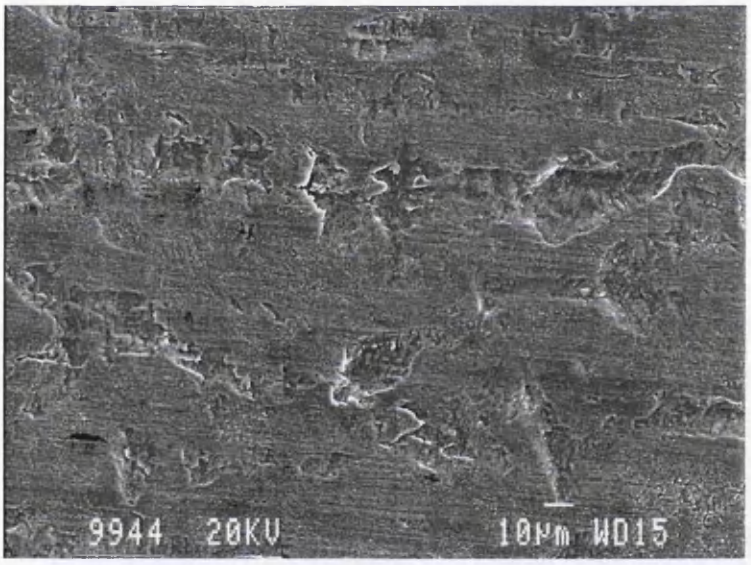

Figure 6.16: SEM Image

Etching time: 5s

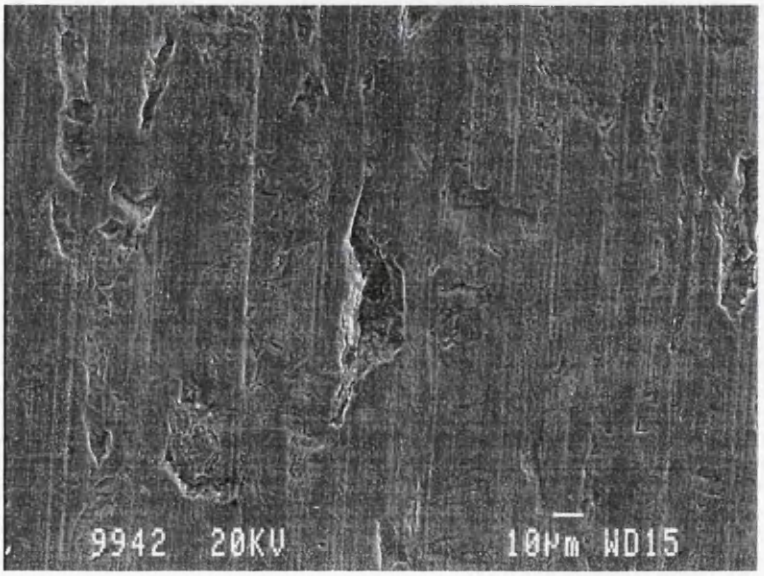

Figure 6.17: SEM Image

Etching time: 20s

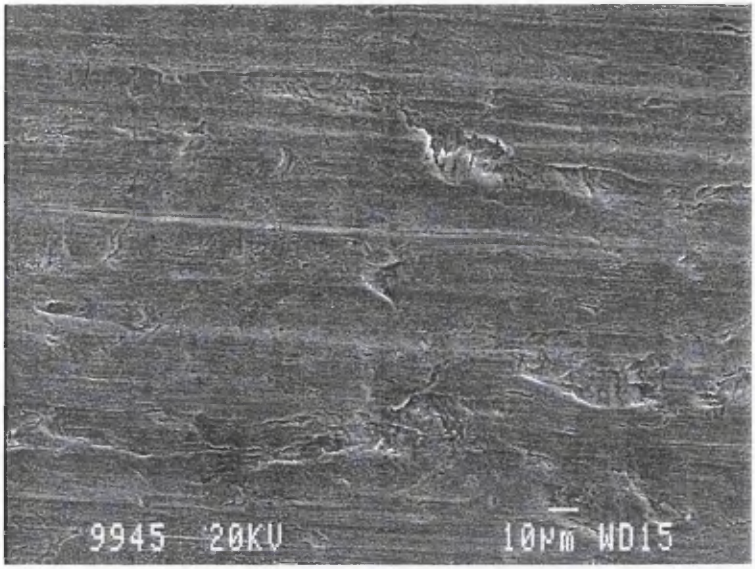

Figure 6.18: SEM Image

Etching time: 40s

Bottom of trough

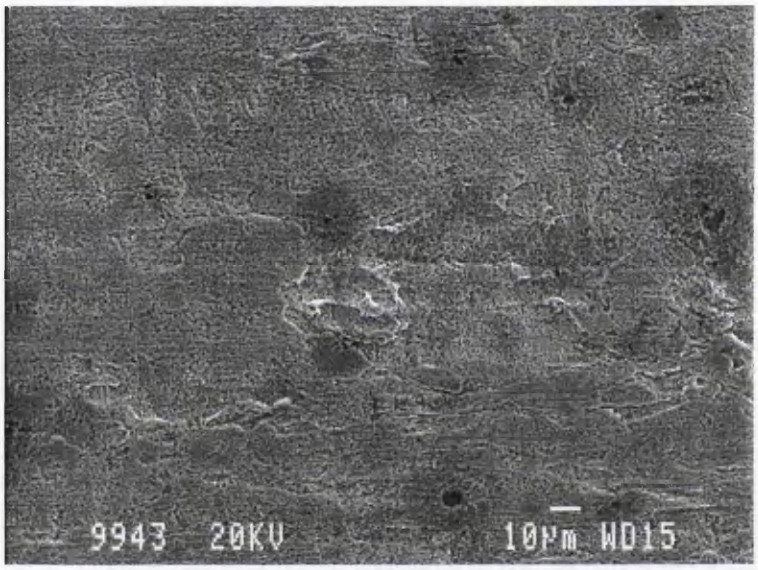

Figure 6.19: SEM Image

Etching time: 90s

Halfway between trough and peak 1

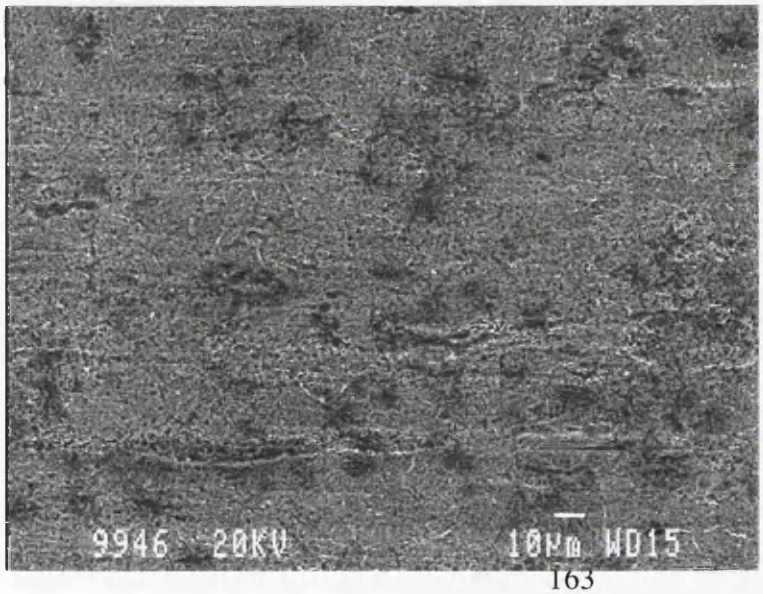

Figure 6.20: SEM Image

Etching time: 150s (#1)

Top of peak 1

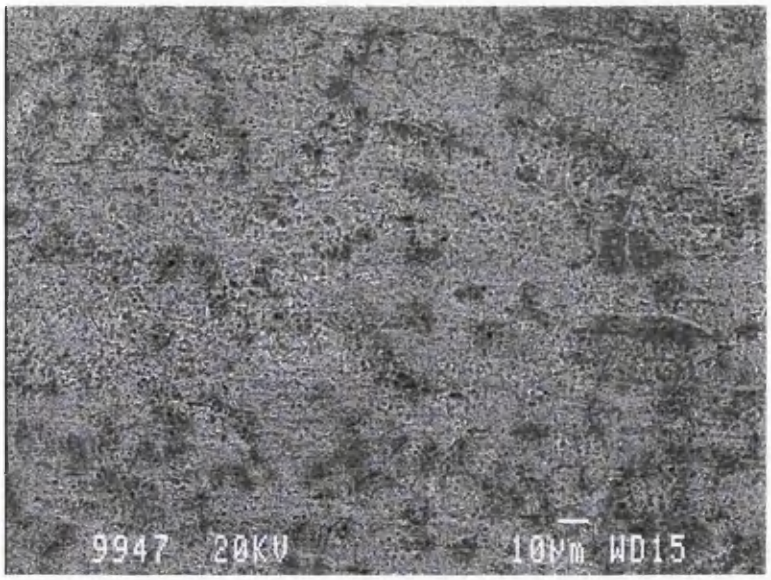

Figure 6.21: SEM Image

Etching time: 150s (#2)

Top of peak 1

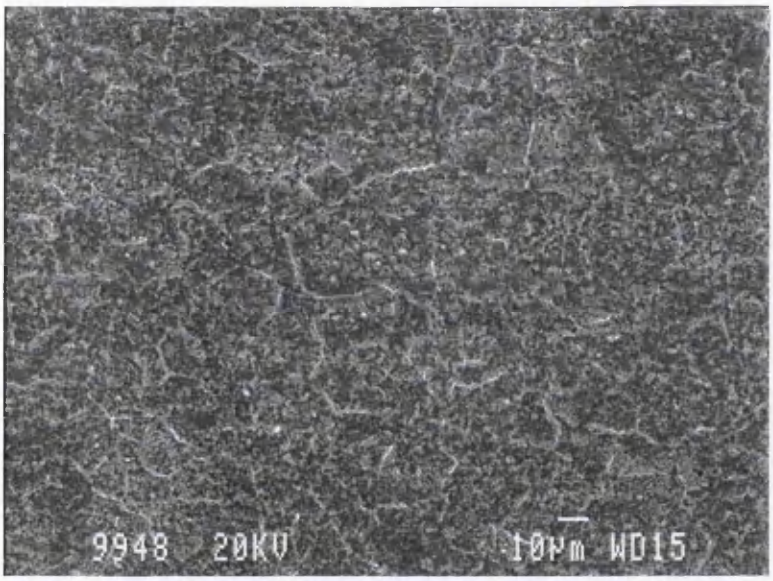

Figure 6.22: SEM Image

Etching time: 230s

Just after peak 1

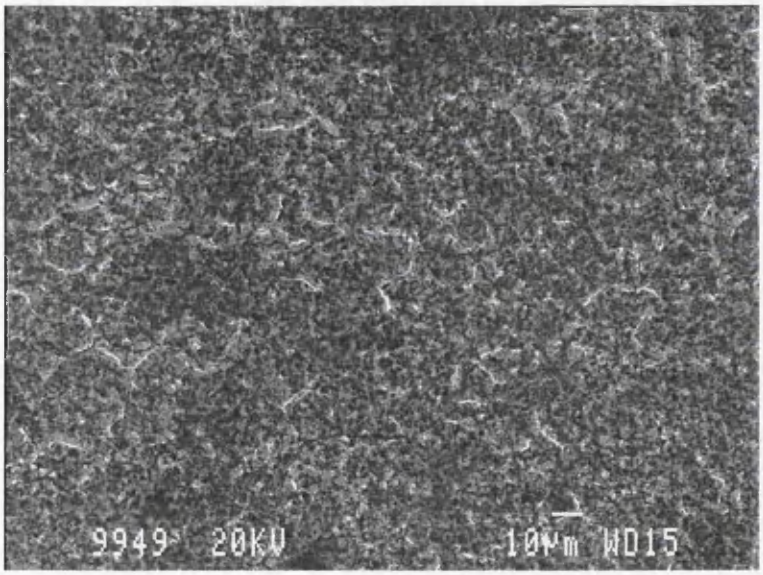

Figure 6.23: SEM Image

Etching time: 300s

Top of peak 2

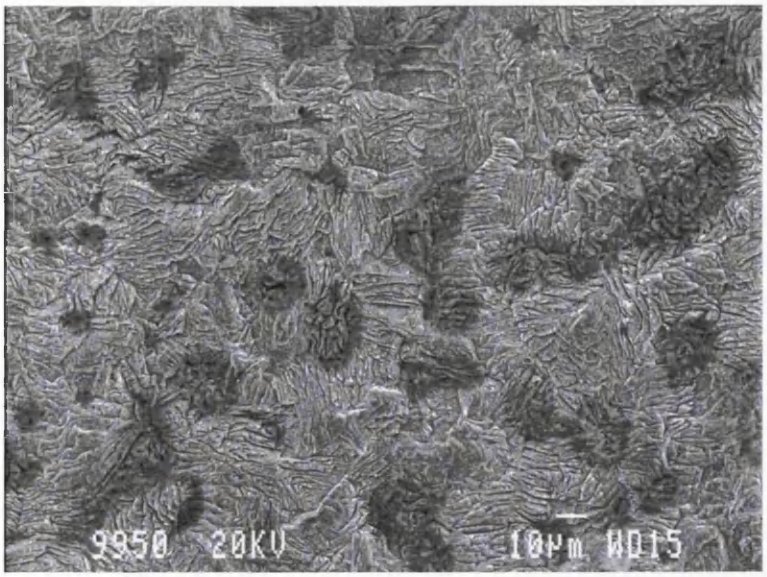

Figure 6.24: SEM Image

Etching time: 1000s

Baseline

Figure 6.19 shows a number of darker spots spread across the area of the sample. It is likely that these correspond to areas of silica, found under the initial fayalite-rich layer. These darker areas then appear to cover a progressively increasing area of the samples as the etching time is increased, until that shown in Figure 6.24. This figure corresponds to the fully etched material (base steel substrate with no oxide layer present) and the SEM image relates to what is expected, with evidence of the grains being seen.

Energy-Dispersive X-ray (EDX) analysis was also carried out in conjunction with the above SEM work. This provided data relating the elemental content at the surface for each sample. However, analysis of EDX results is complicated by the fact that the technique supplies only data relating to the separate elements, and is unable to distinguish the compound in which each element is present. This causes particular problems when considering oxygen and silicon, as these elements are present in fayalite and silica, as well as some other compounds that may be present in smaller quantities (e.g. $FeSiO_3$).

The variation in the amount of iron, oxygen and silicon as the ECP etching progressed is shown in Figures 6.25 – 6.27. Figure 6.28 shows the data from these figures on the same chart, enabling the trends to be easily compared.

The values for the un-etched material were slightly distorted due to the inclusion of magnesium. This was due to residual MgO powder that remained on the surface following cleaning. Ideally, this magnesium content, at approximately 4% (weight), could simply be removed from the calculations as it is not linked to the oxide layer. However, the situation is not that straightforward as the magnesia also contains

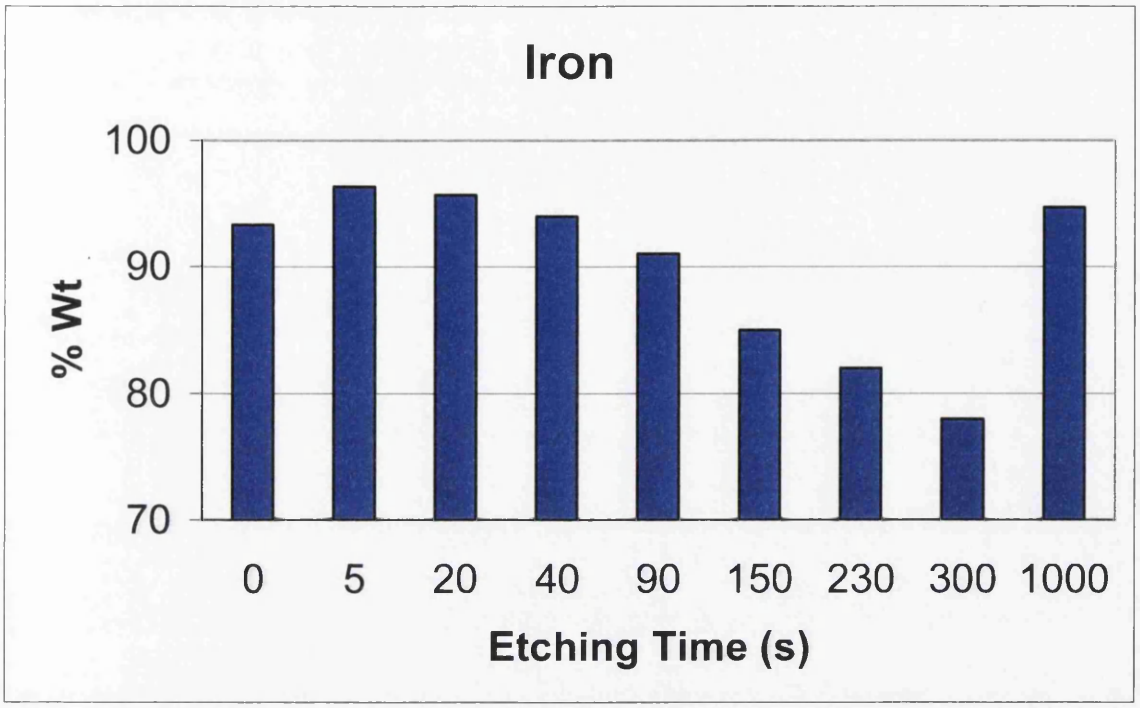

Figure 6.25: EDX iron content at various etching times.

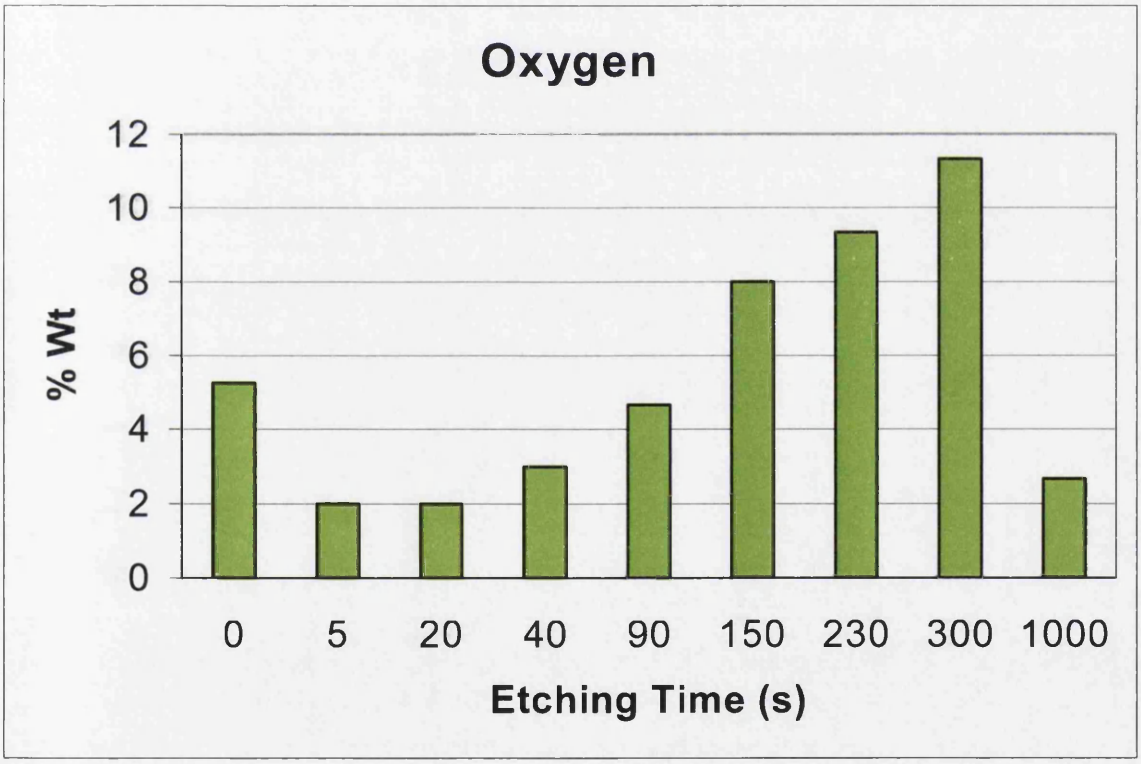

Figure 6.26: EDX oxygen content at various etching times.

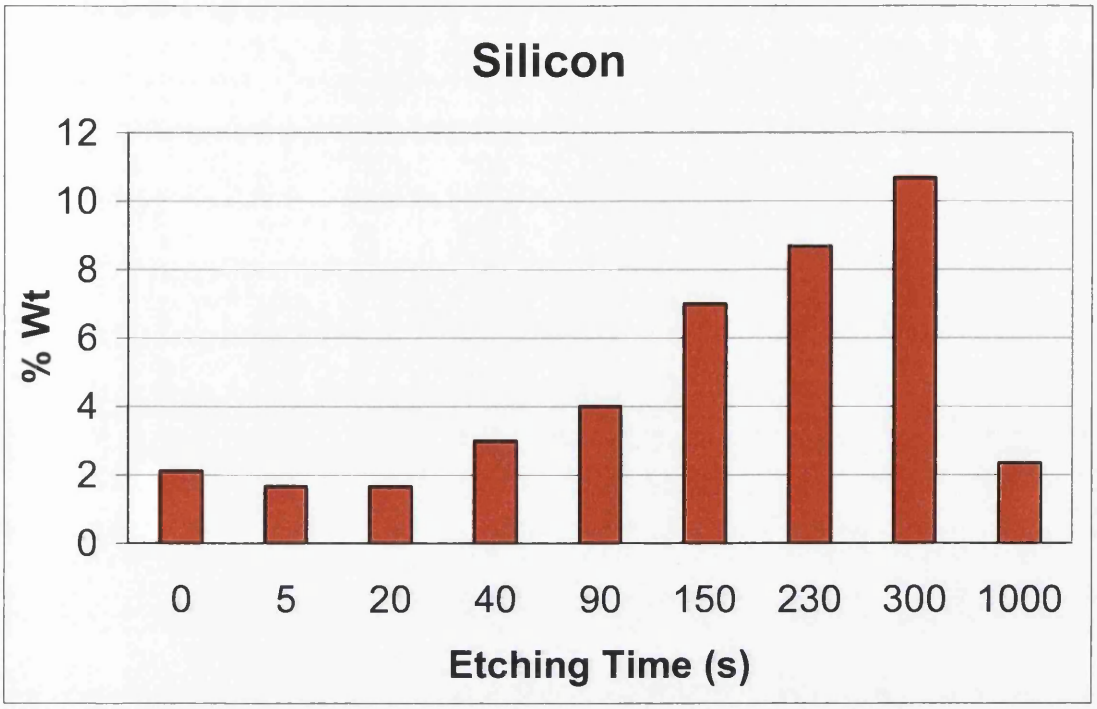

Figure 6.27: EDX silicon content at various etching times.

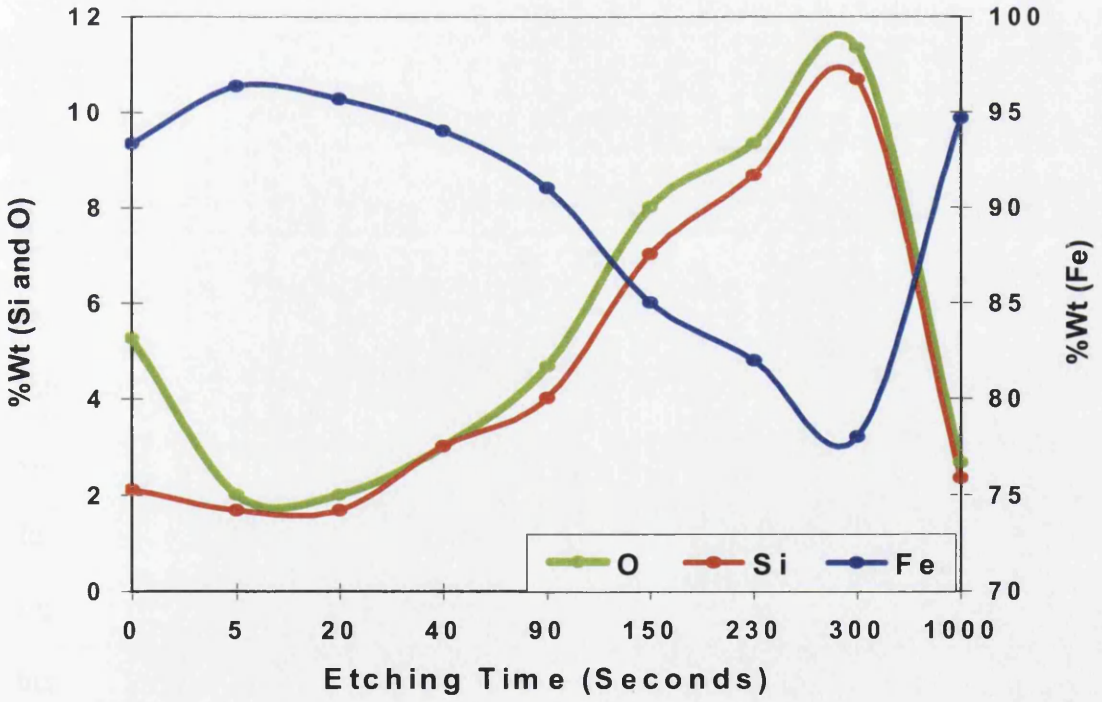

Figure 6.28: Comparison of the EDX elemental variation at various etching times.

oxygen, and so it is not clear how much of the oxygen is related to the magnesia, and how much is present in the form of MgO, Fe_2SiO_4, SiO_2 or other oxides. Therefore, the data relating to the un-etched sample should be treated with some degree of caution.

It can be seen in Figures 6.26 - 6.28 that the trends seen for silicon and oxygen are almost identical. They both show the %Wt increasing at the same rate from 5-300 seconds, with a sharp decrease at 1000 seconds. It is at this point that it is believed that bare steel has been reached. The only point at which these two sets of data significantly differ is for the un-etched material, where the oxygen content is far higher. This is likely to be due to the oxygen being combined with the magnesium to form MgO, as mentioned previously.

Figure 6.29 shows the correlation between the amounts (in %Wt) of silicon and oxygen present as the etching time increases. It should be noted that the data point associated with the un-etched material has been removed from this graph due to the potential errors in the oxygen content caused by the presence of MgO. It can be seen that the correlation is extremely good, with an R^2 value of 0.996. It is also interesting to note the equation of the trendline that has been fitted to the data. The gradient of the line can be seen to be 0.9405 and intersects the x-axis very close to zero. If we consider the increasing content of silica and oxygen in terms of their atomic mass, it is found that it provides evidence that a majority of these two elements are present in the form of SiO_2. The atomic masses of silicon and oxygen are 28.1 and 16 respectively, but there are obviously two atoms of oxygen in this compound with a combined atomic mass of 32. Therefore, as the amount of silica present at the surface increases, the silicon and oxygen should increase with a constant ratio of 0.88 between them

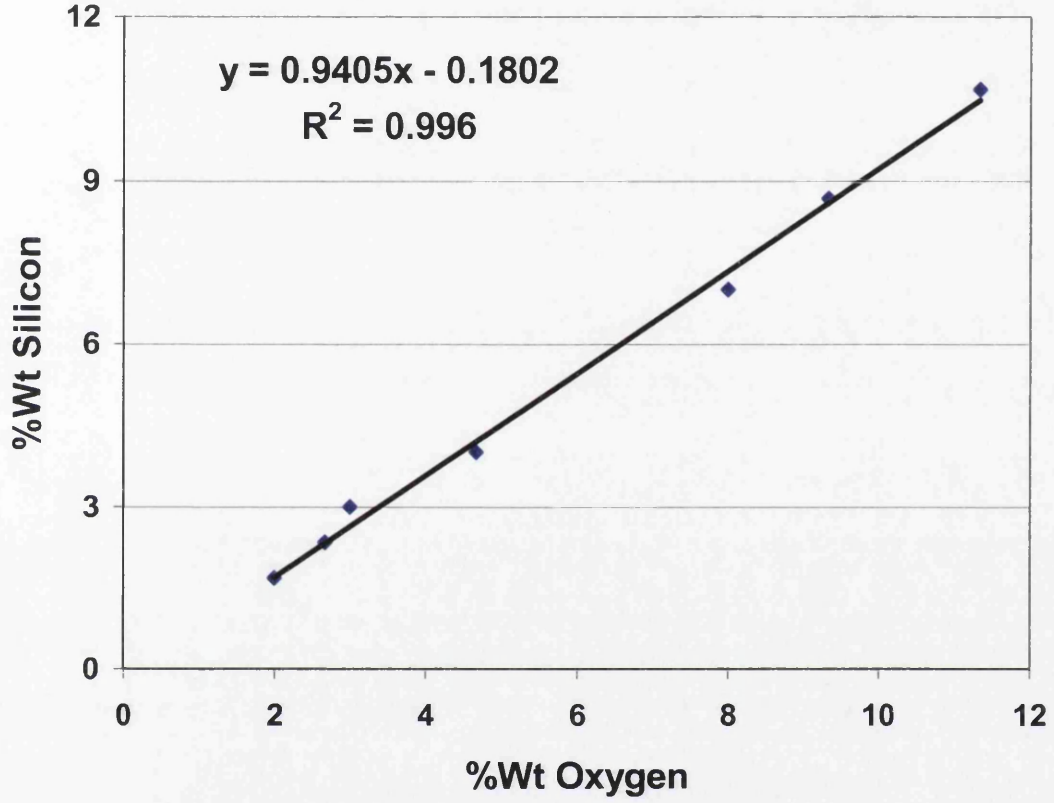

Figure 6.29: Correlation between the content of Si and O when measured using EDX.

(calculated by 28.1 / 32). This is very close to the 0.9405 of the gradient of the trendline, which is easily within the errors associated with a semi-quantitative method such as EDX. Furthermore, if the trendline is adjusted to intercept at the x-axis at 0 (as silicon would not be present without oxygen if this SiO_2 hypothesis were correct), then the gradient is altered to 0.92, which is even closer to what is predicted by the theory. The fact that this ratio is not identical to the predicted value for SiO_2 can be explained either by the errors associated with this technique, or by the possible presence of small amounts of other more oxygen rich compounds, such as SiO_3 or iron oxides. It is believed that these other compounds are often present in the oxide layer, but are in such small amounts as to be deemed negligible with respect to the amount of SiO_2.

It is clear that the trend seen for iron, shown in Figure 6.25, is significantly different to that for oxygen and silicon. This shows a decrease in iron content from 5-300 seconds, before a sharp increase at 1000 seconds. In fact, the graphs show that the data for the iron content was almost the exact opposite to the trend seen for the other two elements. As an example, Figure 6.30 uses the comparison between silica and iron contents to demonstrate this.

6.3.3 Conclusions of Section 6.3

From this work, it can be concluded that there are clear trends in the composition of the oxide layer as the layer is etched away.

The SEM images show evidence of darker areas at etching times greater than when the trough is reached. These dark areas are most likely to be associated with silica,

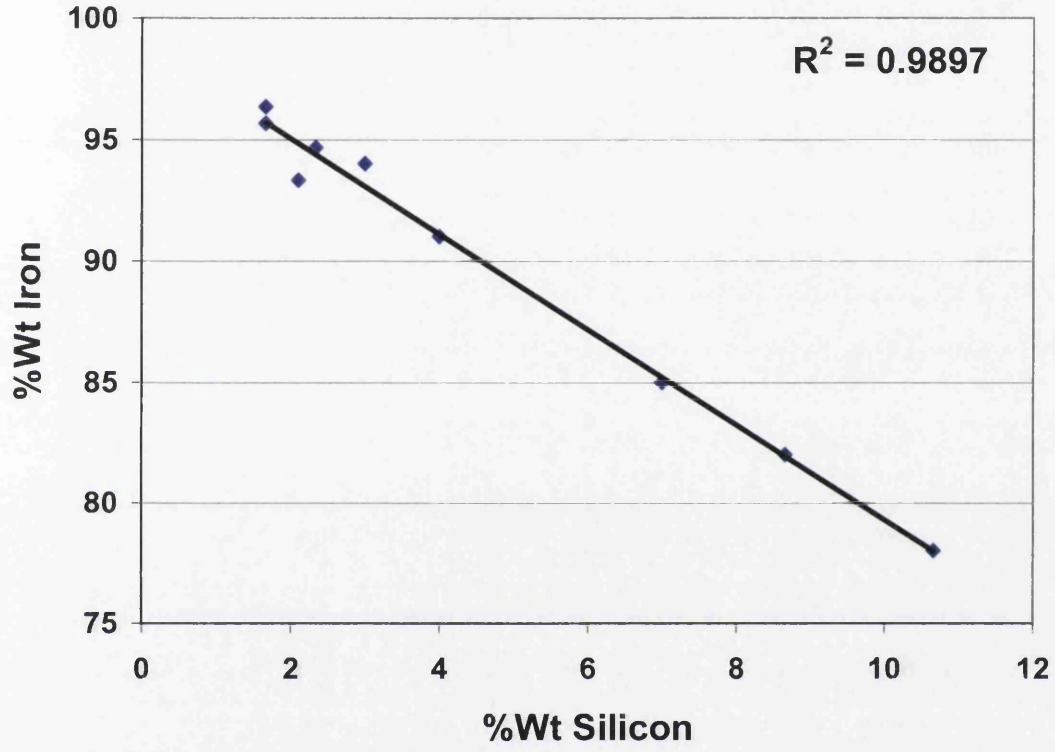

Figure 6.30: Correlation between the content of Fe and Si when measured using EDX.

and increase in number as the etching time is increased. The image observed for the sample at which the baseline has been reached shows a structure associated with the base metal, confirming full removal of the oxide layer.

Analysing the EDX data, it is clear that the silicon and oxygen show a distinct correlation suggesting that they are bonded together, with the expected SiO_2 being the most likely compound. Both of these sets of data begin to increase as soon as the etching duration begins to increase, until a maximum is reached at 300 seconds. After this point, the content of both silicon and oxygen drops dramatically when the sample that was etched to the baseline is analysed. This is where the steel substrate has been reached, and the iron content increases accordingly.

The results obtained from the EDX analysis appear to correspond with those obtained from the FTIR analysis of interrupted ECP samples, which suggests that SiO_2 is present at each etching interval.

Although these results show the trends associated with etching through the oxide layer, it should be clearly acknowledged that these results are only semi-quantitative, and therefore do not provide perfectly accurate values in terms of %Wt. They may also be slightly distorted as the penetration depth varies slightly according to the atomic mass of the element under consideration.

6.4 Combination of X-ray Photoelectron Spectroscopy (XPS) and Interrupted ECP Techniques

X-ray Photoelectron Spectroscopy (XPS) was carried out on interrupted ECP samples to complement the results from FTIR, SEM and EDX work carried out in Sections 6.2

and 6.3. This technique provides both qualitative and quantitative data relating to the composition of the surface layer. The experimental aspect of this work was carried out using the XPS apparatus located at Swinden Technology Centre (STC). A detailed description of this technique can be found in Section 2.2.4.

6.4.1 Experimental Procedure

The ECP apparatus was assembled at STC so that the samples could be quickly and easily transferred to the XPS equipment. In the case of both methods of analysis (ECP and XPS), the method and conditions used were as standard.

A representative sample from the sheet was first used as a sacrificial sample. This also provided information on the shape of the profile that was to be expected for all related samples. This was useful as a good estimate could be made as to the duration the sample would need to be etched before it reached the desired point of the profile. It was found that the material in question produced an ECP profile that exhibited a smaller secondary peak. The samples used in this investigation were from the same coil as those used for the FTIR investigation described in Section 6.2, and were etched to the same points on the profile as the FTIR samples. Therefore, the eleven points at which the samples were removed from the acid corresponded to those shown in the ECP profile in Figure 6.2. These times and positions were as follows:

A – after 10 seconds, where the sample had only briefly been immersed in acid

B – after 20 seconds, further towards trough

C – after 30 seconds, just prior to the trough being reached

D – after 60 seconds, at the base of the trough

E – after 85 seconds, where the profile has started to ascend following the trough

F – after 95 seconds, prior to the first peak being reached

G – after 125 seconds, at the top of the first peak

H – after 215 seconds, between the first peak and second trough

I – after 275 seconds, at the bottom of the second trough

J – after 360 seconds, descending towards the baseline

A further sample (K) was etched to the point at which the potential difference had stabilised at the baseline, where it is believed that the oxide layer has been completely removed.

A sample of the un-etched material was also analysed to determine what was present on the surface of the strip as it was taken from the decarburisation line. To minimise the likelihood of the results being distorted by the presence of magnesia on the strip (as occurred with the EDX results), the sample was cleaned in an ultrasonic bath prior to analysis. This was considered sufficient to remove any excess MgO.

As mentioned previously, the samples were rinsed with tap water upon removal from the acid and dried with a hot air dryer. To prevent contamination of the sample, they were not wiped dry with paper towels, or bought into contact with any other material. As soon as they were dry, an XPS sample (in the form of a disc measuring approximately 5mm in diameter) was punched from the ECP sample. This was then mounted on an appropriate unit using tweezers and placed within a preliminary vacuum chamber, before being moved into the main vacuum chamber where it could be analysed.

6.4.2 Results and Discussion

It was found that the profile was of the type classified previously as a 'Type 1a' profile (Figure 5.3), where the base of the trough is at a higher level than the baseline and there is a second, less-pronounced, peak following the first.

The results from the XPS analysis have been summarised in Table 6.1, and the data for the three elements of greatest interest (Fe, O and Si) is also shown graphically in Figure 6.31. Carbon was also included on this figure due to the magnitude of the amount present in the results.

In the table, the elements refer to the following orbitals:

Iron –	$2p^3/_2$	Nitrogen –	1s	Calcium –	2p
Carbon –	1s	Sulphur –	2p	Manganese –	$2p^3/_2$
Oxygen –	1s	Tin –	$3d^5/_2$	Magnesium –	2s
Silicon –	2p	Chlorine –	2p	Phosphorous –	2p

Figures 6.32 – 6.35 show the data for each of the separate elements for clarity. A representative ECP profile is also included on these figures so that a comparison can be made between the composition of the oxide layer and the respective position on the profile. It should be noted that the x-axis relates directly to the particular etching times, and is therefore not linear.

It can be seen from these results that:

- There is a relatively large presence of magnesium on the un-etched material, but not even trace amounts in any of the etched samples,

Time	Fe	O	C	Si	S	Sn	Ca	N	Cl	Mn	Mg	P
0	5.69	56.92	21.87	1.00	0.00	0.00	0.00	0.00	0.00	0.00	14.44	0.08
10	18.09	49.47	30.12	0.63	0.28	0.03	0.58	0.10	0.12	0.30	0.00	0.29
20	17.76	51.64	27.89	0.37	0.44	0.12	0.59	0.34	0.00	0.31	0.00	0.54
30	16.60	48.71	31.37	1.32	0.30	0.06	0.77	0.18	0.13	0.28	0.00	0.26
60	15.61	53.68	25.27	3.38	0.44	0.00	0.76	0.29	0.15	0.27	0.00	0.15
85	15.76	52.32	23.71	7.04	0.16	0.17	0.42	0.10	0.00	0.32	0.00	0.00
95	9.47	47.44	35.16	6.64	0.00	0.06	0.75	0.19	0.00	0.13	0.00	0.15
125	7.13	51.30	28.96	11.83	0.00	0.00	0.61	0.07	0.00	0.11	0.00	0.00
215	2.56	56.38	23.41	17.00	0.00	0.05	0.30	0.17	0.14	0.00	0.00	0.00
275	1.14	62.19	15.97	20.30	0.00	0.11	0.18	0.06	0.00	0.05	0.00	0.00
360	10.94	48.27	37.46	0.92	0.57	0.05	0.52	0.40	0.00	0.45	0.00	0.42
1200	12.49	48.92	35.13	0.57	0.42	0.06	1.13	0.27	0.18	0.29	0.00	0.56

Table 6.1: XPS data from interrupted ECP investigation.

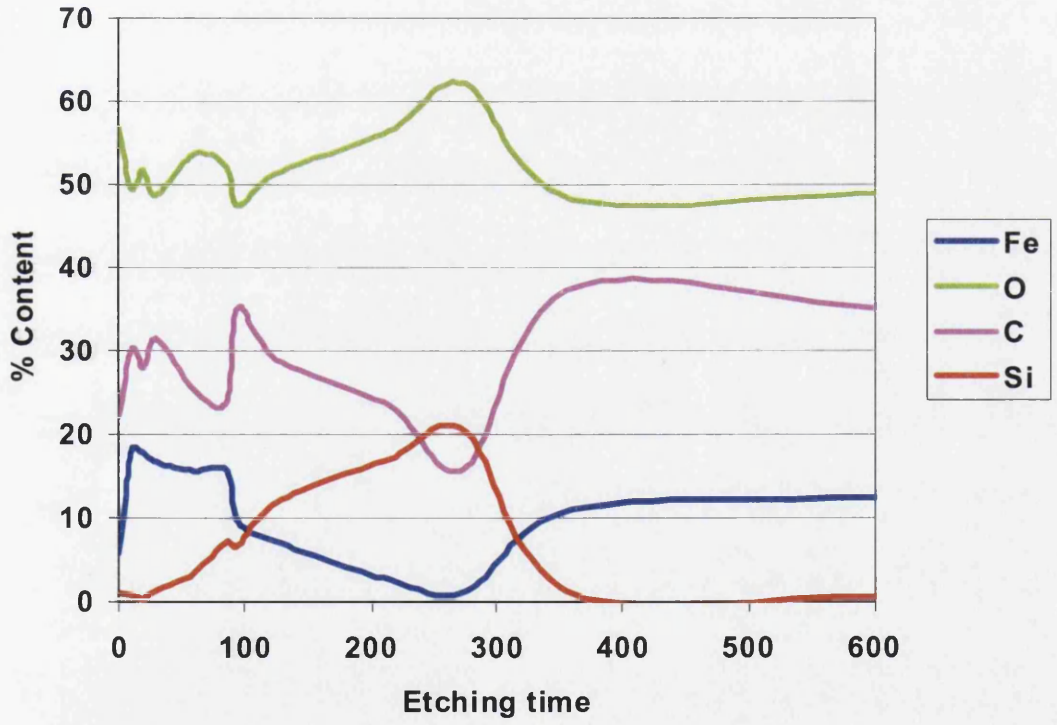

Figure 6.31: Graphical representation of XPS data from interrupted ECP investigation.

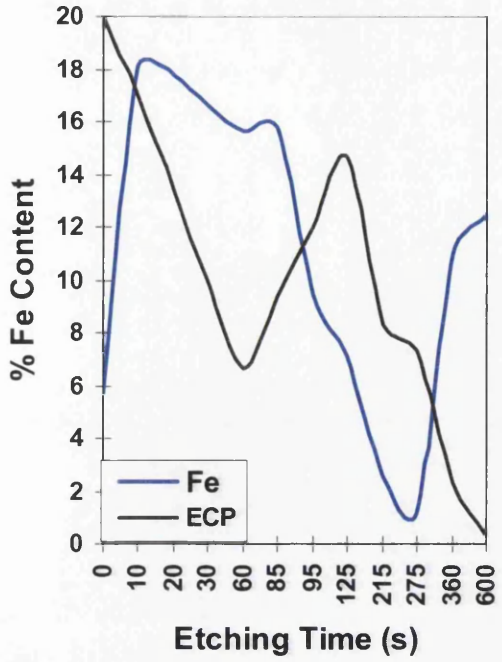

Figure 6.32: Fe Content Compared to ECP Profile

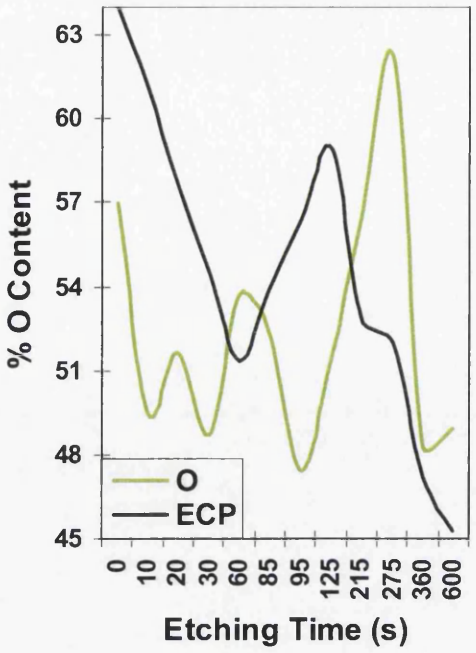

Figure 6.33: O Content Compared to ECP Profile

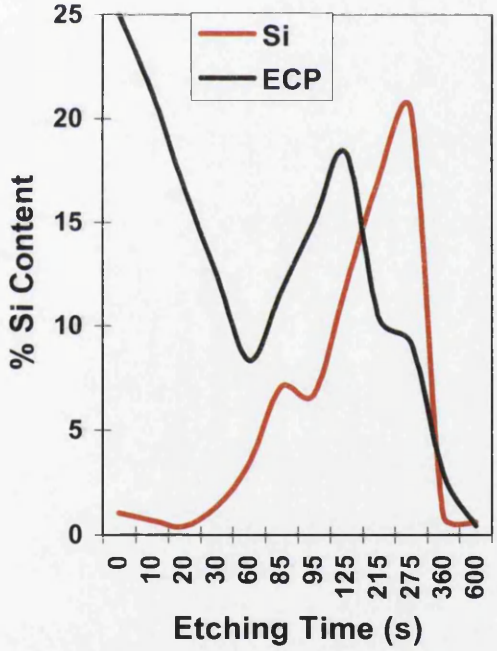

Figure 6.34: Si Content Compared to ECP Profile

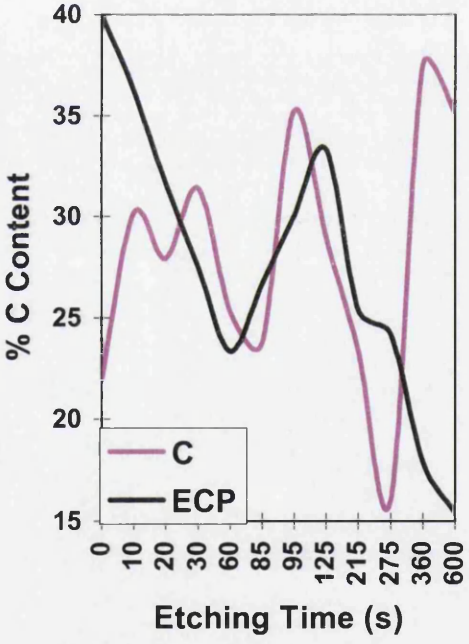

Figure 6.35: C Content Compared to ECP Profile

- The amount of silicon increases as the etching time increases, until the result for 360 seconds is reached, at which point it drops away to almost zero (Figure 6.34),
- There are trace amounts of sulphur tin, calcium, nitrogen, chlorine, manganese and phosphorous, all of which do not appear to vary in any way that is related to the etching time,
- There appears to be a very high presence of carbon, varying approximately between 16 and 36% (Figure 6.35).

The magnesium that is present in the first sample is related to the magnesia coating applied to the strip following the decarburisation process. All visible evidence of the magnesia powder was brushed from the surface, but it appears that even subsequent ultrasonic cleaning could not remove all traces. It is likely that this is due to areas of particularly good adhesion between the magnesia and the surface due to the degree of roughness.

The results relating to the silicon are slightly surprising due to the low values for the last two samples. At these etching times, the profile was either close to, or actually at, the baseline. It was assumed that this baseline was related to the point at which the oxide layer had been completely removed and the base steel had been reached. Although the silicon content was expected to decrease as the oxide layer was completely removed, silicon values of 0.92% 0.57% were unexpected as the amount of silicon present in the base steel itself is approximately 3%.

Due to the nature of the steel making process, it is not unusual to find trace amounts of a number of different elements. Those seen in this investigation are some of those commonly observed. Those observed here are not at levels that are significant to be of concern.

The carbon data is highly unexpected, as one of the main purposes of the decarburisation process is to remove carbon from the steel itself. It was thought possible that the carbon is only being removed as far as the oxide layer, at which point it is becoming trapped. This would have serious consequences in terms of the quality of the final product, and it was necessary to investigate this effect further.

Therefore, as an extension of this work, a representative sample of the un-etched material was also analysed using a technique known as Sputtered Neutral Mass Spectrometry (SNMS), described in Section 2.2.5. This could provide an elemental analysis of the oxide layer by sputtering through the material until the base steel was reached. The high-energy incident beam of ions used in this technique has an erosive effect that acts to etch into the surface layer. This provides a continual depth profile for the composition of the layer, without having to use the acid of the ECP method to etch through the layer in stages. It would clarify whether this technique would correlate with the unexpected carbon results obtained from the XPS investigation, and whether the XPS carbon data was the result of contamination.

The results from the SNMS analysis are shown in Figure 6.36, which shows the smoothed data. It should be noted that the elemental content for SNMS is in atomic percent (compared to weight percent for EDX), the scale on the y-axis is logarithmic, and the etching time for SNMS is completely different to that of the ECP etching

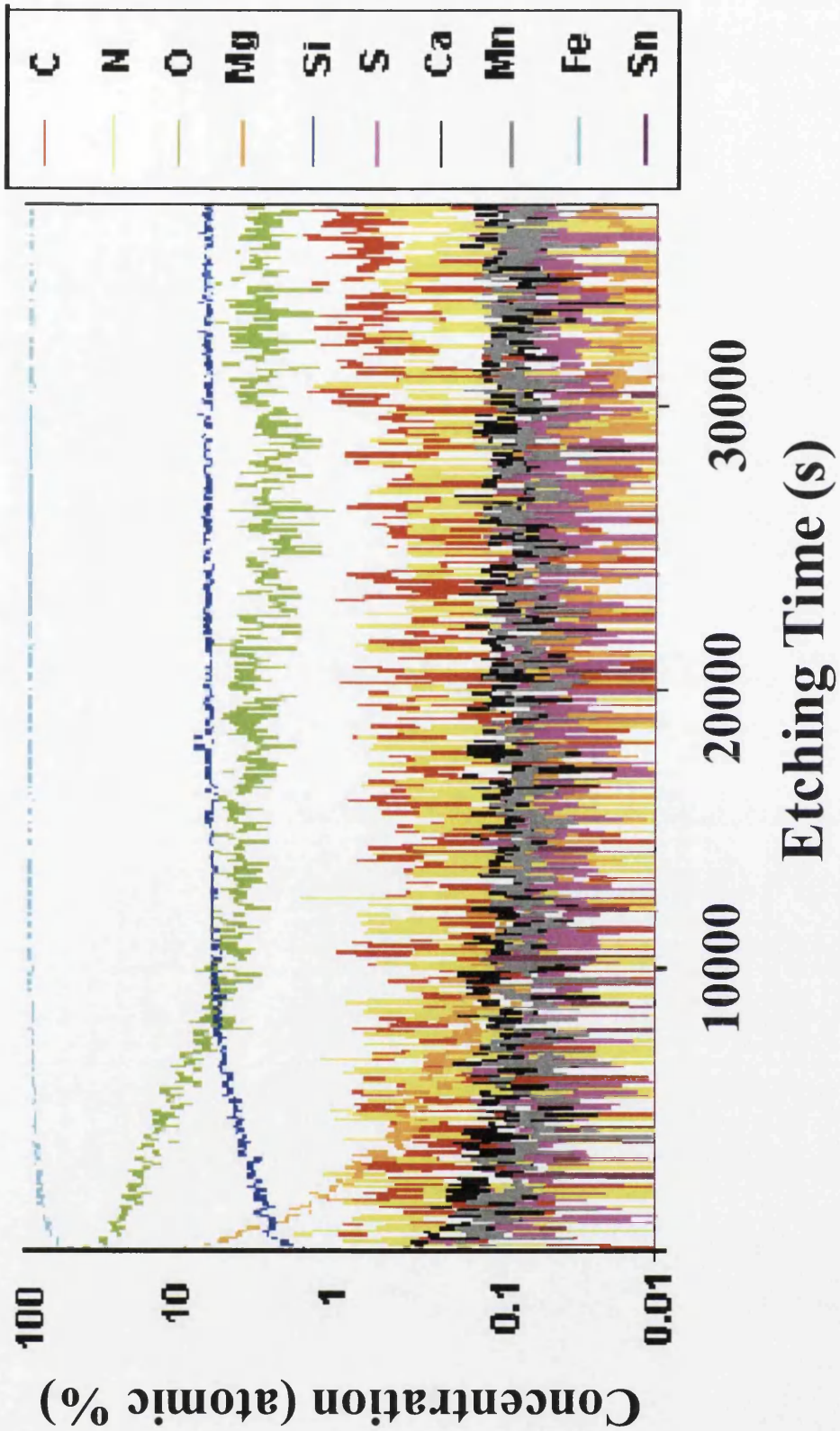

Figure 6.36: Smoothed SNMS data for the Decarburisation Oxide Layer

times. For clarity, the data for the more relevant elements are shown in Figures 6.37 – 6.40.

By comparing the SNMS data in Figure 6.36 to the relevant data from the XPS investigation (Figure 6.35), it can clearly be seen that the carbon data for these two techniques is not in agreement. The XPS data showed a presence of up to approximately 36%, whereas the SNMS data shows the carbon level to remain relatively steady at around 0.5 - 1%, and not increasing above 1.6%. This lower level is much closer to the level of carbon that was originally expected to be found.

Due to the sputtering nature of the SNMS, the oxide layer can only be contaminated on the very outer layer, as the lower levels have previously been unexposed to the atmosphere or any other potential contaminants. Therefore, these results suggest that the sample used for XPS analysis must have somehow been contaminated following the ECP etching process, but prior to the XPS analysis itself. It is not possible for the sample to be contaminated once it had been placed in the XPS apparatus, as each chamber was held under vacuum. Only the water with which it was rinsed and the apparatus used for punching the smaller disk from the etched sample came into direct contact with the surface to be analysed prior to XPS analysis. However, it is deemed highly unlikely that mains tap water would contain such high carbon content. The sample punch is used purely for this purpose and is regularly used in conjunction with the XPS apparatus. If this were the cause of the contamination, then it would occur on all samples analysed using this apparatus, which was not the case.

Another alternative is that the dryer used following the rinse could have dispensed hot air that deposited carbon-rich particles on the surface. Again, such a high level of carbon would not be expected from this. Following further investigation, the most

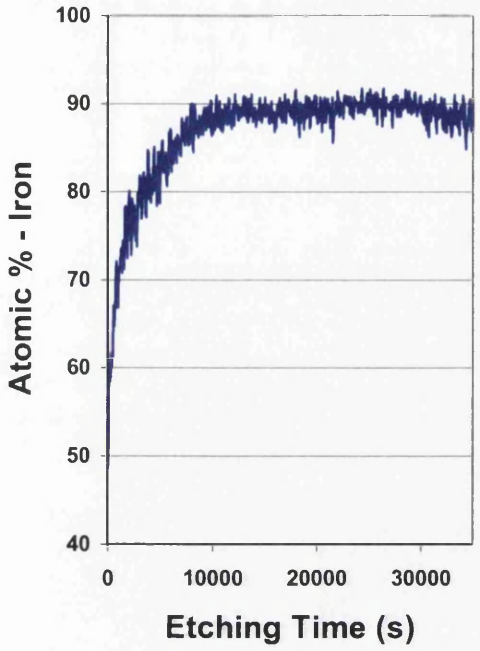

Figure 6.37: SNMS Data For Iron

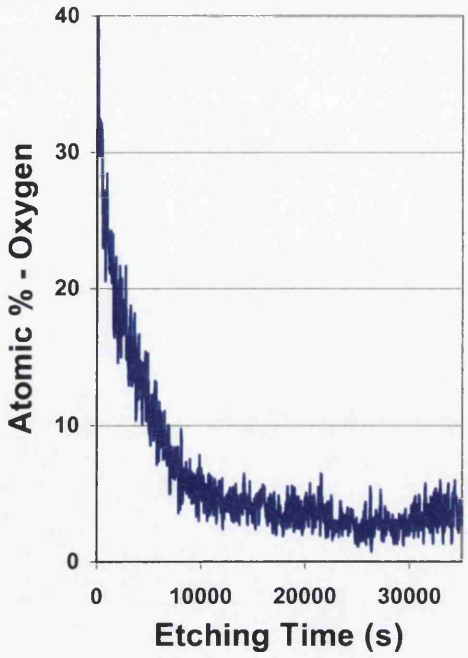

Figure 6.38: SNMS Data For Oxygen

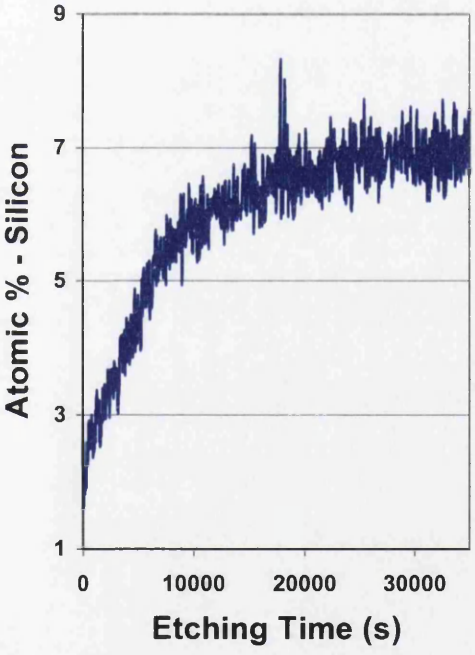

Figure 6.39: SNMS Data For Silicon

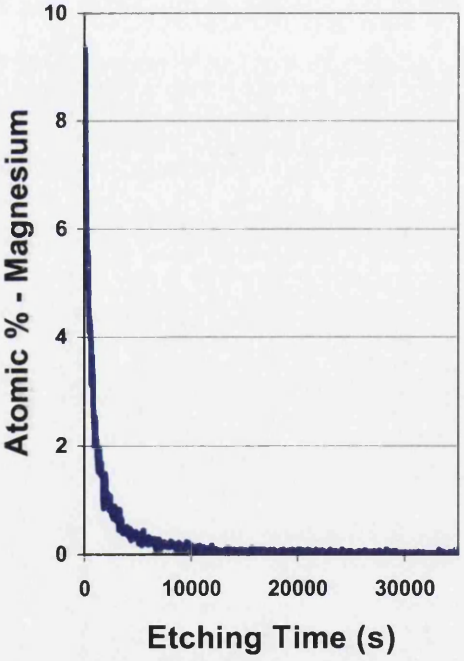

Figure 6.40: SNMS Data Magnesium

likely cause of contamination is related to the tape with which a section of each ECP sample is covered to ensure a constant surface area is exposed to the acid. Although this acid-proof tape prevents acid from attacking the area that it covers, it has been noticed that the areas at the very edge of the tape begin to peel away from the steel surface during the etching process. This provides a possible mechanism for the acid to attack the underside of the tape and the associated glue, which can then be absorbed into the acid solution. The organic substances could then be deposited onto the surface of the sample.

As well as providing evidence of contamination in the XPS investigation, the SNMS data also exhibited a number of other interesting trends.

It was found that there was a very good correlation between the amount of iron and oxygen in the surface layer being analysed. Figure 6.41 clearly shows the expected result that the relationship between these two elements is inversely proportional, illustrating the difference between the oxide layer and the base steel. This is expected as the amount of oxygen, combined within compounds in the oxide layer, decreases as larger amounts of the base steel are exposed.

However, the SNMS data also showed data that contradicts the results of other investigations. It was found that the relationship between silica and oxygen was inversely proportional as shown in Figure 6.42, which was the opposite of what was established from the EDX results. This seems a strange result, as it is believed that the oxygen predominantly combines with silicon in the form of SiO_2, and therefore these two elements should increase in proportion to one another. It can be explained by looking at the amount of both elements present in the two investigations; the SNMS data appears to show evidence of a much higher proportion of oxygen in

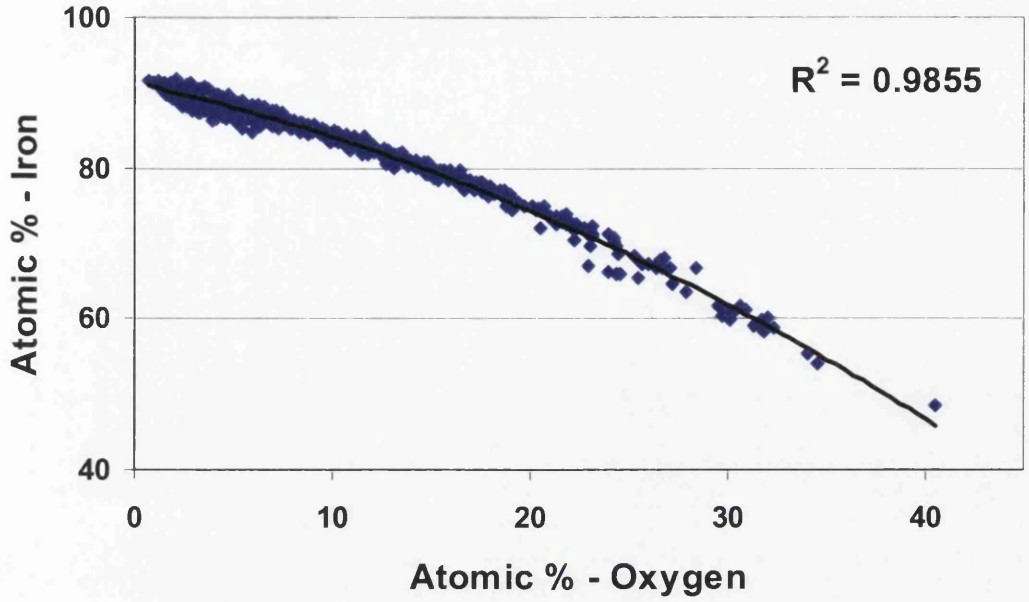

Figure 6.41: Correlation between Iron and Oxygen Content from SNMS Data.

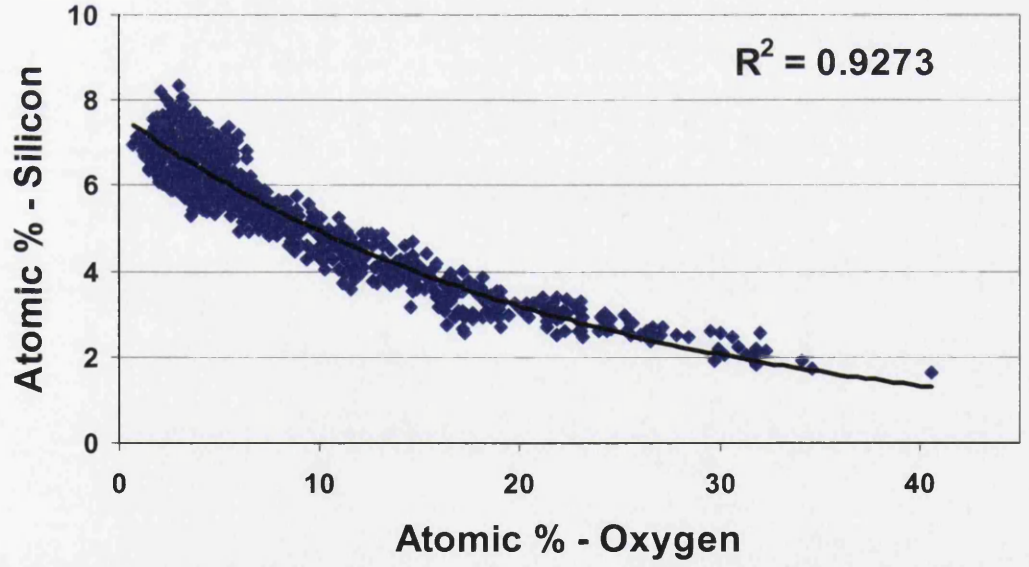

Figure 6.42: Correlation between Silicon and Oxygen Content from SNMS Data.

relation to the silicon content that the EDX data. This suggests that the oxygen is combining with other elements to form compounds other than SiO_2. In the first stages of the SNMS analysis, it is likely that a majority of this oxygen will be combined in the MgO, and this is the region that gives the greatest discrepancy. As the results are given in atomic percentages, it is likely that this MgO distorts the data for all of the other elements. As the amount of magnesium is seen to reduce to normal levels (i.e. after magnesia has been removed) it is seen that the composition of both silicon and oxygen level out and remain constant. This suggests that a region of SiO_2 has been reached.

6.4.3 Conclusions of Section 6.4

Although x-ray photoelectron spectroscopy (XPS) is a useful surface analysis tool for a number of applications, it was found that it could not be utilized in conjunction with interrupted ECP. This was due to the large amount of carbon detected at each stage of etching. The sputtered neutral mass spectrometry (SNMS) was used to prove that this amount of carbon was not a genuine constituent of the decarburisation oxide layer, but was present due to contamination of the samples. This contamination was most likely to be due to organic compounds contained within the adhesive of the acid-proof tape being deposited on the surfaces during the etching process. If further work on this apparatus is anticipated, a sample could be tested without tape to test this hypothesis. However, both techniques did show that, once the region relating to the surface magnesia had been passed, the levels of oxygen and silica remained constant in relation to each another.

6.5 Chapter Summary

The investigation using the 'interrupted ECP' technique was proved to be more successful when combined with the FTIR and EDX methods of evaluation.

Due to carbon contamination of the samples, the results obtained from the XPS apparatus were uncertain, as the presence of such high levels of carbon distorted the results for all other elements of interest. The SNMS was used to prove that these high carbon levels were a result of contamination, and were not a constituent part of the oxide layer. However, it was found that both of these techniques showed a clear correlation between the presence of silicon and oxygen, agreeing with previous opinions.

It was found that the images obtained using the SEM technique were generally inconclusive, although they did appear to show changes in the silica as the etching time increased. The associated EDX analysis was proved to be a useful method of analysing the elemental variation at different etching times. It showed that the amount of both silicon and oxygen increased almost as soon as etching began, and also that they increased at similar rates of weight percentage. When the atomic mass of the two elements is considered, this suggests that the silicon and oxygen are present in the ratio of 1:2, and that the compound is silica (SiO_2).

Of all the techniques used in conjunction with the interrupted ECP, the FTIR method of analysis proved to give the greatest insight into the compounds present on the surface at various etching times. It established that there is a layer of fayalite on the very surface of the oxide layer when the sample is in an un-etched state. However, this is quickly removed when the sample is etched in sulphuric acid, and no trace of fayalite is seen in the spectra relating to any of the etched samples. The spectra relating to the samples etched to regions before the trough on the ECP profile showed

evidence of a main band at around 1135cm^{-1}. As the etching time increased, it was found that this band shifted to higher wavenumbers, reaching a maximum of ~1250cm^{-1}. This occurred on the spectrum relating to the peak of the ECP profile. As the potential then decreased towards the baseline, the band at ~1100cm^{-1} again became more dominant. Interestingly, the change between these two bands appeared at the distinctive points of the peak and trough of the ECP profile, suggesting that there is a link between the composition and / or morphology of the oxide layer and the shape of the ECP profile.

Although the presence of the two bands (~1100 and 1250cm^{-1}) initially appeared problematic, it is believed that both of these bands are due to the presence of silica, but relate to differing forms of the compound. Alternatively, the band at ~1250cm^{-1} could be linked to other silicates or oxides found in the oxide layer, although it has not been possible to obtain any spectra to prove this.

Chapter Seven

Evaluation of Forsterite Glass Film Using FTIR

7.1 Introduction

The formation of the forsterite glass film occurs during a high temperature anneal, as a result of a reaction between compounds in the decarburisation oxide layer and the magnesia (MgO) coating. This is covered in greater detail in Sections 1.2.5 and 1.3.2. Due to the success in obtaining FTIR spectra from other surface layers, it was decided to establish whether this technique could be adapted to the analysis of the forsterite glass film layer. This could be adapted to give an insight into the consistency of the composition of the layer, or the variation in thickness.

7.2 Obtaining FTIR Spectra for Forsterite

7.2.1 Experimental Procedure

At this stage, it was unknown if an FTIR spectrum could be generated for a sample of forsterite coated electrical steel. Therefore a sample was taken from a coil that had been processed in the HTCA furnace where the forsterite is formed. This sample was taken at the entry of the final coating and thermal flattening line, prior to being coated with the phosphate coating. However, some of the magnesia that had not reacted during the formation of forsterite was still on the surface. This was removed simply by brushing.

The sample was analysed using the standard FTIR attachment (26.5° grazing angle), as it was established that this produced an adequate spectrum. Unlike the

decarburisation oxide layer, it was not necessary to use the 80° grazing angle attachment. A number of spectra were obtained from a selection of areas across the sample to establish the reproducibility.

7.2.2 Results and Discussion

It was found that all of these spectra were very similar in terms of both the position and size of the infrared absorption bands. Figure 7.1 shows the four spectra obtained for each surface. This figure illustrates the reproducibility of the results, with each spectrum being very similar to the other three in the set. It can also be seen that the position and relative sizes of each of the bands remains constant from one surface to another. Figure 7.2 shows one of these spectra, with the bands labelled. It can be seen that the major bands appear at 981, 864, 835, 607, 565 and 502cm^{-1}. Other, less distinctive bands can also be seen at wavenumbers of 1008, 956, 886, 522 and 477cm^{-1}.

7.2.3 Effect of MgO

It was suggested that the sample might have been slightly contaminated by small amounts of magnesia, as brushing does not provide a thorough cleaning of the surface. Therefore, the sample that previously had MgO brushed from the surface was thoroughly cleaned using acetone. The three spectra obtained from this sample were averaged using the spectral calculator, which is a software program able to manipulate spectra according to standard mathematical principles (see Section 8.3 for further detail). This averaged spectrum was then compared to the averaged spectrum obtained when the sample was brushed clean. This comparison can be seen in Figure 7.3.

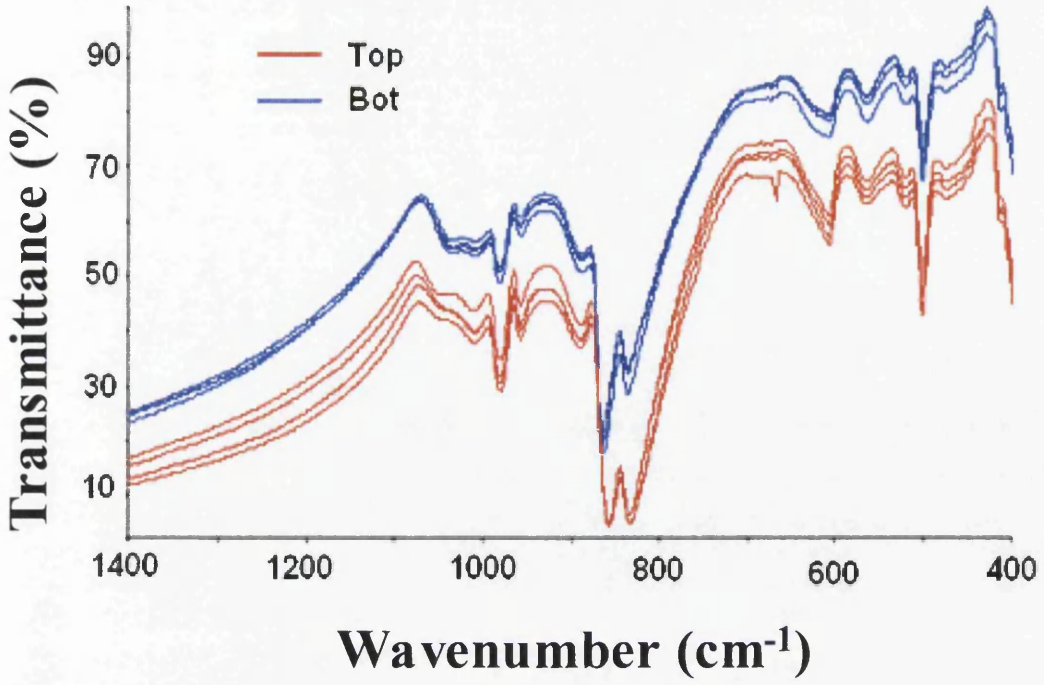

Figure 7.1: Spectra obtained from both surfaces of a forsterite sample (brushed).

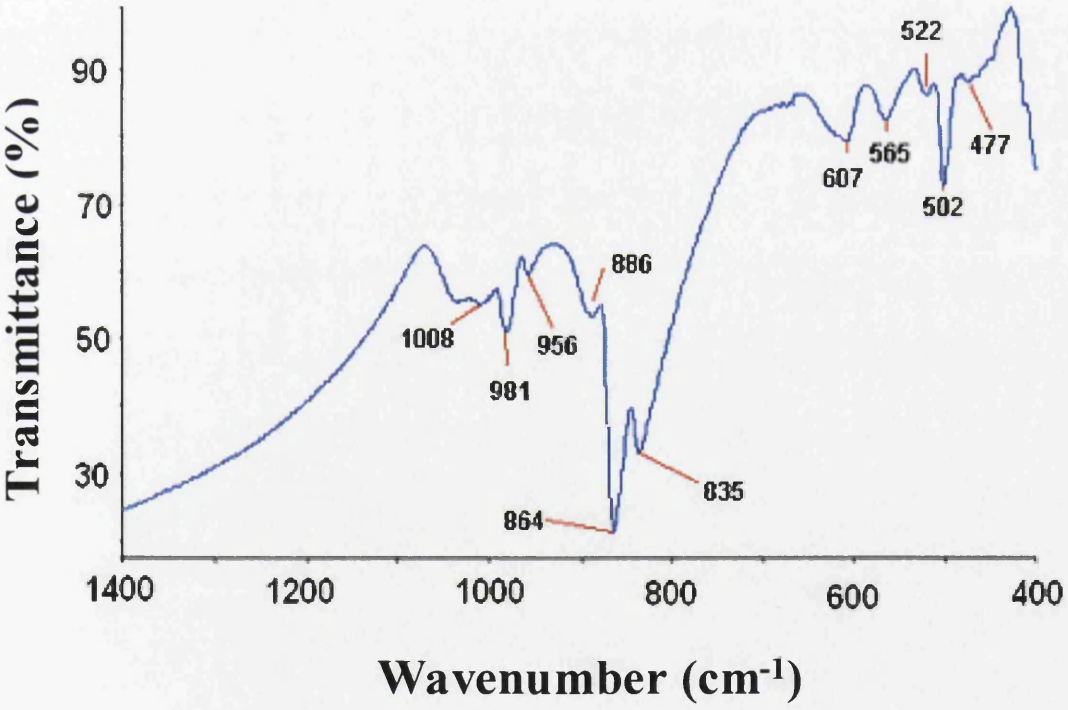

Figure 7.2: Typical spectrum obtained for forsterite (brushed).

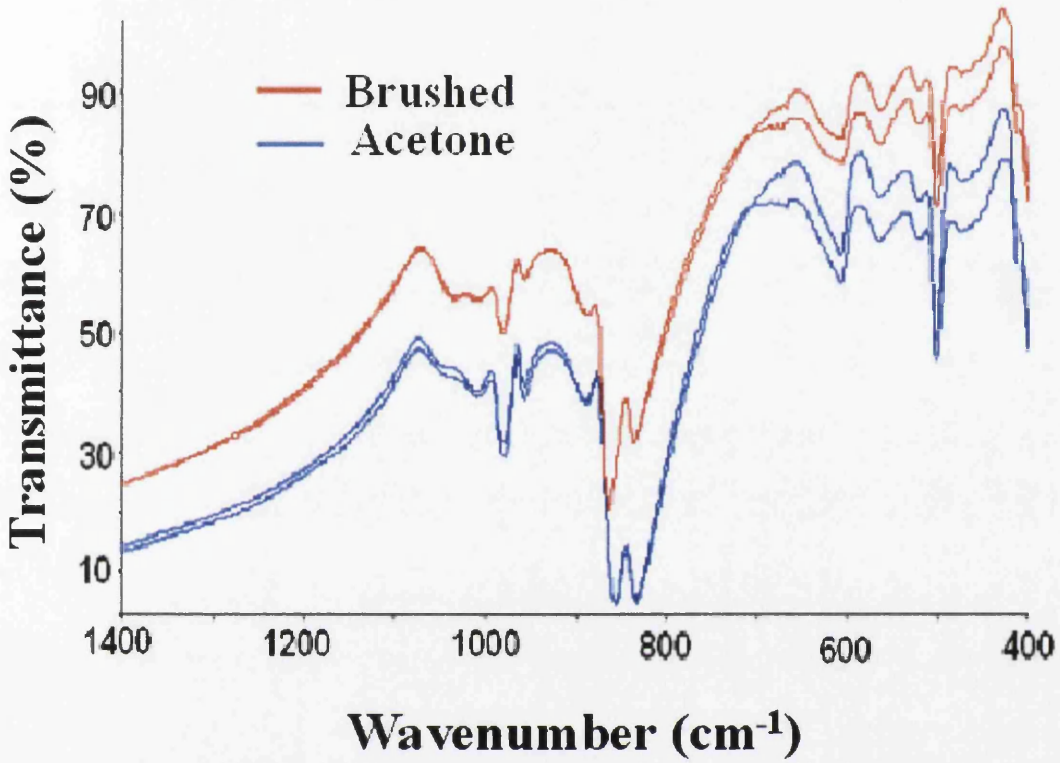

Figure 7.3: Comparison between samples cleaned by brushing and with acetone.

The colours of the spectra relate to the two surfaces of each sample that were analysed (i.e. top and bottom), and it can be seen that the two cleaning methods resulted in very little difference in the spectra.

To further determine whether magnesia coating has an effect on the spectra, a sample was taken from the end of the decarburisation line. This has the oxide layer on the surface of the strip instead of the forsterite glass film, but a layer of magnesia several microns thick covers this. It is very unlikely that the radiation from the FTIR apparatus would penetrate through this magnesia layer, and therefore the resultant spectrum would be that of the magnesia coating. This can be used to determine the wavenumbers at which the magnesia-related bands would be positioned. This spectrum is shown in Figure 7.4. It can be sent that the main bands are located at wavenumbers of 1481, 1421 and 854cm^{-1}, with smaller bands at 1647, 805, 581 and 424cm^{-1}, and that few of these appear to be in positions that would affect the forsterite spectrum. The bands at 1481 and 1421cm^{-1} are out of the wavenumber range of the forsterite spectrum shown in Figure 7.2. However, this scale was chosen as it contained all of the bands that were seen for forsterite. Therefore it can be concluded that these two bands were not observed in the forsterite spectrum. The only band that is similar to one seen in the forsterite spectrum is the one at 854cm^{-1}, which is close to the forsterite band located at 864cm^{-1}. However, as well as these two bands differing in wavenumber by 10cm^{-1}, it would be expected that there would be more than one magnesia related band present, which did not occur. Therefore, it can be concluded that the forsterite spectrum as seen in Figure 7.2 is not contaminated by traces of the magnesia coating.

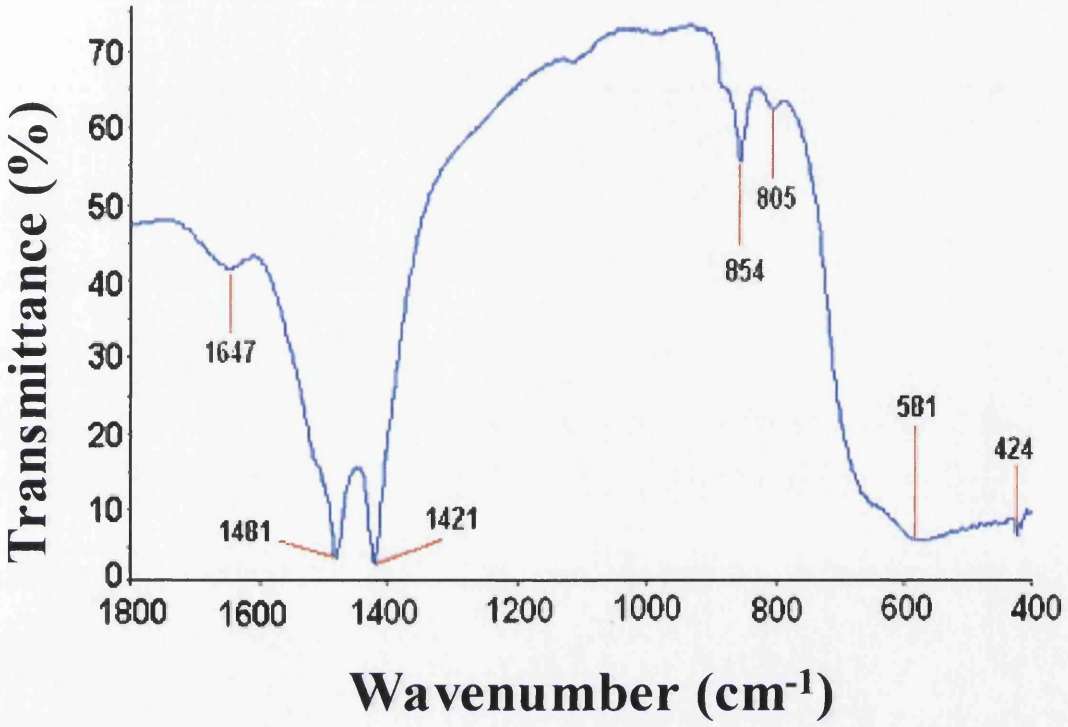

Figure 7.4: Typical spectrum of MgO coated CGO material.

7.2.4 Effect of Acid Pickling

During the production process, the strip undergoes a light pickle in dilute sulphuric acid to remove the magnesia coating prior to final coating. As it had been proved that the FTIR method could obtain a spectrum from forsterite, the effect of this pickling on the forsterite glass film could be established.

A sample was taken from the entry end of the final coating and thermal flattening line, and pickled in sulphuric acid under laboratory conditions. The conditions under which this was carried out were as close as possible to those that the strip experiences on the production line. Figure 7.5 shows a typical spectrum obtained from this sample, and compares it with typical spectra obtained previously in this investigation. It can be seen that the pickling appears to have had very little effect (in terms of the wavenumber at which the absorption bands occur) when this spectrum is compared to samples that were cleaned less vigorously by brushing and cleaning with acetone.

For an investigation to be carried out to establish the level of variation in the forsterite glass film layer, a large number of samples would be required from a number of coils to ensure a large degree of variation in the processing conditions. The most straightforward way of obtaining these would be to use the samples taken from the end of the final coating and thermal flattening line for magnetic testing. These are taken from each coil on a routine basis, and are of a size that is compatible with the FTIR apparatus. However, using the samples in this form is complicated by the fact that these samples have the final phosphate-based coating on top of the underlying forsterite layer.

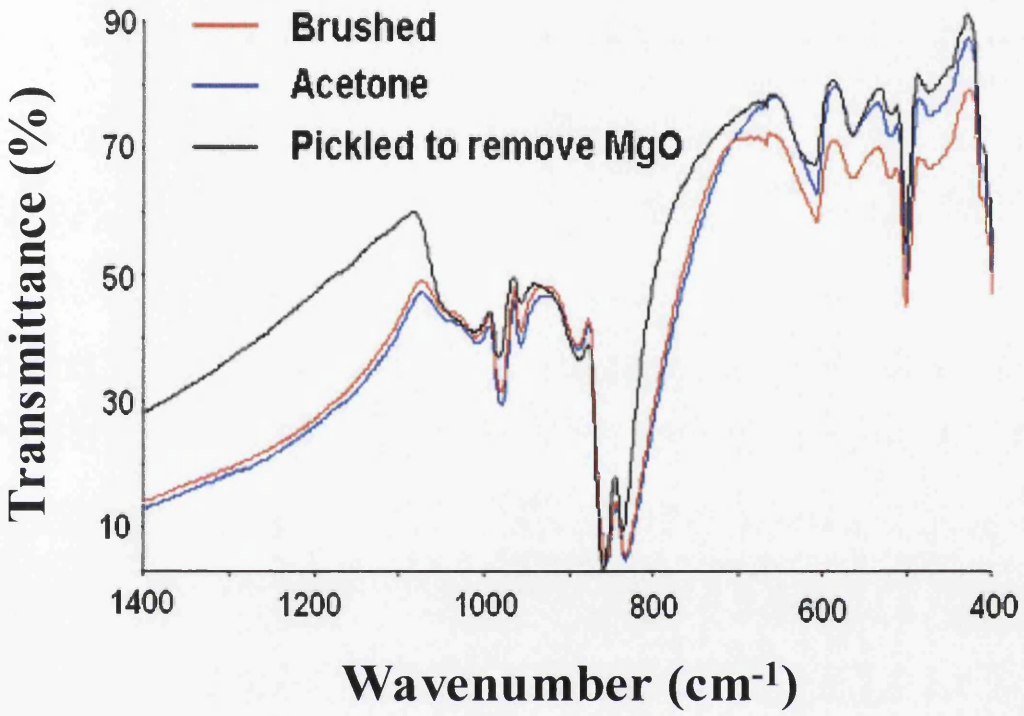

Figure 7.5: Spectra of CGO samples which have had MgO removed in a number of different ways.

Following consultation with Chemistry Department personnel, it was found that sodium hydroxide (NaOH) could be used to pickle these samples in order to remove the phosphate coating without affecting the forsterite layer. A solution of 20% sodium hydroxide was heated until its boiling point was reached, and the phosphate-coated samples were submerged in this solution for 12 minutes. This was sufficient to remove all traces of the final coating from the sample, but leave the forsterite layer intact. However, it was not known whether this pickling process would have an effect on the resultant spectra.

The FTIR apparatus was used to obtain spectra from both surfaces of this sample, which were subsequently averaged using the spectral calculator. Again, the spectra on both sides of the sample were found to be very consistent. One of these spectra was analysed to determine the position of each of the bands, and the labelled spectrum is shown in Figure 7.6.

By comparing this spectra to the three sets of spectra previously obtained in this investigation i.e. removing magnesia by brushing, acetone and pickling in dilute sulphuric acid (Figure 7.7), it can be seen that the spectra are very similar, irrespective of the method that was used to expose the forsterite layer.

7.2.5 Conclusions of Section 7.2

From this work, it has been clearly established that it is possible to obtain an FTIR spectrum from a sample upon which a forsterite glass film had been formed. This was possible using the standard 26.5° grazing angle FTIR attachment.

A number of methods were used to remove the magnesia or final coatings from the surface, thus exposing the forsterite. It was thought that the variation between these methods might lead to differences in the resultant spectra. However, it has been

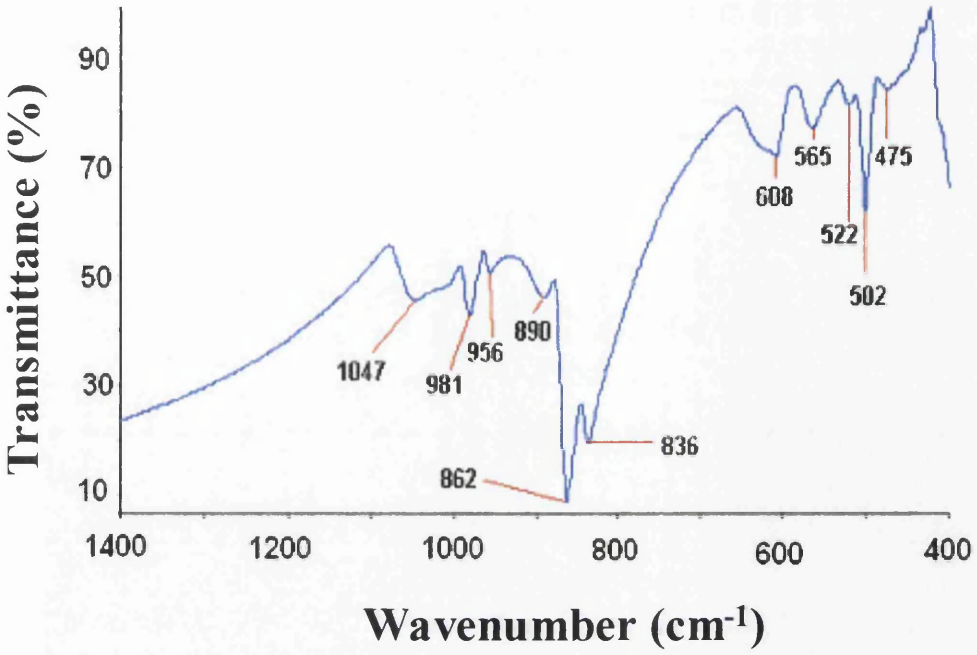

Figure 7.6: Spectrum of sample that has had final coating removed by pickling to expose forsterite.

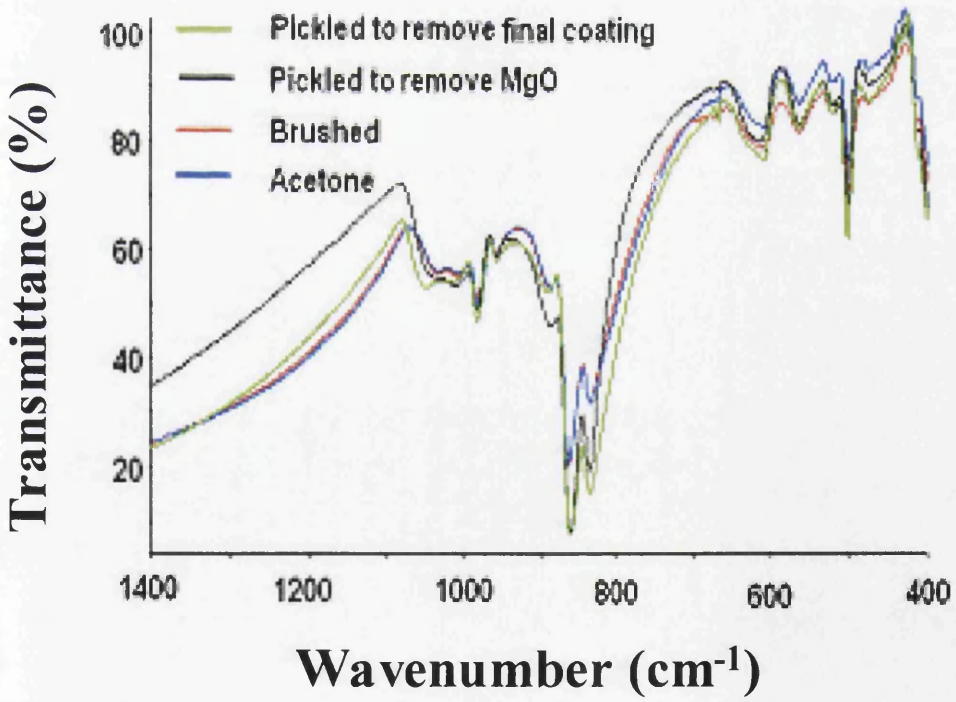

Figure 7.7: Spectra of CGO samples which have had MgO removed using four different methods.

proven that the different techniques have very little impact on the positions and relative sizes of the absorption bands. Therefore, there is no optimum method of exposing the forsterite layer in future investigations, as each of the four methods detailed here are equally as valid. However, the most convenient way to gain access to material from a large number of coils is to use the Epstein samples routinely cut for magnetic testing. A brief pickle in a dilute solution of sodium hydroxide (NaOH) has been shown to efficiently remove the final coating without detriment to the spectra.

During this investigation, it was necessary to obtain a spectrum from a magnesia-coated sample. It was found that none of the bands associated with this magnesia appear to have an effect on the spectra in any of the four aforementioned cases.

From this investigation, it appears that forsterite produces a very distinctive spectrum. As the spectra were obtained from a number of samples, the spectra are seen to be very consistent, with very little variation in the size, shape or position of the bands. This suggests that the forsterite glass film layer varied very little in terms of composition between samples, and has no other significant compounds present other than the forsterite.

7.3 Forsterite Thickness Measurements Using FTIR

7.3.1 Introduction

The Fourier Transform Infrared (FTIR) apparatus at Orb has previously been used to determine the coating thickness of the final phosphate based coating. This application utilised the transmittance value at a specified wavenumber. Previous work has shown that this value has a direct correlation to the coating weights as measured accurately by chemical analysis and by the Fischer Permascope.

Recent work has shown that a spectrum can be obtained from the forsterite glass film that is formed during the HTCA stage of processing (Section 7.2). These spectra exhibit a large number of distinctive peaks that are consistently found at the same wavenumbers. The bands that are observed are also sharp and well defined. These are both characteristics that aid the analysis of FTIR spectra.

It has therefore been decided to undertake an investigation to establish whether a method can be developed to measure the thickness of the forsterite glass film using the FTIR apparatus. If successful, this would provide a technique that would be significantly less time consuming than the methods that are currently used. However it is necessary that this be achieved without compromising on accuracy.

7.3.2 Experimental Procedure

Initially, four samples of forsterite-coated samples were obtained from the entry end of the M2 final coating and thermal flattening line. At this stage of processing, the material has been through the high temperature coil anneal (HTCA) process, and hence the forsterite glass film has been fully formed on the surface of the steel. This surface also has a layer of excess magnesia that did not react in the forsterite forming process, but has not been coated with the final phosphate-based coating at this stage of processing. The majority of the magnesia was removed simply by brushing, ensuring that the brush used was not abrasive enough to damage the glass film. To ensure that none of the excess magnesia remained, acetone was used to further clean the samples prior to analysis.

Once cleaned and cut to an appropriate size, the samples were analysed using the FTIR apparatus at Orb. Two spectra were obtained from different areas from each

side of the four samples, and the spectral calculator software was then used to obtain an average spectrum for each surface.

The Fischer Permascope was used to provide coating thickness data with which to compare the FTIR spectra. This is a technique used as standard at Orb to determine the thickness of the forsterite glass film. When using this equipment, it is necessary to obtain a result by averaging a minimum of 20 readings, each of which is taken by holding a measurement probe in contact with the surface under analysis. At least two sets of measurements were obtained on each surface so that an average value could be calculated to increase the accuracy of this data. This number of samples was required to gain an accurate average value as the forsterite layer is quite undulating in nature, and there are also areas where the forsterite will protrude into the steel substrate, resulting in a greater thickness.

Due to the probe coming into physical contact with this technique, and a minimum of 40 measurements carried out on each surface, it was decided to perform these measurements after the FTIR spectra had been obtained to ensure that any destructive effect that the probe may have on the surface does not affect the spectra.

7.3.3 Results and Discussion

At this stage it was possible to compare the results from the two methods. Upon visual inspection of the spectra, it initially appeared that there was little correlation between the area or positions of the distinctive bands and the thickness of the forsterite layer. The bands all appeared to be at the same wavenumbers, with no obvious shifts observed, and the areas were generally similar for a range samples with varying forsterite thickness. However it was apparent that the thickness of the forsterite appeared to have an effect on the overall transmittance level of the whole

spectrum, particularly between the wavenumbers of 1300 and 400cm^{-1}. This is demonstrated by the spectra shown in Figure 7.8. This shows the average spectra from two surfaces, with forsterite thicknesses of 1.10 and 1.73 microns, as measured by the Fischer Permascope. It is clearly seen that the spectrum relating to the greater thickness is seen at significantly lower levels of transmittance over the entire range of wavenumbers.

To test this hypothesis, the results were used in conjunction with FTIR software (Beer's Law [42]). This enables concentration, or in this case coating thickness, to be compared with certain specified characteristics. The coating thickness values obtained from the Fischer Permascope are entered into the computer, along with the corresponding spectra. The software then performs calculations on the input data according to certain parameters set by the operator. In this case, it was the area above the curve that was specified. The result was that this software determined a very high degree of correlation between the spectra (in terms of area) and the thickness as measured using the Fischer Permascope. However, it was clear that an increased number of samples were required to prove the reliability of this method. It was also necessary to obtain samples that would increase the range of thickness over which this technique could be applied. For these reasons, a further three samples (i.e. six surfaces) were acquired and analysed in the same way, although one surface was found to be contaminated, and was removed from the investigation.

Preliminary visual analysis of the resultant spectra suggested that they followed the same trend as seen previously, and using the aforementioned Beer's Law software confirmed this. This software is able to determine a coating thickness based on all

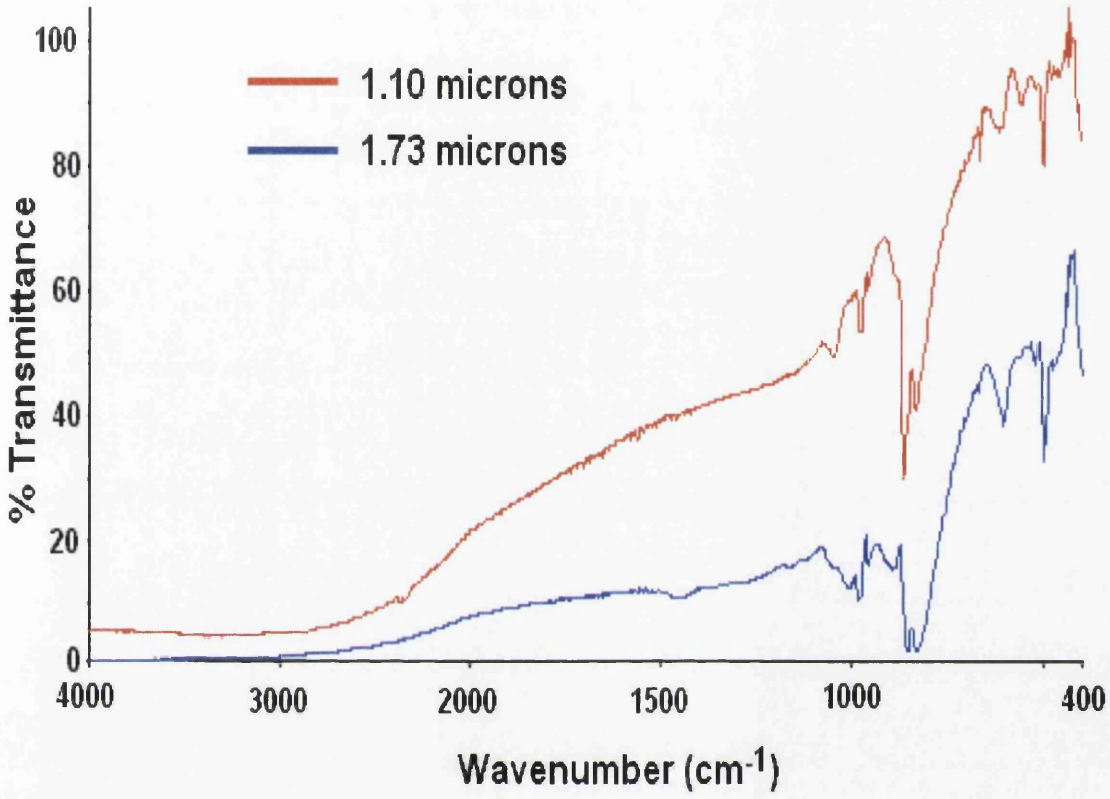

Figure 7.8: Spectra showing correlation between forsterite thickness and overall transmittance levels.

points of the spectrum. However, the range over which the calculations were based was refined to 400-890cm^{-1} following further analysis of all of the spectra.

A plot was obtained, comparing the calculated area with the measured forsterite thickness. This can be seen in Figure 7.9. It can be seen that the correlation between these two parameters is very good, with a correlation value, calculated by the software, of 0.988. This is particularly impressive when it is considered that the standard error of the Fischer Permascope is !0.1 microns.

The software uses this result to be able to predict a coating thickness based on the standards that have been set. Figure 7.10 illustrates the correlation between the measured coating thickness and that predicted according to the area calculations, based on the samples already observed.

The correlation remains good over the entire range of samples, from 0.76③ to 2.21③, which covers a significant range of forsterite thickness that are expected to be produced under standard production conditions.

7.3.4 Conclusions of Section 7.3

From the work detailed above, it can be concluded that there is a clear correlation between the area above the transmittance spectrum for a sample with a forsterite glass film layer, and the coating thickness of that layer, as measured using a Fischer Permascope.

It has also been established that the Beer's Law software, linked to the FTIR apparatus, can be used to take advantage of this relationship and predict the coating thickness of forsterite.

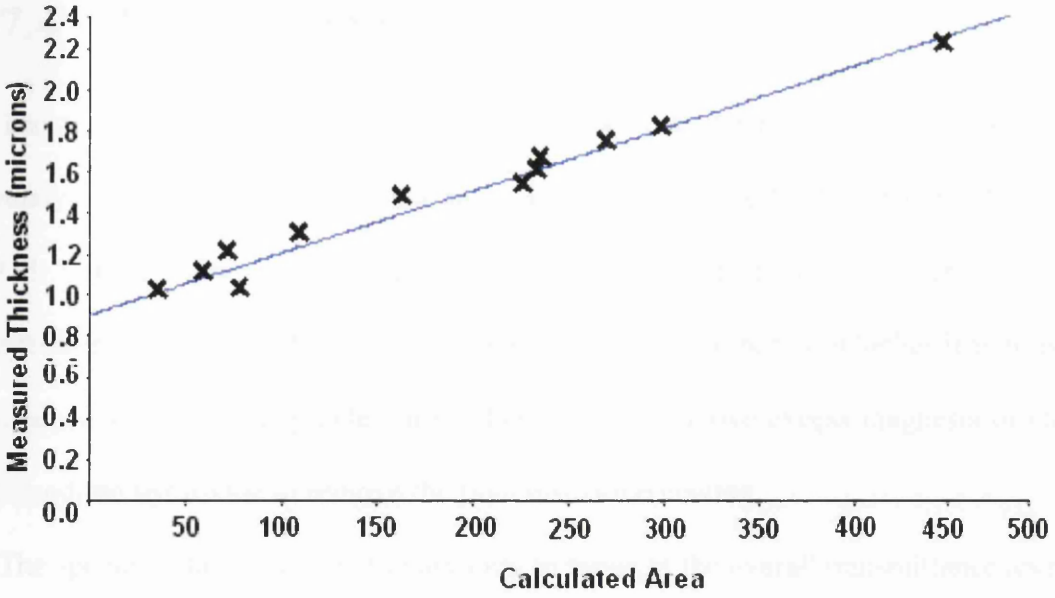

Figure 7.9: Graph showing the correlation between calculated area and measured forsterite thickness.

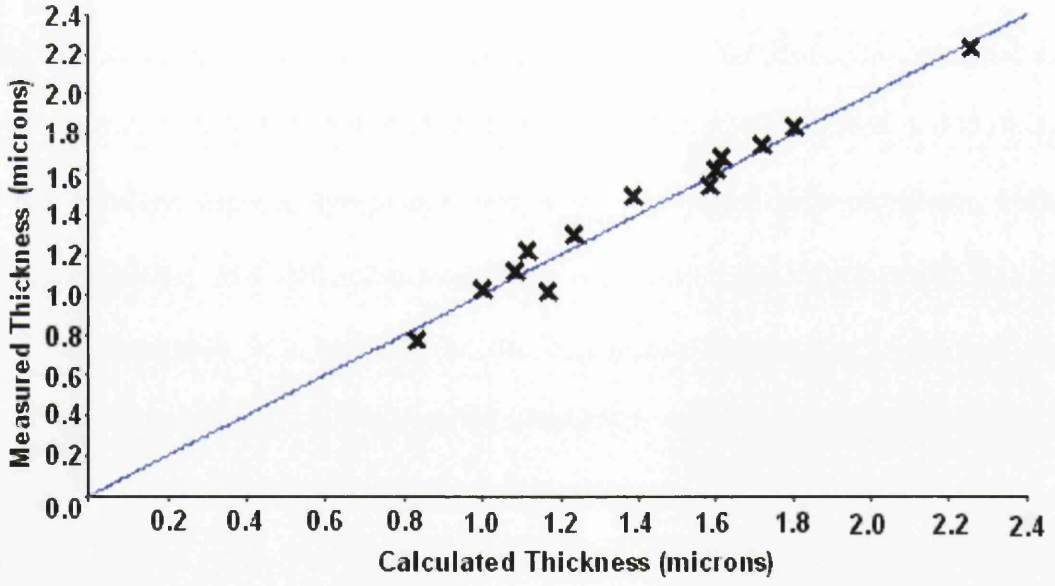

Figure 7.10: Correlation between measured coating thickness and coating thickness predicted by Beer's Law software.

7.4 Chapter Summary

The work performed in this chapter has shown that the forsterite glass film can be analysed using the 26.5° grazing angle attachment on the FTIR apparatus located at Orb works. The spectra obtained show that forsterite produces a very consistent spectrum in terms of the position, shape and size of the bands, whether it is brushed, cleaned with acetone, pickled in sulphuric acid to remove excess magnesia or etched in sodium hydroxide to remove the final insulation coating.

The spectra obtained appear to vary only in terms of the overall transmittance level. It has been proved that this deviation is due to the thickness of the forsterite glass film layer. Software linked to the FTIR apparatus can subsequently be used to predict the thickness of the layer based on the area above the spectral curve in the range of 400-890cm^{-1}.

Chapter Eight

Evaluation of Final Insulation Coating Using FTIR

8.1 Introduction

Once the grain oriented coils have been removed from the High Temperature Coil Anneal furnaces at Orb Works, the material passes through a line known as M-line, which is a final coating and thermal flattening line. For many years, the coating mix that has been applied to grain oriented material on this line has been a phosphate-based solution. This coating layer provides the dual benefits of reducing losses by inducing further tension on the surface of the strip, and also providing greater electrical insulation. Until the recent development of alternative chrome-free coatings (described in Chapter 9), the formulation that has been used to coat GO material at Orb Works has remained constant for approximately 25 years. This was the standard coating formulation that was used on a routine basis on production material at the time of this work, and is therefore the coating that has been evaluated in this chapter. This standard coating formulation comprises aluminium orthophosphate, colloidal silica, chromic acid and water, and these components are mixed at the site of the coating apparatus. It is believed that the final magnetic properties of the steel can be substantially affected by the ratio of aluminium orthophosphate to colloidal silica [18].

Although the coating is mixed according to strict practices on-site at Orb, it is possible that some settlement may occur in the mixing tanks and coating overflow trays. This causes the exact composition that is coated onto the strip to remain unknown unless

very time consuming wet chemistry techniques are applied to the coated material. Therefore it is highly desirable to establish a method that can accurately and rapidly assess the final coating to determine if the optimum coating is being applied in terms of its tensioning capabilities.

During initial investigations, it was found that a suitable spectrum could be obtained from coated material using the standard FTIR procedure and attachment (i.e. the 26.5° attachment). It was envisaged that this technique could provide a rapid and straightforward method of determining variations in the coating composition.

The spectra obtained from these primitive investigations were observed to contain a large number of clear, broad absorption bands. However, the relevance of each separate peak and trough was unknown and could not be linked to any of the separate constituent components of the mix from this basic analysis alone.

Therefore, an investigation was carried out to determine the origin of these bands, so that the composition of the coating mix could be evaluated and monitored. This would enable an optimal coating mix to be maintained and would ensure that any variations in the final coating layer that may occur as a result of subtle differences in composition between mixes were reduced. Also, if the difference in density of the separate components is significant enough, the mix may change in composition as the coating in the tank is consumed due to a settling effect. This is a further effect that could be easily monitored if FTIR was established to be a suitable method of analysis.

8.2 Separate Constituents

8.2.1 Experimental Procedure

To establish which of the spectral characteristics are related to each of the constituent parts of the coating, it was decided to first coat separate steel samples with the two substances thought to have an effect on the final magnetic properties (colloidal silica and aluminium orthophosphate). A number of Epstein samples (305 x 30mm) of grain oriented material were selected from a pack taken from M-line for routine magnetic testing and grading. These samples were pickled to remove both the final coating and the forsterite glass film from the surface. This provided samples with a clean base steel substrate, upon which the constituents could be coated. It also ensured that the base steel would be as similar as possible for each of the coatings in order to minimise any effect that the steel surface could have on the results.

The samples were coated with a steel coating bar with a groove depth of 3.5③m, with the colloidal silica and aluminium phosphate having been obtained from the same source as used for standard Orb Works production.

The samples were cured in a laboratory furnace at a temperature of 800°C. During the laboratory investigation, it was difficult to accurately reproduce the curing conditions experienced by the material on the process line. The time of cure in the laboratory furnace was therefore varied to ascertain whether the amount of curing would affect the spectra produced. The different times were 5, 10 and 20 seconds for both coatings, with an extra aluminium orthophosphate sample cured for 30 seconds to ensure that it was fully cured. Once cured, each sample was placed on the 26.5°

grazing angle attachment and analysed using the FTIR apparatus located at Orb Works.

8.2.2 Results and Discussion

This procedure gave the infra-red spectra for pure colloidal silica and pure aluminium orthophosphate (i.e. no mixing, either with each other or with any other compounds), and should therefore show only the characteristic bands associated with each of these two components. These spectra are shown in Figures 8.1 and 8.2.

The scans were obtained over a range of 400-4000cm^{-1}, although the wavenumber range shown in these spectra ranges only from 400-1500cm^{-1} as no relevant bands were seen at the wavenumber values omitted.

It can be seen that there are four clear bands associated with the colloidal silica spectrum. These occurred at approximately 1180, 1035, 795 and 450 cm^{-1}.

The spectra relating to aluminium orthophosphate shows a greater number of features, although many of these are not as distinct as those seen for silica. They were located at the following wavenumbers: 1230, 1100, 933, 730, 710, 620 and 480cm^{-1}.

Therefore, it was observed that the two separate constituents had two distinctive spectra with no bands occurring at precisely the same wavenumber, although some, such as those at 450 cm^{-1} (colloidal silica) and 480cm^{-1} (aluminium orthophosphate), were in close proximity with one another which may cause difficulties when trying to distinguish which compound it relates to.

In theory, it is only the bands that have been observed at these exact wavenumbers that can be related to the two components. However, this may not be as straightforward as it appears, as mixing the components may distort the spectra. For

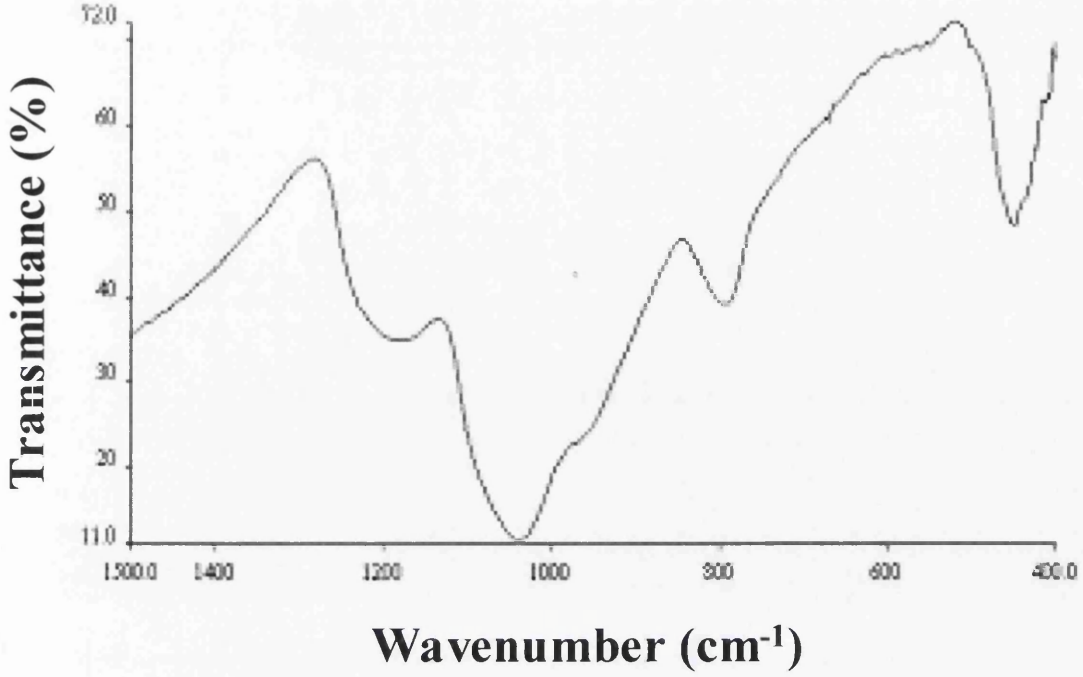

Figure 8.1: Typical FTIR spectrum obtained for colloidal silica.

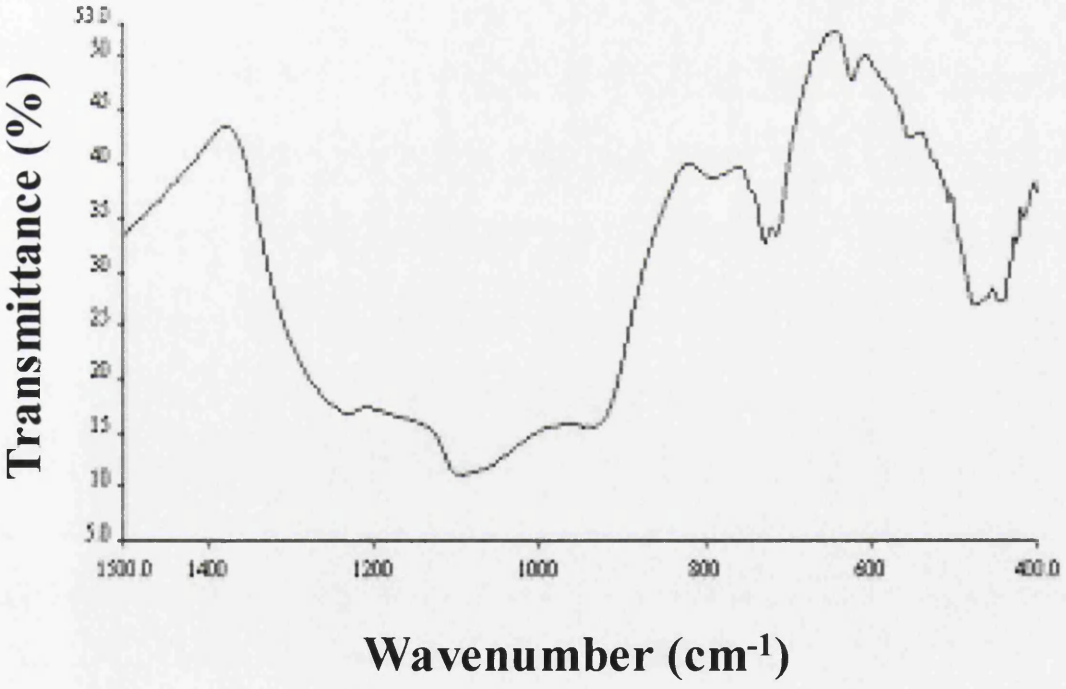

Figure 8.2: Typical FTIR spectrum obtained for aluminium orthophosphate.

example, when two or more components are mixed, the peaks and troughs of the bands that are related to each component will be superimposed onto one another. This may cause some features to disappear, or other features may appear to move, as the apparatus may not be able to resolve between each of the different peaks.

Furthermore, it was found that the length of time for which the samples were cured did not greatly affect the spectra obtained. This is demonstrated by the spectra in Figure 8.3. It can be seen that the spectra show certain bands at different levels dependant on curing time, but it is the position of the bands that is of interest and these generally remain constant. The only noticeable variation is between approximately 900 and 1100cm^{-1}, when the curing time increases above 10 seconds. Under these conditions the shape of the trough changes slightly and a small band appears at approximately 1030cm^{-1}. The size of this small band is almost negligible when compared to the size of the wider band within which it is located, and is probably not relevant for further studies, but note should be taken of this particular wavenumber in case any effects are seen in this region during further investigations.

8.3 Spectral Calculator

The 'Spectral Calculator' is a component of the software provided for the Perkin-Elmer FTIR equipment. It allows a previously obtained spectrum, or a number of spectra, to be manipulated in a way that is related to a basic standard numerical calculator. For example, a chosen spectrum can be multiplied by a specific factor, or a number of spectra may be added together or subtracted from one another. A combination of addition and division of spectra may be used to provide an average spectrum from a set of data (i.e. [spectrum 1 + spectrum 2] / 2 = average spectrum).

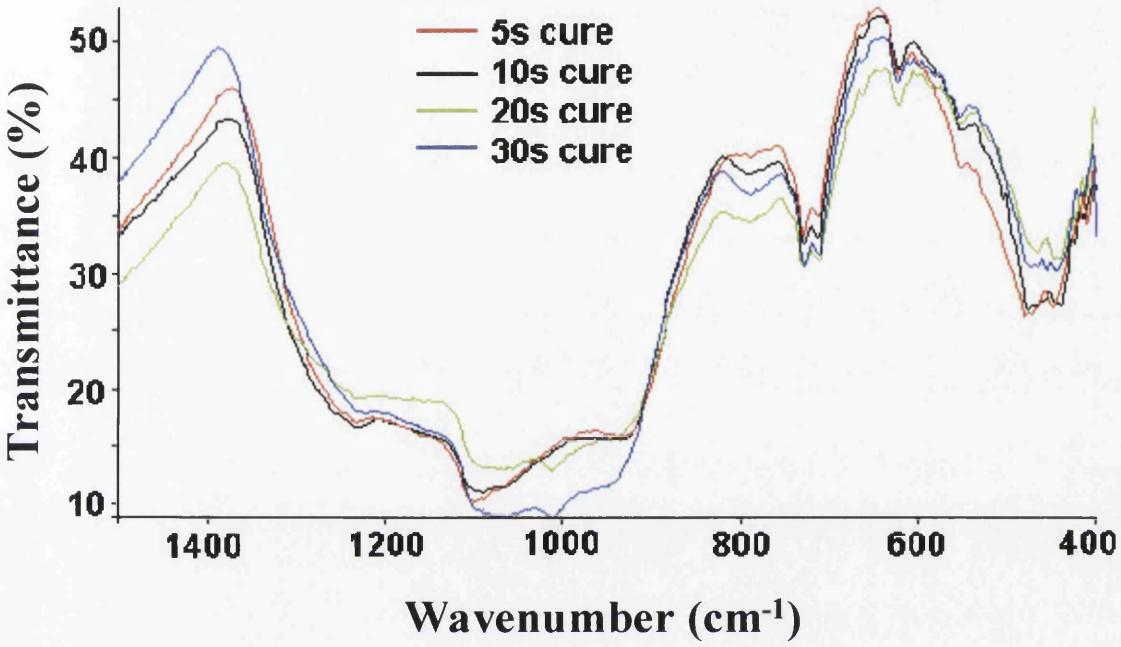

Figure 8.3: Selection of spectra showing the effect of curing time (all spectra relate to aluminium orthophosphate)

The previous section (Section 8.2) described how the separate components of the insulating coating were coated onto steel samples under laboratory conditions. This enabled spectra to be obtained for 100% colloidal silica and 100% aluminium orthophosphate. However, these components are not applied to the strip on their own under production conditions, but are mixed according to a specified formulation.

The Spectral Calculator software has therefore been utilised to manipulate the spectra to produce a number of theoretical mixes that show how the spectra change as the ratio of the constituents is varied.

Figure 8.4 shows this variation as the theoretical mix varies from [100% colloidal silica + 0% aluminium orthophosphate] to [0% colloidal silica + 100% aluminium orthophosphate] in incremental steps of 10%. Although the ratio between these two components would be expected to vary over a much smaller range under production conditions, the combinations used cover the maximum range of variation possible, which gives the greatest chance of establishing the spectral changes that occur due to changing composition.

It can be seen that there are obvious changes to the spectra as the ratios of the constituents within the 'mixes' are varied. The most significant observations are:

- There are three points that stay approximately fixed as the mix changes (at approximately 1380, 1050 and 800 cm^{-1}). This suggest that these regions are unaffected by either of the components. These points could prove useful as they have potential to be used as reference points to which other coordinates may be compared.
- There is significant variation between approximately 1380 and 900cm^{-1}. The spectrum relating to 100% colloidal silica shows two clearly defined bands at

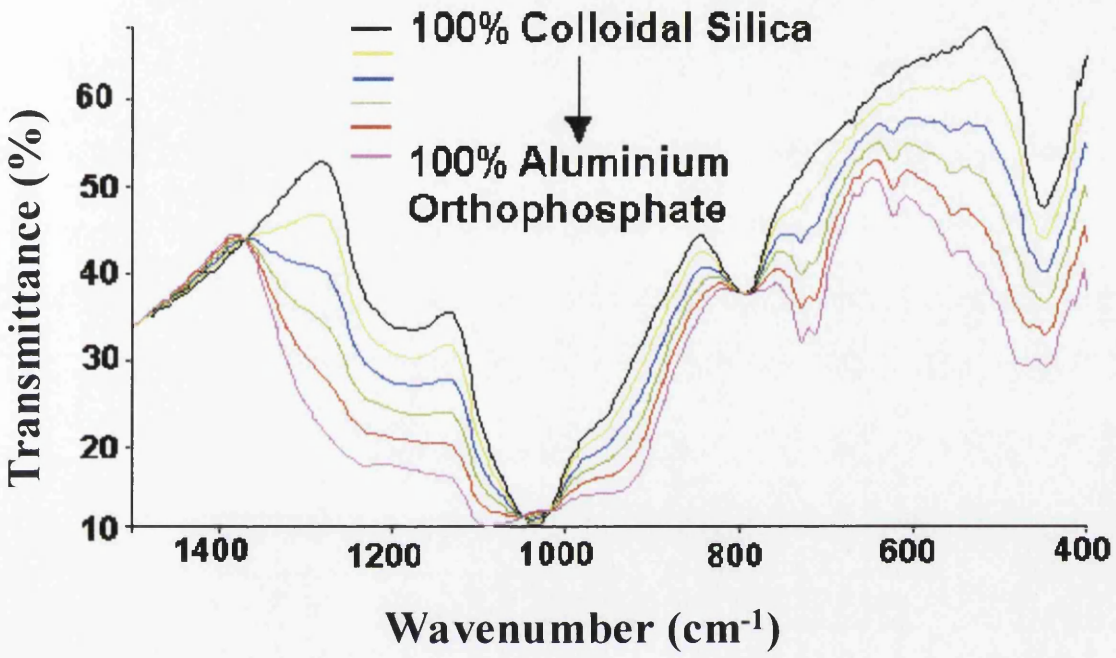

Figure 8.4: Variation of the FTIR spectra as the composition of the coating is varied using the spectral calculator

approximately 1180cm^{-1} and 1035cm^{-1}. However, as the aluminium orthophosphate content increases, a number of changes are seen. Firstly, the band at 1180cm^{-1} becomes shallower, moves to regions of increasingly lower transmittance and also shifts to a slightly greater wavenumber. The band at 1035 cm^{-1} also becomes less well defined, and appears to separate into two bands at 1100 cm^{-1} and 930cm^{-1}. The level of transmittance in this region also decreases as the aluminium orthophosphate content increases.

- The band at ~800cm^{-1} remains fixed at that wavenumber, although the depth of the trough decreases as the aluminium orthophosphate content increases.
- At ~730cm^{-1}, the band also remains at a fixed wavenumber. However, this band increases in depth as the amount of aluminium orthophosphate increases.
- The band at approximately 450cm^{-1} becomes broader and shallower as the aluminium orthophosphate content increases.

These spectra clearly demonstrate the benefits of the 'Spectral Calculator' software, and show that significant differences are seen in the FTIR spectra when the colloidal silica and aluminium orthophosphate spectra are manipulated to provide theoretical mixes. However, the variation seen here remains theoretical and requires practical experimentation to confirm the findings. This work is described in Section 8.4.

8.4 Laboratory Coating Mixes

8.4.1 Experimental Procedure

An investigation was carried out to discover what the effect of mixing the main two components of interest (colloidal silica and aluminium orthophosphate) would have on the spectra obtained.

Three different formulations were chosen with varying $Al(H_2PO_4)_3$: SiO_2 (aluminium orthophosphate : colloidal silica) ratios. They were:

Mix 1: 30ml SiO_2 : 10ml $Al(H_2PO_4)_3$ (3:1 i.e. 25% Aluminium orthophosphate)

Mix 2: 30ml SiO_2 : 20ml $Al(H_2PO_4)_3$ (1.5:1 i.e. 40% Aluminium orthophosphate)

Mix 3: 20ml SiO_2 : 20ml $Al(H_2PO_4)_3$ (1:1 i.e. 50% Aluminium orthophosphate)

It should be noted that the formulation of mix 2 was based around the approximate ratio used as the standard mix at Orb Works.

The three mixes were deliberately chosen to give a much larger variation in composition than would be found on production material. This was to ensure that any changes in the spectra could easily be seen. If they varied only by the slight amount that was expected to be found on the production line, then it is possible that the changes in the spectra may be too subtle to be detected. If this investigation were to show promise, the technique could be refined further, but at this stage it is only necessary to ascertain the feasibility of using this apparatus to determine changes in composition. Relating this to a production situation would require far greater study.

Water and chromic acid were not used in the mix during this investigation, as it is the ratio of the colloidal silica to the aluminium orthophosphate that is of interest, due to its direct influence on magnetic properties. It was decided that the bands due to these other substances would only interfere with the bands of interest, making the determination of any changing features more problematic.

In each case, the aluminium orthophosphate and colloidal silica were mixed together by rapidly stirring the solution with a glass rod. This was carried out so there would be no localised areas of one particular component once the mix had been coated onto the steel. This would cause the spectra obtained to give misleading information.

The samples used in this investigation are known as Epstein samples. These are samples measuring 305mm x 30mm, and are routinely taken from each production coil for analysis after the final coating and thermal flattening line. In this particular investigation, the sheet sample they were taken from was referenced as MS399025. These samples were pickled in acid to provide a consistent, bare steel substrate for this investigation, as carried out when samples were coated with the two separate constituents in Section 8.2. The top surface of each sample was also coated using the same steel roll (3.5③m groove depth) that had previously been used. Curing was again carried out for a duration of 15 seconds in a laboratory furnace set at a temperature of 800°C.

To determine the reproducibility of results along the length of the sample, three FTIR spectra were obtained from each sample; one in the centre of the sample, and one towards either end. Each set of scans were taken in the same position along the length

of each of the samples to ensure that the position in the furnace did not have an effect (i.e. different curing effects due to temperature differentials within the furnace).
Each coating formulation was repeated using a second sample to discover how reproducible the results were from one sample to another.

It was noted that, although the coating equipment utilized is commonly used as a standard method of one-sided laboratory coating, the coating sometimes appeared to coalesce in certain areas before it could be cured. This is an occurrence commonly known as de-wetting. It is possible that this may result in different spectra being obtained due to thickness effects at various points on the sample. However, the composition of each mix should remain the same and therefore the spectra should be similar for each sample coated with the same formulation, irrelevant of the non-uniformity of the application. A thickness effect should only result in either an increase or decrease in the level of transmittance, depending on whether the coating was thicker or thinner. This is because as a thicker coating will result in a greater absorption of the radiation, and hence a decrease in the transmittance values on the spectra. The position of the bands themselves should remain relatively unchanged.

8.4.2 Results and Discussion

An average spectrum for each laboratory mix was calculated using the spectral calculator software, explained in Section 8.3. A comparison between the average spectra for the three different coating formulations is shown in Figure 8.5.
The consistency of the spectra for a particular mix, comparing both spectra from different areas of the same sample and also between two different samples (Figure 8.6), appeared to be acceptable. This shows that the results given by this method are

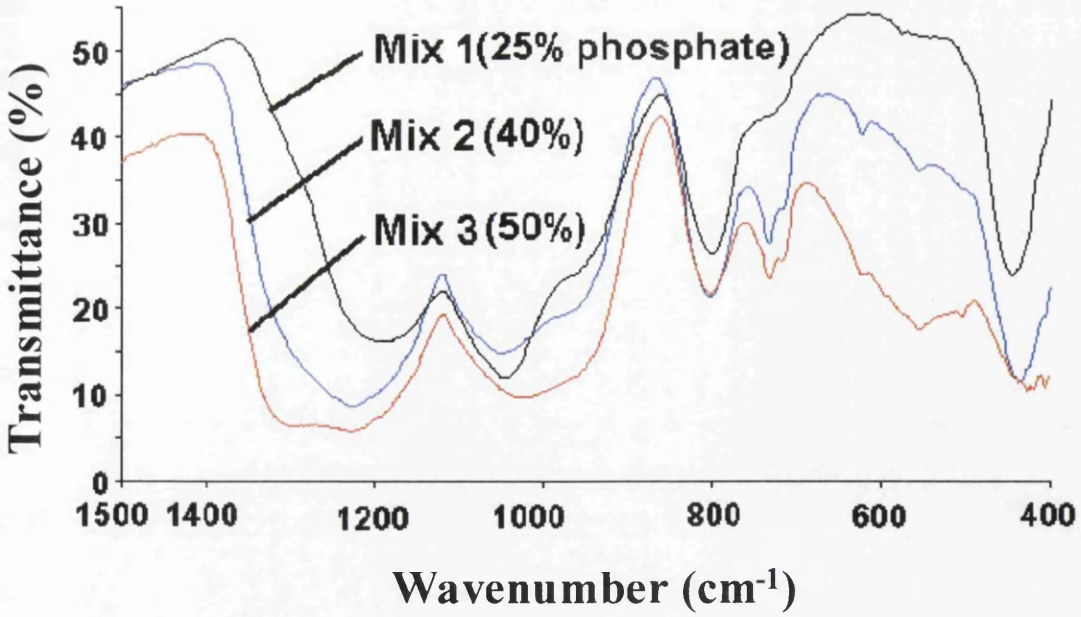

Figure 8.5: A comparison between the average spectra obtained for each of the three laboratory mixes.

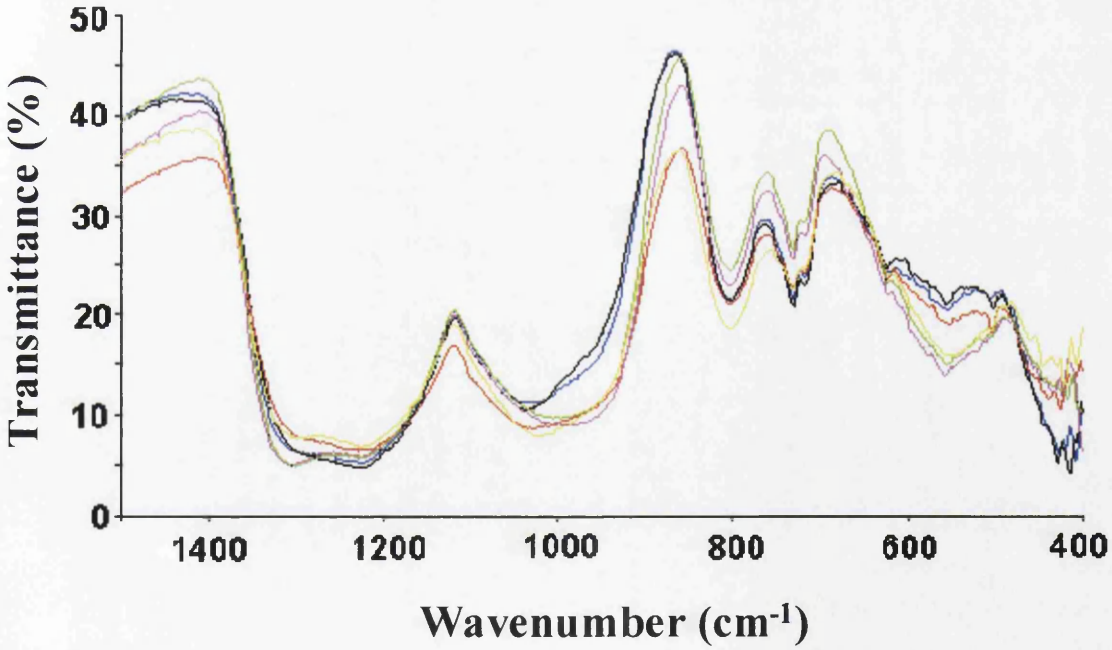

Figure 8.6: Spectra showing the level of repeatability for a particular mix.

reasonably reproducible, which is often difficult to achieve under laboratory conditions such as these. It also confirms that there was not a large amount of variation along the length of each sample, which it was thought might potentially occur due to the different temperatures at various points within the furnace

In Figure 8.5, it can be seen that there is a definite trend in the variation between spectra when the amount of aluminium orthophosphate is considered. The general level of transmittance tends to decrease as the aluminium orthophosphate percentage increases i.e. from 25% for mix 1 to 50% for mix 3.

A number of changes in the shape of the spectra could also be seen. The main observations were:

- An increase in aluminium orthophosphate led to a widening of the band at ~1100-1300cm^{-1}. The right hand extremity of this band remained at a fixed wavenumber, but the left hand side moved significantly to higher wavenumbers. There also appeared to be a flattening of the base of the trough of the band, as if evidence of another band was becoming more apparent
- The band at ~1050cm^{-1} showed a similar effect. The band appeared to become much broader as the amount of aluminium orthophosphate was increased. Mix 1, and to a slightly lesser extent Mix 2, showed quite a sharp band with what appeared to be a slight second band superimposed upon it at approximately 950cm^{-1}. The spectrum relating to Mix 3 shows just one broad band where these two bands appeared to have joined.
- The area of the trough relating to the band at ~800cm^{-1} changes according to the coating formulation. This is due to the transmittance at the right hand end of the band reducing as the amount of aluminium orthophosphate increases.

However, this may be difficult to use quantitatively, as it is affected by the band at 730cm^{-1}.

- The band at 730cm^{-1} becomes much more apparent for Mixes 2 and 3, but is hardly observed for Mix 1. However, the band relating to Mix 2 has a larger than that for Mix 3, signifying that there may not be a direct correlation with composition.
- The same is true of much smaller bands at approximately 640 and 580cm^{-1}.
- The band at ~450cm^{-1} becomes much smaller as the amount of aluminium phosphate is increased. However, this may also be difficult to quantify in terms of area, as the point that defines the edge of the band appears to be at a wavenumber below 400cm^{-1}, which is the lowest wavenumber at which this apparatus can scan.

As expected from the results of the separate constituents, it appears that there are clear and distinguishable differences between the spectra relating to the three mixes. It can also be seen (Figures 8.4 and 8.5) that there are many strong similarities between the results predicted from the theoretical mixes produced using the spectral calculator and the spectra produced by the practical laboratory mixes. The bands appear where expected, along with the variations in band size, the occurrence of band shifts and changes in the levels of transmittance all occurring as predicted.

There appeared to be five main bands of importance on the spectra relating to each of the coating formulations. It is the troughs of the bands that are of relevance in this investigation, as transmittance was being measured and the troughs show where the

radiation is being absorbed by the coating. The base point of these troughs appeared at wavenumbers of approximately 1250, 1050, 800, 730 and 450 cm^{-1}.

From the spectra obtained from coating samples with the separate constituents (Figures 8.1 and 8.2), attempts can be made to allocate certain bands to certain components of the coating mix.

- The band seen at ~1250cm^{-1} is likely to be due to the silica. However, the broadening of this band to areas of greater wavenumbers is likely to be due to the aluminium orthophosphate.
- A similar occurrence is also seen with the band at ~1050cm^{-1}, which is mainly linked to silica. The broadening of this band, this time in the direction of lower wavenumbers, is again due to aluminium orthophosphate.
- The increasing depth of the trough at 800cm^{-1} is due to an increase in the silica content.
- The band at ~730cm^{-1} is linked to aluminium orthophosphate.
- A deeper, sharper band at ~450cm^{-1} is linked to increased silica content.

In all cases, visually analysing these spectra shows that the bands observed in Figure 8.5 agree with predictions that can be made from the spectra of separate constituents. However, although the bands and trends can be attributed to certain components, a quantitative analysis tool must be able to link the characteristics of the spectra in a more mathematical manner. Therefore, it was necessary to analyse these spectra in greater detail.

Two main characteristics of a band that may be used for quantitative analysis are the height and area i.e. a change in one or both of these parameters can be linked to a change in concentration between mixes. It is possible to test this hypothesis in this case as the coatings were mixed according to known formulations. Therefore, the area of each of these troughs was calculated using the standard baseline method in an attempt to discover a trend.

The areas of the troughs were plotted against the percentage of aluminium orthophosphate in the mix. The greatest correlation was found to be associated with the trough at ~ 450cm^{-1} (Figure 8.7). This provided an R^2 value of 0.8262. However, it was found on a number of coated samples that there was not always a trough associated with this wavenumber due to the trough extending outside the region of which the apparatus can scan. Therefore using it for quantitative analysis would be unreliable.

All of the other trendlines associated with the graphs of trough area versus concentration had an R^2 value of less than 0.6, and could not be used for future analysis of the coatings, as the scatter at each wavenumber would make it ineffective.

The ratios of the areas of each of the absorption were also calculated (e.g. area of the band at 1250cm^{-1} divided by the area of the band at 1050cm^{-1}). Although there is still a degree of scatter about the trendline, Figure 8.8 indicates that there is a link between the amount of aluminium orthophosphate present, and the ratio of the bands at 1170 cm^{-1} and 800 cm^{-1}. The potential for this to be used to determine the composition of

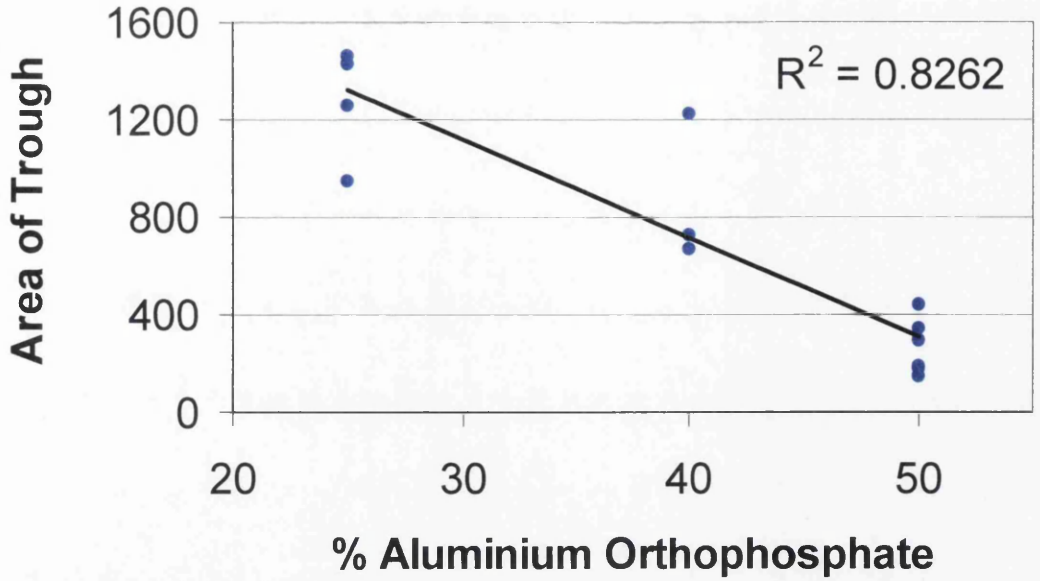

Figure 8.7: Correlation between the percentage of $Al(H_2PO_4)_3$ in the coating mix and the area of the trough at 450cm^{-1}.

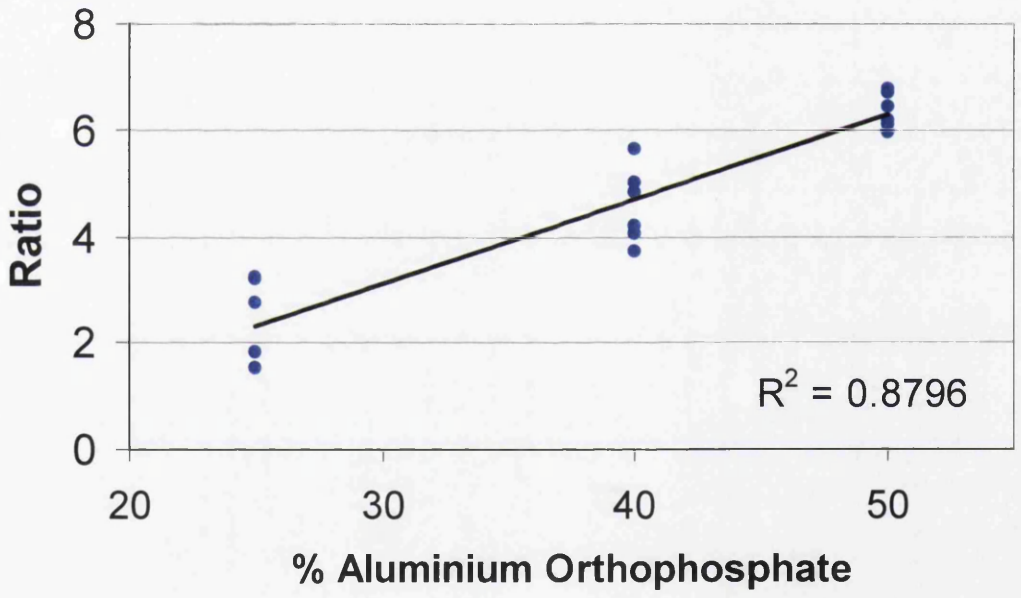

Figure 8.8: Correlation between the percentage of $Al(H_2PO_4)_3$ in the coating mix and the ratio between the areas of the bands at 1170cm^{-1} and 800cm^{-1}.

the coating would have to be further examined by establishing the same link on standard Works produced material.

Due to the nature of infrared analysis, each compound that is detected is associated with a number of bands at particular wavenumbers. In spectra obtained from a combination of two or more components, any shift in the position of the bands must be due to a change in composition of the coating being analysed. It was therefore considered that observing the effects at certain wavenumbers may be more relevant than the size of the troughs themselves, and so it was decided to use the transmittance (%T) values at the wavenumbers that appeared to be relevant. These wavenumbers were chosen to be 1373, 1278, 1130, 1035, 846, 795, 730 and 446 as these correspond to the positions that a majority of the peaks and troughs occur. When the transmittance value was analysed for each separate peak, it was found that a correlation with the amount of $Al(H_2PO_4)_3$ was only apparent for the troughs at 1373, 1278 and 730 cm^{-1}. The correlation, including the appropriate R^2 values, is shown in Figure 8.9.

Other methods of analysis were used to determine the extent of any correlation between these spectra and the coating composition. This included calculating the ratios between the above transmittance values and also the wavenumber separation between the points. Again, the averaged data showed some promise in many cases, but the full sets of original data showed a large amount of scatter, meaning the accuracy of a single, one-off analysis was not quite up to the standard required.

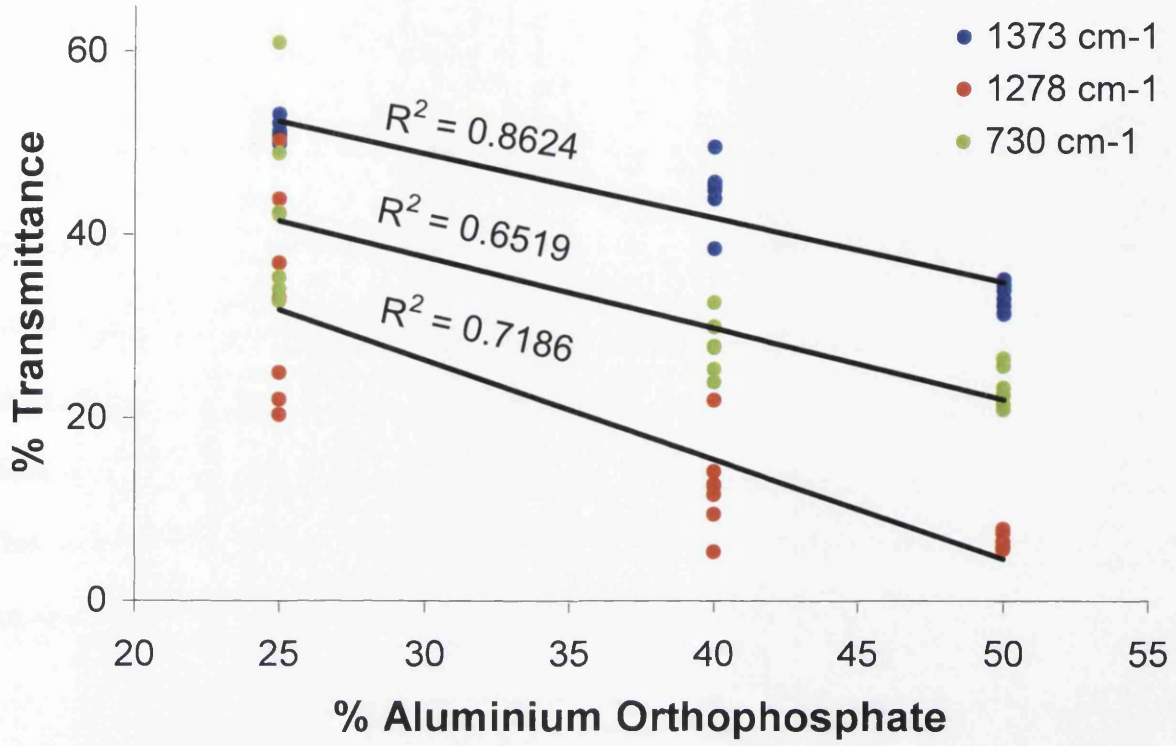

Figure 8.9: Correlation between transmittance and the amount of $Al(H_2PO_4)_3$ for the troughs at 1373, 1278 and 730 cm^{-1}.

As the number of spectra observed increased, it became increasingly evident that, as well as the bands changing size, the spectra were also changing shape. This is an important observation, as it interfered with the area calculations in some cases. For example, when the band at approximately 1100-1350cm^{-1} on the laboratory mix spectra is considered, it can be seen that the height of the boundary of the band at ~1100cm^{-1} varies according to the composition. This affects the calculated areas, but is directly influenced by the second band at 850-1100cm^{-1}. Therefore it was decided to re-examine a large number of spectra to establish any trends as this could be a factor that is responsible for introducing errors

From this visual inspection, it was found that the band centred around 1200 cm^{-1} is more likely to start splitting into two separate peaks as the amount of silica decreases. This visual observation is far less exact than the calculations carried out previously, but should be considered when carrying out further work.

8.5 Evaluation of Works Mixed Phosphate Coating

The results obtained from the previous section (coating steel samples with a laboratory mixed coating formulation) did not give a completely accurate indication of the coating mix used during Works production. The laboratory mix consisted of only colloidal silica and aluminium orthophosphate, as it is these components that are believed to affect the properties of the coating. Using just two components also allowed the basic understanding of their distinctive absorption characteristics to be obtained more easily. However, the coating mix used on the Works production line also contains water and chrome (in the form of chromic acid), which may have an effect on the overall shape of the spectra obtained. Previous work has shown where the bands associated with both colloidal silica and aluminium orthophosphate are to

be expected to be found, and has also shown some trends that are observed when the ratio of these two components is varied. However, it was necessary to investigate the different aspects of the coating under 'real life' conditions, and to establish the effect of these two extra components.

8.5.1 Experimental Procedure

Five samples of the coating mix were taken from the production line over a period of four days. The samples were taken as the coating was mixed, before being transferred to the main mixing tank. Each solution underwent chemical analysis in the Chemistry Laboratory in order to discover the content (%w/v) of silicon, aluminium and chrome present in the mix. If necessary, this data can be converted from these figures to give the amount of colloidal silica, aluminium orthophosphate and chromic acid that was used to make up the mix (i.e. the respective volumes).

The data is shown in the Table 8.1, including the ratio of silicon to aluminium that is believed to be the most important factor in relation to final magnetic properties. Figures are also shown for the target specification of the mix, according to the standard operating procedures for the production line.

A selection of Epstein samples were selected and subsequently pickled so that they could be used as a bare steel substrate. They were taken from the same Epstein pack as the samples used for the laboratory mixes in the previous investigations. Therefore, they would be expected to have the same steel chemistry. The various coatings were applied to the top surface using a roll with a 1.2 thou (30 microns)

Mix	(Shift, date)	Si	Al	Cr	Si / Al ratio
A	6-2, 10/4,	9.4	1.65	2.51	5.70
B	10-6, 11/4	9.6	1.47	2.29	6.53
C	2-10, 12/4,	10.7	1.38	2.35	7.75
D	10-6, 12/4,	8.9	1.71	2.44	5.20
E	2-10, 13/4,	10.3	1.31	2.38	7.86
	Specification	8.2	2.20	2.0-2.1	3.73

Table 8.1: Composition of Works mixed coating solutions.

groove depth, and the samples were cured at 800°C for 15 seconds. Each mix was used to coat two samples. The coated surface was then analysed using the FTIR apparatus. Three measurements were taken on each surface, one at each end and one in the middle, to establish the level of consistency along the length of the sample.

8.5.2 Results and Discussion

The spectra obtained from each of the coatings were compared by overlaying them using the FTIR software. Although the shapes of the spectra varied from one coating to another, a majority exhibited similar shapes based around four distinctive troughs. A typical example of these spectra is shown in Figure 8.10.

Initial observations found that these troughs occurred at approximately 1170, 950, 800 and 450cm^{-1}. Some spectra also exhibited a slight peak at around 730 cm^{-1}.

When compared to the spectra of the separate components, it could be seen that each of these bands could be linked to one of the components, with the spectrum for colloidal silica showing the greatest similarity. Colloidal silica also exhibited bands at approximately 1170, 800 and 450cm^{-1}, whereas the aluminium orthophosphate had bands at approximately 950 and 730cm^{-1} in common, as well as a possible similarity at 480cm^{-1} (compared to 450 in the Works mix spectrum).

It should also be noted that the spectra obtained with these mixes also showed good comparison with the spectra from mixes formulated with just two components in the laboratory (see Figure 8.5 for comparison).

The area of each of the troughs relating to each band was calculated using the standard baseline procedure, as with the laboratory coatings.

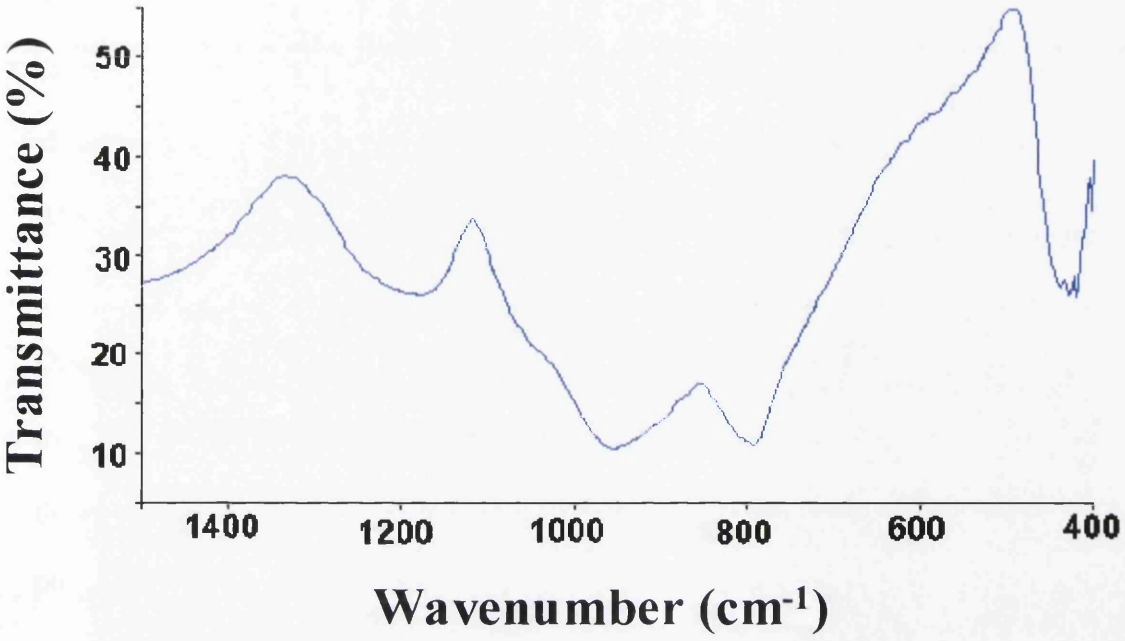

Figure 8.10: A typical coating mix showing 4 main troughs.

These areas were plotted against the Si:Al ratio of the mixes. It was found that the data points appeared to show almost random scatter, with the trend line showing the greatest correlation having an R^2 value of 0.0083.

It was also considered that the ratio of the areas of various troughs might show a trend in their variation as the concentration of the mix changed. Ratios were calculated for each combination possible. However, again no trend was found, with the data points showing a similar degree of scatter. The highest value for R^2 in this case was only 0.0859.

During the examination of the spectra, it was noticed that the base of some of the troughs did not always occur in exactly the same place, in terms of both wavenumber (x-axis) and transmittance (y-axis). It was deemed possible that there may be a possible shift occurring due to the change in Si:Al ratio. For this reason, the coordinates of the base of each trough was found and was plotted against the Si:Al ratio.

There appeared to be very little correlation between the ratio and the transmittance, but when the wavenumber shift was considered the troughs at approximately 1260 and 1170cm^{-1} appeared to show a slight trend. However, the variation averaged only ~20 cm^{-1}on the x-axis, which is quite insignificant when the large range of coating compositions is considered i.e. small changes in coating composition would not be detected by using this method. The study of these peaks was also slightly hindered by the fact that they occasionally merged to a varying degree.

The differences in wavenumber and transmittance values between the points at the bases of each trough were also calculated i.e. differences in height between troughs and distances between troughs.

When this data was plotted, it was found that there was a greater separation of the bases of troughs at ~1260 cm^{-1} and 1170 cm^{-1} (where the main peak appeared to separate in a number of cases) as the Si:Al ratio decreased. This had an R^2 value of 0.6336, which does not prove that this can be used as an accurate method, but does show that the change in composition of the formulations is having a clear effect on the spectra.

As mentioned previously, the shape of some of the troughs appeared to vary. This could also be affected by the Si:Al ratio. This appeared to be most obvious at 1160-1260cm^{-1} and 950-1050cm^{-1}.

Upon further study, it was found that as the Si:Al ratio increased, the troughs at ~1170cm^{-1} and ~1260 cm^{-1} were more likely to merge with each other to form a more elongated trough. The spectra obtained from mix D (lowest ratio of Si:Al = 5.20) clearly showed two distinctive peaks, whereas the spectra of mix E (highest ratio Si:Al = 7.86) showed only one. The region of the trough(s) also appeared to get shallower as the ratio increased.

To a lesser extent, separation and elongation also occurred in the 950-1050cm^{-1} region, but no link with the Si:Al ratio could be found. This was most likely due to the variation being much more slight, making the analysis more difficult.

8.6 Analysis of Works Coated Material

The previous sections have shown the spectra obtained from the two main components of the final insulation coating, the combination of these two coating constituents, and also the standard coating formulation as mixed on the Works production line. This has given a useful grounding of what is to be expected. However, all of the coating and curing procedures that have been carried out as part of those investigations has been performed in the laboratory. The overall aim of this work is to establish whether the FTIR can be used to directly determine the composition of the formulations that have been coated onto the final product. Therefore, now that a greater understanding of the components has been gained, it is necessary to analyse the coated steel as produced on the Works production line.

8.6.1 Experimental Procedure

As mentioned previously, Epstein samples (305 x 30mm) are routinely taken from each coil that has been processed on the final coating and thermal flattening line so that the material can be graded for customers. This provided a convenient supply of a large number of coated, Works produced material from a wide range of coils. They were also of dimensions that could be easily modified to suit the FTIR apparatus.

A large number of these samples were collected, and analysed using the FTIR apparatus at Orb Works, in conjunction with the 'standard' 26.5° attachment used for all analysis of final coatings and their constituents.

8.6.2 Results and Discussion

Once the spectra had been obtained from a number of samples it was instantly obvious that they were significantly different to what was expected. An example of one of these spectra can be seen in Figure 8.11. It is immediately apparent that there are far more bands present than had previously been seen for any other coating formulations. For example, the spectrum shown in Figure 8.11 shows at least twelve obvious bands. This was unexpected, as the work carried out in Section 8.5 had used a number of coating formulations taken from the mixing tanks on the same production line as these samples had been coated, and none of these had resulted in spectra of such complexity. Although the samples of the coating formulations were taken a number of weeks prior to these Epsteins being coated, it was deemed very unlikely that such a dramatic change of composition would occur. Therefore, the changes must be due to an effect that is unrelated to the composition.

Initial thoughts were centred on the coating and curing techniques, as the production conditions were significantly different to those in the laboratory, even though effort was made to replicate the same conditions. The coating was carried out with grooved rubber rolls and the curing was carried out at the same temperature as in the Works (800°C), but it was difficult to truly replicate the conditions due to the large scale of the production line.

The method of curing the samples could possibly introduce some discrepancies, as the temperature gradient and heating rate experienced by the sample may differ when it is static in a furnace, compared to when it is in strip form passing through a furnace. However, previous work in this section has shown that curing may slightly affect the levels of transmittance of a spectrum, but did not introduce any obvious new bands such as those seen on the Works produced material. This was expected, as it would

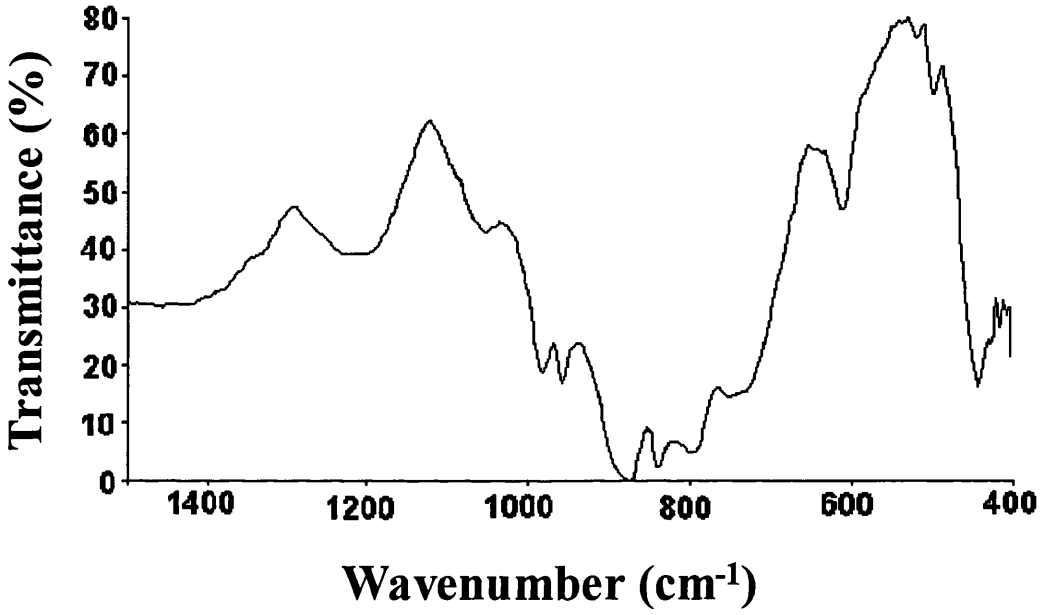

Figure 8.11: Spectrum obtained from material coated on Works final coating and thermal flattening production line.

take a very high temperature to cause the formation of any different compounds, as it is only new compounds being detected by the FTIR apparatus that could cause new peaks to be observed. Therefore the possibility of the curing conditions being responsible for the unexpected spectra was eliminated.

Samples have already been coated with coating formulations taken from the production line, and it was therefore known that the many bands were not all due to the components that are mixed to form the solution. It was initially thought possible that the coating mix could be contaminated. However, an in-depth evaluation of the line did not show any areas in which this could occur. It was also deemed very unlikely that the coating could be contaminated either between coating and curing, or post-cure.

The reasons for the numerous bands became evident when previous work relating to the FTIR analysis of the decarburisation oxide layer (Chapter 4) was considered. In this work, it was found that the penetration depth associated with the grazing angle attachment that was used hindered the analysis.

When the spectrum for forsterite (obtained in Chapter 7) was re-evaluated with respect to the Works coated samples, it was found that a number of the bands coincided with the wavenumbers associated with the forsterite glass film. This is clearly shown in Figure 8.12. It can be seen that, not only do a majority of the bands appear to be a result of the presence of forsterite, but also that other bands are affected by forsterite bands, causing them to be distorted. This results in a majority of the bands being ineffective for quantitative analysis. However, the bands at approximately 730, 800 and 1200cm^{-1} appear to be relatively unaffected, suggesting that these could potentially be used to give an insight into the composition of the

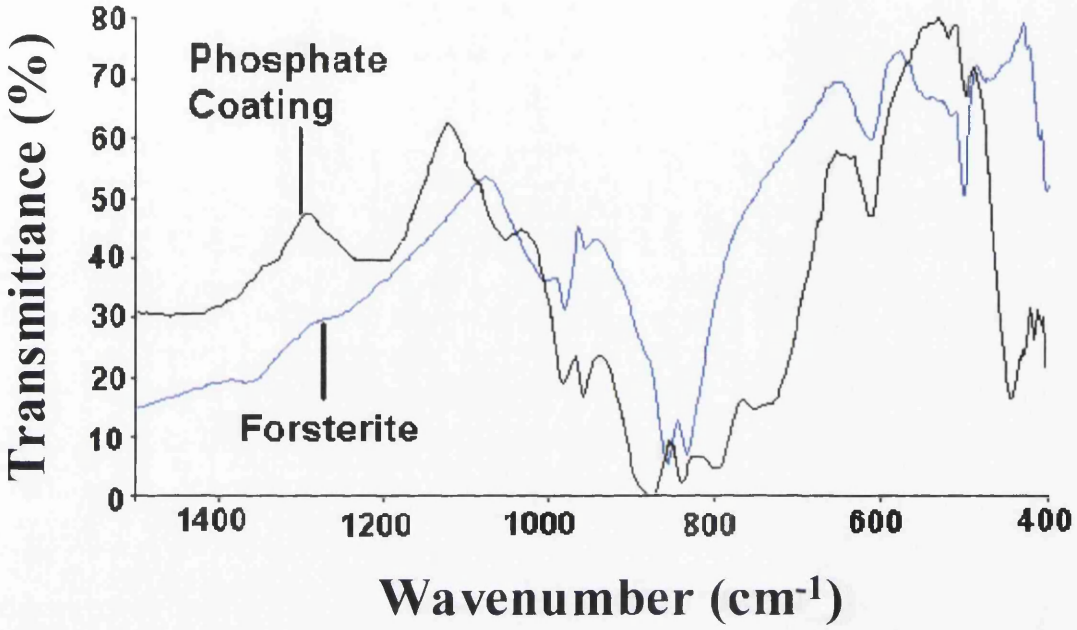

Figure 8.12: Comparison between spectra of Works coated and forsterite coated samples.

coating, although accurately determining the boundaries of these absorption bands is still problematic due to the underlying forsterite. The work carried out in Section 8.2 has already confirmed that the bands at 800 and 1200cm^{-1} are most likely to be associated with colloidal silica, and the band at 730cm^{-1} is related to aluminium orthophosphate.

8.7 Chapter Summary

The work carried out in this section has greatly increased the amount of knowledge relating to the FTIR analysis of the final insulating coating used on the final coating and thermal flattening line at Orb Works, as well as the separate constituents of the mix.

It has been shown that the FTIR apparatus at Orb, in conjunction with a 26.5° grazing angle attachment, is able to produce a clear spectrum for both of the coating components that are believed to have an effect on the final magnetic properties on the steel (colloidal silica and aluminium orthophosphate).

These spectra of the separate components could then be used to predict the spectra that would be produced when the constituents were mixed according to certain theoretical ratios, and this forecast was proved to be accurate when various mixes were coated onto steel samples under laboratory conditions.

Steel samples were also coated with a variety of coating solutions obtained from the Works production lines, and many of the spectra obtained also agreed with what was expected.

However, quantifying the results using the baseline method to calculate the peak areas and taking the coordinates of the peaks and / or troughs proved very difficult. Many

trends were found, although there was a high degree of scatter around the average value; it was only when the average value was calculated that a lot of the trends became evident. The reason for this is likely to be subtle variations in the spectra between scans and samples due to ineffective mixing of the constituents that make up the coating solution. In hindsight, although the samples appeared to be completely mixed, a more thorough mixing procedure should have been followed to eliminate the possibilities of localised areas with a greater content of a particular coating component.

Although it was difficult to predict the exact coating composition from the data extracted from the spectra, it was found that a number of changes could be observed when the ratio of components changed. This was particularly evident in the region around 1250cm^{-1}, where the band became more elongated, and in some cases separated) as the concentration of aluminium orthophosphate increased.

FTIR analysis of samples coated and cured on the Works production line further complicated matters, as a much larger than expected number of bands was observed on the resultant spectra. It has been shown that a large number of these bands are related to the underlying layer of the forsterite glass film. It appears that the radiation can pass easily through the cured insulation coating, allowing the layer underneath to be detected. It is this underlying layer that results in the extra bands, and also distorts those that are present due to the coating solution.

At present, it is not possible to quantitatively determine the composition of the final insulating coating due to the detection of the underlying forsterite. It was initially believed that the Spectral Calculator may be used to subtract the forsterite spectrum from that of the coated samples, but the variation in final coating thickness prevented this from being a practical solution, as the thickness affected the degree to which the

infrared radiation could reach the forsterite layer. However, the technology associated with FTIR is still improving, with a large number of software solutions entering the market. It is likely that these advances will shortly result in programs which can detect much more subtle variations in the spectra than can be seen visually, or can be discovered by the methods used during this work. The FTIR method has been proven to give results, both to a high degree of accuracy, and within a very short time frame. It therefore provides the correct type of analysis that is required for the constantly changing conditions of a production line, and effort should be made to exploit these benefits as the capabilities of FTIR equipment continue to improve.

Chapter Nine

Development of a New Chrome-Free Coating

9.1 Introduction

The work carried out in Chapter 8 of this thesis has included an in-depth evaluation of the FTIR spectra obtained from samples coated with the final insulation coating. However, variations in the composition can have many different effects on the properties of both the coating and the final product, such as appearance, magnetic properties, adhesion etc. There are a large number of measurement techniques that are currently employed at Orb Works to assess the quality of the finished material, and it was envisaged that these could be utilised to determine the effects that would result from changes in coating composition.

It was decided that it would prove beneficial to combine this work with a more in-depth study concerning the development of a new, alternative chrome-free coating.

The coating applied to grain oriented electrical steel on the final coating thermal flattening line at Orb Works has, for a number of years, contained chrome as a constituent. The presence of chrome in the coating formulations improves a number of characteristics such as solution stability and wettability, and also aids curing. Furthermore, the use of chrome enhances the appearance of the cured coating and improves the magnetic performance of the material.

A number of recent directives that govern the use of chrome have recently been issued, such as WEEE (waste electrical and electronic equipment) and RoHS

(restriction of the use of certain hazardous substances in electrical and electronic equipment) [43]. As a result of this, it has become evident that the use of hexavalent chrome should be eliminated at Orb, and hence removed from the coatings. It was therefore necessary to develop a replacement coating that satisfied all of the criteria specified by the standards of both Cogent and its customers.

The overall suitability of a new coating would primarily be assessed by the effect it has on improving the magnetic properties of the material. It is known that this will be largely dependent on the tension that it applies to the steel. However, other characteristics of the coating are of great importance, such as:

- A low enough curing temperature to ensure it would cure during production
- Constituents that mix easily
- Good adhesion to the strip when cured
- Good appearance when cured
- Good punching characteristics

Other safety considerations must also be taken into account, such as any heat and / or fumes given off when the components are mixed together.

In order to gain an insight into the substances that may be used for coating grain oriented electrical steel, a review of a large number of previous coatings was undertaken [44]. This included discussions with Technical personnel at Orb Works who have had a number of years experience of using different coatings, as well as reviewing published patents and Orb Research and Technical Reports which have been written since the 1970's. From this, it became evident that a number of

constituents are commonly used. These include magnesium or aluminium phosphate, MgO, phosphoric acid, silica, kaolin (aluminium silicate), gasil (powdered silica), boric acid and water, along with many other additions. It is on these components that the trial mixes were based.

9.2 Trial 1

As coating trials of this type had not been undertaken for a number of years, and each of the new the coating formulations had not previously been tested, it was necessary to undergo a preliminary investigation. This would enable the coating and curing procedures to be established, and the basic properties of various coatings to be ascertained.

9.2.1 Experimental Procedure

A number of sheet samples of both CGO and Hi-B types were cut from coils at the entry end of the final coating and thermal flattening line. At this stage, the strip has been annealed in the H.T.C.A to form the forsterite glass film on the surface, but has not yet been coated with the final coating. The sheets were still covered in excess magnesia, and so this was removed by brushing. These sheets were then cut into smaller samples with dimensions of 200mm x 80mm for coating. This size was chosen, as it would allow insulation measurements to be performed using a Franklin insulation tester. It was necessary to de-burr these samples to prevent any damage to the coating rolls. The samples were also annealed to remove shape defects caused from previous coiling operations.

In order to replicate the conditions experienced on the production line prior to coating, the samples were briefly pickled in a weak sulphuric acid solution. This cleans the sample of any remaining magnesia and provides a surface that the coating is more able to key in to, improving adhesion. Following the pickling process, the samples were rinsed with water and dried using tissue paper and a hot air dryer.

A powered coating unit, previously used by technical personnel for magnesia coating trials, was used to coat the samples. The rubber rolls used were re-grooved to an appropriate specification for final coating formulations (26 grooves per inch, 90° angle). The depths of the grooves on the two rolls were different, having depths of 101 and 165 ③m. This enabled both a thin and a thick coating to be evaluated from the two sides of the same sample.

The coating solutions were placed into a tray located beneath the bottom roller. When filled to the correct level, the lower roll was partially submersed in the solution, as shown in Figure 9.1. The coating was picked up onto the top roll from the bottom roll due to the contact between the two rolls. It was found that passing the sample through these rolls four times produced an adequate, uniform coverage.

The coating formulations were based on a number of previous trials, reports and patents. Seven types of coating mix were proposed, with varying proportions of each of the coating constituents. The coatings can be grouped according to their combination of components, as shown in Table 9.1.

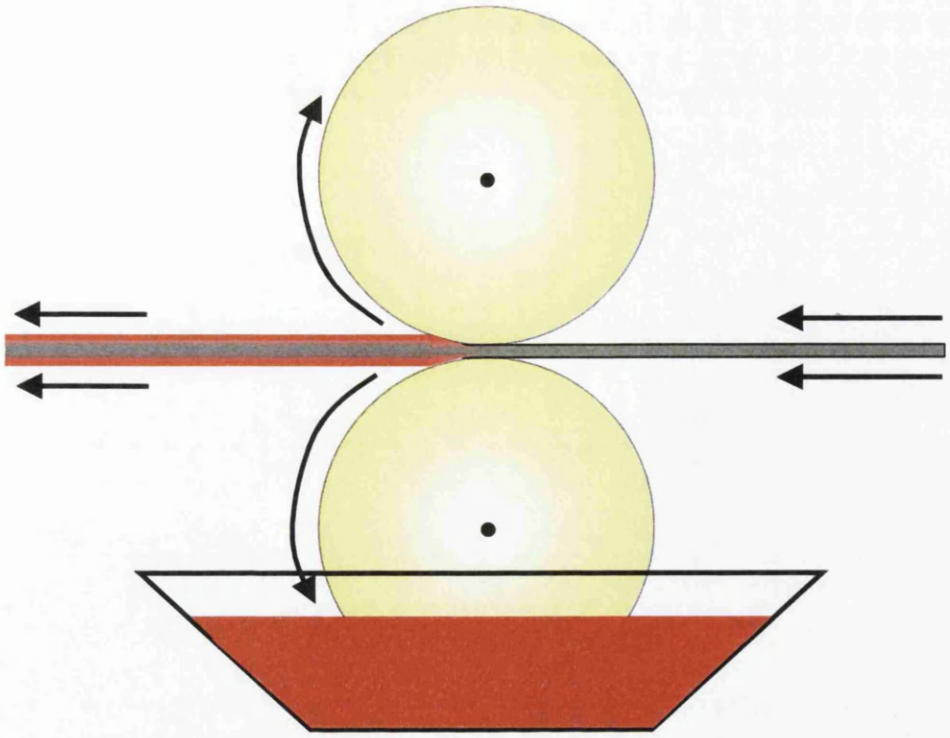

Figure 9.1: Schematic diagram of the laboratory coating unit.

	Aluminium Phosphate	Colloidal Silica	MgO	Phosphoric Acid	Water
Type 1	✓	✓	×	×	✓
Type 2	×	×	✓	✓	✓
Type 3	✓	×	✓	✓	✓
Type 4	×	✓	✓	✓	✓
Type 5	✓	✓	✓	✓	✓
Type 6	✓	×	×	✓	✓
Type 7	✓	✓	×	✓	✓

Table 9.1: Coating formulations used in Trial 1.

Water was added to each of the formulations in varying amounts. For each coating, the amount was chosen to ensure that the specific gravity for each of the coating mixes remained the same.

It was hoped that kaolin additions could be used for a number of these coatings, but upon mixing the particles were found to be too coarse to achieve a good coating mix. Therefore it was necessary to omit kaolin from the investigation.

The constituents of these coatings were mixed together in a large glass beaker using a magnetic stirrer. Some of these formulations were exothermic when the constituents were added together, and so each was left to cool to below 25°C before they were used to coat any samples.

Six different combinations for curing conditions were used for each coating formulation. Curing times of 5, 40 and 50 seconds were used in each of the two furnaces, which were set to maintain temperatures of 500°C and 800°C. These parameters were set for the following reasons:

- 5 seconds – to ascertain any problems relating to under-cure at a time that the strip would be reaching the first furnace roll on the production line
- 40 seconds – this is the time taken for the strip to pass through the furnace according to standard operating practice
- 50seconds – discover the effects of possible over-cure. This could occur due to the necessity of reduced line spend

- 500°C – recommended by chemistry laboratory personnel who advised that curing effects would be seen more easily at this lower temperature
- 800°C – this is the temperature at which the furnace on the production line is maintained.

Inside the furnace, two ceramic bricks supported the samples as shown in Figure 9.2. These were shaped to provide the minimum amount of contact with the sample whilst still keeping the sample flat.

The samples were manoeuvred into and out of the furnace using a set of tongs that gripped one end of the sample.

Once coated and cured, various properties of each of the samples were tested in the following ways:

- Insulation resistance using the laboratory Franklin tester. Two measurements were taken on each side of the sample. The coatings were graded between Grade 1 (greater than 29 ohm.cm^2) and Grade 5 (all results less than 10 ohm.cm^2).
- Loss on boiling. An area of the sample measuring 50mm x 40mm was cut from the coated sample and weighed. It was then submerged in boiling water for 10 minutes before being re-weighed. The loss on boiling (LOB) value in grams/m^2 is calculated by multiplying the weight loss by 500. A loss on boiling value of <0.2 grams/m^2, and preferably 0.1 grams/m^2, is considered to relate to a good degree of cure. This test also allows the free phosphate and hygroscopic tendency to be tested.

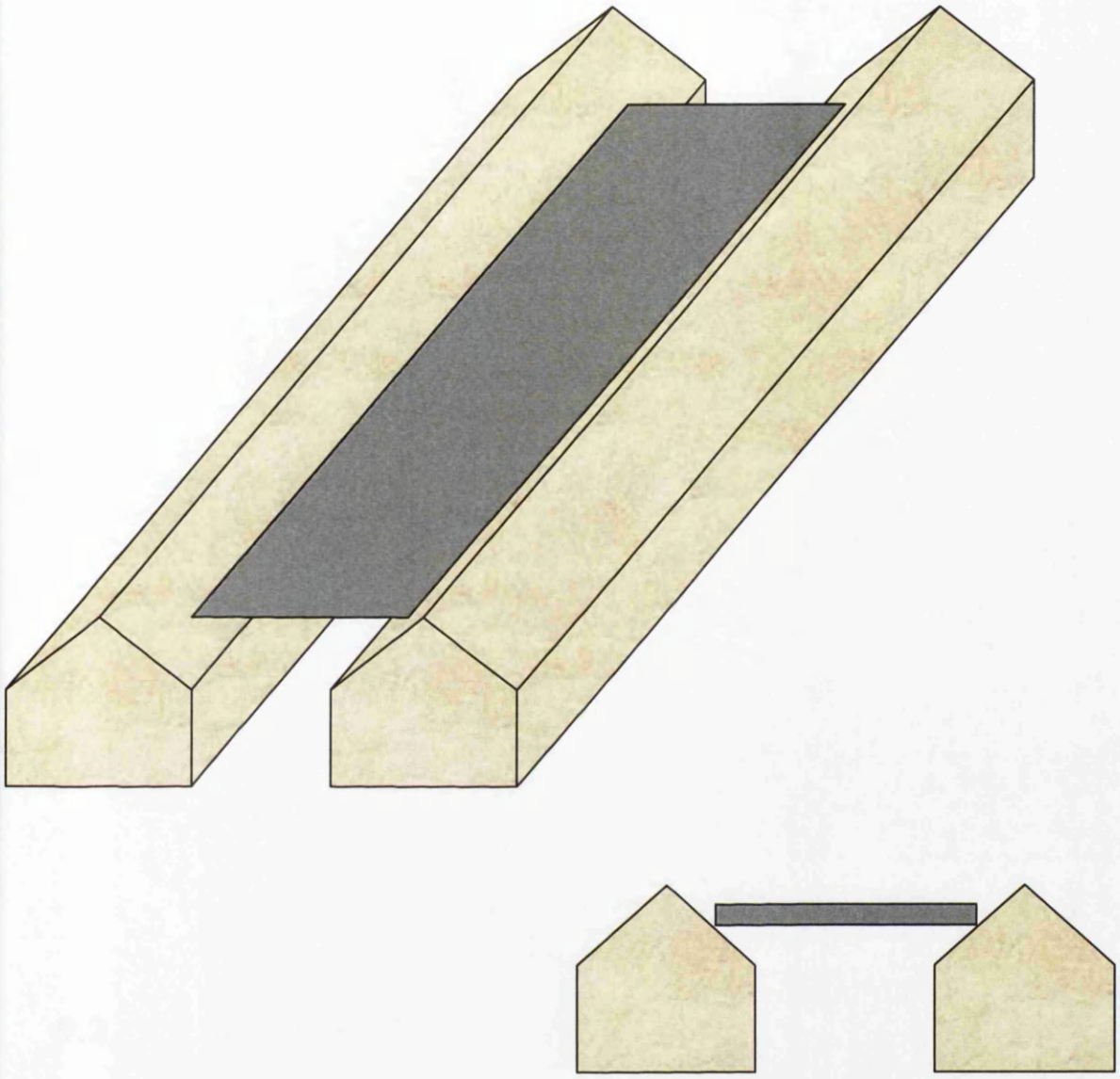

Figure 9.2: Schematic diagram showing the sample being supported by refractory bricks in the furnace.

- Adhesion test using a 25mm diameter bar. Coatings were monitored following both compression and tension.
- Coating thickness using apparatus known as a Fischer Permascope. The thickness value for each sample was calculated from an average of a minimum of 25 readings from each surface. Recalibration was carried out before each set of samples.
- Surface roughness using a Surtronic 3 instrument. Roughness average (Ra) and peak count (Pc) values were obtained from both the 'with' and 'against' rolling directions. Only the top surface of the sample was evaluated due to time constraints.
- Appearance was evaluated visually. The colour of the coating was noted along with whether it was glossy or matt, uniform, and whether it had lines associated with the coating roll grooves.
- Stability of the coating solution was established by leaving the mix in a glass beaker without any stirring for a number of days and monitored on a regular basis. It could then be seen how quickly the solutions gelled, if at all.

9.2.2 Results and Discussion

Although some of the coatings appeared to gel slightly quicker than others, all of the coatings were found to be relatively stable. None were found to gel after 3 days which is the time considered adequate for use on production lines.

Other characteristics of the coatings varied between mixes, such as the surface roughness. It was found that the Type 1 coatings were generally smoother than the other formulations. Other variations between coatings are described below:

Type 1

All samples were found to cure well at 800°C for 5 seconds, and the values for insulation resistance were satisfactory.

Appearance was generally good, although some samples exhibited a slightly whiter coating than others. Other coatings appeared to have a slightly pink appearance. It is thought that this must be due to an effect of the underlying material, as all other conditions remained consistent for each sample.

These results are for both CGO and Hi-B material. It can be seen that this type of coating appears to be quite promising.

Type 2

The appearance of samples coated with this type of formulation appeared to be good, and the insulation values for the CGO material were very good. However, the insulation values for the Hi-B material were not quite up to the same standard.

It was also observed that, although these coatings had been well cured after 40 and 50 seconds at 800°C, none were reasonably cured after just 5 seconds. Therefore, at this stage it appears that this type of coating would be unsuitable for production methods.

Type 3

The insulation resistance values and appearance for these samples appeared to be good. Unfortunately, the loss on boiling assessment was unsuccessful and did not provide any useful results. Therefore the ability of this coating to cure in 5 seconds at 800°C is unknown. However, the coating did not appear to be tacky, and so it is likely that the samples were well cured.

Type 4

Insulation resistance values for this coating were found to be satisfactory, with the better results being seen on the CGO material. However, a number of samples were found to be of a tacky nature that caused the appearance to be poor. This was due to the samples being slightly uncured, as proved by the resultant loss on boiling analysis. This under-curing was found to affect not only the samples cured for 5 seconds, but also some of those cured for both 40 and 50 seconds.

Some of the samples appeared to be of a higher quality that others, and also with better curing, and so it is possible that this formulation could be re-evaluated in any further investigations.

Type 5

The samples coated with this formulation were of a grey matt appearance. The insulation values were found to be very good on both the CGO and Hi-B material, and the samples were well cured, even after 5 seconds.

From all of the samples evaluated in Trial 1, the samples coated with this formulation appear to show the most promising results.

Type 6

This coating provided good insulation results and was very well cured on the CGO material. It was similarly well cured on the Hi-B. However the insulation values obtained from the Hi-B material did not achieve the same standard.

Type 7

This coating formulation is very similar to that of Type 6, and the results were also similar, with the insulation values for the CGO being an improvement on those seen from the Hi-B material. However, at one silica level on CGO, the coating was found to be under-cured and would therefore require further investigation. A number of the Hi-B samples also exhibited a slightly pink appearance, although this may be an effect due to the underlying material and not the coating itself.

9.2.3 Conclusions for Trial 1 (Section 9.2)

A comprehensive study has been carried out into different coating formulations that may provide a chrome-free alternative to the final coatings presently used. Many of the coatings evaluated during Trial 1 showed encouraging results. The only coating formulations which do not appear to be suitable for production material at present are those of Types 2 and 4 which both exhibited under-cured samples, particularly after 5 seconds at 800°C. An under-cured coating caused by these curing conditions would be likely to cause an undesirable build up of coating on the furnace rolls. However, the under-curing was not seen on all samples, and requires further investigation.

From these results, the most promising of the seven types of coatings appeared to be the formulation of Type 5. However, it should be considered that this coating contains five separate components, which is more than any other formulation that has been considered. This may make the use of this coating formulation more complicated than others, and the practicality of using this coating would require further trials.

Although many of these coatings show potential to be used on the production lines, further research is necessary. The effect of the tensioning properties of the coatings needs to be investigated, particularly for the Hi-B material. This further work was carried out as a second trial, detailed in Section 9.3, below.

9.3 Trial 2a

The trials carried out in Section 9.2 have shown a number of coating formulations that have the potential to be used on production material as a viable chrome-free alternative to the chrome-bearing coating that has previously been used. However, although previous work has assessed characteristics such as insulation resistance, appearance and ability to cure under certain conditions, it has not evaluated the tension that these coatings apply to the steel. This is one of the most important characteristics of the final coating, and can have a significant effect on the magnetic performance of the final product.

Therefore, further investigations have been carried out to assess the tensioning properties of a number of coatings that appeared promising.

9.3.1 Experimental Procedure

A number of Epstein samples were cut from the same Hi-B sheet that was used in Trial 1. It is possible to test samples of these dimensions on a single-strip tester to determine the magnetic properties of the material. This material had been taken from a coil at the entry end of the coating line and thermal flattening final, and therefore had a forsterite layer on the steel surface. The samples were annealed at 800°C to remove the shape defects caused by the coil-set, and then lightly pickled in dilute

sulphuric acid as before. However, prior to coating, each of these samples were magnetically tested at Bpk = 1.7T, 50Hz using the PMS 3000 single strip tester located at Orb Works. This allowed them to be sorted into groups of 20 samples exhibiting similar properties. This provided groups that were essentially identical in terms of the mean loss and loss range of the samples, which would ensure that any variations observed would be due to the coatings and not the material on which it was coated.

The coating formulations used were made according to the types specified for Trial 1. However, a number of mixes used in the previous investigation were not used again during this investigation due to the poor results seen previously. For example, the formulations containing the certain proportions of each component that related to the under-cured coatings were not repeated. However, variations of coating mixes relating to some coating types that showed promise were increased to gain a further understanding of the effect of certain variations e.g. to discover the effect of increasing the colloidal silica content.

The coatings were applied in the same manner as Trial 1, and each sample was cured for 50 seconds at 800°C. These conditions would ensure that the coatings were fully cured, as the ability for these coatings to cure for shorter times had already been established.

Once coated, the samples were re-tested on the single-strip tester to determine whether the coatings had caused any changes to the properties of the steel.

9.3.2 Results and Discussion

Following re-testing of the magnetic properties of each of the samples, it was found that none of the samples showed a significant loss reduction due to the coatings, as shown by the average values for each coating type shown in Table 9.2. This seemed a very strange result as the coatings were of types known to provide a tension on the steel surface, thus providing a reduction in magnetic losses.

A detailed evaluation of the coating procedure and other variables was carried out and a number of possible explanations for these results were highlighted. These are described below, along with remedial actions that were evaluated in an attempt to eliminate each effect.

Due to the necessity of sorting the samples into similar groups, it was essential that every sample for this entire investigation was pickled and single-strip tested prior to starting the coating procedure. It was thought that this delay might cause a layer to form on the surface of the samples that would affect the ability of the cured coatings to adhere to the surface. Therefore, a small number of samples were selected so they could be pickled, tested and coated within a much shorter time frame, thus reducing the delay prior to coating. However, it was again found that the applied coating did not result in a significant loss reduction.

The use of refractory bricks in the furnace ensures that the samples are kept flat when they are curing. However, when the samples are removed from the furnace, using a pair of tongs to grip one end, the samples bend until they are placed on a further set of refractory bricks for cooling. Although the samples were flat during cooling, it was considered possible that this procedure for removing the samples from the furnace may introduce stress into the material as it immediately starts to cool. It may also

Loss before coating	Loss after coating	% Loss Reduction
1.026	1.104	-7.60
1.045	1.099	-5.17
1.06	1.056	0.38
1.065	1.093	-2.63
1.068	1.094	-2.43
1.074	1.085	-1.02
1.076	1.165	-8.27
1.08	1.064	1.48
1.084	1.055	2.68
1.086	1.059	2.49
1.09	1.089	0.09
1.094	1.06	3.11
1.097	1.111	-1.28
1.1	1.122	-2.00
1.106	1.117	-0.99
1.111	1.144	-2.97
1.115	1.127	-1.08
1.119	1.132	-1.16
1.125	1.196	-6.31
1.09	**1.10**	**-1.72**

Table 9.2: Average loss data showing no response for samples coated during Trial 2a.

cause the sample to be in a bowed position when the coating starts to solidify, preventing the coating from providing its correct tensioning properties. To negate these possible effects, a number of stainless steel trays, upon which the samples could be placed, were fabricated. These provided support along the entire length of the sample from the moment the sample entered the furnace until it was cooled down to room temperature i.e. the sample was kept flat at all times that the sample was heated above room temperature. A further selection of samples was coated using this new technique, but it was found to have no effect on improving the magnetic losses.

It was possible that the single-strip tester, used to obtain the magnetic data for each sample, was not functioning properly and was not picking up the effects of the coatings. However, the apparatus was checked against a number of reference samples and was found to be functioning correctly.

To determine whether these results were due to the coating procedure, a number of samples were coated with the chrome-bearing coating that had successfully been used on production material for a number of years. Although it was known that this coating should reduce the losses of the material, no effect was seen on the samples upon which this coating was applied, even when the samples were pickled immediately prior to coating and when the supporting tray was used during curing. This suggested that it was not the coating or curing procedures that were responsible for the unexpected results.

It was therefore considered that the results must be due to the material being unresponsive, either due to the steel itself or the forsterite coating on its surface.

9.3.3 Conclusions for Trial 2a (Section 9.3)

Each of the coating formulations, including the chrome-bearing coating used as standard on the Works production line, was found to have no effect on the magnetic losses of the data for the set of samples utilised in this investigation. Following a number of investigations into the possible causes of this, it can be concluded that this is an effect of the material itself being unresponsive. The reasons for this have yet to be established.

A number of other possibilities were suggested and discounted following efforts to eliminate the effects. Although it was eventually determined that the material was responsible, it is recommended that the improved coating and curing techniques (i.e. using a stainless steel supporting tray during curing and minimising the time between pickling and coating) are used as standard during future investigations as this will reduce the variability in the technique.

It still remains necessary for the tensioning properties of these coating formulations to be established. Therefore it is required that this investigation is repeated on a different material in order for valid conclusions to be made.

9.4 Trial 2b

Trial 2a was carried out in an attempt to gain an insight into the tensioning properties of a number of coating formulations. However, this trial was unsuccessful as the material was found to be un-responsive; each of the coating formulations tested, including the mix that had previously been used successfully on the production

material, were not found to provide any loss reduction on this material. Therefore, the investigation was repeated using exactly the same formulations that were used in trial 2a. In order to minimise the chance of un-responsive material being selected again, it was decided to use samples from more than one coil source.

9.4.1 Experimental Procedure

As the reasons for the material not responding to final coatings were unknown, there was no way of knowing which coils were most likely to respond. Sheet samples were taken from two coils at the entry end of the final coating and thermal flattening line (K39169 and K39170), from which Epstein samples were cut. A number of preliminary tests were carried out on this material using the coating mix used for standard production, and it was found that the material from both coils was responsive. The reasons for this were unknown, as there appeared to be no obvious physical differences between this material and the unresponsive material.

The same experimental procedure was followed as for trial 2a. The samples were pickled, magnetically tested and sorted into groups that were as similar as possible in terms of magnetic properties. A group of 20 samples was used for every different coating formulation. During this trial, the samples also underwent a very brief secondary etch prior to coating. This was to minimise any surface oxidation effects caused by the delays during magnetic testing. A preliminary study established that the effect that such a brief pickle had on the material was negligible.

The samples were coated with mixes of the same formulations as used in trial 2a, and cured in a furnace at 800°C for 50 seconds. This was carried out using all coating types, with the exception of the type 6 formulation as problems were encountered

when trying to use this coating. The modified curing procedure, using a stainless steel tray to support the sample, was used.

The samples were then re-tested on the single-strip tester and evaluated in terms of appearance and coating thickness. The coating thickness measurements were carried out using the Fischer Permascope apparatus. Five readings were taken from each of the 20 samples in a group so that an average could be taken from the 100 separate readings. It was considered unnecessary to carry out further tests on the insulation resistance, as the grading for each coating type has previously been established in Trial 1.

9.4.2 Results and Discussion

The appearance of each type of coating formulation is shown in Table 9.3. This gives a general view of each particular set, but does not account for slight variations between samples.

It can be seen that a majority of the coatings were found to be too thick and that the uniformity over the area of the sample was also generally poor. It is believed that this is due to the coating rolls used, and is not necessarily related to the coatings themselves. It should be noted that samples coated in the laboratory generally tend to be of an inferior appearance to those coated on the production line.

It was found that the coating thickness on the bottom surface of the samples was significantly greater than that on the top surface. This was due to the greater groove depth on the bottom roll, which was a requirement of previous trials in order to assess two separate thicknesses of coating.

	Colour	Uniformity	Thickness	Smoothness	Gloss
Type 1	Grey	Med - poor	Too thick	Smooth	Shiny
Type 2	Grey	Poor	Too thick	Variable	Variable
Type 3	Grey / black	Poor	Too thick	Variable	Matt
Type 4	Grey / black	Medium	OK	Smooth	Matt
Type 5	Grey / black	Variable	Variable	Variable	Matt
Type 6	----	----	----	----	----
Type 7	Grey	Poor	Too thick	Rough	Matt

Table 9.3: Appearance of samples coated during Trial 2b.

For a particular coating type, subtle variations in the composition of the mix, such as varying the content of colloidal silica, were also found to have an effect on the physical characteristics of the coating.

For a Type 1 coating, it was found that a reduction in the proportion of colloidal silica resulted in a coating of improved uniformity, but with a less glossy appearance.

A lower silica content for Type 4 coatings resulted in a darker coating.

Type 5 formulations were also found to be affected by variations in the proportions of the components. Similar to Type 4 coatings, a decreased proportion of silica led to a darker coating. However, it also resulted in an improvement in the uniformity and smoothness of the coatings.

The results obtained from the magnetic testing, both before and after coating, are shown in Table 9.4. This data is displayed graphically in Figure 9.3. This shows the percentage loss reduction for each type of coating tested. In the case of some coating types, subtly different coatings were obtained by using the same components, but in different proportions. Increasing the colloidal silica content, while the amount of all other components in the mix remained constant achieved this. The lower case letters (i.e. a, b, c etc) denotes the different variations within each coating type.

It was thought possible that the thickness of the coatings might have an effect on the loss data. Therefore, the mean coating thickness was calculated for each coating (considering both the top and bottom surfaces) and plotted against the percentage loss reduction. Figure 9.4 shows that the effect of the coating thickness appears to have very little effect on the loss reduction achieved. This suggests that the coating only

Type	Reference	Original Loss	Pickled Loss	Coated Loss	% Reduction
Type 1	1a	1.127	----	1.088	3.46
Type 1	1b	1.108	1.124	1.078	2.71
Type 1	1c	1.108	1.124	1.084	2.17
Type 2	2	1.108	1.115	1.078	2.71
Type 3	3	1.108	1.134	1.057	4.60
Type 4	4a	1.107	1.121	1.067	3.61
Type 4	4b	1.114	----	1.084	2.69
Type 5	5a	1.108	1.132	1.059	4.42
Type 5	5b	1.126	----	1.063	5.60
Type 7	7	1.107	1.115	1.076	2.80
Standard Production Mix	Std.	1.095	----	1.052	3.93

Table 9.4: Appearance of samples coated during Trial 2b.

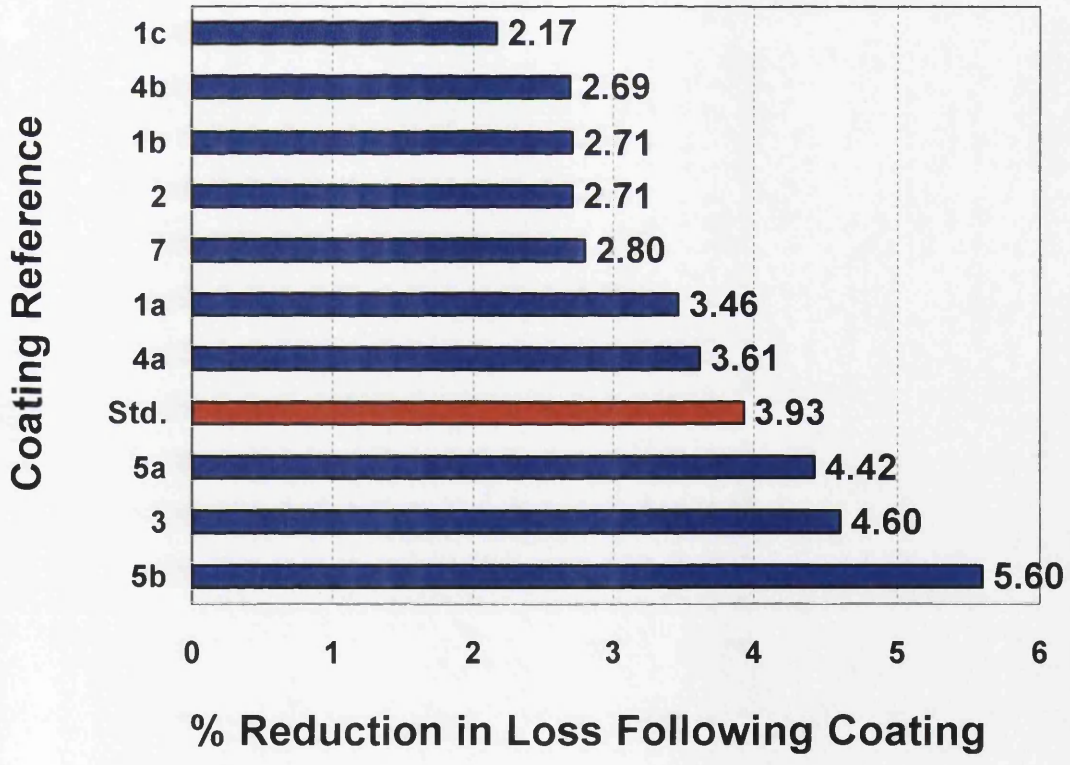

Figure 9.3: Loss reduction achieved with various coatings.

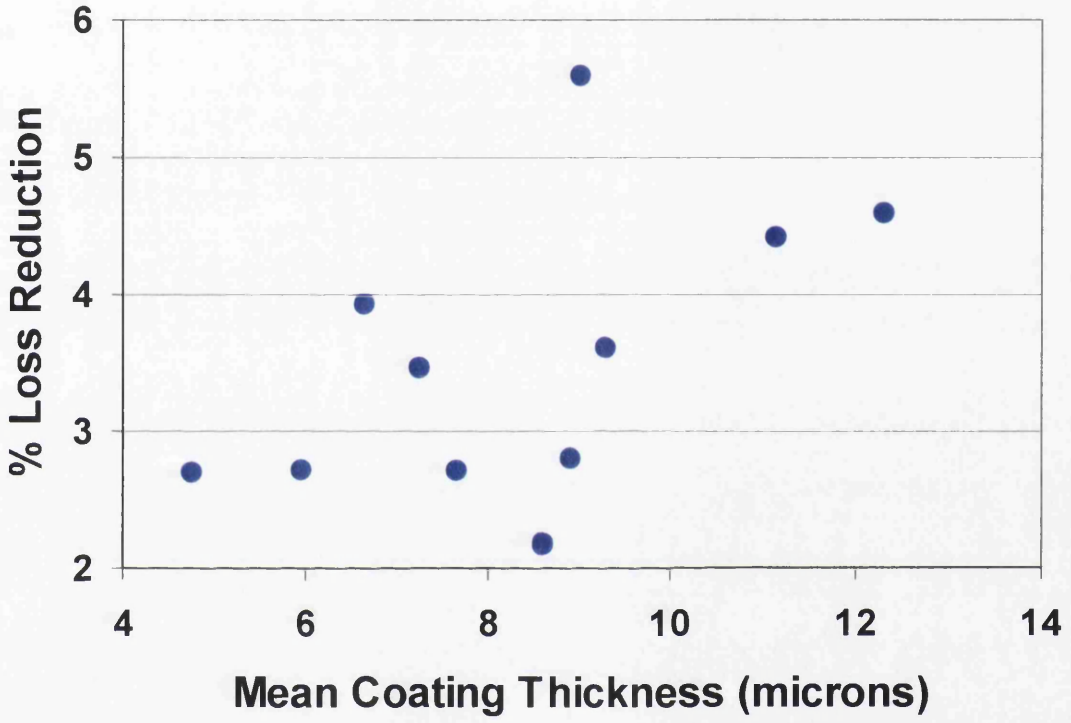

Figure 9.4: Effect of mean coating thickness on loss data.

has to be of a certain thickness to provide its maximum amount of tension, and any extra coating will have very little impact.

It was found that there was a spread of loss reduction values for each coating mix. An example of this is shown in Figure 9.5. The range over which the loss reduction varied can be seen to be quite large. It is believed that this variation is due to some underlying steel and / or forsterite being more responsive to coatings than others, as seen in trial 2a. However, it is considered that the number of samples used for each coating should give a good indication of the loss reduction that can be expected, based on averaging the data from each sample in the set.

It can be seen from the magnetic data that these coatings give a significant improvement in the magnetic properties of the samples, with the samples coated with coating mixes 3, 5a and 5b showing an improvement on the chrome-bearing formulation previously used for production coatings.

The sets of samples relating to coatings 1a, 1b and 1c were found to have loss reductions of 3.46%, 2.71% and 2.17% respectively. These coating mixes contained the same three components (aluminium phosphate, colloidal silica and water), but there is a clear trend that shows an increasing silica content is associated with a smaller loss reduction. Plotting this data (Figure 9.6) shows that there is a very good correlation between these two parameters.

The effect of silica was also seen in results for Type 4 coatings. These coatings consisted of silica, MgO, phosphoric acid and water, with Type 4a containing a

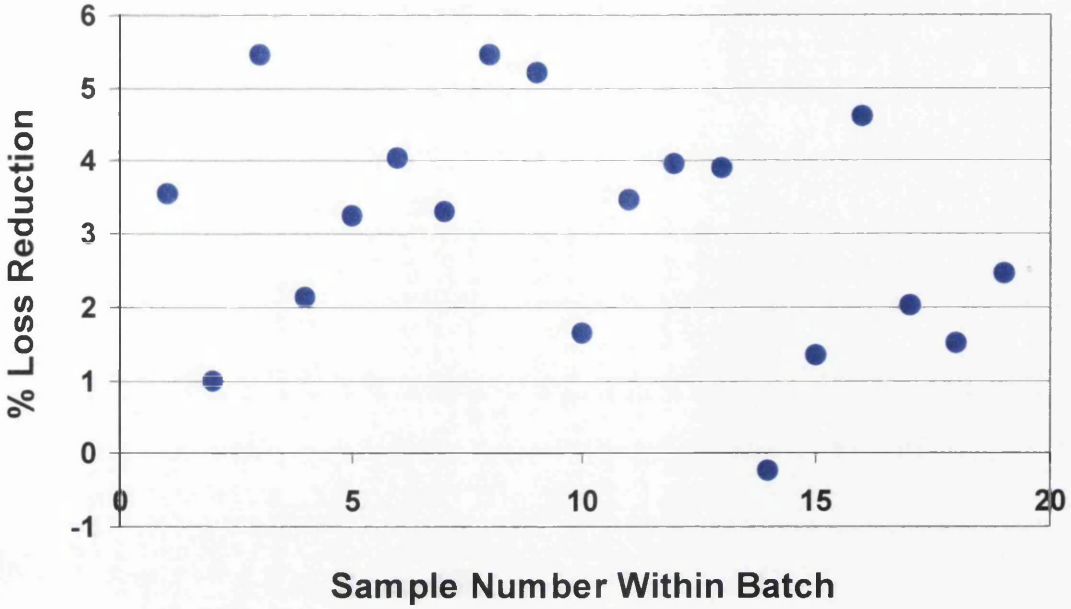

Figure 9.5: Graph showing an example of the spread of loss values that occurred within a batch.

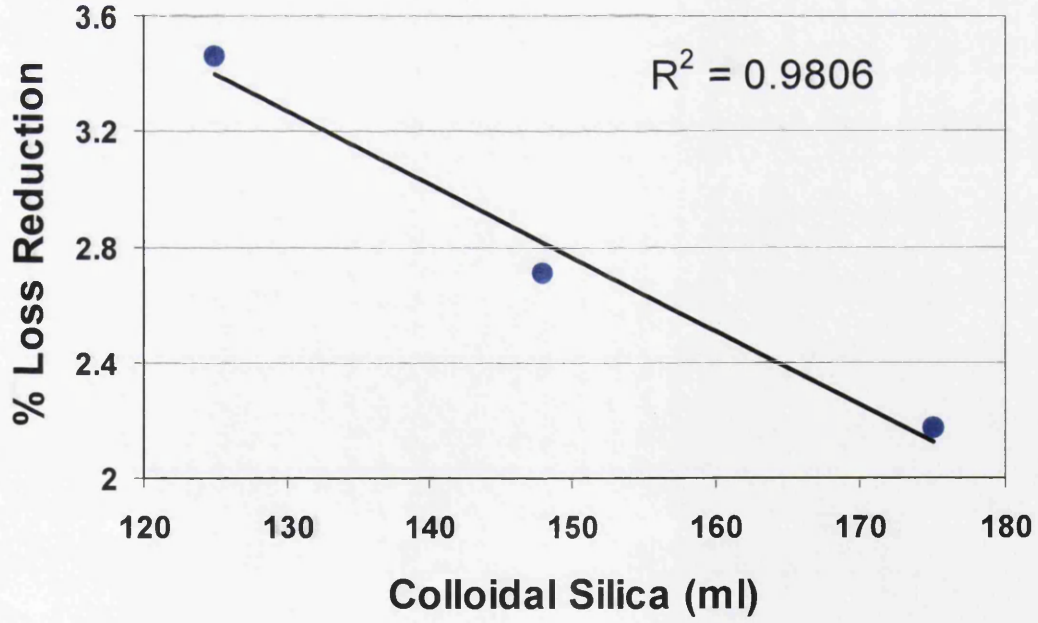

Figure 9.6: Effect of silica variation for Type 1 coatings.

greater proportion of silica than type 4b. We can also consider the data for the type 2 coating, as this can be considered as type 4 without the presence of any silica. Plotting this data (Figure 9.7) shows that the effect is the opposite to that seen for type 1 coatings, with an increased silica content resulting in greater loss reduction values, although the correlation is not as good. These results do not contradict each other, but instead show the different effects that result from mixing assorted components to create a coating mix.

Silica content was also found to have an effect on Type 5 coating formulations, as shown in Figure 9.8. The Type 3 coating has also been considered here, as it is essentially a Type 5 formulation without any colloidal silica. Unlike previous trends, it suggested that there was potentially a certain amount of silica that resulted in an optimum formulation, with either more or less silica having a detrimental effect on the loss data.

It was noted that the formulation that provided the greatest loss reduction was also the coating with the best appearance. However, although Type 5b resulted in the greatest loss reduction, it can be seen that all three of these formulations give good results when compared to some other coating types.

9.4.3 Conclusions for Trial 2b (Section 9.4)

A wide selection of coating formulations has now been evaluated to determine their ability to impart tension onto the steel surface. It has been established that all of the mixes investigated in this trial had a positive effect on the magnetic performance of the steel samples. The improvement in the losses ranges from 2.17%, which itself is a considerable improvement, up to 5.60%. This latter value was in fact found to result

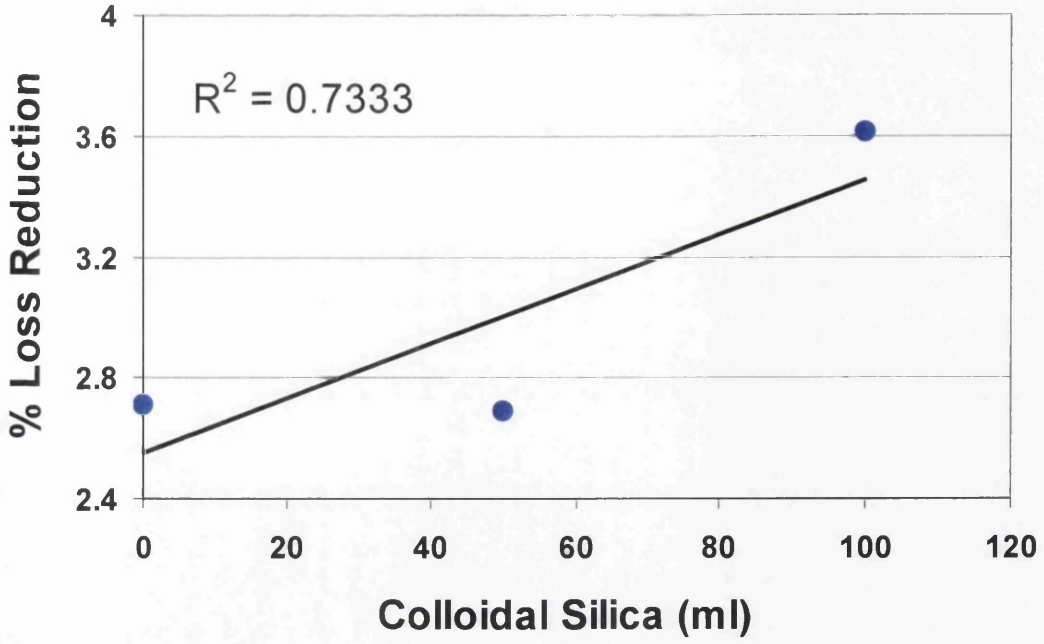

Figure 9.7: Effect of silica variation for Type 4 coatings (Type 2 data included).

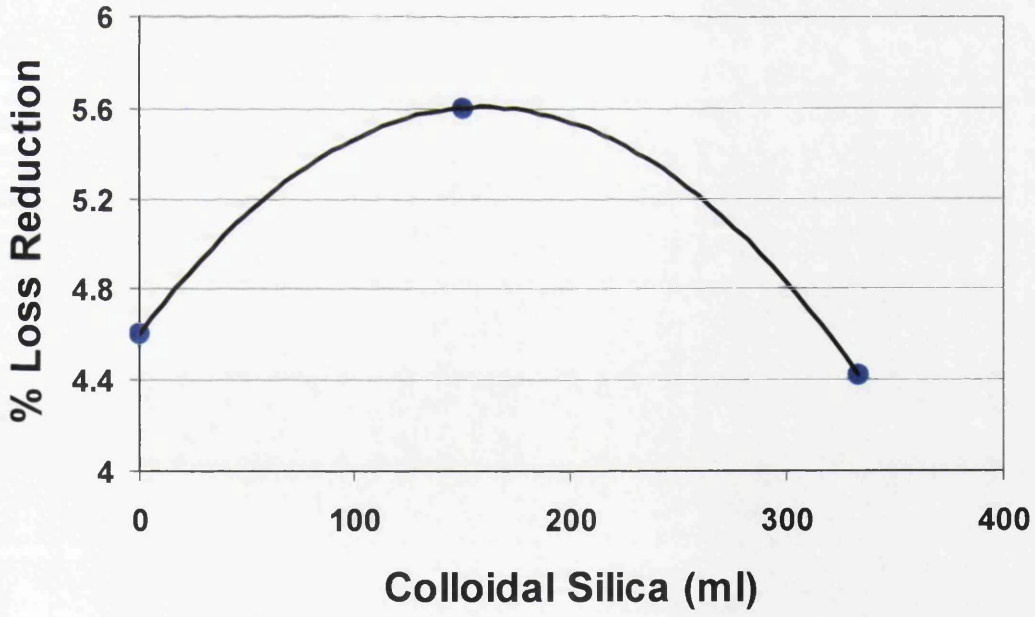

Figure 9.8: Effect of silica variation for Type 5 coatings (Type 3 data included).

in an improvement of over 40% on the coating that had previously been used for production material. This is a significant outcome as it provides a replacement coating that is not only chrome-free, but also has the potential to improve the magnetic performance of the final product.

A number of trends were found that suggest that the proportion of colloidal silica in the coating mix has a significant effect on the loss reduction. Although a number of the results have been impressive, these trends should be used as an indicator of further formulations that should be investigated, as it may be possible to improve the coatings further still.

Type 1 coatings, consisting of aluminium phosphate, colloidal silica and water, showed a loss reduction of between 2.17% and 3.46%. The data showed that the loss reduction increased as the silica content decreased (i.e. a lower silica content resulted in the coating having better tensioning properties). Therefore, a further coating formulation should be tested with the silica content reduced further. This will determine whether the coating can be further improved, or whether the formulation for Type 1a is the optimum for this combination of components.

Analysing the data obtained from the Type 4 coatings (containing colloidal silica, MgO, phosphoric acid and water), plus the data for the Type 2 formulation (essentially a Type 4 coating minus the colloidal silica), it was found that an increased silica content caused an increase in the tensioning properties of the steel. Therefore, the potential of a coating of higher silica content must be investigated.

The coating formulations containing various proportions of all five components (aluminium phosphate, colloidal silica, MgO, phosphoric acid and water) were also found to cause a variation in magnetic properties. The data suggested that there was an optimum level at which colloidal silica should be present in the mix, and any amount either side of this resulted in lower loss reduction values. As only three coatings of this type were considered (3, 5a and 5b) it is deemed necessary to evaluate a further formulation close to the perceived optimum in an attempt to establish whether further improvements are necessary.

From these results, it is clear that the proportion of silica within a coating mix can have a significant effect on the amount of tension that the coating imparts onto the steel. During this investigation, only one mix was made of a Type 7 formulation (aluminium phosphate, colloidal silica, phosphoric acid and water. Therefore, the effect of varying the colloidal silica content in this type of coating should also be investigated.

9.5 Trial 3

A number of previous trials have been carried out in order to develop a new chrome-free coating for use as a final insulation coating with high tensioning characteristics. Trial 1 established whether various formulations would satisfy a number of the basic requirements for a final coating, such as insulation, appearance, adhesion and the ability to cure within the required time frame. It was envisaged that trial 2a would give an insight into the tensioning properties of the different formulations. However, this trial was unsuccessful due to unresponsive material, and a further trial (trial 2b)

was required. A number of recommendations were made based on the results obtained in trial 2b that would lead to the optimum coating formulations. These recommended coatings were evaluated in trial 3.

9.5.1 Experimental Procedure

Further Epstein samples were cut from a sheet sample obtained at the entry end of the final coating and thermal flattening line. Once these samples had been annealed at 800°C to remove coil-set, they were pickled, magnetically tested and sorted into groups containing similar magnetic properties in the same manner as for previous trials. However, in view of time constraints, groups containing 15 samples were deemed adequate, instead of the groups of 20 that had been used for previous trials. Coating and curing of the samples was performed following exactly the same procedure that was used during trial 2b, with the curing being carried out in an 800°C furnace for 50 seconds.

The coating formulations used during this trial are based on the recommendations from the previous trial, which can be found in Section 9.4.3. They are variations of Types 1, 4, 5 and 7; Type 1d was chosen to have a lower silica content than the mixes of 1a-1c that have previously been used, 4c had an increased proportion of silica compared to other Type 4 formulations, 5c had a significantly lower silica concentration than 5a and 5b and coatings mixes 7b and 7c had lower silica contents than the original type 7. As it was only the effect of varying the silica content that was being investigated, the amounts of each of the other coating components remained unchanged.

9.5.2 Results and Discussion

The coatings were all considered to have a reasonable matt grey appearance. They all appeared to be reasonably uniform, except for some of the samples that had been coated with the 7b and 7c formulations, which had a slightly blistered appearance, particularly on the bottom surface.

Insulation resistance values for each of the coatings, measured using the Franklin Insulation Tester, were found to be 'infinite'. Although this is a very good result, the coating thickness values were found to average 6.2③ and 8.7③ for the top and bottom surfaces respectively. These figures are higher than would be found on the production material, and this could account for the impressive insulation results. The bottom surface generally had a thicker coating due to the bottom roll having a different roll specification for the groove depth. It was also observed that the coatings containing MgO (4c and 5 c) were of a greater coating thickness than those not containing MgO.

Samples coated with each of the formulations were bent around a bar of a diameter of 25mm to test the adhesion of the coating to the steel. The adhesion was found to be satisfactory in each case.

Testing the samples before and after coating using the PMS 3000 at Bpk = 1.7T, 50Hz enabled the loss reduction due to the coating to be calculated. The results are as follows:

1d = 2.51% loss reduction
4c = 4.12% loss reduction
5c = 4.83% loss reduction
7b = 3.00% loss reduction
7c = 2.01% loss reduction

This data is shown graphically in Figure 9.9, which includes loss reduction results, obtained previously in trial 2b, for comparison.

It can be seen that formulation 1d did not perform as well as either 1a or 1b. Figure 9.10 shows the effect of colloidal silica on Type 1 coatings. From the trend seen in trial 2b, it was expected that the reduced silica content could potentially increase the reduction in losses. However, this was not found to be true. The loss reduction value for formulation 1d (2.51%) was found to decrease significantly (by 0.95%) from the formulation with the next lowest silica content. Therefore, instead of a linear agreement between loss reduction and silica content, it appears that an optimum formulation is reached around that used for mix 1a.

The loss reduction that resulted from coating the samples with mix 4c averaged 4.12%. This followed the trend seen in trial 2a, where increased silica content resulted in improved loss reduction figures. This trend is shown in Figure 9.11. This is an impressive result, and appears to reduce the losses by a greater amount than the chrome-bearing coating that had previously been used on production material (labelled 'Std.' in Figure 9.9).

It was found that variation in the proportion of colloidal silica in Type 5 coating formulations did not have a great effect on the loss reduction achieved, as shown in Figure 9.12. It appears that silica values in the middle of the range evaluated result in the greatest loss reduction, although all of these formulations have led to reductions of at least 4.4%, which is a significant improvement on the chrome-bearing coating previously used.

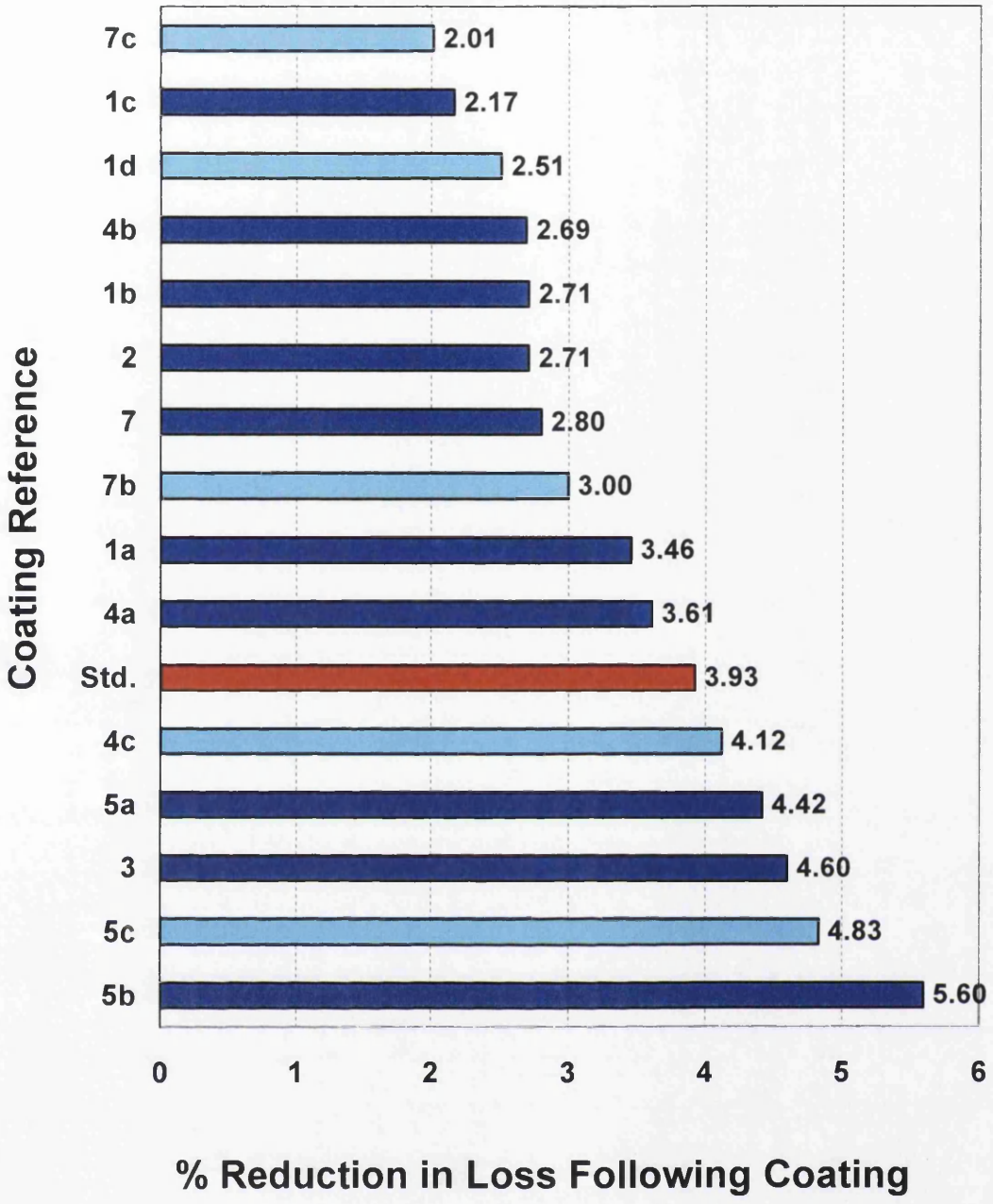

Figure 9.9: Comparison of loss reduction data from various coating formulations used in Trials 2b and 3.

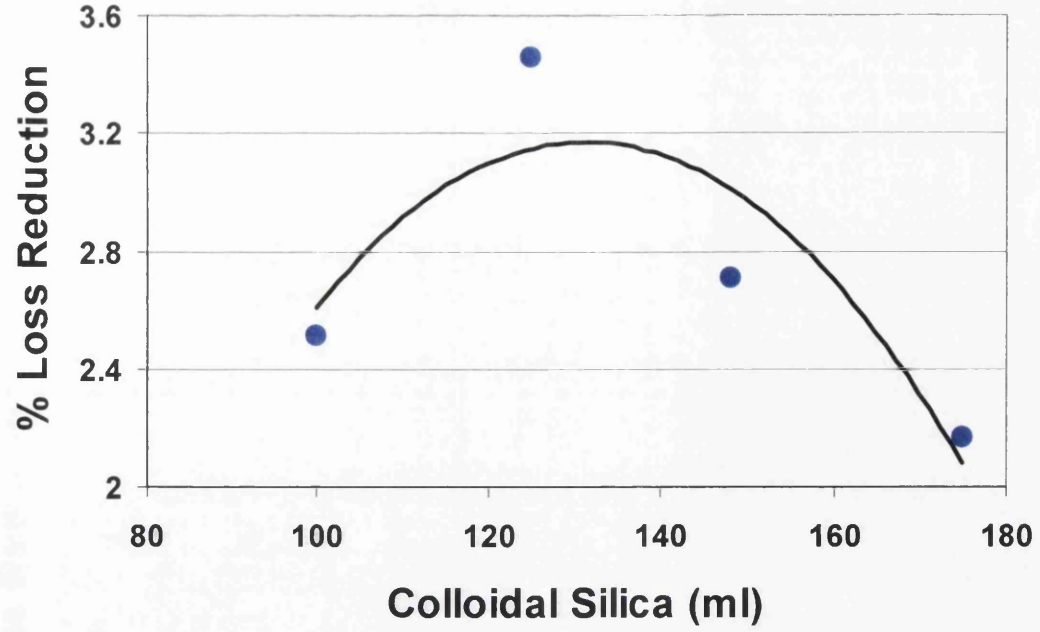

Figure 9.10: Effect of silica on Type 1 coating formulations - Trials 2b and 3.

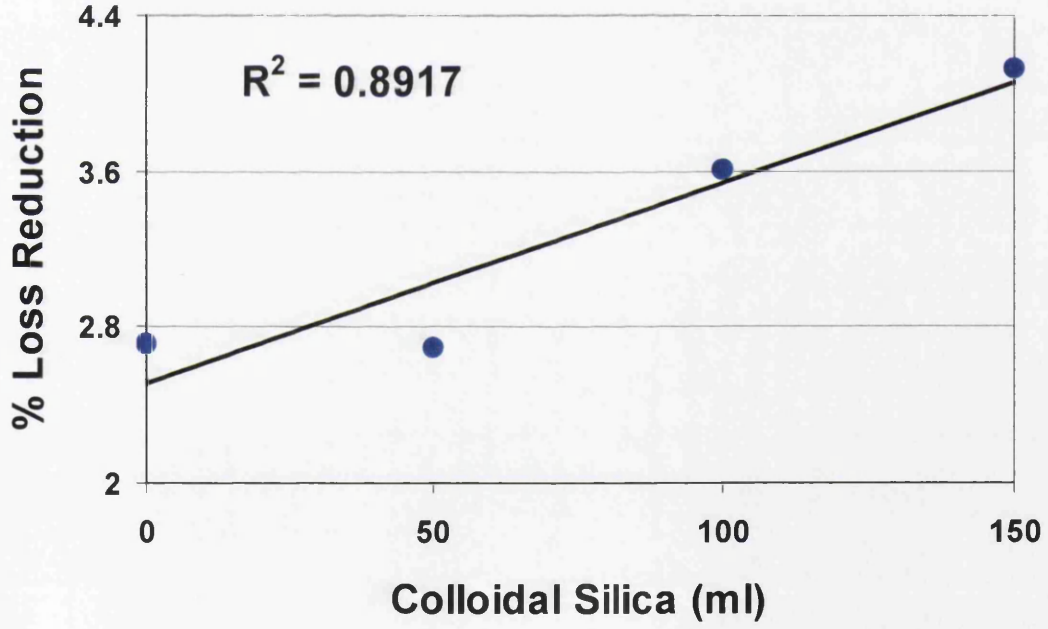

Figure 9.11: Effect of silica on Type 4 coating formulations (Type 2 Data included) - Trials 2b and 3.

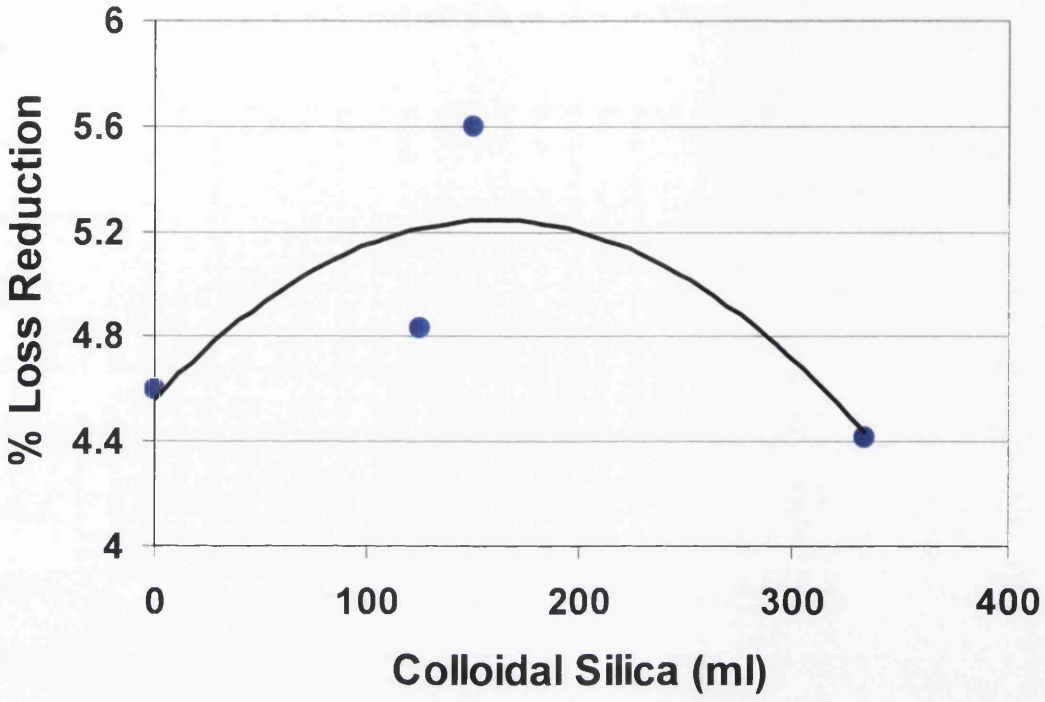

Figure 9.12: Effect of silica on Type 5 coating formulations (Type 3 Data included) - Trials 2b and 3.

The type 7 coating formulations shown in Figure 9.13 also appeared to exhibit greater results for silica contents in the middle of the range tested (100ml). However, these coatings produced a maximum loss reduction of just 3.00%, which is 0.93% below the standard set by the chrome-bearing coating.

9.5.3 Conclusions for Trial 3 (Section 9.5)

Following an in depth study into a number of different coating formulations, it has been found that a coating containing aluminium phosphate, colloidal silica, MgO, phosphoric acid and water (mix 5) results in the greatest reduction in losses. The loss reduction achieved by Type 5b averages 5.60%, which is a vast improvement on the chrome-bearing coating that has previously been used for coating the steel strip on the production line (3.93%). However, the silica content does not appear to have a great impact on the loss reduction, and all coatings of this type showed good results. It should be considered that as this coating mix contains all five components, it is likely to be more complicated and time consuming to mix, and may also have cost implications. However, the benefits may make the extra effort worthwhile.

Type 1 coating formulations are far simpler to mix, as they consist of just aluminium phosphate, colloidal silica and water. These coatings also showed potential, particularly Type 1a, although they could not quite attain the same loss reduction values as the chrome-bearing coating. This would be a useful coating to use if it was found impractical to use a Type 5 coating mix.

Type 4 coating formulations, containing colloidal silica, MgO, phosphoric acid and water, have also shown potential for application as a chrome-free alternative coating. At present, the formulation of this type resulting in the greatest loss reduction has been 4c with a loss reduction of 4.12%. This is already a greater value than the

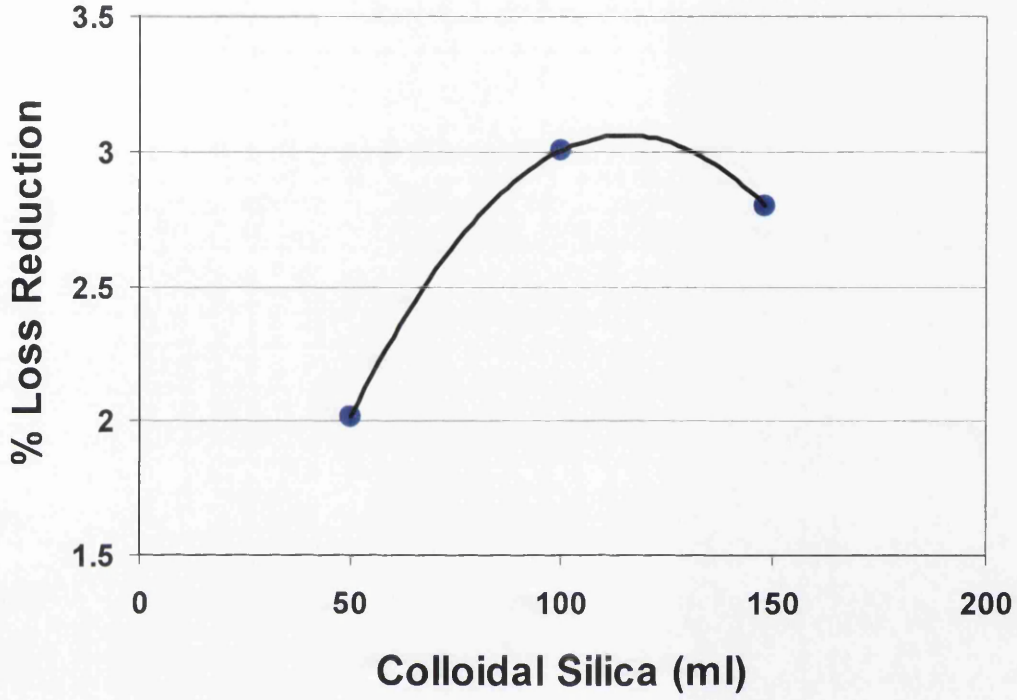

Figure 9.13: Effect of silica on Type 7 coating formulations - Trials 2b and 3.

chrome-bearing coating, and there was a clear trend suggesting that increasing the content of colloidal silica could result in greater reductions in loss. However, the proportion of silica used in formulation 4c is already considered quite high and a further increase could possibly lead to problems associated with dusting.

Coating formulations have been developed that appear to have all the characteristics required from a final insulation coating. They have been found to have a satisfactory appearance, good insulation and adhesion properties, and are also fully curable within the required times. In formulations 3, 4c, 5a, 5b and 5c, coatings have also been observed to not only match the loss reduction provided by the chrome-bearing coating, but also actually improve upon it.

Project work on these chrome-free coatings has been completed with respect to the Engineering Doctorate scheme. Internal reports, containing recommendations for further work, have been written and issued to the relevant technical and production personnel [45-47]. Plant trials of coating formulation 1a have taken place on the production line at Orb Works. This coating formulation was initially chosen over the other successful formulations due to the ease with which they can be mixed on the site of the coating unit. The resultant samples suggested that this coating provides a suitable chrome-free alternative to the coating previously used, and extended trial was carried out to determine the result of slight modifications. A chrome-free coating is now used on all coils as the standard production coating as a result of this work.
Further coating materials have been ordered so that a coating trial can be carried out using the 5b coating formulation. It is hoped that the loss reduction achieved by this trial will correspond to the results achieved during this investigation. This trial will

also provide an opportunity for the production mixing and coating procedures to be assessed in order to establish whether it is practical to coat the strip using a more complex formulation.

Chapter 10

In-Depth Analysis of Two Alternative Chrome-Free Coatings

10.1 Introduction

Due to the introduction of recent legislation, the decision was taken to eliminate all traces of chrome from every process on-site at Orb Works. Work has previously been carried out to establish a number of recommendations for alternative chrome-free coating formulations, and this is described in Chapter 9. This work concentrated primarily on the more practical aspects of the coating, such as curability, wettability, adhesion to the strip surface etc.

To further develop the chrome-free coatings, further investigation was necessary to establish the effect of the coating formulation on magnetic loss reduction. It was found that some of the formulations were not just able to satisfy the practical requirements of a coating, but also provide a loss reduction equivalent to the previous chrome-bearing S2 coating, and in some cases surpass it.

A number of coatings were found to provide the characteristics suitable for use on production material. One formulation was subsequently recommended and now provides the basis for the coating that is currently being used as the standard coating on the production line at Orb Works.

Although the chosen chrome-free coating appears to be a satisfactory replacement, it is necessary to further investigate this coating with respect to its effect on magnetic

loss reduction. It is also desirable to establish the effect of the coating on the magnetostriction properties of the steel, as this affects the noise that the material will produce when assembled as the core in a transformer.

10.2 Analysis of Magnetic Loss Reduction

The magnetic losses of the chrome-free coating currently used at Orb is to be evaluated using the PMS 3000 single strip tester, as has been used in previous investigations. The chrome-bearing S2 coating that was previously used on-site is to be used to provide a direct comparison. A further coating known as 'Mix 26' is also to be used, as this provided the basis for the formulation that resulted in the greatest loss reduction in the previous investigation.

10.2.1 Experimental Procedure

Strip samples were taken from four Hi-B coils at the entry end of the final coating and thermal flattening line at Orb Works. All samples were taken from the front end of the coil, with the exception of one coil where a sample was also cut from the middle section. Although the mid-coil samples are desirable due to the possible reduction in variability, it is not viable to obtain these samples from a large number of coils due to the disruption that it causes to production.

At this stage of processing, the steel had a forsterite 'glass film' on both surfaces, and was covered in MgO from the decarburisation line. A majority of this magnesia was removed simply by brushing (the remainder was removed with the samples undergoing a brief pickling prior to coating).

Each strip sample was labelled with a letter as follows:

Sample	Coil	Section	Gauge
A	L04125	Front	0.30
B	L04126	Front	0.30
C	L04126	Mid	0.30
D	L04128	Front	0.27
E	L04136	Front	0.27

The samples were to be coated as Epstein sized samples (305x30mm), and so samples of the correct dimensions were cut from the strip and labelled as shown in Figure 10.1 (coil A used for example).

It is believed possible that the strip may be more consistent along the length that it is across its width. Therefore, approximately 20cm was removed from each edge prior to Epstein samples being cut to ensure that the samples were as similar as possible.

For each coating formulation, ten samples were selected from each of the 5 coils used (A-E). Therefore, there were 50 samples to be coated with each formulation, and 150 samples in total. The samples were chosen in a way that arranged them into groups with similar characteristics. Therefore S2 was coated onto A4, A7, A10 etc, chrome-free onto A5, A8, A11 etc and Mix 26 onto A6, A9, A12 etc.

To investigate the effects that the different coatings have on the material, it was necessary to analyse the samples both before and after coating. However, prior to any testing, it was necessary to stress relief anneal the samples to remove any coil-set. It was also necessary to pickle the samples for approximately 6 seconds in 5% (w/v)

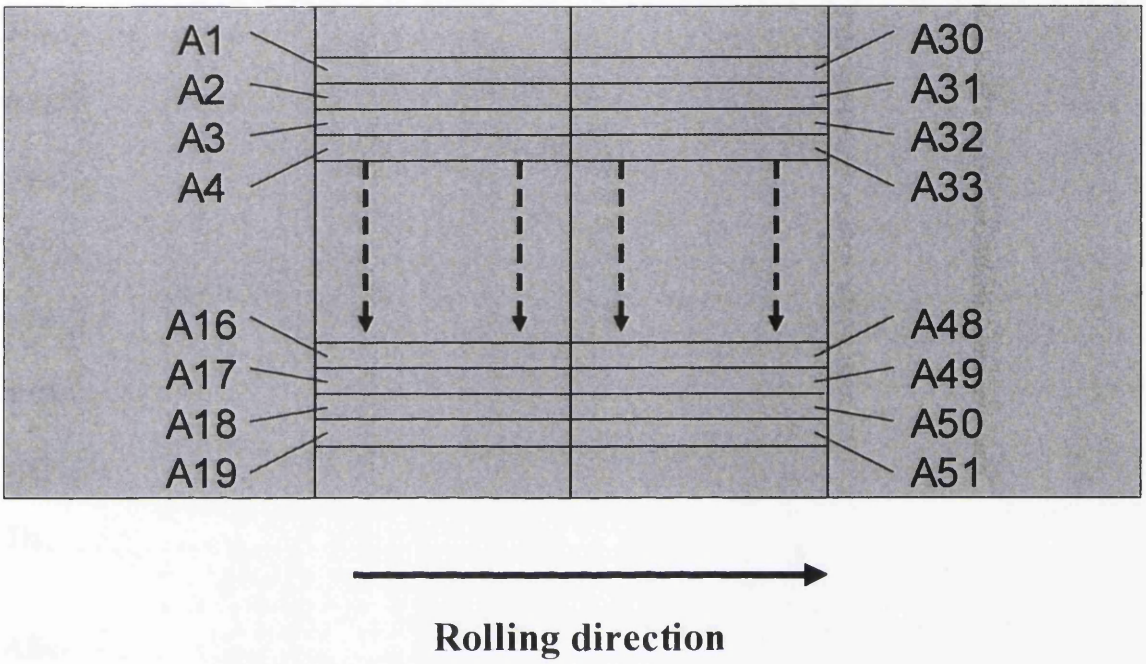

Figure 10.1: Diagram illustrating the labelling system for the samples.

sulphuric acid at 70°C. This is to replicate the production process at the entry of the final coating and thermal flattening line, and remove the remaining MgO from the steel surface. It was decided that the samples should be pickled before the testing was carried out, as this would give a more accurate representation of the results for the samples in their 'before coating' state.

The samples were first tested on the PMS 3000 single-strip tester to assess their initial magnetic properties prior to coating. Following this, they were analysed on the magnetostriction test-rig located at Orb Works. This was able to provide information on the magnetostriction, magnetic loss, permeability and VA's at intervals of ~1MPa over a stress range of -10MPa to +10 MPa. Although it has the function for measuring the losses of the material, these are not calibrated against the PMS 3000 apparatus and would only give relative results, instead of being fully quantitative.
The testing parameters for both of these techniques were Bpk = 1.5T and 1.7T, 50Hz.

After these tests had been performed, it was necessary to pickle the samples for a further 1-2 seconds. This was necessary to clean the surfaces due to the time taken for the testing, as it was possible for oxides to form on the surface. This could cause problems with de-wetting or prevent the coatings from adhering to the surface correctly. This second pickle was for a much shorter duration than the first, main pickle, and previous work has shown that the effect of this pickle on the properties of the steel is negligible.

Samples were coated using a mechanically driven, laboratory, two-roll coating system. The rolls used were grooved rubber rolls (see Section 9.2.1 for further details), and the roll pressure could be adjusted using a screw mechanism. The

bottom roll was submerged in the coating, which was held in a coating tray. The top roll was lowered so that it was in contact with the lower roll, causing some of the coating solution to be transferred onto the top roll. This allowed 2-sided coating of the sample.

Prior to the coating of each of the groups of samples (one group per coating formulation), a number of preliminary samples were coated and cured to assess the coating weights that were achieved at various roll pressures. When the results had been obtained, the apparatus was adjusted accordingly so that the desired coating weights could be attained.

Each sample was passed between the rolls twice, turned over, and then passed through again (twice). This was to ensure that both sides of the sample were coated as uniformly as possible.

Once coated, the sample was placed onto a metal support tray that acted to keep the sample flat throughout the curing process. The support tray was also designed to minimise contact with the sample, so that as little of the coating as possible was affected prior to the sample entering the curing furnace.

The tray supporting the coated sample was placed onto refractory bricks within a laboratory furnace set at 800°C, for a duration of 30 seconds, to ensure that the coating was fully cured.

Once coated and cured, the samples were re-tested, both on the PMS 3000 single-strip tester and then on the magnetostriction apparatus. Again, the tests were carried out at Bpk = 1.5T and 1.7T, 50Hz.

10.2.1.1 Coating Thickness

The coating rolls used for previous coating trials had a groove depth of 4.5 thou (114μ), which was a similar specification to the rolls used on the production line. However, it was believed that to match the coating weights attained on the production line (8-10g/m^2 for both sides combined), the roll specification would have to be changed, as previous trials have resulted in coating thicknesses greater that those required.

Before this investigation could begin, it was necessary to carry out an investigation to establish the coating weight that would be generated by the current rolls.
Six plate samples (approximately 70mm x 200mm) of Hi-B material were selected and pickled in 5% (w/v) H_2SO_4, according to the standard procedure followed for previous coating investigations. This was to remove the excess MgO powder and prepare the surface for coating. The samples were taken from the entry of M-line, so had not been coated with the final coating.

The first two samples were coated with the rolls set so that they were just touching, allowing the maximum amount of coating solution to be deposited on to the surface. The top roll was then lowered to its mid position, decreasing the gap between the rolls, and the next two samples were coated. For the final two samples, the top roll was lowered once more so that the gap between the rolls was as small as could be achieved. A slight modification was made to the position of the top roll between the coating of the final two samples, as it became clear upon coating that the roll was not completely horizontal.

The results were as follows:

Sample 1	23.1 g/m^2
Sample 2	22.5 g/m^2
Sample 3	15.3 g/m^2
Sample 4	14.9 g/m^2
Sample 5*	18.6 g/m^2
Sample 6	11.5 g/m^2

* Top roll not horizontal. Adjusted prior to coating sample 6

These are total coating weights, and include both surfaces.

The desired coating weight is between 8 and 10 g/m^2, as this is what is regularly achieved on the production line. It can be seen that none of these results were within the range required.

The coating weight for sample 6 was the closest, and was probably within a range that would be tolerable for this investigation. However, it was the opinion of the operator that this thickness would not have been achieved consistently and that the average would have been somewhat higher.

It was therefore necessary to obtain coating rolls of a different specification, with a groove depth of less than 4.5 thou (114μ).

In previous investigations, coating had also been carried out with a bar coater with a groove depth of 1.2 thou (30μ). It was known that this had resulted in coating weights slightly less than that required in this investigation, which further refined the grove depth range that was necessary to achieve a coating weight of 8-10 g/m^2.

Due to the time constraints of this project, it was decided to re-grind the rubber of the existing rolls instead of having new rolls fabricated. The grooves were skimmed off to give a smooth surface before further grooves could be cut. All parameters except for the groove depth were kept the same as the previous specification (i.e. 26 grooves per inch, 55^{o} angle, rounded edge).

It is believed that the coating rolls may give a variation in coating weight due to the variation in viscosity between the three coatings. Therefore, to ensure the correct coating weight could be achieved, two different roll groove specifications were chosen. These were of groove depths 2 thou and 3.5 thou (51 and 89 microns respectively). The rolls were re-ground with two different sections on each half of the roll, ensuring that the areas of each roll with the same specifications matched up (see Figure 10.2). This was to guarantee that both the top and bottom surfaces of any sample would have a similar coating weight.

With the two different groove specifications and control over the roll pressure, this set-up allowed an accurate adjustment of coating weight over a wide range of values, particularly around those required for this investigation.

10.2.2 Results and Discussion

Each group of ten samples from each coil, and for each coating, were averaged. From these values, the percentage loss reduction was calculated. The results for the tests at Bpk = 1.5T, 1.7T, 50Hz are shown in Tables 10.1 and 10.2 respectively. They are also illustrated in Figures 10.3 and 10.4.

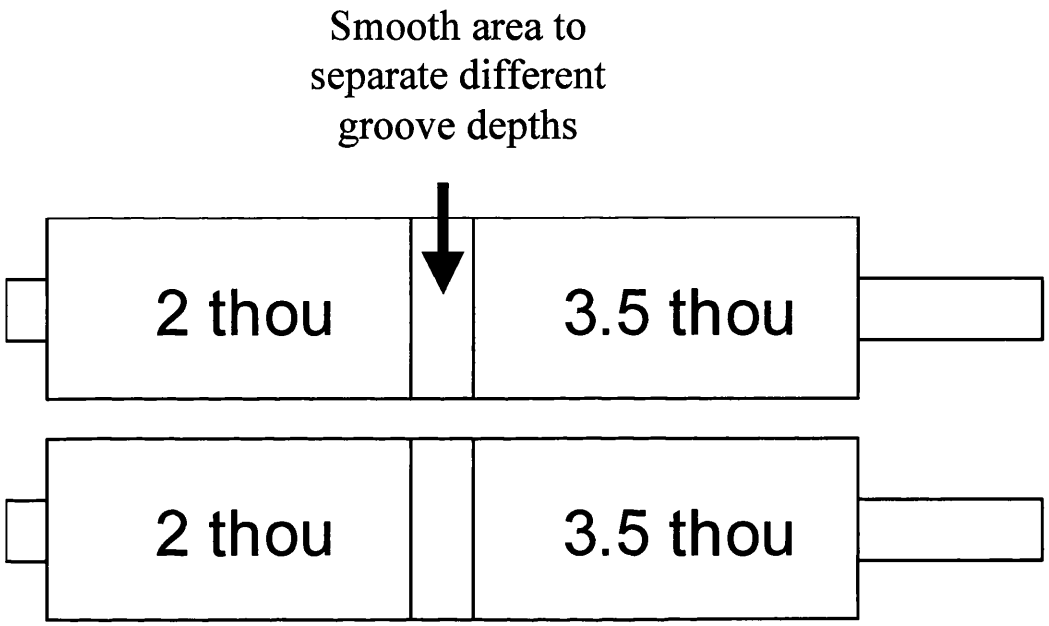

Figure 10.2: Schematic diagram of the 2-section coating rolls.

	S2			Cr-free			Mix 26		
	Before Ct.	After Ct.	%Loss Red.	Before Ct.	After Ct.	%Loss Red.	Before Ct.	After Ct.	%Loss Red.
Coil A	0.887	0.867	2.20	0.894	0.888	0.66	0.886	0.836	5.73
Coil B	0.955	0.924	3.30	0.952	0.923	2.99	0.944	0.887	6.01
Coil C	0.959	0.910	5.14	0.958	0.926	3.31	0.968	0.894	7.65
Coil D	0.925	0.884	4.35	0.925	0.898	2.87	0.930	0.888	4.56
Coil E	0.866	0.809	6.61	0.852	0.844	0.66	0.876	0.851	2.88
Average	0.918	0.879	4.32	0.916	0.896	2.10	0.921	0.871	5.37

Table 10.1: Loss reduction values for samples measured at Bpk =1.5T, 50Hz using PMS3000.

	S2			Cr-free			Mix 26		
	Before Ct.	After Ct.	%Loss Red.	Before Ct.	After Ct.	%Loss Red.	Before Ct.	After Ct.	%Loss Red.
Coil A	1.168	1.152	1.38	1.173	1.164	0.80	1.160	1.079	6.98
Coil B	1.234	1.197	2.98	1.234	1.202	2.58	1.212	1.123	7.33
Coil C	1.268	1.213	4.35	1.271	1.225	3.55	1.274	1.156	9.24
Coil D	1.198	1.159	3.28	1.200	1.164	3.02	1.201	1.145	4.62
Coil E	1.166	1.094	6.18	1.148	1.137	0.74	1.178	1.141	3.05
Average	1.2068	1.163	3.63	1.2052	1.1784	2.14	1.205	1.1288	6.24

Table 10.2: Loss reduction values for samples measured at Bpk =1.7T, 50Hz using PMS3000.

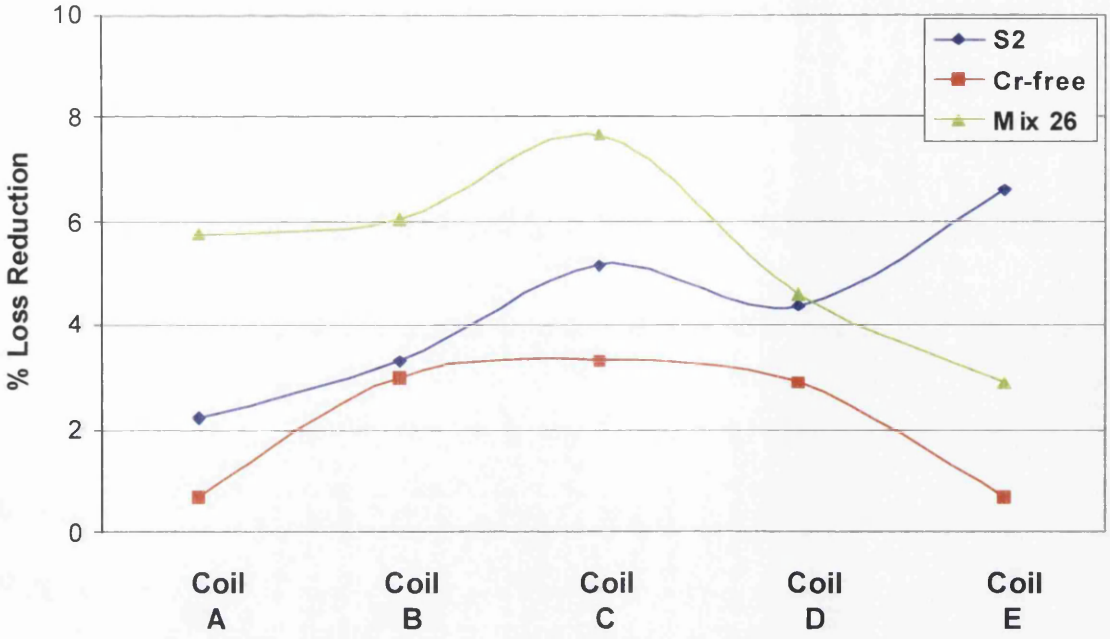

Figure 10.3: Variation in percentage loss reduction between coils at Bpk =1.5T, 50Hz

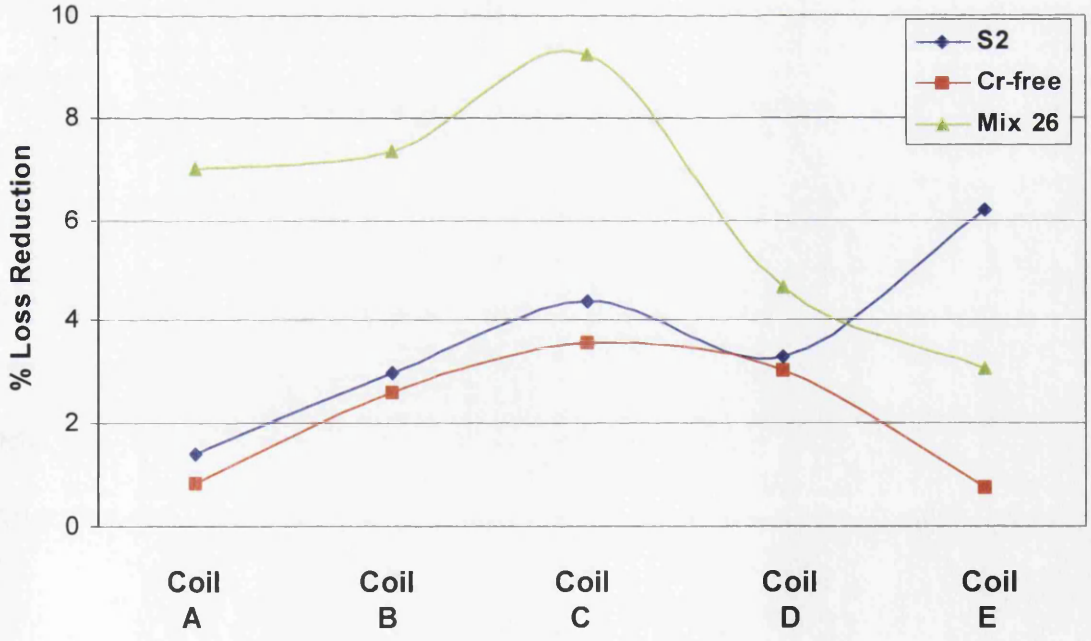

Figure 10.4: Variation in percentage loss reduction between coils at Bpk =1.7T, 50Hz

It can be seen that, for each coating formulation, there is a variation in the percentage loss reduction between different coils. However, the performance from coil to coil is generally matched for each of the coatings. For example, the highest loss reduction for each coating occurs on Coil C, which is incidentally the only material taken from the middle of the coil and is therefore likely to be of the highest quality. This effect is seen for the results from the tests at both Bpk = 1.5T and 1.7T, 50Hz. The only point on the graphs that does not follow the trend is that of the S2 coating on Coil E. The reasons for this cannot currently be explained, but it is suspected that it is a result of malfunctioning of the single-strip tester, as the trends for every other data point seem to be so respectable.

If the data point discussed above is omitted, it can be seen that the percentage loss reduction results for the S2 and C-free coating currently used on the production line are very similar, particularly at Bpk = 1.7T, 50Hz. The results for S2 are generally the higher of the two in this investigation, but no noticeable effect in the magnetic losses has been observed on production material when the standard coating has switched from S2 to the chrome-free coating.

The loss reduction results of the 'Mix 26' coating are seen to be significantly better that seen for the other two coatings, with a maximum loss reduction of 9.24% achieved on Coil C. This confirms the findings of the previous investigation, and is significantly better than any coating formulations that have previously been trialled at Orb. Most promisingly, it suggests that the percentage loss reduction on Hi-B material could approximately be doubled if the 'Mix 26' was employed.

10.3 Magnetostriction Apparatus – Shift of the Fundamental Component of Magnetostriction

The samples analysed in Section 10.2 were also used to investigate the effect that the different coatings had on the magnetostriction properties of the steel. This was done by using apparatus that had been specifically built at Orb Works for the measurement of magnetostriction. The magnetostriction apparatus varies the stress from +10MPa (extension) to -10MPa (compression), and takes readings of the magnetostriction and magnetic loss at intervals of approximately 1MPa. The magnetostriction results consist of the fundamental (100Hz for 50Hz excitation), which is commonly believed to be related to transformer noise, along with the 2^{nd}, 3^{rd}, 4^{th} and 5^{th} harmonics. Values of VA/kg and permeability are also given at each stress value.

Effects of the higher harmonics are very important but at present it is uncertain how best to combine the harmonics of magnetostriction to best relate to noise.

One method for evaluating the magnetostriction curves has been based around the stress value at which the magnetostriction value becomes positive (the stress intercept). However, a problem was encountered with the software associated with the magnetostriction apparatus during this investigation, as it was failing to correctly distinguish between positive and negative magnetostriction values that were close to zero. Further to discussions with the system designer, it was decided to modify the results that were generated by altering some of the signs (i.e. changing between positive and negative). Some of the values were simple to interpret as having an incorrect sign, as they were far more negative than considered possible for electrical steel. However, other data points were not as straightforward. Unfortunately, the stress value at which the magnetostriction became positive was now a direct result of

personal interpretation of the data, and specifically which values were made positive. Therefore, this parameter was not used for the analysis of the data obtained.

It was decided to only consider the fundamental component of magnetostriction and also to make each magnetostriction value positive in order to ensure that each curve was smooth. This is shown in Figure 10.5, which shows the curve in its original and modified forms. Note that μS = microstrain = 10^{-6}.

Although this was not a conventional technique, it was considered acceptable to do this in this incidence since it mainly affected the data that had magnetostriction values close to zero, and it is the higher values that are of most interest. It is aimed to establish the difference between coated and uncoated samples, and not provide definitive, quantitative data for one-off samples.

Other techniques for analysing the curves have been based around the magnetostriction value at either -5MPa (5MPa compressive stress), or the point of inflection (which commonly occurs at a similar stress value). However, the variation in magnetostrictive properties of a material over the entire range of stress is of interest in this investigation, not just at one particular value.

It was decided that the optimal method for demonstrating the effect of coatings on the magnetostrictive properties over the entire stress range was to calculate the magnetostriction shift (on the vertical axis) between the absolute (positive) values of a particular sample, when comparing the sets of data for both the coated and uncoated sample. This resulted in a small value when the curves were similar, and a higher

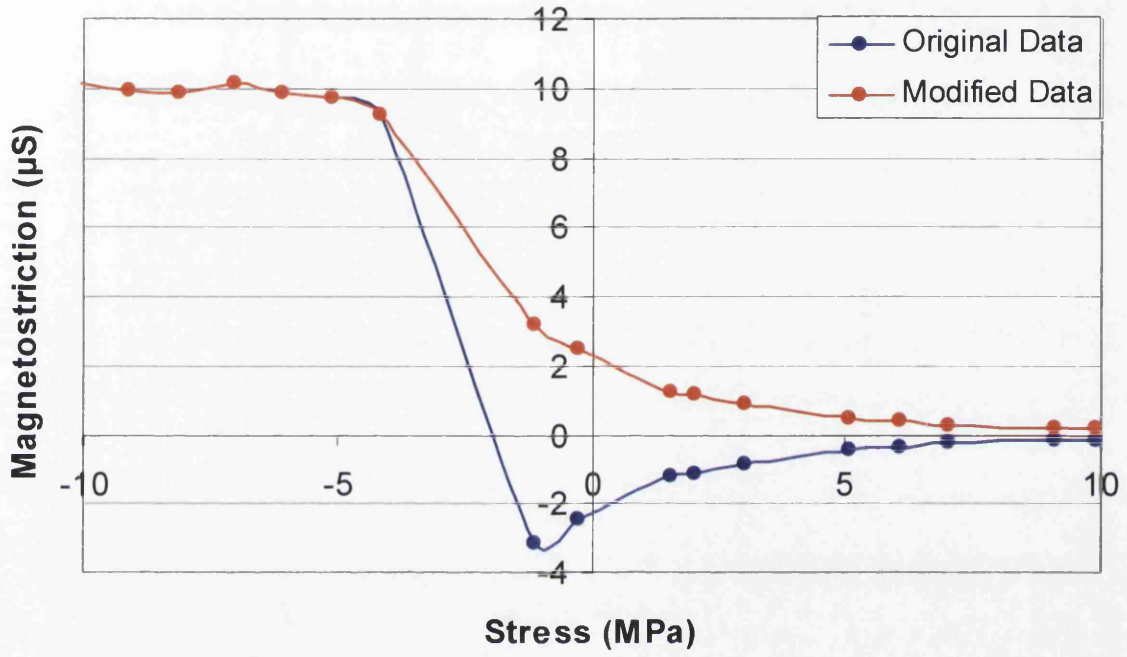

Figure 10.5: Original and modified curves for sample A7 at 1.7T.

value with improvement due to the coating. Hence, the greater the magnitudes of the magnetostriction shift, the greater the influence of the coating on reducing the magnetostriction.

Figure 10.6 shows the adjusted curves for sample A44, both uncoated (red) and when it had been coated with the S2 formulation (blue). The green curve on this figure shows the difference in the magnetostriction value at each stress value.

This shows an example where there is a significant difference in the magnetostriction curves, particularly at compressive stress >4Mpa. Two similar curves would result in a shift curve that was far more flat.

The magnetostriction shift values were calculated for a large number of samples. However, due to the large number of samples and certain time constraints, it was decided to concentrate only on those results obtained at Bpk = 1.7T, 50Hz. Also, only the samples from coils A, B and C (all 0.30mm) were selected to be analysed in this way. Although this prevented a large number of samples from being considered, it was still sufficient to provide a large amount of data on all three coatings, and their effects on material from two different coils, including material from both the end and the middle sections of one of these coils. Coil C also relates to the material which exhibited the highest values for magnetic loss reduction, and so the magnetostrictive properties of this material are of particular interest.

It was found that for the 10 samples from the same material and with the same coating, there was a large amount of spread for the magnetostriction shift curves. This was expected due to minor fluctuations during the testing procedure, unavoidable differences in the pickling, coating and curing of the samples and the variation in the

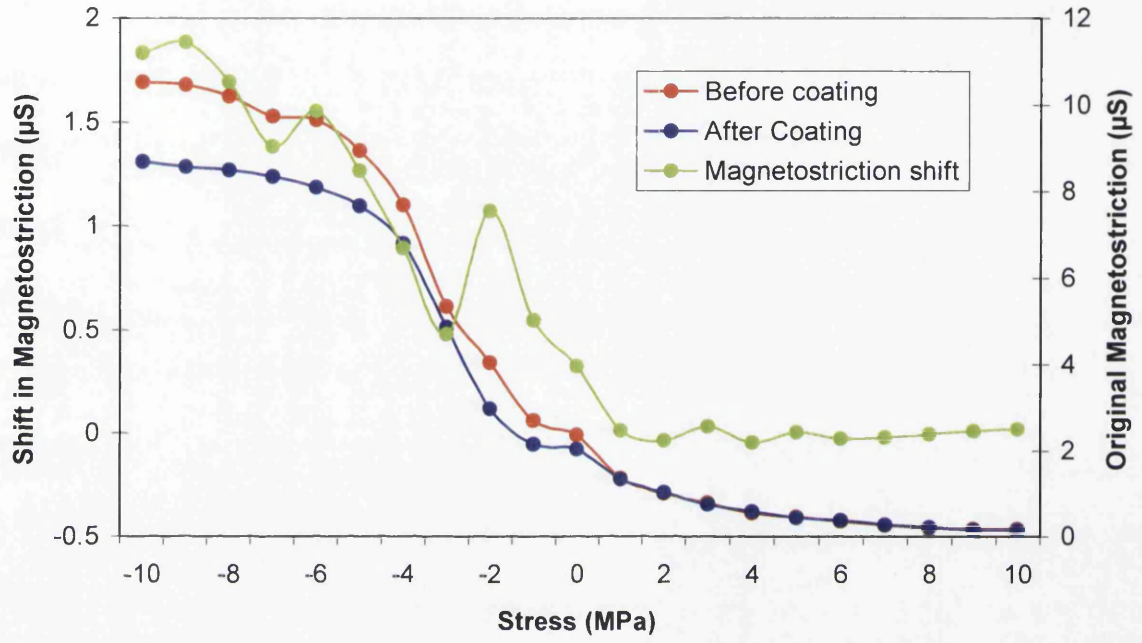

Figure 10.6: Magnetostriction curves for sample A44 before and after coating, and the resultant shift curve.

characteristics of the base steel. However, this variation between samples was not seen to be problematic as the data for the 10 samples was averaged, giving a good overall view of a particular group.

The averaged magnetostriction shift data for coils A, B and C can be seen in Figures 10.7, 10.8 and 10.9 respectively.

In each of the three Figures (10.7-10.9), it can be seen that the greatest magnetostriction shifts (in relation to the fundamental component), and therefore the greatest reduction in magnetostriction, are for the samples coated with the S2 formulation. The chrome-free coating gives the second greatest shift, with the least difference in magnetostriction curves being seen for the samples coated with the 'Mix 26' formulation.

For each of the three coils, the 'Mix 26' formulation appears to have very little effect on the magnetostriction at all, with it having a negative impact for most of the stress values for coil C i.e. the magnetostriction curve of the coated sample is actually worse than that of the uncoated steel.

In each graph, it is apparent that the magnetostriction in the areas of tension (positive stress values) is largely unaffected by coating the samples, and that the main shifts occur under compression.

An interesting observation, particularly apparent for coil A (and to a lesser extent for coil B), is the behaviour of the curve relating to the chrome-free formulation. It appears to remain close to the curve for 'Mix 26' when under tensile stress and then, as the compressive stress increases, steps up to a similar level as the S2 coated

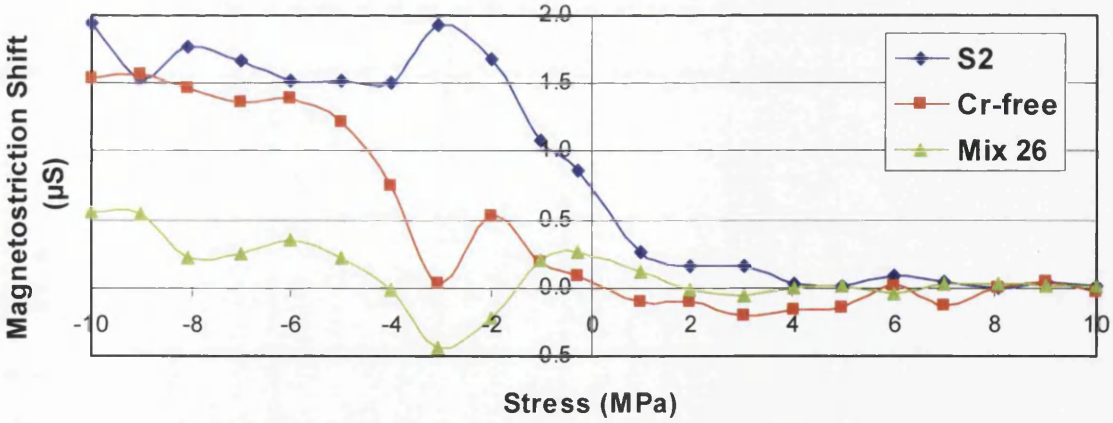

Figure 10.7: Average magnetostriction shift curves for the 3 coatings on Coil A.

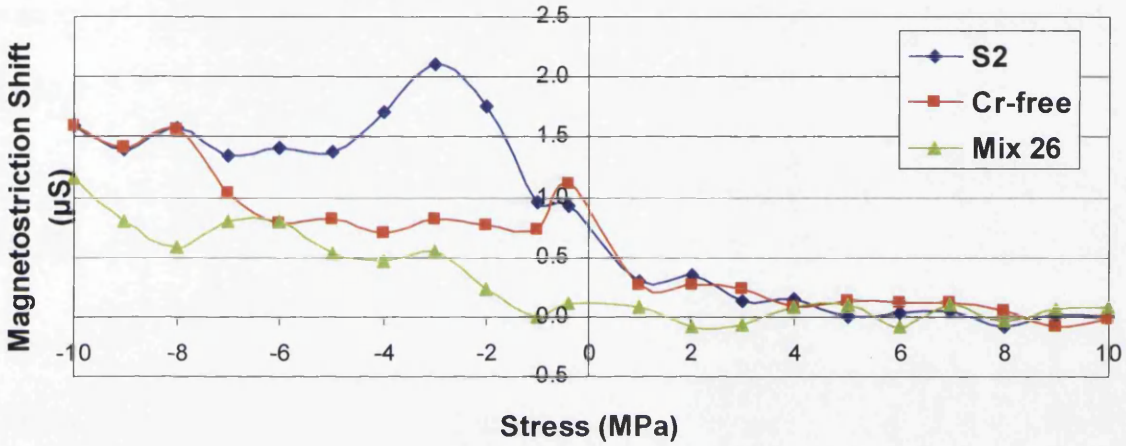

Figure 10.8: Average magnetostriction shift curves for the 3 coatings on Coil B.

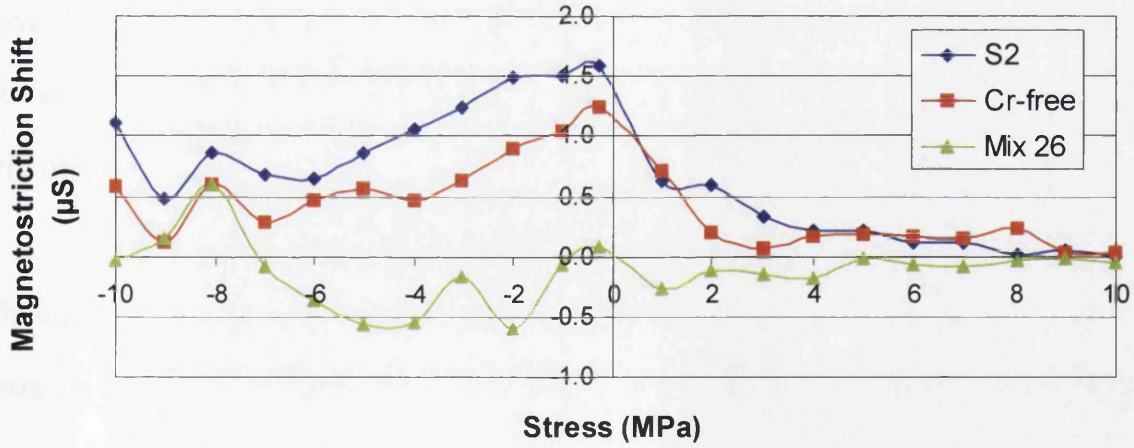

Figure 10.9: Average magnetostriction shift curves for the 3 coatings on Coil C.

samples. This effect is also seen when considering the data that has been averaged for each coating formulation across all three coils, shown in Figure 10.10.

These magnetostriction shift curves are not as expected, as it has previously been considered by various personnel that the magnetic losses and the magnetostriction are closely linked. However, it can be seen that the coating that resulted in the lowest loss reduction (chrome-free) did not have the least effect on the magnetostriction. More evidently, the 'Mix 26' formulation has the least effect on the magnetostriction, even though it clearly gave rise to the greatest loss reductions seen from any of these coatings.

10.4 Conclusions

This investigation has shown that the 'Mix 26' formulation may be used as a final insulating coating on grain oriented electrical, and will result in substantially greater reductions in magnetic losses than those previously achieved. However, it appears that there will also be a corresponding reduction in the effect that this coating will have on the magnetostrictive characteristics of the material. Therefore, the benefits of this coating must be weighed up against this effect, and the viability of this coating will depend largely on the requirements and priorities of the customer.

The contradictory results between the magnetic losses and the magnetostriction curves were unexpected. These results warrant further investigation, which is due to be carried out on new magnetostriction apparatus that has recently been commissioned.

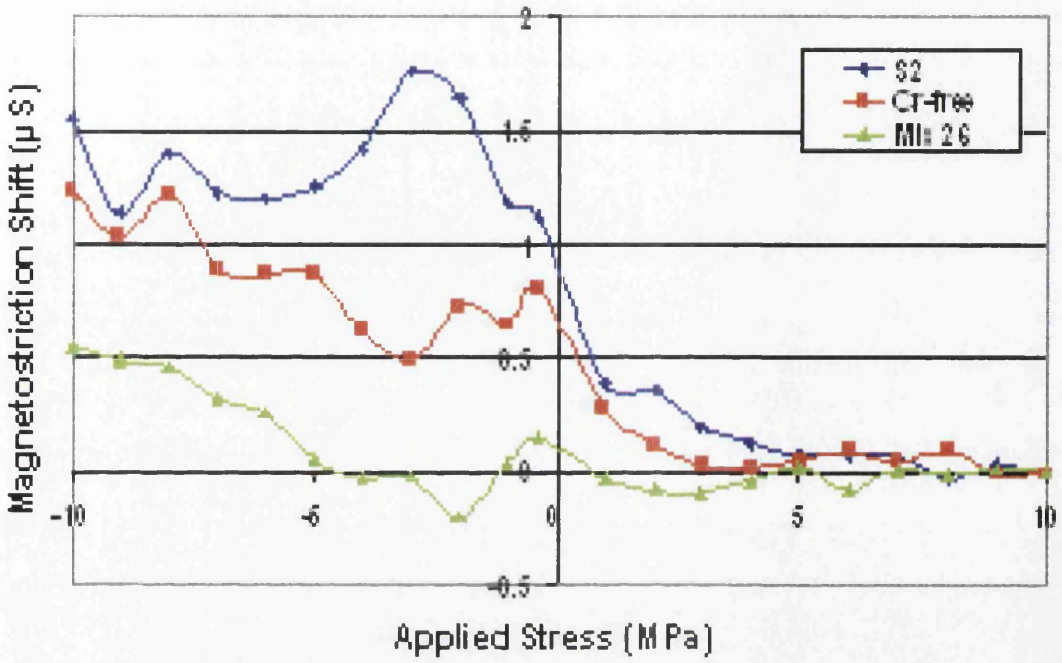

Figure 10.10: Magnetostriction shift curves for each of the three coatings, averaged over coils A to C.

Chapter 11

11.1 Conclusions

This investigation had studied the feasibility of using a wide range of different analytical techniques for the assessment of various surface layers on grain oriented electrical steel. From this work, the following conclusions can be drawn:

11.1.1 Decarburisation Oxide Layer

- Fayalite (Fe_2SiO_4) is found in the uppermost section of the decarburisation oxide layer, and is the only compound detected when a decarburised sheet is analysed using the 80^o grazing angle attachment in conjunction with the Fourier Transform Infrared (FTIR) apparatus. The underlying layer of silica is only exposed upon subsequent acid etching of the sample, due to the rapid removal of the fayalite. It was established that use of a variable grazing angle attachment was not able to sufficiently alter the penetration depth of the infrared radiation in order for the entire oxide layer to be examined using FTIR.
- The Electrochemical Potential (ECP) method has been used to assess the consistency of the surface oxide layer formed during the decarburisation process. It has been found that the Works produced material generally results in ECP profiles that can be separated into four slightly different categories, but that these different profiles appear to show no trends in relation to the position on the strip from which each sample originated. However, analysis of samples annealed under varied atmospheric conditions in a laboratory tube furnace showed significantly different ECP profiles. This suggests that the technique is reproducible, and that

the consistency of the material on the Works production lines might be better than was initially anticipated, as the variation in the four types of ECP profiles was far less than seen in the laboratory furnace trials.

The ECP technique is therefore very useful for the classification of groups of samples for studies relating to decarburisation layers.

- The ECP technique was found to provide a successful method for closely monitoring the slow etching of the decarburisation oxide layer. This effectively enabled analysis to be carried out at various depths within the layer.

    - Images obtained from Scanning Electron Microscopy (SEM) were generally inconclusive, but the associated Energy Dispersive X-Ray (EDX) showed an increase in both silicon and oxygen as the depth within the layer increased. They increased consistently according to an atomic weight ratio of 1:2, suggesting that the compound could be identified as silica (SiO_2).

    - X-ray Photoelectron Spectroscopy (XPS) also showed a link between the silicon and oxygen present in the lower regions of the oxide layer. However, this technique could not be used quantitatively, as subsequent analysis using Sputtered Neutral Mass Spectrometry (SNMS) proved that the XPS results were distorted due to carbon contamination.

    - Fourier Transform Infrared (FTIR) analysis provided a useful insight into changes in the composition of the oxide layer. It was found that the fayalite on the very surface was removed as soon as the sample was etched in the acid. Further etching showed that the ECP profile was directly related to the observation of two separate absorption bands,

believed to be two different forms of silica, with the peak and trough of the profile associated with the points at which the spectra changed from one band to another. This proves a direct link between the ECP profiles and the composition and / or morphology of this surface oxide layer.

11.1.2 Forsterite Glass Film

- Use of the FTIR apparatus, in conjunction with the 26.5° grazing angle attachment, has proved that the forsterite glass film produces a very consistent spectrum in terms of the position of its absorption bands. Software associated with the FTIR apparatus has enabled this fact to be exploited by using a section of the spectra (400 to 890cm^{-1}) for the determination of the forsterite thickness using.

11.1.3 Final Insulation Coating

- The main constituents of the coating (aluminium orthophosphate and colloidal silica) were found to give distinctive spectra when analysed using the FTIR apparatus. These spectra were used in conjunction with a software program (Spectral Calculator) to produce a theoretical prediction of specific mixes of these components, which was subsequently found to exhibit a good correlation with the spectra obtained from laboratory mixes.
- When the FTIR technique was used to analyse material coated on the Works production line, it was found that the resultant spectra could not be used to determine the ratio of silica and aluminium orthophosphate as desired. This was due to the presence of many absorption bands relating to the underlying forsterite

glass film layer, which caused the bands associated with the coating to be distorted.

- A number of trials were carried out to develop a chrome-free insulation coating. Many techniques were used to assess a number of characteristics of the cured coatings in order to establish whether they were a viable alternative to the chrome-bearing solution. Once their practicality had been proven (solution stability, wettability etc.), the potential coating formulations were assessed to determine the effect that they had on the magnetic properties of the steel. It was found that there were a number of coatings that exceeded the results produced by the chrome-bearing coating, including a formulation that gave an improvement of approximately 40%. As a result of this investigation, an alternative chrome-free coating is now used as the standard production coating on all grain oriented steel produced at Orb Works.

11.2 Future Work

11.2.1 Decarburisation Oxide Layer

- The work combining the FTIR and ECP techniques appeared very promising in terms of assessing the decarburisation oxide layer. It is necessary to make an attempt to definitively identify the compounds relating to the spectra at various stages of etching. This would enable an exact correlation to be made between the shape of the ECP profiles, and particularly the points of inflection, and the composition of the oxide layer.
- A large number of samples were analysed using the ECP method. However, the aim was to analyse a large number of samples from a small area of strip.

This work needs to be developed to determine the variation in ECP profiles between a much larger number of coils. To achieve this, the ECP technique should be used on a more routine basis to analyse a few samples from many coils over a number of months.

11.2.2 Final Insulation Coating

- FTIR analysis of the Works coated material was found to be problematic due to the underlying forsterite glass film distorting the absorption bands associated with the final phosphate coating. This is due to the penetration depth of the infrared radiation being too great. Therefore attempts should be made to utilise variable grazing angle apparatus to vary the penetration depth, in a similar way as was used in the investigation for the decarburisation oxide layer. Reducing the power of the infrared source could also have a similar, beneficial result. Due to the mixing of the coatings, the cured coatings should be of a consistent formulation throughout, suggesting that the FTIR apparatus could be used to determine the composition if the effect of the forsterite could be eliminated.
- The loss reduction results from a number of alternative chrome-free coatings were very promising, and one of the formulations now provides the basis for the standard production coating. However, this was not the formulation that provided the greatest loss reduction, but the one that could be applied on the production line with most ease. Therefore, coatings remain that have shown great loss reduction potential, but further investigation is needed to determine the requirements for them to be used under production conditions.

- During the evaluation of various formulations of the final coating solution, the loss reduction was calculated from a number of samples, taken across a range of 5 different coils. It was found that some of the coils appeared to show a better response to the coating than others. The reasons for this are currently unknown, but establishing the reasons for this would be highly beneficial when trying to consistently reduce losses to the minimum that is achievable for each production coil. Therefore, an investigation should be carried out using a number of coils with known differences in a number of characteristics, such as surface roughness, grain size etc. to determine the reasons for this effect.
- The magnetostriction apparatus located at Orb was originally commissioned as part of a PhD project, and was not intended for long term use, and has also not been used on a routine basis for more than a year. A new magnetostriction set-up has recently been commissioned and is currently being built. With further advances in technology and knowledge of the system, it is hoped that this apparatus will measure the characteristics of both magnetostriction and loss to a greater degree of accuracy. Once this new apparatus is operational, further measurements can be taken to confirm the results obtained during this investigation, and modifications can be made to the coatings, where necessary, in order to satisfy the customers needs.

References

1. W.F.Barrett, W.Brown and R.A.Hadfield, Scientific Transactions, Vol 7, p67, 1900.

2. W.F.Barrett, W.Brown and R.A.Hadfield, Journal of Elec. Eng., Vol 31, p674, 1902.

3. T.D.Yensen Trans. Amer. Inst. Elect. Eng 34 2601, 1915.

4. K.Honma et al, Development of Non-Oriented and Grain Oriented Silicon Steel, IEEE Transactions on Magnetics, Vol. MAG-21, No.5, September, 1985.

5. N.Goss, US Patent 1,965,559, 1934.

6. S.Taguchi, A.Sakakura and H.Takashima, U.S. Patent 3,287,183, 1966.

7. A.J.Moses, Electrical Steels: Past, Present and Future Developments, IEEE Proc. Vol 137, Sep, 1990.

8. Philip Beckley, Electrical Steels, European Electrical Steels, 2000.

9. Victor William Carpenter and John Martin Jackson, Production of Insulative Coatings on Steel Strip, Patent Specification, March 11 1959.

10. Armco International Corporation, British Patent 810 039, March 1959.

11. MgO-based Annealing Separator for Grain Oriented Silicon Steel Strips, UK Patent Application, 2 041 343 A, 1979

12. Robert.G.Hirst and George.J.Desnoyers, Insulating Coating and Method of Making the Same, U.S.Patent, Dec 12 1972.

13. Ichida et al, Method of Forming a Forsterite Insulating Film on the Surface of a Grain Oriented Steel Sheet, U.S. Patent, Feb 10 1981.

14. R.A.Chapman, The Formation of an Inorganic Insulating Coating on Electrical Sheet Steel, PhD Degree Thesis, 1973.

15. Method for Forming Forsterite Insulating Film on an Oriented Silicon Sheet Steel, United states patent, Feb 26, 1980.

16. S.Akatsu, Methods of Deposition of Silicon Oxide Films on Silicon Sheet Steel, 1967.

17. P. Cummings, Coating defects in Fully Finished GO Material, Internal Cogent Power Research Report No.004, 1997.

18. O. Tanaka, H.Kobayashi, E.Minematsu, New Insulating Coating for Grain Oriented Electrical Steel, J.Mater.Eng. 13:161 – 168, 1991.

19. M.J.Davies et al, Measurement of Coatings and Surface Oxide Layers on Grain Oriented Electrical Steel, Ironmaking and Steelmaking, Vol.25 No.2, 1998.

20. Developments of Grain-Oriented Silicon Steel Sheets With Low Iron Loss, Kawasaki Steel Technical Report, No. 22, May 1990.

21. Dan S. Loudermilk and Robin A. Murphy, Overview of Technology of Insulating Coatings for Grain-Oriented and Non-Oriented Electrical Steels, Conference Proceedings, 15th Annual Conference on Properties and Applications of Magnetic Materials, 1996.

22. Obtained by technical personnel (P. Cummings) at Orb Works.

23. R.W.Hannah and J.S.Swinehart, Experiments in Techniques of Infrared Technology, Perkin-Elmer Corporation, 1974.

24. P.Beckley and H.Boniface, Electrochemical Assessment of Oxide Layers, British Steel Technical Note No. E/309, 17th June 1982.

25. Nigel Martyn, The Electrochemical Potential Analysis of Decarburised Surface Oxide Layers Of Electrical Steel, EPSRC MRes Degree Thesis, 2000.

26. Young and Freedman, University Physics Ninth Edition, Addison-Wesley Publishing Company, Inc., 1996.

27. Philip Anderson, A Novel Method of Measurement and Characterisation of Magnetostriction in Electrical Steels, Ph.D. Thesis, 2000.

28. P.I. Anderson, A.J. Moses, H.J. Stanbury, An automated system for the measurement of magnetostriction in electrical steel sheet under applied stress, Journal of Magnetism and Magnetic Materials Vol 215-216 pp 714-716, 2000.

29. Methods of Measurement of the Magnetic Properties of Electrical Steel Sheet and Strip by Means of an Epstein Frame, British Standard, BS 6404: Part 2: 1996, IEC 404-2: 1996, Magnetic Materials. Part 2, 1996.

30. Website: Products Finishing Online, Coating Thickness Measurement: The Fundamentals, http://www.pfonline.com/articles/0206qf1.html.

31. G. Thomas, Determination of Fayalite Layer Composition Using Infrared Analysis, Orb Technical Note, 1997.

32. Perkin-Elmer Spectrum™ User's Reference, January 1998.

33. Website: http://webbook.nist.gov/chemistry - NIST Chemistry WebBook.

34. P. Beckley and H.Boniface, Electrochemical Assessment of Oxide Layers, British Steel Technical Note No. E/309, 17th June 1982.

35. Nigel Martyn, The Electrochemical Potential Analysis of Decarburised Surface Oxide Layers Of Electrical Steel, EPSRC MRes Degree Thesis, 2000.

36. D. Snell, Preliminary Evaluation of Surface Oxide Layers on Decarburised Conventional Grain Oriented Electrical Steel, British Steel Technical Note No. E/348, 12th September, 1986.

37. D. Snell, Further Assessment of Surface Oxide Layers on Decarburised Grain Oriented Electrical Steel Using the Electrochemical Method, British Steel Technical Note No. E/351, 1st October, 1986.

38. D. Snell, Assessment of Surface Oxide Layers on Decarburised Grain Oriented Electrical Steel Using the Electrochemical Potential Difference Method, Orb Electrical Steels Ltd. Technical Note No. 179, 22nd February, 1994.

39. D. Snell and H. Silverthorn, Comparison of Different Methods of Assessment of the Surface Oxide Layers on Decarburised Grain Oriented Electrical Steel Using the Potential Difference Method, Orb Electrical Steels Ltd. Technical Note No. 218, 6th September 1994.

40. H. Toda, K. Sato and M. Komatsubara, Characterisation of Internal Oxide Layers in 3% Si Grain-Oriented Steel by Electrochemical Methods, Journal of Materials Engineering and Performance, Volume 6 (6), p. 722- 727, December 1997.

41. J. R. Ferraro., The Sadtler infrared spectra handbook of minerals and clays, Philadelphia, Pa: Sadtler, (ISBN 0-8456-0080-x), 1982.

42. Perkin-Elmer Technical Publication, Spectrum Beer's Law User's Reference, January 1998.

43. http://www.rohs.gov.uk/content.aspx?id=9

44. D. Snell, Review of Chrome Free Coatings for Grain Oriented Electrical Steels, Cogent Internal Research Note (RN 348), 19/5/05.

45. D. Snell, D. Poultney, A. Nolan, A. Green, D. Power and G. Thomas, Laboratory Evaluation of Chrome Free Coatings for Grain Oriented Electrical Steel RN 350, June 2005.

46. D. Snell, D. Poultney and A. Nolan, Tension Coatings for High Permeability Grain Oriented Electrical Steel, Cogent Internal Research Note (RN 356), 30th March, 2006

47. D. Snell, D. Poultney and A. Nolan, Further Trial on Tension Coatings for High Permeability Grain Oriented Electrical Steel, Cogent Internal Research Note (RN 357), 24th April, 2006.